

1-1-2015

Synthesis And Biological Evaluation Of Nitrile-Based Inhibitors Of Cysteine Proteases Caged With Ruthenium Complexes

Rajgopal Sharma
Wayne State University,

Follow this and additional works at: https://digitalcommons.wayne.edu/oa_dissertations

 Part of the [Chemistry Commons](#)

Recommended Citation

Sharma, Rajgopal, "Synthesis And Biological Evaluation Of Nitrile-Based Inhibitors Of Cysteine Proteases Caged With Ruthenium Complexes" (2015). *Wayne State University Dissertations*. 1380.
https://digitalcommons.wayne.edu/oa_dissertations/1380

This Open Access Dissertation is brought to you for free and open access by DigitalCommons@WayneState. It has been accepted for inclusion in Wayne State University Dissertations by an authorized administrator of DigitalCommons@WayneState.

**SYNTHESIS AND BIOLOGICAL EVALUATION OF
NITRILE-BASED INHIBITORS OF CYSTEINE PROTEASES
CAGED WITH RUTHENIUM COMPLEXES**

by

RAJGOPAL SHARMA

DISSERTATION

Submitted to the Graduate School

of Wayne State University,

Detroit, Michigan

in partial fulfillment of the requirements

for the degree of

DOCTOR OF PHILOSOPHY

2015

MAJOR: CHEMISTRY (Organic)

Approved By:

Advisor

Date

© COPYRIGHT BY
RAJGOPAL SHARMA
2015
All Rights Reserved

DEDICATION

I dedicate my dissertation work to my wonderful parents, Navratan and Kiran Sharma who have made many sacrifices in their life to make me a better person. I could achieve this only because of your support, love and blessings. I also dedicate my work to my lovely wife Priyanka Sharma for her endless love and encouragement. Finally I also dedicate this dissertation to Mukesh, Kavitha, Bhagyashree, Sanjana, Tanushree and Jatin Sharma who have been my greatest strength.

ACKNOWLEDGMENTS

Firstly, I would like to thank my PhD advisor Professor Jeremy Kodanko for his guidance throughout graduate school. He has been an incredible source of knowledge and inspiration to me. Apart from laboratory training he has put an extra effort in teaching me writing skills. He has always motivated me in coming up with new ideas towards my research, which gave me an opportunity to understand and think as an independent chemist. He has been a great mentor and guide both professionally and personally, and I don't know if I will ever be able to express how thankful I am for that.

I would like to extend my acknowledgements to my committee members, Professor Jin K. Cha, Professor H. Bernhard Schlegel and Professor Maik Huttemann who have given me valuable advice on my thesis work and presentation skills. I am very grateful for the cooperation and flexibility shown by them for scheduling my meetings and talks.

I would like to thank our collaborators Professors Turro, Podgorski, Endicott, Schlegel and Sloane for their contributions towards my projects. None of my projects could have been completed without their contributions and suggestions. I would like to thank Professor Izabela Podgorski who has trained me in conducting bioassays and made me feel comfortable with biochemistry.

I would like to thank my friend, Shaheen Ali who has motivated me for pursuing graduate studies in U.S and has been a great guide both professionally and personally. I would like to thank my uncle, Dr. Ghanshyam Sharma who has always been an inspiration and guide. I would also like to thank Dr. Santhana Krishnan, Dr. Raghu Mortala, Dr. Satyanarayana Mavurapu, Basanti, Paramesh, Kalyan and Chary who have been my mentors and friends at Dr. Reddy Laboratory.

I would like to thank the entire current and past Kodanko group and other chemistry research students that I had the opportunity to interact with. I am in particular thankful to my coworkers: Tomasz, Jai, Eric, Nick, Ao, Karan, Veronica and Matt for providing a joyful environment in the lab and outside the department. I also would like to thank all the staff members from the chemistry department and Science Stores for their help and support in numerous aspects of graduate life.

I would like to thank all the people whom I met in Michigan including Jessica, Lindsey, Matt, Tanya and Becky who made me feel that Michigan was my home away from home.

Finally none of this would have been possible without the love and support of my family in India who believed in me and supported me in every situation. I also thank all my friends including Rajendar Salla, Yogitha Mantri, Sadhana Reddy, Raj Kumar, Sachin Khandelwal, Ram Khandelwal, Shiv Sagar, Ravi Vatepu, Ibrahim Mohammad, Vinod Chiluka and Narsimha Nagavaram who have been part of many memorable events in my life. I also thank Balkrishna, Jayshree, Nandu and Mayur for their support and love.

TABLE OF CONTENTS

Dedication	ii
Acknowledgments	iii
Table of Contents	v
List of Tables	x
List of Figures	xi
List of Schemes	xv
Chapter 1. Introduction.....	1
1.1 General introduction	1
1.2 Light in therapeutics	1
1.3 Metals in medicine	2
1.4 Photocages in biological applications.....	6
1.5 Photodynamic therapy (PDT)	12
1.6 Photoactivated ligand dissociation	15
1.7 Cysteine cathepsin proteases.....	16
1.8 Proof of concept (background work)	24
1.9 Thesis statement	25
Chapter 2. Inhibition of cathepsin K activity in a cell-based assay by light activated caged ruthenium complexes.....	27
2.1 Introduction	27
2.2 Results and discussions.....	28
2.2.1 Synthesis of metal complexes 62 and 63 and characterization data.....	28
2.2.2 Stability studies	31
2.2.3 Light activated inhibition of cathepsin K.....	34

2.2.4 Toxicity studies -----	36
2.2.5 Light activated inhibition of cathepsin activity in a cell-based assay -----	37
2.3 Discussions -----	42
2.4 Conclusion -----	45
2.5 Experimental procedures -----	45
2.5.1 General considerations -----	45
2.5.2 Experimental procedures for synthesis of complexes (62 and 63) and characterization data -----	46
2.5.3 Stability study -----	48
2.5.4 Photochemical quantum yield -----	48
2.5.5 Cell assays and imaging -----	49
2.5.6 Experimental procedure for cathepsin K inhibition studies -----	50
2.5.7 Experimental procedure for toxicity studies -----	51
Chapter 3. Imaging inhibition of cathepsin B activity in real-time in situ 3D MAME cultures	
3.1 Introduction -----	53
3.2 Results and discussions -----	55
3.2.1 Synthesis of metal complex (65) and characterization -----	55
3.2.2 Stability studies and photolysis data -----	57
3.2.3 Light activated inhibition of purified cathepsin B and cell lysates -----	58
3.2.4 3D MAME cell culture assay for breast cancer cell lines -----	60
3.3 Discussions and conclusions -----	69
3.4 Experimental procedures -----	70
3.4.1 Cathepsin B inhibition studies -----	70

3.4.2 Inhibition of cellular cathepsin activity	71
3.4.3 Live cell proteolysis assay	71
3.3.4 Cell viability studies	72
3.4.5 Experimental procedure for synthesis of complex 65	73
3.4.6 Photoinduced ligand dissociation	74
Chapter 4. Caged nitrile-based CA-074 analog for inhibition of cathepsin B activity	75
4.1 Introduction	75
4.2 Results and discussions	77
4.2.1 Synthesis of CA-074 analog (66) and corresponding caged complex (73)	77
4.2.2 Stability and photolysis	79
4.2.3 Cathepsin B isolated enzyme inhibition studies	80
4.3 Discussions and conclusions	81
4.4. Experimental procedures	82
4.4.1 Synthesis of inhibitor (66) and characterization data	82
4.4.2 Synthesis of metal complex (73) with characterization data	84
4.4.3 Inhibition assay	85
Chapter 5. Ru(TPA) as an effective photocaging group for nitriles	87
5.1 Introduction	87
5.2 Results	89
5.2.1 Synthesis and characterization of two Ru(TPA)-based complexes	89
5.2.2 Photolysis study	91
5.2.3 Stability	95
5.2.4 Isolated enzyme inhibition study	95

5.2.5 Discussions and conclusions	96
5.3 Experimental procedures	97
5.3.1 Experimental procedures for synthesis of complexes (76 and 77) and tabulated data	97
5.3.2 Photochemical quantum yield.....	98
5.3.3 Stability	99
5.3.4 Cathepsin K inhibition study procedure	99
5.3.5 X-ray data for [Ru(TPA)(CH ₃ CN) ₂](PF ₆) ₂	100
Chapter 6. Solid phase synthesis as a platform for developing new caging groups.....	116
6.1 Introduction	116
6.2 Results	118
6.2.1 Synthesis of ligands (85 a-j) on solid phase.....	118
6.2.2 Synthesis of metal complexes (88 a-j) on solid phase	122
6.2.3 Synthesis of metal complexes (89-91) by solution phase	130
6.2.4 Photolysis study of metal complexes.....	133
6.2.5 Discussions	137
6.2.6 Conclusions.....	140
6.3 Experimental procedures	140
6.3.1 Synthesis of compound 80	140
6.3.2 Synthesis of resin bound pyridine precursor and resin bound ligands.....	141
6.3.3. Optimization studies for metallation and synthesis of 87 and 88	150
6.3.4 Synthesis of metal complexes (89-91) by solution phase	152
6.3.5 Synthesis of secondary amine 94 for TQA ligand.....	154
6.3.6 X-ray Data for 89 and 91	156

Chapter 7. Tuning excited state lifetimes of Ru complexes -----	196
7.1 Introduction -----	196
7.2 Results -----	198
7.2.1 Synthesis of metal complexes -----	198
7.2.2 Excited state lifetime studies and quantum yield calculations -----	199
7.2.3 DFT calculations -----	201
7.3 Discussions and conclusions -----	204
7.4 Experimental procedures -----	204
7.4.1 Synthesis and characterization of metal complexes -----	204
7.4.2 UV studies -----	206
Chapter 8. Conclusions -----	209
8.1 Goals achieved and future directions -----	209
Appendix -----	215
References -----	239
Abstract -----	264
Autobiographical statement -----	266

LIST OF TABLES

Table 1: IC ₅₀ values (μM) for 64 and 65 and dark/light ratio (with and without irradiation) against human cathepsin B, MDA-MB 231 lysate and Hs578T lysate.	60
Table 2: Observed rate constants for decomposition of 76 and 77 in 100% DMSO or pH 6.5 phosphate buffer (1.0% DMSO) at 298±2K	99
Table 3 - 8: X-ray crystallographic analysis of [Ru ^{II} (TPA)(CH ₃ CN) ₂](PF ₆) ₂ . (76)	101
Table 9: Conditions and Ru(II) sources examined for conversion of resin-bound ligand 85a to Ru(II) complexes [Ru(86a)(DMSO)Cl]Cl (87a) and [Ru(86a)(MeCN) ₂]X ₂ (88a , X = OTf, O ₂ CCF ₃)	126
Table 10: ESMS data for compounds 88a-j showing major <i>m/z</i> values observed and molecular formulas for dications	129
Table 11: Synthesis of compounds 83 and 84	142
Table 12 - 18: X-ray crystallographic analysis of [Ru ^{II} (DPAbpy)(MeCN)](PF ₆) ₂ . (89)	156
Table 19 - 25: X-ray crystallographic analysis of [Ru ^{II} (TQA)(MeCN) ₂](PF ₆) ₂ . (91)	173
Table 26: Excited state lifetimes (τ _{in}) and emission quantum yields (Φ _{em}) of some [RuL(X) ₂] ^{m+} complexes at 77K	200
Table 27: Relative energies of the ³ MLCT and ³ MC states and orbital contributions (%) of Ru and ligands to the SOMOs of A) [Ru(TQA)(MeCN) ₂] ²⁺ (91); B) [Ru(TQA)(CN) ₂] (101); C) [Ru(bpy) ₂ (MeCN) ₂] ²⁺ ; D) [Ru(bpy) ₂ (CN) ₂]	203

LIST OF FIGURES

Figure 1: Structures proposed for Salvarsan.....	3
Figure 2: Mn- and Ru-based complexes as NO and CO releasing metal complexes.....	5
Figure 3: Platinum- and ruthenium-based anticancer agents.....	6
Figure 4: Photocaging approach for two different biological applications; A) ligand acts as biological agent and B) caging group acts as therapeutic agent.....	7
Figure 5: Common functional groups caged using organic and inorganic photocages.....	8
Figure 6: Examples of platinum- and ruthenium-based photocages used as therapeutic agents that are anticancer agents similar to cisplatin.....	11
Figure 7: Ruthenium-based photocages used for caging bioagents.....	11
Figure 8: Photosensitizers used in PDT.....	12
Figure 9: (a) Pictorial representation of PDT and (b) Jablonski diagram of PDT showing energy transfer to tissue oxygen for the generation of ROS.....	13
Figure 10: Jablonski diagram of photoactivated ligand dissociation.....	16
Figure 11: Examples of cathepsin inhibitors with different warheads.....	21
Figure 12: First discovered nitrile-based cathepsin inhibitors.....	21
Figure 13: Nitrile-based inhibitors of cathepsins with their corresponding IC ₅₀ values.....	23
Figure 14: Nitrile-based CTSK inhibitors with their corresponding IC ₅₀ values.....	29
Figure 15: Structure of Δ - 62 or 63 and Λ- 62 or 63	30
Figure 16: Changes to electronic absorption of (a) 62 (52 μM) in a 1% DMSO aqueous solution irradiated at 0, 2, 3, 4, 5, 6, 7, 8, 10 and 15 min (λ _{irr} ≥ 395 nm); inset 0 and 1 min; and (b) 63 (51 μM) in a 2% acetone solution at irradiation times 0, 10, 13, 16, 20, 25, 30, 40, 50 and 60 min (λ _{irr} ≥ 395 nm); inset 0, 1, 2, 3, 5 and 7 min.....	33
Figure 17: (a) IC ₅₀ curves for inhibitor 60 (red = dark; green = light) and <i>cis</i> -[Ru(bpy) ₂ (60) ₂]Cl ₂ (62) (black = dark; blue = light) and (b) IC ₅₀ curves for inhibitor 61 (red = dark; green = light) and <i>cis</i> -[Ru(bpy) ₂ (61) ₂]Cl ₂ (63) (black = dark; blue = light) against isolated cathepsin K.....	35

Figure 18: Cytotoxicity of *cis*-[Ru(bpy)₂(**60**)₂]Cl₂ (**62**) (A and D), *cis*-[Ru(bpy)₂(**61**)₂](BF₄)₂ (**63**) (B and E) and the control compound *cis*-[Ru(bpy)₂(MeCN)₂](PF₆)₂ (C and F) on BMM cells (A-C) and prostate cancer PC3 cells (D-F) 37

Figure 19: Expression of cathepsins B and K in BMM and BMM derived osteoclast cells. Western blot analysis (A and C) and densitometric analysis of CTSB (B) and CTSK (D) performed using Fuji Multimodal Imager..... 38

Figure 20: Confocal microscopy images of mouse osteoclast cells treated with **60** at different concentrations. The intensity of green fluorescence is a direct measure of the quantity of hydrolyzed and precipitated substrate (A-D) also visible on DIC images (E-H). The quantified data are shown as column (I) and dot (J) plots. * Indicates p<0.05 and ** indicates p<0.001 40

Figure 21: Confocal microscopy images of mouse osteoclast cells treated with the ruthenium-caged inhibitor **62**(A-D) or *cis*-[Ru(bpy)₂(MeCN)₂](PF₆)₂ (E-H). Cells were preincubated with either complex (0-1000 nM) for 30 min at 37 °C in the presence of cathepsin B inhibitor CA-074Me (1 μM), then exposed to dark (no irradiation) or light (irradiation; 250W, 395-750 nm) conditions for 15 min. ** indicates p<0.001 42

Figure 22: Changes to the electronic absorption of **65** (25 μm) in a 2 % acetone aqueous solution at irradiation times, t_{irr}, of 0, 3, 5, 7, 10, and 15 min (λ_{irr} ≥ 395 nm); the * denotes the mono-aqua intermediate. Inset: t_{irr} = 0.0, 0.5, 1.5, and 3.0 min 58

Figure 23: The uncaged inhibitor **64** (30 μM) reduces degradation of DQ-collagen IV (*green*) by MAME cultures of MDA-MB-231 (A) and Hs578T (B) breast carcinoma cells. Top views at 4 days of culture were reconstructed in 3D with Volocity software from optical sections of 16 contiguous fields acquired on a Zeiss LSM780. Fluorescent intensity per cell (C) was quantified in the entire volume; nuclei were stained with Hoechst 33342 (*blue*) at the time of imaging and counted..... 62

Figure 24: The uncaged inhibitor **64** (30 μM) reduces total and pericellular degradation, but not intracellular degradation of DQ-collagen IV by 3D MAME cultures of MDA-MB-231 and Hs578T breast carcinoma cells imaged at 4 days of culture. Quantification of total proteolytic fragments (black bars) and segmentation into pericellular (open bars) and intracellular (gray bars) fragments was performed by image arithmetic in Volocity software 64

Figure 25: The caged inhibitor **65** (ruthenium-caged compound, 1 μM) when uncaged by light exposure reduces degradation of DQ-collagen IV (*green*) by MAME cultures of MDA-MB-231 and Hs578T breast carcinoma cells. Structures treated with **65** were incubated in the dark (no irradiation) or light (λ_{irr} = 395-750 nm) for 45 min. Top views at 4 days of culture were reconstructed in 3D. Fluorescent intensity per cell (C) was quantified in the entire volume; nuclei were stained with Hoechst 33342 (*blue*) at the time of imaging and counted..... 66

Figure 26: The ruthenium complex <i>cis</i> -[Ru(bpy) ₂ (MeCN) ₂](PF ₆) ₂ used to cage the inhibitor did not affect degradation of DQ-collagen IV (green) by 3D MAME cultures of MDA-MB-231 and Hs578T breast carcinoma cells. Top views at 4 days of culture were reconstructed in 3D. Structures were incubated in the dark (no irradiation) and light ($\lambda_{\text{irr}} = 395\text{-}750\text{ nm}$) for 45 min. Fluorescent intensity per cell (C) was quantified in the entire volume; nuclei were stained with Hoechst 33342 (<i>blue</i>) at the time of imaging and counted.....	68
Figure 27: Structure of CA-074 (43) and its corresponding nitrile-based analog (66).....	76
Figure 28: Changes to the electronic absorption of 73 in a 2 % acetone aqueous solution at irradiation times, t_{irr} , of 0, 1, 3, 5, 7, 10, and 15 min ($\lambda_{\text{irr}} \geq 395\text{ nm}$); the * denotes the mono-aqua intermediate. Inset: $t_{\text{irr}} = 0, 1, \text{ and } 3\text{ min}$	80
Figure 29: IC ₅₀ curves for ruthenium-caged inhibitor 73 (blue with irradiation and black without) and uncaged inhibitor 66 (red with irradiation and green without) against human cathepsin B.....	80
Figure 30: Structures of complexes releasing bidentate ligands on photolysis.....	88
Figure 31: Structures of new nitrile-based Ru(TPA) complexes 76 and 77	88
Figure 32: ORTEP diagram of dication [Ru(TPA)(MeCN) ₂] ⁺²	90
Figure 33: Changes in the electronic absorption spectra upon irradiation with $\lambda > 350\text{ nm}$ in H ₂ O (2% acetone) of 76 (A) for 0, 1, 2, 3, 5, and 10 min and 77 (B) for 0, 1, 3, 7, 10, and 15 min.....	91
Figure 34: Photochemical reaction of 76 (0, 120 and 240 min) in C ₆ D ₆ O: D ₂ O – 9: 1 showing the release of <i>cis</i> -MeCN (2.47 ppm) and formation of free MeCN (2.05 ppm).....	93
Figure 35: Photochemical reaction of 77 (0, 120 and 240 min) in C ₆ D ₆ O: D ₂ O – 9: 1 showing the release of <i>cis</i> - 60 (4.40 ppm) and formation of free 60 (4.16 ppm).....	94
Figure 36: IC ₅₀ curves for ruthenium-caged inhibitor 77 (blue with irradiation and black without) and uncaged inhibitor 60 (red with irradiation and green without) against human CTSK.....	95
Figure 37: Ligands used in Ru(II)-based caging groups.....	117
Figure 38: Structures of polypyridyl ligand library bound to resin (85a-j) and cleaved for analysis (86a-j).....	121
Figure 39: Changes in the electronic absorption spectra upon irradiation with visible light ($\lambda_{\text{irr}} > 400\text{ nm}$) in H ₂ O of complexes 88a-j for 0 (black), 5 (red), 15 (green) and 30 (blue) min.....	128

Figure 40: ORTEP diagrams of the dications $[\text{Ru}(\text{DPAbpy})(\text{MeCN})]^{2+}$ (A) and $[\text{Ru}(\text{TQA})(\text{MeCN})_2]^{2+}$ (B) derived from 89 and 91 , respectively. Thermal ellipsoids are shown at 50% probability. Hydrogen atoms are omitted for clarity.....	132
Figure 41: Electronic absorption spectra of 90 irradiated for 0, 0.5, 1, 4, 7, and 15 min (A) and 15, 40, and 85 min (B) and 91 irradiated for 0, 0.5, 1, and 2 min (C) and 2, 5, 20, and 60 min (D), in H_2O upon irradiation with $\lambda \geq 395$ nm.....	134
Figure 42: ^1H NMR spectra following irradiation of 91 in D_2O with $\lambda_{\text{irr}} \geq 395$ nm for 0, 15, 45, 90, and 180 min; the label M indicates signal from the mono-aqua intermediate and B from the bis-aqua product formed upon irradiation with selected integrations shown parentheses (A) and schematic representation of the first ligand exchange process of the complex (B)	136
Figure 43: ^1H NMR spectra following irradiation of 90 in D_2O with $\lambda_{\text{irr}} \geq 395$ nm for 0, 30, 60, and 120 min. Stars indicate new signals evolved upon irradiation.....	137
Figure 44: Examples of Ru-based photosensitizers.....	197
Figure 45: A) Lifetime determination for 91 ; B) Emission spectra for $[\text{Ru}(\text{TQA})(\text{L})_2]^{m+}$ complexes 91 (L = MeCN, black), 101 (L = CN, red) and 102 (L = SCN, blue).....	201
Figure 46: Metal-based SOMOs (corresponding orbitals with isovalue of 0.03 a.u.) and orbital contributions (%) of Ru and ligands for A) $[\text{Ru}(\text{TQA})(\text{MeCN})_2]^{2+}$ (91); B) $[\text{Ru}(\text{TQA})(\text{CN})_2]$ (101); C) $[\text{Ru}(\text{bpy})_2(\text{MeCN})_2]^{2+}$; D) $[\text{Ru}(\text{bpy})_2(\text{CN})_2]$ in the $^3\text{MLCT}$ optimized geometries	202
Figure 47: Absorption spectrum of 91 at RT (black) and at 90 K (red)	207
Figure 48: Absorption spectrum of 101 at RT (black) and at 90 K (red)	207
Figure 49: Absorption spectrum of 102 at RT (black) and at 90 K (red)	208

LIST OF SCHEMES

Scheme 1: Organic molecules as photocages - Carboxylic acid functionality protected with organic photocaging group and its corresponding photolysis products.....	8
Scheme 2: Metal complexes as photocages - Ru-based photocaging group and its corresponding photolysis products	9
Scheme 3: Proteolysis mechanism by cysteine protease.....	17
Scheme 4: Interaction of cysteine proteases with nitrile-based inhibitors.....	22
Scheme 5: Photodissociation of <i>cis</i> -[Ru(bpy) ₂ (Inh) ₂] ⁺²	25
Scheme 6: Synthesis of caged inhibitor complexes 62 and 63	30
Scheme 7: Synthesis of ruthenium-based CTSB inhibitor 65 and structure of 64	56
Scheme 8: Synthesis of nitrile-based analog of CA-074 (66).....	77
Scheme 9: Synthesis of Ru(bpy) ₂ -based caged complex (73).....	78
Scheme 10: Synthesis of nitrile-based Ru(TPA) complexes 76 and 77	89
Scheme 11: Synthesis of pyridine precursor 80	119
Scheme 12: Solid phase synthesis of the polypyridyl ligand library (85a-j).....	120
Scheme 13: Three methods (A-C) explored for synthesis of Ru(II) complexes [Ru(86a)(DMSO)Cl]Cl (87a) and [Ru(86a)(MeCN) ₂]X ₂ (88a , X = OTf, O ₂ CCF ₃).....	124
Scheme 14: Synthesis of Ru(II)-MeCN complex library (88a-j).....	125
Scheme 15: Synthesis of Ru(II) MeCN complexes 89-91 by solution phase methods.....	131
Scheme 16a: Synthesis of polypyridyl ligand library (85a-85e).....	143
Scheme 16b: Synthesis of polypyridyl ligand library (85f-85j).....	144
Scheme 17: Synthesis of secondary amine (94) for the synthesis of TQA ligand.....	154
Scheme 18: Synthesis of Ru(TQA) complexes 101 and 102	198

CHAPTER 1. INTRODUCTION

1.1 General introduction

Spatial distribution and temporal release of specific biologically active molecules by light activated compounds help researchers to study how various chemical events mediate different biological processes. This thesis is directed towards developing new tools for achieving spatial and temporal control for enzyme inhibitors using light and caged complexes. An effort has also been made to introduce various aspects involved in developing caged compounds for biological applications. This chapter also outlines the applications of light, metals and photocages in biology. Current work involves developing light-activated metal-based complexes for caging enzyme inhibitors. A brief introduction of cathepsins is provided, because we wanted to develop caged cathepsin inhibitors. We have shown that ruthenium-based caged cathepsin inhibitors can be used for achieving spatial and temporal control over enzyme inhibition.

1.2 Light in therapeutics

The electromagnetic spectrum consists of oscillating electric and magnetic waves whose wavelengths range from a few picometers to thousands of kilometers. Based on the frequency of vibrations, the electromagnetic spectrum is subdivided into different waves. These waves are made of the same kind of vibrations but differ in their frequencies. While different waves have different applications, light has been widely used in therapeutics against many disease states.¹ Light has numerous effects on animal and plant life; it acts as a vital stimulant and has numerous effects on the skin, nervous system, blood circulation and cutaneous glands. Light also increases the hemoglobin content of the blood. Apart from stimulating eyes, which sends signals to our brain and enables to see things around us, light

has also found its application in therapeutics. In the late 18th century, patients were advised by physicians to sunbathe for health benefits. Later light therapy, exposure to artificial light, gained therapeutic importance. The first electric light bath was developed in 1891 for treating patients at the Battle Creek sanitarium. Since then the electric light bath was introduced in many hospitals for treating various diseases such as acne vulgaris, ulcerating lupus, dermatitis and neck abscesses. Light therapy affects neurotransmitters and helps in treatment of physiological conditions like depression and sleep disorders.² Numerous book chapters have been dedicated towards explaining the importance of light in medicine and provide a better understanding of the topic.³⁻⁵

Absorption of light by various molecules can dramatically influence their reactivity. This unique feature can be used in numerous applications, as molecules in their excited states have different electronic properties compared to their ground states. Photo-excitation can also cause changes in geometries, bond angles and bond lengths in the molecule. Thus light can also be used in the activation of many molecules such as photosensitizers for photodynamic therapy, metal complexes for anticancer applications and caged complexes for drug delivery systems. These applications of light are directly related to this dissertation topic and will be briefly discussed in subsequent sections of this chapter.

1.3 Metals in medicine

Metal ions play a very crucial role in numerous biological processes, which include gene regulation, neurotransmission, respiration, synthesis of antibiotics and DNA repair.^{6,7} Bioinorganic chemistry, which deals with the study of metals in biology, is a rapidly growing area of research with a high potential for developing metal complexes as therapeutic agents with novel mechanisms of action. While organic molecules dominate the pharmaceutical

industry and drug market, novel drugs containing metal ions are finding their way into medicine. The first metal-based drug, Salvarsan (Arsphenamine), introduced in 1910 was an organoarsenic agent developed for treatment of syphilis.⁸ The initial structure proposed for Salvarsan was a bimetallic compound **1** containing an As=As double bond. More recently the structure of Salvarsan was proposed with As-As single bonds and containing a mixture of cyclic-As₃ (**2**) and cyclic-As₅ (**3**) species (Figure 1).⁹

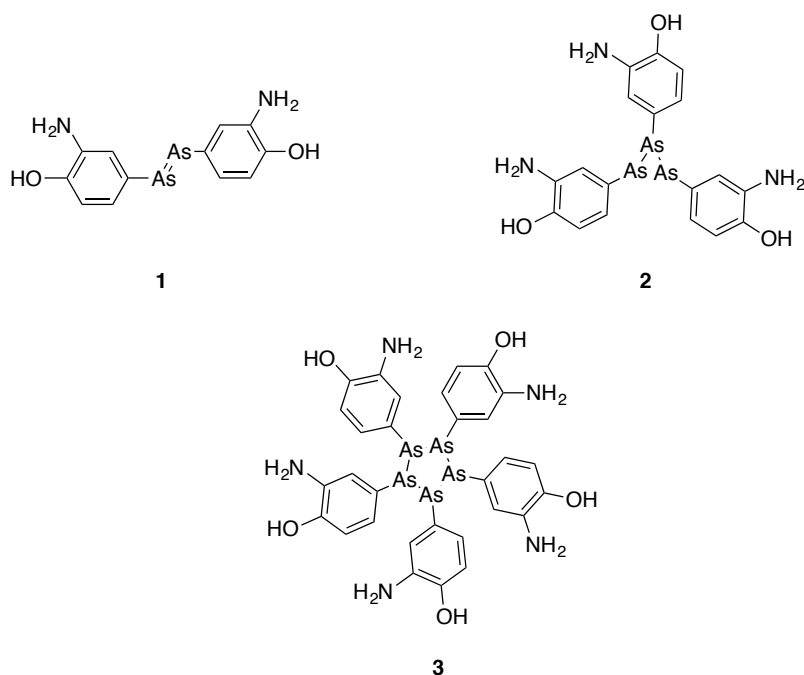


Figure 1: Structures proposed for Salvarsan

Medicinal inorganic chemistry received its largest breakthrough with the success of cisplatin, which is renowned as the best selling anticancer drug.¹⁰ Fifty percent of cancer chemotherapy uses cisplatin for inducing cell apoptosis by interacting with DNA.¹¹ Apart from platinum complexes, numerous polynuclear platinum (II) complexes were also developed for anti-cancer applications.¹² Despite being widely used for cancer treatments, cisplatin has many neurotoxic and nephrotoxic effects. These drawbacks have driven researchers to develop new platinum and other metal ion containing drugs for oncology.

^{10,11,13-20} Apart from oncology, bioinorganic chemistry has produced innovative drugs for numerous therapeutic applications such as silver-containing antimicrobial agents, iron chelators as antimalarial agents,²¹ vanadium complexes as insulin mimetics and gadolinium complexes for diagnostic purposes.¹⁰ More recently, Au(I) and Au(III), two different classes of gold-containing compounds have been developed for anticancer applications.²² Thermodynamically both Au(I) and Au(III) oxidation states are unstable when compared to Au(0) and can act as oxidizing agents causing cytotoxic effects.

Compared to organic small molecules, metal complexes have distinct electronic, chemical and photophysical properties, which could be utilized in many biological applications. Biology utilizes numerous inorganic elements for various functions such as Na⁺, K⁺ and Ca²⁺ for charge balance,²³ Ca²⁺ and Zn²⁺ for propagation of biochemical signals, Fe and Cu complexes for electron transport²⁴ and various metals for redox catalysis.²⁵ In addition to naturally bioavailable inorganic elements, researchers have applied transition metals and lanthanide elements to biology. Ru- and Pt-based complexes are used for interactions with biomolecules such as DNA.^{26,27} Iron, copper and zinc chelators are developed to alter bioavailability of metal ions in cell biology for studying the effects of metal ions in cell processes.²⁸ Mn- and Ru-based complexes were developed for releasing small molecules such as NO (**4** and **5**, Figure 2) and CO (**6**, **7** and **8**, Figure 2) by breaking M-NO or M-CO bonds *in vivo*.^{29,30} Gd and Mn complexes are being developed as MRI agents.²⁵ Research in the area of metals in medicine is abundant; therefore in subsequent sections focus will be laid on ruthenium complexes in medicine as it is directly related to the projects described in this dissertation.

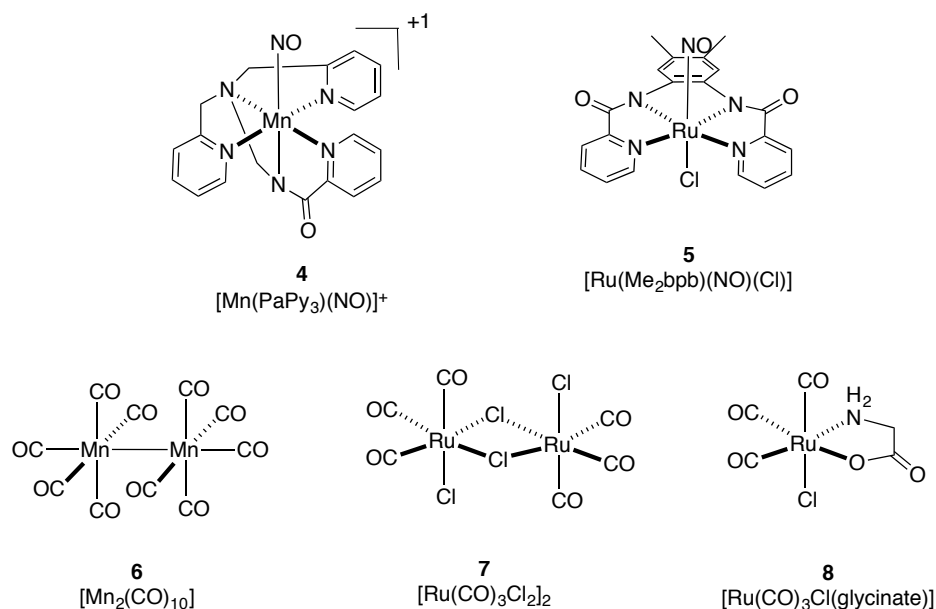


Figure 2: Mn- and Ru-based complexes as NO and CO releasing metal complexes.

Ruthenium complexes are developed for many medicinal applications where they act as anticancer, antibiotic, immunosuppressant and antimicrobial agents.^{31,32} Excess NO can result in physiological conditions such as stroke, epilepsy and septic shock. Nitric oxide forms stable ruthenium (II) mononitrosyls when they are treated with different Ru(III) complexes. Thus ruthenium compounds can act as nitric oxide scavengers.³³ Properties like rates of ligand exchange and range of accessible oxidation states make ruthenium-based complexes suitable for medicinal applications. While cisplatin has revolutionized the bioinorganic field, drug resistance and toxicity arising from platinum drugs has fueled the screening process for discovering other metal ion based anticancer drugs. Similar to platinum drugs, ruthenium compounds also cause DNA interaction and damage.³⁴ FDA approved platinum-containing anticancer drugs are cisplatin (**9**), carboplatin (**10**) and oxaliplatin (**11**) (Figure 3). NAMI-A (**12**) was the first ruthenium-based anti-cancer drug to enter clinical trials. NAMI-A contains inert Ru(III), which upon entering into tumor cells is reduced to Ru(II), which is the active anti-cancer agent. KP1019 (**13**) was the second ruthenium-based

anti-cancer drug to enter clinical trials. KP1019 induces apoptosis by bending and untwisting DNA.³⁵ Ruthenium complexes are also used for photocaging applications of bioagents.³⁶⁻⁴⁰ Applications of ruthenium complexes in biology are well summarized by Tomasz Respondek, a fellow graduate student from our group, in his thesis.⁴¹

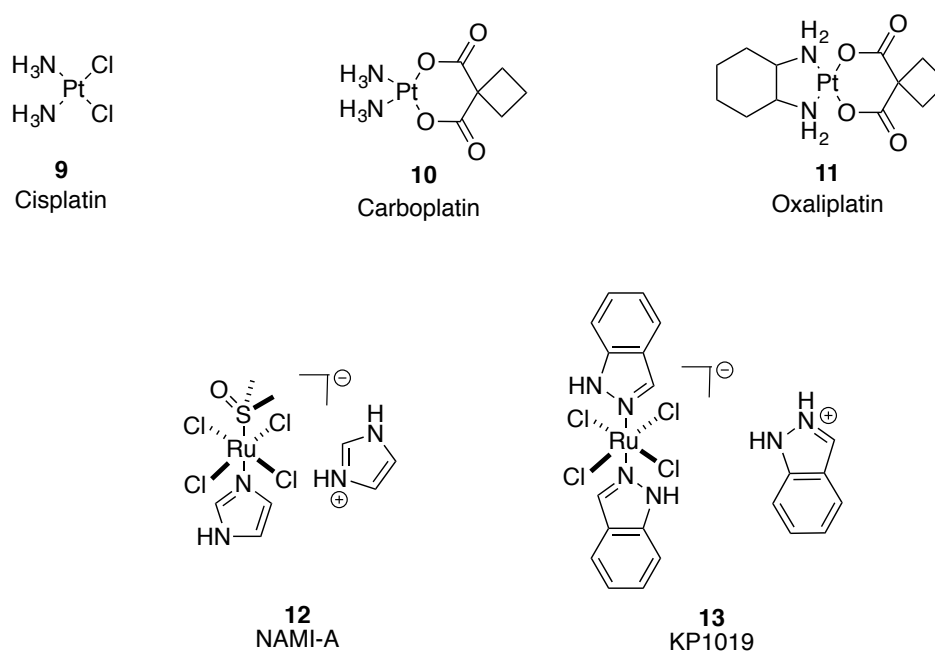


Figure 3: Platinum- and ruthenium-based anticancer agents.

1.4 Photocages for biological applications

Photolabile caging groups (photocages) are molecules that can be cleaved using light. Light can be controlled both spatially and temporally with great precision; thus it can be used in activation of biomolecules leading to targeted release. Based on the target biomolecules, either the caging group or the caged molecule interacts with the biomolecules (Figure 4).

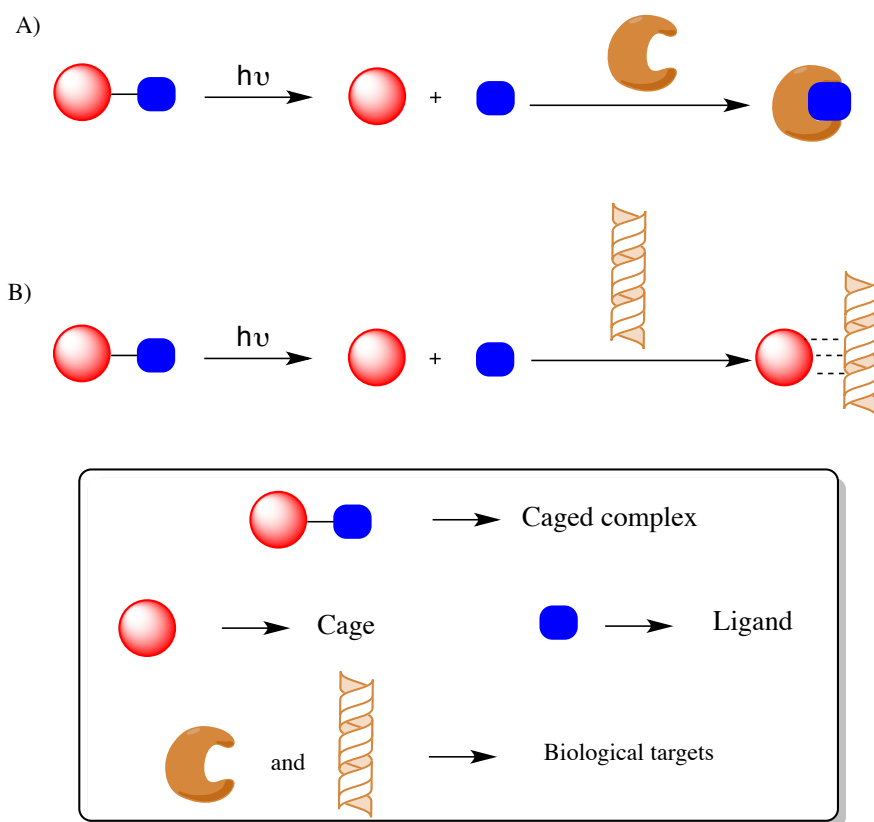
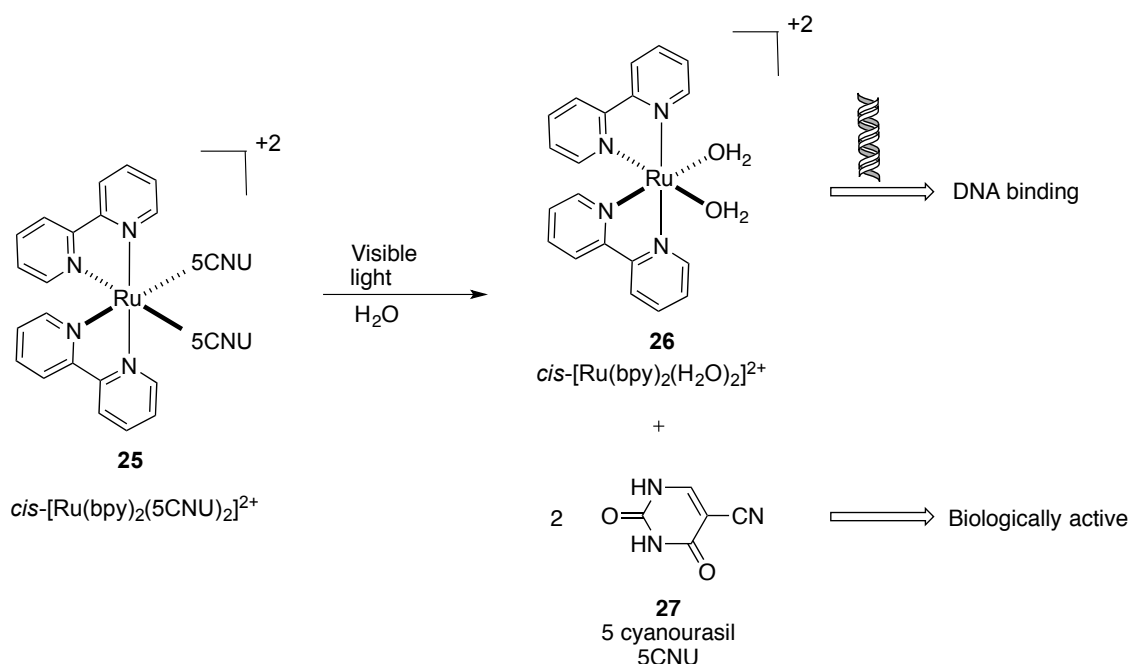


Figure 4: Photocaging approach for two different biological applications; A) ligand acts as biological agent and B) caging group acts as therapeutic agent.

Many different photocages are being developed for bioagents, including enzymes, neurotransmitters, fluorophores, insecticides and enzyme inhibitors for different biological applications. Initially, organic groups were developed for photocaging applications. Different functionalities such as amines, carboxylic acids, alcohols, amides, and phosphates can be caged using organic photocages, which was summarized in a recently published review article.⁴² Factors such as high quantum yields for the release of bioagents, strong absorption of light of $\lambda > 300$ nm (to prevent damage of biological entities by light), solubility of the photocages in the targeted media, distribution and nontoxic byproducts govern the usefulness of the organic photocaging groups. Numerous caged bioagents (**14** - **19**) are commercially available and used. For example, the widely used *o*-nitrobenzyl organic protecting group can

More recently metal complexes are being developed for photocaging applications. With single-photon excitation, most of the organic photocages are uncaged using UV light, but metal complexes show photo-cleavage in visible region. Also, metal complexes can be used for caging functional groups such as nitriles,^{47,48} thioethers⁴⁹ and pyridines,⁵⁰ which cannot be caged using standard organic photocaging groups (**20** and **21** in Figure 5). Thus, metal complexes provide an orthogonal approach for researchers in caging bioactive molecules.



Scheme 2: Metal complexes as photocages - Ru-based photocaging group and its corresponding photolysis products.

An advantage of using metal-based photocages is the reduction of risk of damage to biomolecules due to the usage of less energetic visible light. In biology, metal-based photocages are utilized for two different applications. First, they can be developed for targeting biomolecules, where the metal complex itself acts as a bioagent after photo-excitation (Figure 4B). Here photocaged complexes act as prodrugs, and light of a suitable

wavelength serves the purpose of converting the prodrugs into their active forms.^{10,31,51-55} Numerous platinum- and ruthenium-based complexes can act as anticancer agents after photodissociation (Figure 6).³¹ Secondly, ruthenium complexes act as protecting groups for biomolecules (Figure 4A). One area where metal complexes acting as protecting groups has proven particularly useful is neuroscience. Researchers have utilized ruthenium complexes for caging neurotransmitters such as tryptamine, tyramine, serotonin, GABA and butylamine using the Ru(bpy)₂ caging group **34** (Figure 7).³⁶ They showed that introducing a phosphine-based ligand alters the MLCT and quantum yield of the reaction. Complex **35** shows a higher quantum yield and faster ligand exchange when compared to [Ru(bpy)₂(GluH₂)₂]²⁺. The photorelease of glutamate from **35** occurs at 532 nm (single-photon excitation) or at 800 nm (two-photon excitation).⁵⁶ This dissertation will focus on developing ruthenium complexes for caging enzyme inhibitors for achieving spatial and temporal control over enzyme inhibition.

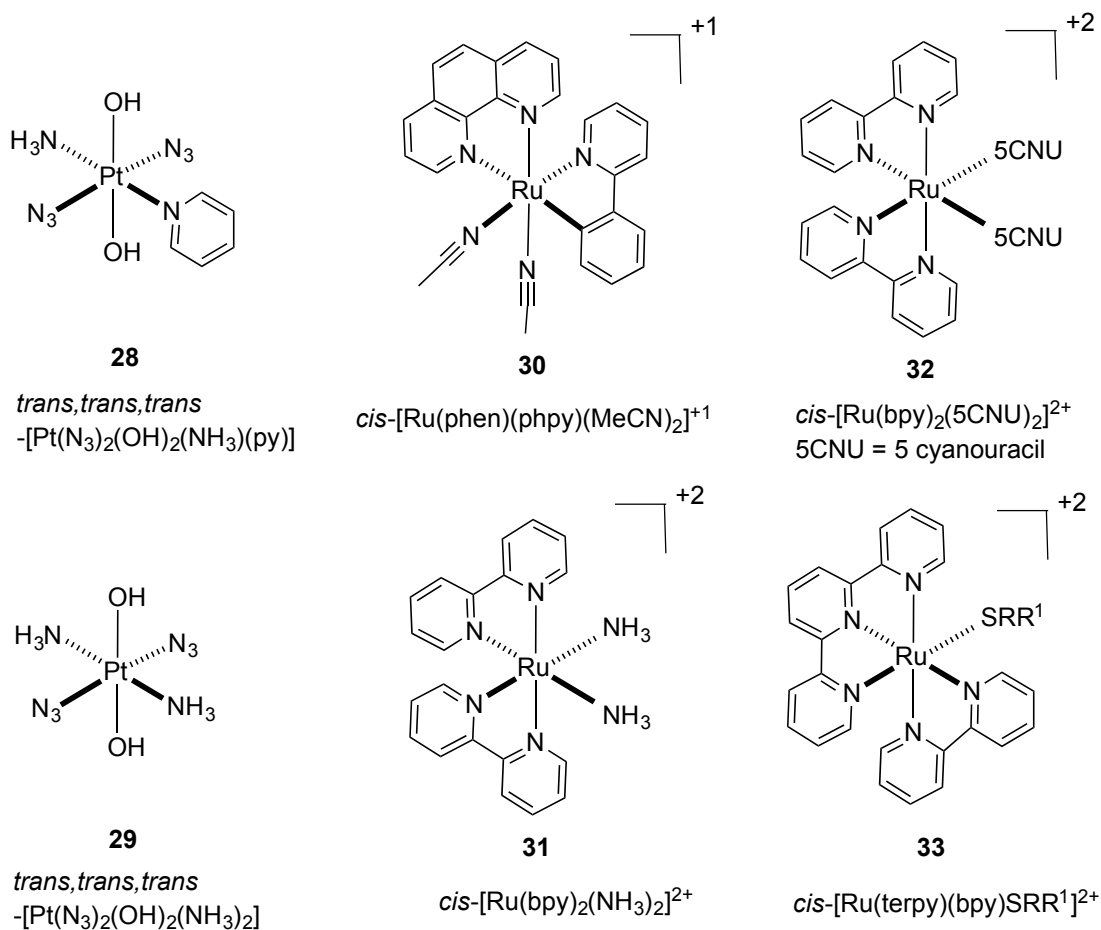


Figure 6: Examples of platinum- and ruthenium-based photocages used as therapeutic agents that are anticancer agents similar to cisplatin.

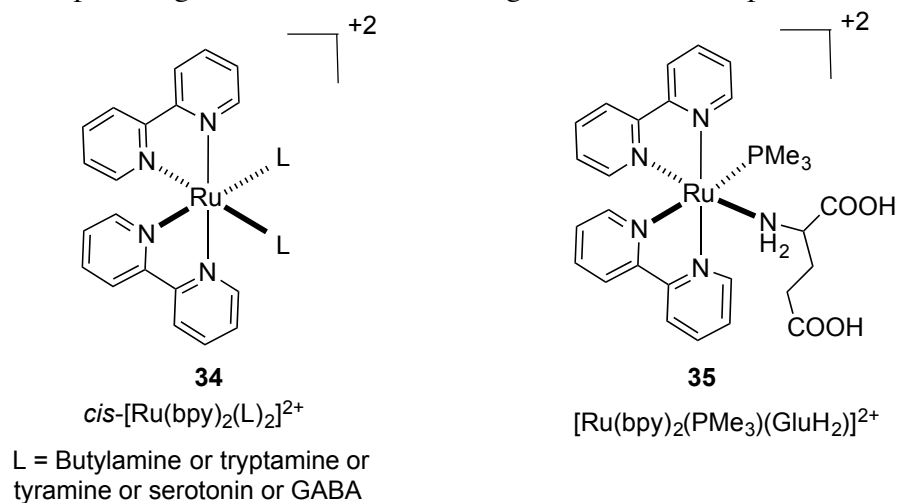


Figure 7: Ruthenium-based photocages used for caging bioagents.

1.5 Photodynamic therapy (PDT)

For decades light has been used for therapeutic applications against many disease states such as depression, vitiligo, rickets and psoriasis. Light therapy involves patient exposure to sunlight or light of a particular wavelength. More recently light has been used for photodynamic therapy (PDT).⁵⁷⁻⁶⁵ The first example of PDT was reported in the early 1900s in which scientists observed that light in combination with other chemical agents could induce apoptosis.⁶⁶ In photodynamic therapy, three nontoxic components; light, a photosensitizer and oxygen; are used for inducing cell death.⁶⁷

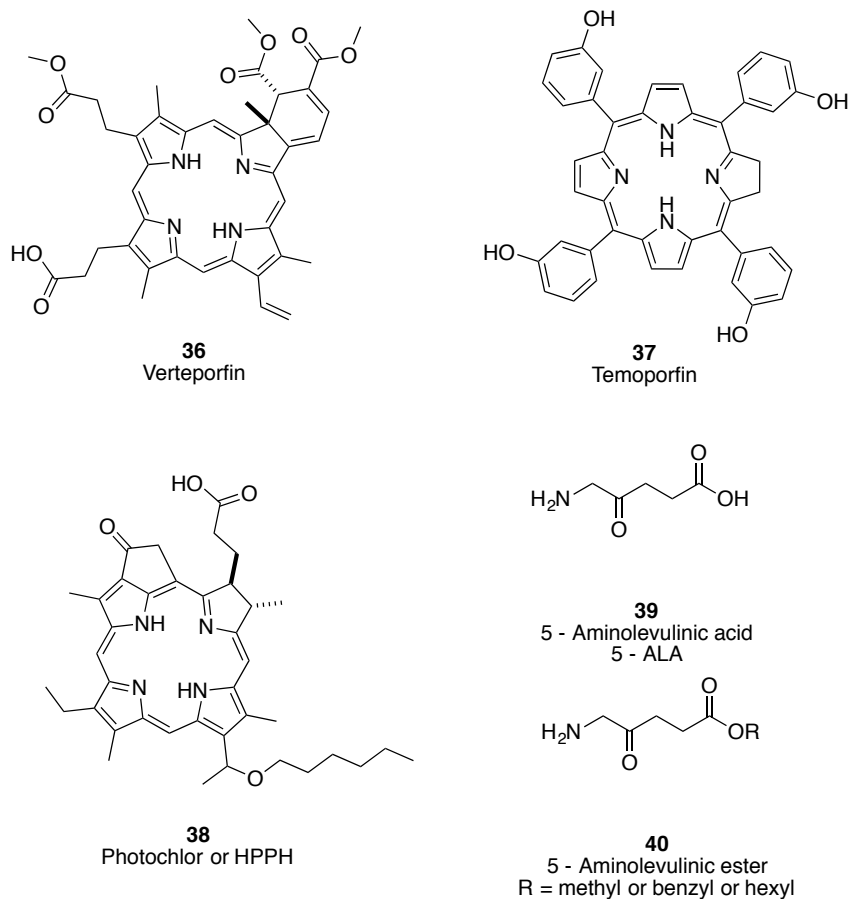
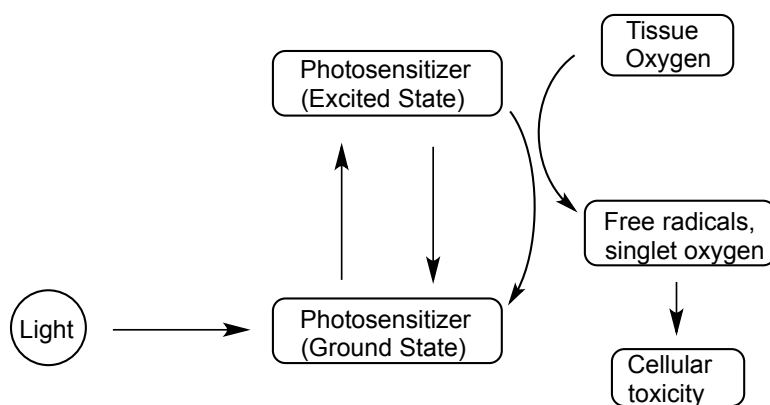


Figure 8: Photosensitizers used in PDT

Photosensitizers are organic molecules that are photosensitive and can be excited using light. Many photosensitizers have been developed for different malignant diseases.^{57,68}

Most of the sensitizers are porphyrin-based compounds such as **36**, **37** and **38** (Figure 8). Porphyrin precursors such as 5-ALA **39** and 5-ALA esters **40** are also used for PDT applications where they are transformed into porphyrins inside human cells. Once the photosensitizers reach the target cells or tissues, they can be activated using light of a suitable wavelength. Due to this unique feature, different photosensitizers and wavelengths of light are used for different malignant diseases. Once the photosensitizers are irradiated with light, the ground state sensitizer is transformed into its corresponding singlet excited state. Through intersystem crossing (ISC) the singlet excited state is transformed into a low-lying triplet excited state. The activated triplet photosensitizer then follows one of the two major reaction pathways for inducing cell death using tissue oxygen. The two pathways are (i) direct reaction with substrate to generate radicals, which can then react with tissue oxygen to generate oxygenated products, or (ii) direct energy transfer to tissue oxygen to generate reactive oxygen species (ROS) (Figure 9). These ROS can then oxidize the surrounding substrates, leading to cell toxicity and cell death.⁵⁷



(a)

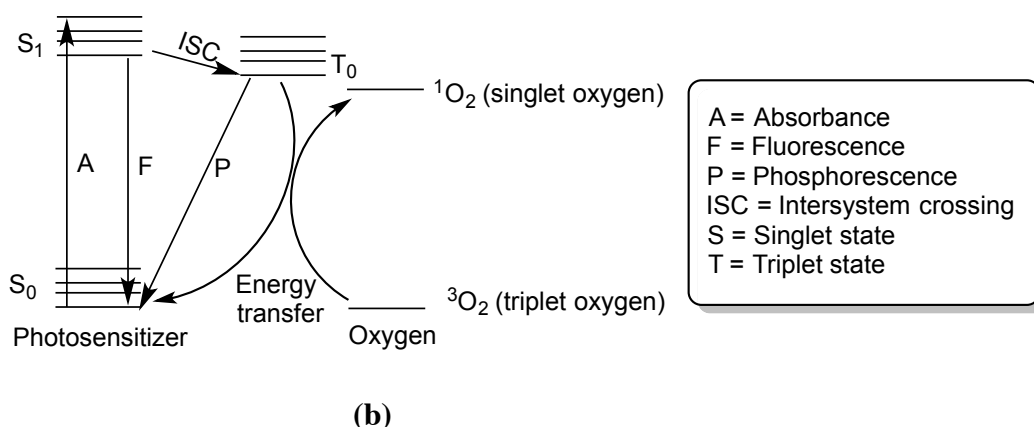


Figure 9: (a) Pictorial representation of PDT and (b) Jablonski diagram of PDT showing energy transfer to tissue oxygen for the generation of ROS.

Reactive oxygen species induce phototoxicity by oxidizing biomolecules such as proteins, lipids and DNA.⁶⁹ ROS can also inhibit enzyme activity by oxidizing enzyme cofactors. Singlet oxygen formed during PDT can oxidize fatty acids and amino acids, which are the building blocks for lipids and proteins. They can also react with double bonds or with C-H bonds of DNA.⁷⁰ Oxidation of DNA can induce cell toxicity through modifications such as strand breakage, removal of nucleotides, nucleotide mismatching and DNA-protein crosslinking.⁷¹ Numerous PDT sensitizers are being developed and are currently under clinical trials. Presently PDT is being tested and used in treatment of many cancers such as advanced esophageal tumors, lung cancer, bladder cancer, brain tumors, head and neck cancers and intrathoracic tumors.⁵⁸

While PDT has found many therapeutic applications, it cannot be used for treating hypoxic tumors. In PDT, tissue damage and cell death are highly dependent on sensitizer distribution, as the formed ROS have very short lifetimes and limited migration from the site of formation.^{58,72,73}

1.6 Photoactivated ligand dissociation

Light is also used in photoactivated ligand dissociation of metal complexes. This novel strategy is being used in developing many therapeutic agents. Utilizing this strategy, numerous platinum and ruthenium complexes are being developed for anticancer applications. This strategy does not require tissue oxygen and can be used against hypoxic tumors. Research has shown that various photolabile Ru complexes can cause DNA damage after photodissociation. For example *cis*-[Ru(bpy)₂(NH₃)₂]⁺² (**31**) undergoes photodissociation when irradiated with visible light and can then interact with DNA, causing cytotoxicity.¹⁵ The mechanism of photodissociation of Ru(bpy)₃⁺² was reported in the 1980s, when they suggested that Ru(bpy)₃⁺² undergoes ligand dissociation by forming a pentacoordinated intermediate, which forms from thermal activation of d-d excited states.⁷⁴ The metal complex reaches the d-d excited state through the triplet charge transfer state, which is formed from initial excitation. The same mechanism is extended to the metal complexes of Ru(bpy)₂(X)₂⁺² type (Figure 10). Upon absorbing light of a suitable wavelength, metal complexes from their ground state reach their corresponding singlet metal to ligand charge transfer state (¹MLCT). These ¹MLCTs reach their ³MLCTs through intersystem crossing (ISC), which upon internal conversion (IC) give triplet metal center states (³MC). Triplet MCs can then facilitate ligand dissociation, leading to photolability. More recently, photocleavage of Ru(bpy)₂(X)₂⁺² type complexes are also shown to proceed via a pentacoordinated Ru species that quickly traps solvent molecules.⁷⁵ Photodissociation opens up coordination sites on the metal center, which can then bind to DNA. Chemists have utilized photoactivated ligand dissociation for developing novel platinum- and ruthenium-based anticancer agents.^{15,51}

This strategy can also be used for spatially controlled delivery of bioagents. Researchers utilize the photoactivated ligand dissociation mechanism for delivery of neurotransmitters³⁸ and NO⁷⁶. More recently it was shown that $[\text{Ru}(\text{bpy})_2(5\text{CNU})]^{2+}$ **25** can be used as a dual therapeutic agent (Scheme 2), where photodissociation leads to the release of the biologically active agent (5-cyanourasil) and generation of a DNA-binding agent.⁴⁷ They have also shown that $[\text{Ru}(\text{bpy})(\text{dppn})(\text{CH}_3\text{CN})_2]^{2+}$ can be used as a dual therapeutic agent which can generate ROS and also produce $[\text{Ru}(\text{bpy})(\text{dppn})(\text{H}_2\text{O})_2]^{2+}$ through ligand dissociation, which can interact with DNA.⁷⁷ One area of research in Kodanko group is utilizing this photoactivated ligand dissociation mechanism in developing new tools for achieving spatial control over enzyme inhibitors.

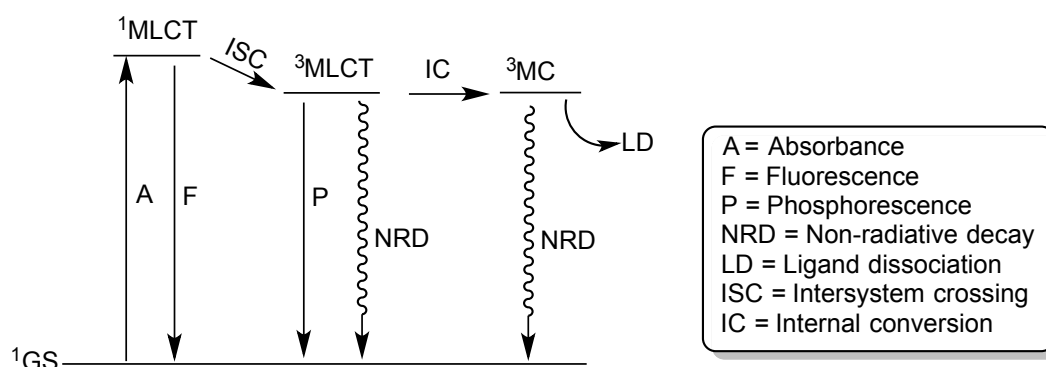


Figure 10: Jablonski diagram of photoactivated ligand dissociation.

1.7 Cysteine cathepsins proteases

Biological systems are extraordinarily complex and possess high levels of spatial and temporal control. This includes enzymes, which carry out many different functions. One such class of enzymes is proteases, which are distributed all over the body. Proteases are a class of enzymes that facilitate hydrolysis of polypeptides by cleaving the peptide bonds between amino acid residues.⁷⁸⁻⁸⁰ Proteases are further classified into endopeptidases and exopeptidases depending on the site of hydrolysis of a protein chain. Endopeptidases cleave

while cathepsins B, C, H and X are exopeptidases. These enzymes are intracellular and are mainly located inside the lysosomal vesicles.

While cathepsins are distributed all over the body, a few cathepsins, like cathepsin K (CTSK), cathepsin W (CTSW) and cathepsin S (CTSS), are more tissue specific.⁸⁵ In osteoclasts, epithelial cells and the synovial fibroblasts of rheumatoid arthritis joints, high levels of CTSK were reported. CTSL is ubiquitously expressed, but CTSV, which is homologous to CTSL, is expressed only in the thymus and testis.⁸⁶ Apart from cellular protein degradation and turnover, cathepsins are found to play a role in bone resorption and remodelling,⁸⁷ brain and skin development,^{88,86} keratinocyte differentiation and other biological processes. CTSS helps in protein loading, as it controls MHC class II antigen presentation pathway.⁸⁹ CTSL localized to the nucleus is associated with the regulation of cell-cycle progression and also shows interactions with histones, opening a new role for these enzymes.⁹⁰ CTSL also helps in regular hair-follicle morphogenesis and its deficiency leads to periodic hair loss.⁹¹ In normal conditions, well-coordinated signaling pathways regulate the production and activity of cathepsins but during abnormal malignancies, well-coordinated signaling systems get altered. These irregularities can lead to overproduction of cathepsins. Increased levels of cathepsin activity are related to various disease states such as obesity, cancer, inflammation and neurological disorders.⁸⁵

For further reading, researchers are referred to many review articles, which are dedicated to understanding the role of cathepsins in relation to various pathological conditions.^{83-85,92-96} Instead, only their role (cathepsins in general, and CTSK and CTSB, in particular) in cancer growth and metastasis will be briefly discussed as they are directly related to the topic of this dissertation.

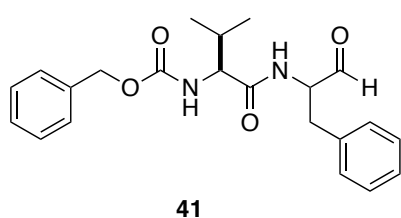
Cysteine cathepsins were previously thought to function primarily intracellularly inside lysosomal vesicles until recently, when evidence was found to show them functioning both extracellularly and intracellularly in cancer.^{97,98} Researchers have shown through experimental models and results that increased cathepsin activity has an important role in tumor growth and progression.⁹⁹⁻¹⁰² Extracellular cathepsins help in tumor progression through collagen degradation,^{85,103} and intracellular cathepsins assist in tumor invasion through proteolysis.¹⁰⁴

Cathepsin B promotes cell migration during wound healing by helping in remodeling the extracellular matrix.¹⁰⁵⁻¹⁰⁸ Overexpression and dysregulation of CTSB is correlated to cancer growth and progression.¹⁰⁶ Aberrant CTSB activity is associated with many kinds of cancers including brain, prostate, breast, colorectal, and lung cancer.^{105,109,110} Studies show that tumor cells secrete CTSB into the extracellular matrix, which then leads to matrix degradation, facilitating tumor progression.^{94,111-113} Numerous research articles have been published summarizing aberrant CTSB activity in tumor invasion and progression, and thus will not be discussed further.^{85,92,100,102,105-107,109-111,114-117}

CTSK, which is predominantly expressed in osteoclasts, plays an important role in bone resorption and remodeling.¹¹⁸⁻¹²⁰ CTSK is responsible for collagen I degradation. Studies relate osteoporosis and tumor-induced bone resorption to aberrant CTSK activity.^{118,120-122} Taken together, these data suggest that aberrant expression and/or activity of CTSB and CTSK is critical for tumors and other related conditions, and they could be viable therapeutic targets.^{93,123-127}

Different classes of small molecule inhibitors targeting cathepsins have been developed by both academia and industry.^{92,93,128,129} All these inhibitors react with the thiol of

the cysteine residue lying in the enzyme active site. Depending upon the warhead present, cathepsin inhibitors react with the thiol either in a reversible fashion or irreversibly.⁹³ Cathepsin inhibitors usually contain a peptide segment, which helps in enzyme recognition, and an electrophilic warhead, which reacts with the cysteine residue. The electrophilic warhead can include, but is not limited to, nitriles, aldehydes, semicarbazones, ketones and epoxysuccinyl derivatives (Figure 11).⁹³ Though overexpressed in the tumor microenvironment, cathepsins are required for normal cell growth and function, and a major drawback with most of the cathepsin inhibitors *in vivo* is their offsite reactivity as small molecules lack spatial control.



MDL 28170 - Cat B and calpain

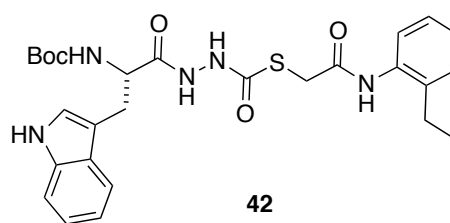
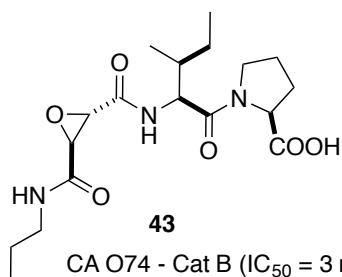
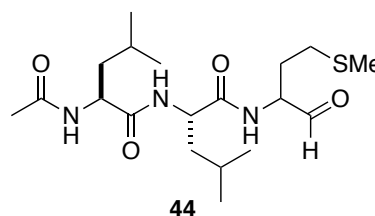
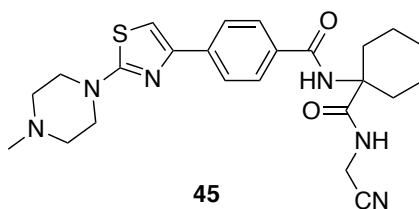
SID 26681509 - Cat L (IC₅₀ = 56 nM)CA O74 - Cat B (IC₅₀ = 3 nM)Cat L (IC₅₀ = 0.6 nM)L 006235 - Cat K (IC₅₀ = 0.25 nM)

Figure 11: Examples of cathepsin inhibitors with different warheads

Numerous review articles have been published describing the use of nitrile-based inhibitors for cysteine proteases.^{127,130-136} Acetamidoacetonitrile (**46**) and benzamidoacetonitriles (**47**) were the first nitrile-based inhibitors developed for cysteine proteases (Figure 12).¹³⁷

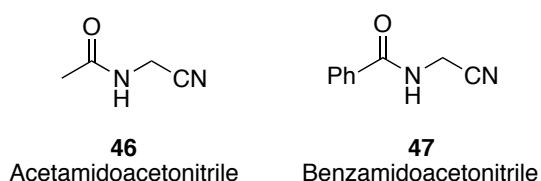
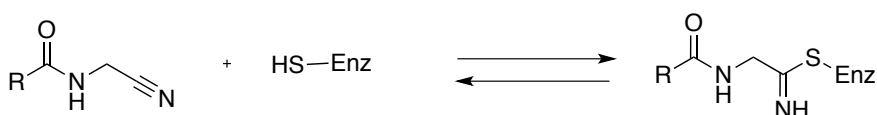


Figure 12: First discovered nitrile-based cathepsin inhibitors.



Scheme 4: Interaction of cysteine proteases with nitrile-based inhibitors.

Based on their electrophilic properties, nitrile inhibitors are further divided into (i) aminoacetonitriles, (ii) aromatic nitriles and (iii) cyanamides. Cyanamides were reported to have the highest electrophilicity, whereas benzonitriles were least electrophilic.^{132,138} Cathepsin inhibitors with nitrile functionality reversibly react with the thiol of the cysteine residue to give thioimidate intermediates (Scheme 4).^{131,133} Numerous research articles have been published dealing with the development of dipeptide nitriles as potent and selective inhibitors of cathepsins.^{127,130-132,139} Dipeptide inhibitors can either inhibit many different cathepsins or they can specifically inhibit one type of cathepsin. For example, compound **51** is a specific cathepsin C inhibitor when compared to cathepsins B, H and L ($IC_{50} > 10 \mu M$).¹³² Compound **52** specifically inhibits CTSK activity ($IC_{50} = 3 \text{ nM}$) when compared to cathepsins B, L and S ($IC_{50} > 2 \mu M$).¹⁴⁰ Although numerous nitrile-based cathepsin inhibitors

are being developed, no molecule has reached the market.¹³⁵ Clinical trials of Odanacatib (**54**), a nitrile-based CTSK inhibitor developed by Merck, have shown promising results for the treatment of osteoporosis, but side effect profiles from phase III clinical trials have forced Merck to delay FDA filing.^{141,142} Odanacatib is a reversible covalent modifier and reacts with thiolates through a Pinner-type mechanism.¹³⁵ Another nitrile-based inhibitor to reach clinical trials is Balicatib (**53**), which was developed by Novartis. Balicatib is a highly selective CTSK inhibitor with an IC_{50} of 1.4 nM. Although promising results were seen initially, phase II trials were discontinued due to numerous nonselective off-target effects.¹⁴³ Compounds **55** and **56** are examples of cyanamide-based cysteine protease inhibitors.

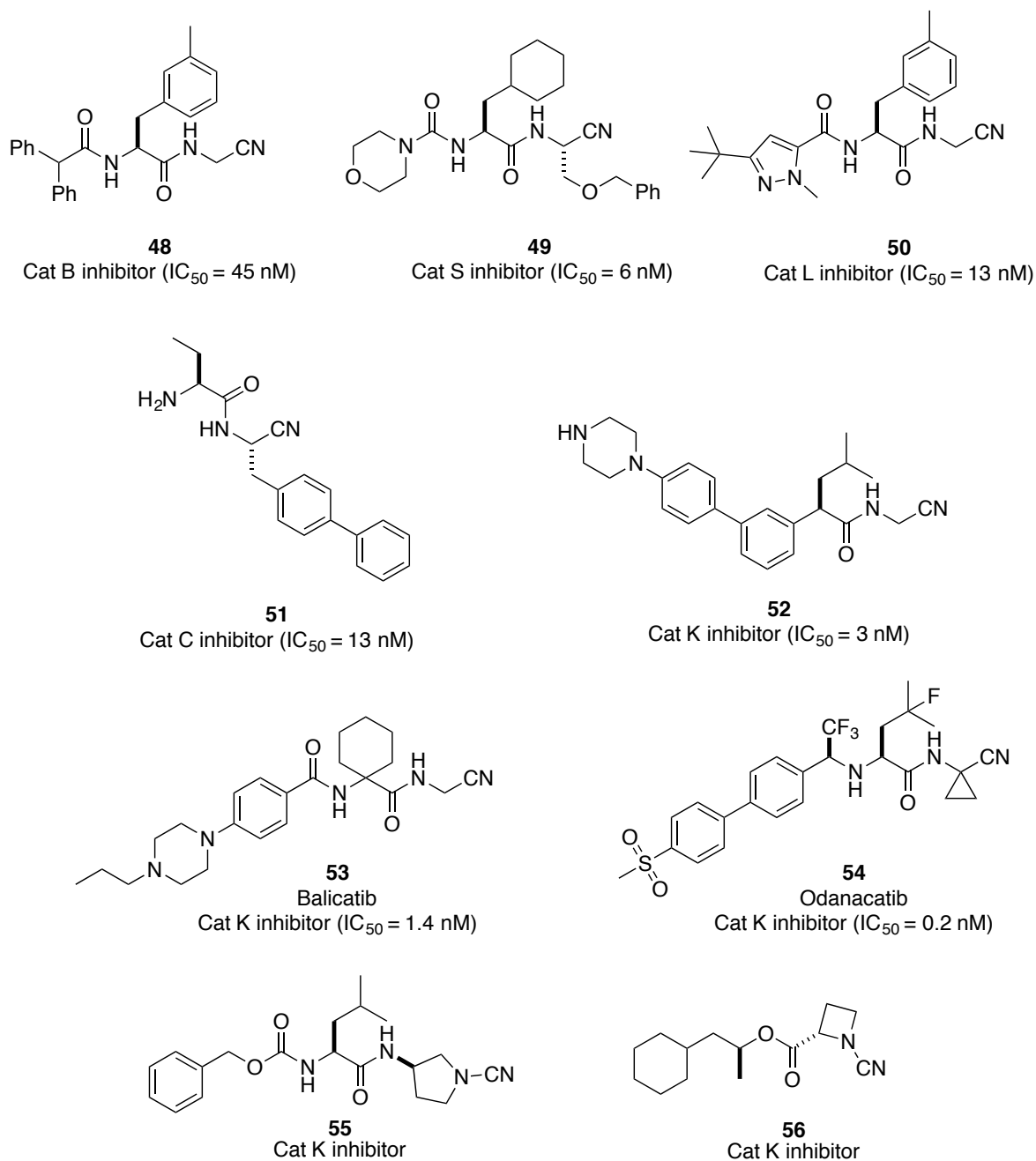


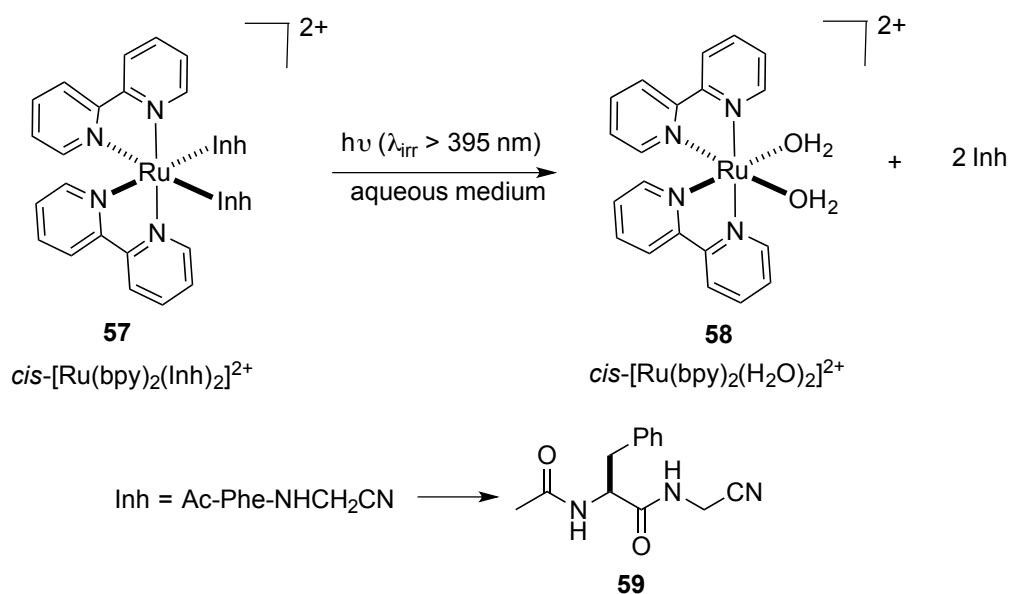
Figure 13: Nitrile-based inhibitors of cathepsins with their corresponding IC_{50} values.

While numerous inhibitors have been developed and tested, there is no FDA approved cathepsin B or cathepsin K inhibitor due to their nonselective off-target inhibition in normal cells.^{144,145} Despite being overexpressed in the tumor microenvironment and other disease states, cathepsins are required for normal cell function and small molecules inhibiting

cathepsins lack spatial control. Small molecules lack the ability to selectively inhibit cathepsin activity in tumor microenvironment. If normal small molecules are used they inhibit cathepsins in normal cells as well, leading to toxicity. Thus new tools for achieving spatial control over enzyme inhibitors should be explored.

1.8 Proof of concept (background work)

While researchers have used $\text{Ru}(\text{bpy})_2$ for caging neurotransmitters, the Kodanko group, in collaboration with the Turro group, has caged nitrile-based cathepsin inhibitors using the same caging group.¹⁴⁶ The compound *cis*- $[\text{Ru}(\text{bpy})_2(\text{Inh})_2]^{2+}$ (**57**) was synthesized where Inh (**59**) was a CTSK inhibitor (Ac-Phe-NHCH₂CN) which binds to ruthenium through the nitrile functional group.



Scheme 5: Photodissociation of *cis*- $[\text{Ru}(\text{bpy})_2(\text{Inh})_2]^{2+}$

Complex **57** shows excellent stability in the dark, and fast dissociation of the caged inhibitor in the light (Scheme 5). Photodissociation proceeds through formation of a mono aqua complex with $\Phi_{\text{R} \rightarrow \text{I}} = 0.080(4)$, which upon further irradiation gives complex **58** with $\Phi_{\text{R} \rightarrow \text{P}} = 0.00091(7)$. Complex **57** was 33 times more potent in the light ($\text{IC}_{50} = 5.4 \mu\text{M}$)

than in the dark ($IC_{50} = 170 \mu\text{M}$) against papain, where the IC_{50} value for free inhibitor (Inh) was $12 \mu\text{M}$. This method of caging cathepsin inhibitors with a ruthenium complex provides a novel approach to achieve control over enzyme activity.

Though photocaging of bioactive agents is being explored for different biological applications, current Ru-based cages utilize planar heteroaromatic ligands such as bpy, phen and terpy. Cages derived from other multidentate nonplanar ligands are under-investigated. The complex $[\text{Ru}(\text{bpy})_3]^{+2}$ is known to lose a bpy ligand upon photoactivation, so multidentate ligands should be developed for caging biomolecules to avoid photodecomposition in the biological system. The ligand structure directly impacts MLCTs and photoreactivity of the caged complexes. Research has recently shown that sterically bulky bidentate ligands enhance photodissociation of a pyridine ligand.^{50,147} Thus, modulating ligand structure opens a window for developing novel ruthenium complexes with high quantum yields for dissociation and photocleavage using less energetic light.

1.9 Thesis statement

Biological systems, which are extraordinarily complex, possessing high levels of spatial and temporal control, sometimes have dysregulations in enzyme activity. Though numerous inhibitors are being developed, their off-target reactivity and lack of spatial control cut back their *in vivo* applicability. Therefore, new strategies for selective activation of bioactive molecules in desired areas need to be developed. Also, the caging strategy provides spatial and temporal control over biological molecules, which could help in understanding various biological processes. One such strategy is the photocaging strategy where the bioactive molecules would be activated only in the desired area by light. While different metal ions can be used for developing caged groups for bioactive molecules, we sought to

use ruthenium-based caging groups as a platform for releasing inhibitors in a spatially controlled fashion. Recently this ruthenium-based caging strategy has been demonstrated for caging neurotransmitters and simple cathepsin inhibitors bearing amine, pyridine and nitrile functionality. The goal of this dissertation is to further explore various ruthenium-based groups for caging different agents and studying their biological applications.

The first goal of this dissertation is to cage nitrile-based cathepsin inhibitors with higher activity using a Ru(bpy)₂ caging group. The caged complexes, *cis*-[Ru(bpy)₂(L)₂]²⁺, with L being the nitrile-based inhibitor, were synthesized and fully characterized. Photodissociation and various enzyme inhibition studies were performed on isolated enzymes and also on 2D and 3D assays under both dark and light conditions. Stability studies were undertaken to show the compatibility of the caged complexes in biological media. Toxicity studies with caged complexes in dark and light were performed to rule out any toxic effects on cell viability.

The second goal of this dissertation is to develop novel ruthenium-based caging groups using multidentate ligands and to study ligand effects on photodissociation of caged ruthenium complexes. We proposed a solid phase-based synthesis and screening method of various metal complexes for caging applications.

The last section of this dissertation deals with studying excited state properties of ruthenium complexes. Efforts were made toward developing novel ruthenium-based photosensitizers with exceptionally long-lived excited states for different applications. Background and strategies implemented for achieving each goal are discussed in the following chapters along with experimental procedures and data. Lastly, conclusions and future directions for each goal are discussed at the end of this dissertation.

CHAPTER 2. INHIBITION OF CATHEPSIN K ACTIVITY IN A CELL-BASED ASSAY BY LIGHT ACTIVATED CAGED RUTHENIUM COMPLEXES¹

2.1 Introduction

Caging biomolecules and releasing them through a light activated ligand dissociation pathway provides an excellent strategy to manipulate biological activity with spatial and temporal control.^{42,148,149} The first example of caged nitrile-based protease inhibitor was described in the last part of the previous chapter, where a nitrile-based cathepsin K inhibitor was caged using the Ru(bpy)₂ caging group.¹⁴⁶ In this approach, the cathepsin K inhibitor was protected from a reactive cysteine thiol by covalently binding to a ruthenium center. The Ru(bpy)₂ caging group was used because pioneering work demonstrated its application in caging neurotransmitters and using it in biological research.^{36,37,40,150-152} Importantly, these ruthenium complexes and their corresponding photolysis byproducts showed no toxic effects.

Cathepsin K inhibitors were chosen for caging because numerous reports outline the relationship between aberrant cathepsin K activity and metastatic bone disease.^{97,118,119,144,153,154} Cathepsin K plays a crucial role in osteoclastic bone resorption,¹¹⁹ macrophage invasion and tumor growth.^{155,156} High levels of cathepsin K activity in bone metastases, when compared to primary tumors and soft tissues, make it a viable target for chemotherapy. Also, growth and progression of prostate carcinoma cells (PC3) implanted into CTSK knock-out mice significantly decreased in comparison to tumors implanted into wild-type mice, suggesting the importance of CTSK activity in bone tumor progression. While numerous small

¹ Portions of the text in this chapter were reprinted and adapted with permission from Respondek, T.; Sharma, R.; Herroon, M. K.; Graner, R. N.; Knoll, J. D.; Cueny, E.; Turro, C.; Podgorski, I.; Kodanko, J. J. *Chem. Med. Chem.* **2014**, 9, 1306.

molecules were developed for CTSK inhibition, lack of spatial control and off-target reactivity lead to side effects and subsequent failure in clinical trials.^{83,142} For this reason, new tools may be needed for achieving localized protease inhibition.

Towards this goal, photoactivated CTSK inhibitors were developed. In the “proof of concept” approach, Ac-Phe-NHCH₂CN, (**59**) (IC₅₀ = 12 μM) was used for testing the caging strategy. Two equivalents of **59** were caged using Ru(bpy)₂ and subsequently both the equivalents were released in 10 min using visible light irradiation. Initial success motivated us to develop a new class of Ru-based caged compounds with more potent inhibitors of CTSK. Herein, two new CTSK inhibitors (**60** and **61**) with higher activity and their corresponding Ru-caged complexes were developed. We also demonstrated that our strategy could be used for protease inhibition in living cells. Subsequent sections in this chapter will provide convincing evidence that our caged inhibitors are nontoxic and can be further developed as chemical tools for understanding the role of different proteases within living systems, including animal models of human disease states.

2.2 Results and discussions

2.2.1 Synthesis and characterization of [Ru(bpy)₂(L)₂](X)₂ (**62** and **63**) complexes

Literature data show that subtle modifications of compound **59**, which was used in the previous study, can lead to significant enhancements for inhibition of CTSK activity.^{127,139} Compounds **60** and **61** were chosen for caging; IC₅₀ values were roughly three orders of magnitude lower than compound **59** (Figure 14). Compound **60** was chosen because it was structurally similar to **59** and was known to inhibit CTSK activity in live cell assays.¹³⁹ Compound **61** was chosen because it had more drug-like properties, possessing longer

plasma stability and around ten-fold longer half-life *in vivo* than **60**. Also, **61** had an alpha-substitution that we were interested in studying to see its effects on properties of the caged complex. Compounds **60**¹³⁹ and **61**¹²⁷ were synthesized by following published procedures from enantioenriched Cbz-Leu-OH and Boc-Ser(OBn)-OH respectively.

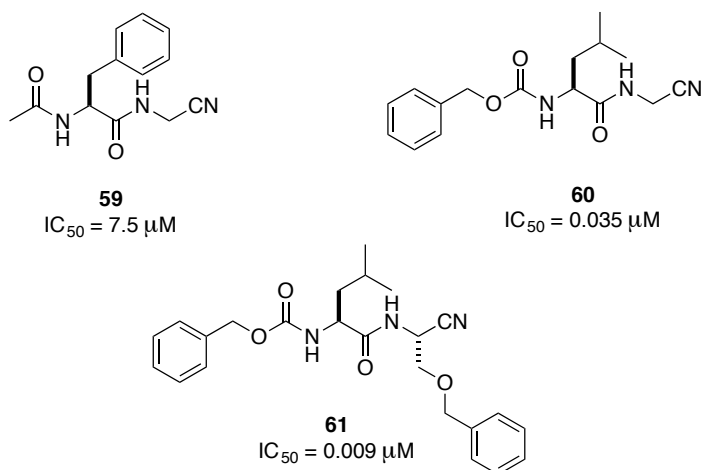
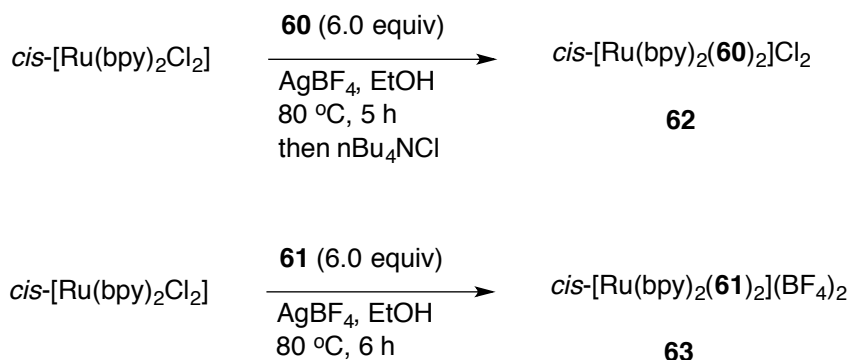


Figure 14: Nitrile-based CTSK inhibitors with their corresponding IC_{50} values.

Upon treating *cis*-[Ru(bpy)₂Cl₂] with **60** (6.0 equiv) in EtOH at 80 °C for 5 h, in the presence of silver tetrafluoroborate, a color change from violet to orange occurred. The reaction mixture was cooled to -20 °C, filtered through celite and concentrated under reduced pressure to obtain an orange solid. Spectroscopic analysis of the crude reaction mixture confirmed that **60** was bound to ruthenium with high conversion, as there were no metal-based byproducts. To remove excess **60** and purify the complex **62**, the crude solid was dissolved in ethyl acetate and treated with *n*Bu₄NCl. Upon cooling to -20 °C, an orange oily residue was observed, which was washed with ethyl acetate and toluene several times to remove excess *n*Bu₄NCl. Subsequent precipitation (layering) from acetone and diethyl ether for multiple cycles, followed by drying in vacuum, gave the caged inhibitor **62** in analytically pure form. Complex **63** was prepared by following a similar procedure; however, the

tetrafluoroborate salt was purified using silica gel chromatography, giving directly the pure caged complex **63** without anion metathesis.



Scheme 6: Synthesis of caged inhibitor complexes **62** and **63**.

Compounds **62** and **63** were isolated as 1:1 mixtures of Δ and Λ isomers, because *cis*-[Ru(bpy)₂Cl₂], **60** and **61** are chiral (Figure 15). Spectroscopic analysis confirms the formation of two diastereoisomers, as two distinct peaks corresponding to amide protons for each of the diastereoisomers were split.

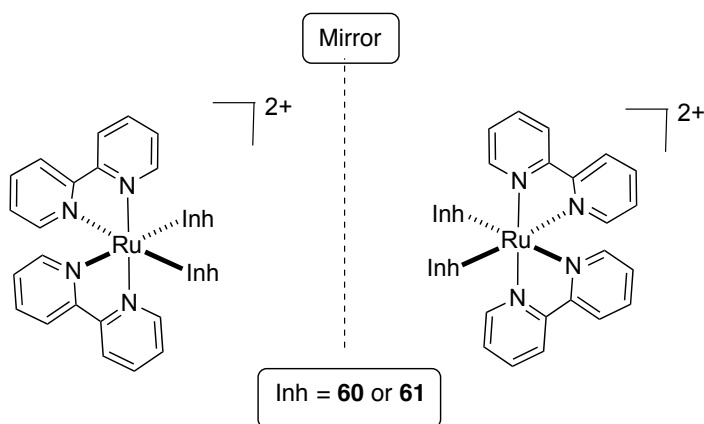


Figure 15: Structure of Δ -**62** or **63** and Λ -**62** or **63**

The IR spectrum for **60** shows the characteristic CN stretching at 2258 cm⁻¹. This resonance is shifted to 2274 cm⁻¹ in the complex **62**, which is consistent with the nitrile binding to the metal center.^{146,157} The UV-Vis spectrum of **62** shows maxima at 281 nm ($\epsilon =$

55,600 M⁻¹ cm⁻¹), associated with ligand-centered bpy $\pi\pi^*$ transitions, and at 412 nm ($\epsilon = 9,600$ M⁻¹ cm⁻¹), associated with metal-to-ligand charge transfer (¹MLCT) transitions, i.e Ru→bpy. These observations are consistent with electronic absorptions of other related complexes such as *cis*-[Ru(bpy)₂(MeCN)₂]⁺² and *cis*-[Ru(bpy)₂(**59**)₂]⁺² (**57**). The electrospray ionization mass spectra of **62** in water shows a prominent peak at *m/z* = 1055, along with a suitable isotopic pattern, consistent with the monocation of the formula [Ru(bpy)₂(**60**)₂](Cl)⁺.

The IR spectrum for **61** shows the characteristic CN stretching at 2257 cm⁻¹. This resonance is shifted to 2270 cm⁻¹ in the complex **63**. The UV-Vis spectrum of **63** shows maxima at 284 nm ($\epsilon = 50,600$ M⁻¹ cm⁻¹) and at 418 nm ($\epsilon = 9,810$ M⁻¹ cm⁻¹). The electrospray ionization mass spectra of **63** in water shows a prominent peak at *m/z* = 1348, along with a suitable isotopic pattern, consistent with the monocation of the formula [Ru(bpy)₂(**61**)₂](BF₄)⁺.

2.2.2 Stability and photolysis of [Ru(bpy)₂(L)₂](X)₂ complexes

The half-life of both the complexes was determined spectrophotometrically in phosphate-buffered saline (PBS, pH = 6.5). The half-life for **62** was about 8.0 days at 293±2 K, as determined by using the rate constant for decomposition of **62** obtained from the slope of a ln A vs. t graph ($k_{\text{obs}} = 1.0 \times 10^{-6}$ s⁻¹). Decomposition was also studied in the dark in pure water and in solutions containing 1% DMSO to mimic the conditions used in the biological assays. Complex **63** was more stable than **62**, giving $k_{\text{obs}} = 5.0 \times 10^{-9}$ s⁻¹ in PBS buffer corresponding to a half-life of >1800 days.

The Turro group characterized the photochemistry of **62** and **63**. Photoactivated ligand dissociation of **62** in water (1% DMSO) results in the sequential exchange of the two monodentate ligands (**60**) for solvent molecules, generating *cis*-[Ru(bpy)₂(H₂O)₂]²⁺. The changes

in the electronic absorption spectrum of **62** (52 μM), which was measured as a function of irradiation time ($\lambda_{\text{irr}} \geq 395 \text{ nm}$), show the decrease of the starting material peak at 412 nm and the formation of an intermediate species in $t_{\text{irr}} = 0\text{-}3 \text{ min}$ with a maximum at around 450 nm (Figure 16A, inset). During this time, two isosbestic points at 322 and 364 nm are apparent, as well as a pseudo-isosbestic point at 427 nm. The intermediate at $t_{\text{irr}} = 2\text{-}3 \text{ min}$ has been shown to correspond to the product formed after the exchange of one CH_3CN ligand for a H_2O molecule in the CH_3CN complex, i.e. $\text{cis-}[\text{Ru}(\text{bpy})_2(\text{CH}_3\text{CN})(\text{H}_2\text{O})]^{2+}$, and is denoted by * in Figure 16.^{75,146} Further irradiation of **62** from 3 min to 15 min leads to the formation of the final photolysis product, $\text{cis-}[\text{Ru}(\text{bpy})_2(\text{H}_2\text{O})_2]^{2+}$, with the known absorption maxima at 340 nm and 486.¹⁵⁸ Three isosbestic points are seen during the final step of photolysis ($t_{\text{irr}} = 3\text{-}15 \text{ min}$) at 332, 384, and 463 nm (Figure 16).

Despite complex **63** showing excellent stability in many solvents, photolysis of **63** is much less efficient than **62**. Photolysis of **63** in water (2 % acetone) results in a similar trend, where sequential exchange of the two **61** ligands with H_2O was observed to be much slower than **62**. Formation of the intermediate $\text{cis-}[\text{Ru}(\text{bpy})_2(\mathbf{61})(\text{H}_2\text{O})]^{2+}$ can be inferred from a decrease in the absorbance at 412 nm and an increase in absorbance at 440 nm that occurs with irradiation ($\lambda_{\text{irr}} \geq 395 \text{ nm}$) up to 10 min. The isosbestic point at 424 nm is similar to that observed for the first ligand dissociation in **62**. The second dissociation of **61** to provide the final photodissociation product, $\text{cis-}[\text{Ru}(\text{bpy})_2(\text{H}_2\text{O})_2]^{2+}$ is very slow. From 13 to 60 min of irradiation, the intermediate absorbance decreases and a new $\text{cis-}[\text{Ru}(\text{bpy})_2(\text{H}_2\text{O})_2]^{2+}$ product transition evolves at 486 nm with an isosbestic point at 462 nm.

The quantum yields for all the conversions were also measured, where for the conversion of the reactant (R) **62** to the intermediate (I) $\text{cis-}[\text{Ru}(\text{bpy})_2(\mathbf{60})(\text{H}_2\text{O})]^{2+}$ ($\Phi_{\text{R-I}}$) and to the product

(P) cis -[Ru(bpy)₂(H₂O)₂]²⁺ (Φ_{R-P}) were 0.050(6) and 0.0067(4), respectively ($\lambda_{irr} = 400$ nm). The corresponding Φ_{R-I} and Φ_{R-P} values for the photoaquation of **63** were measured as 0.021(2) and 0.0045(6), respectively.

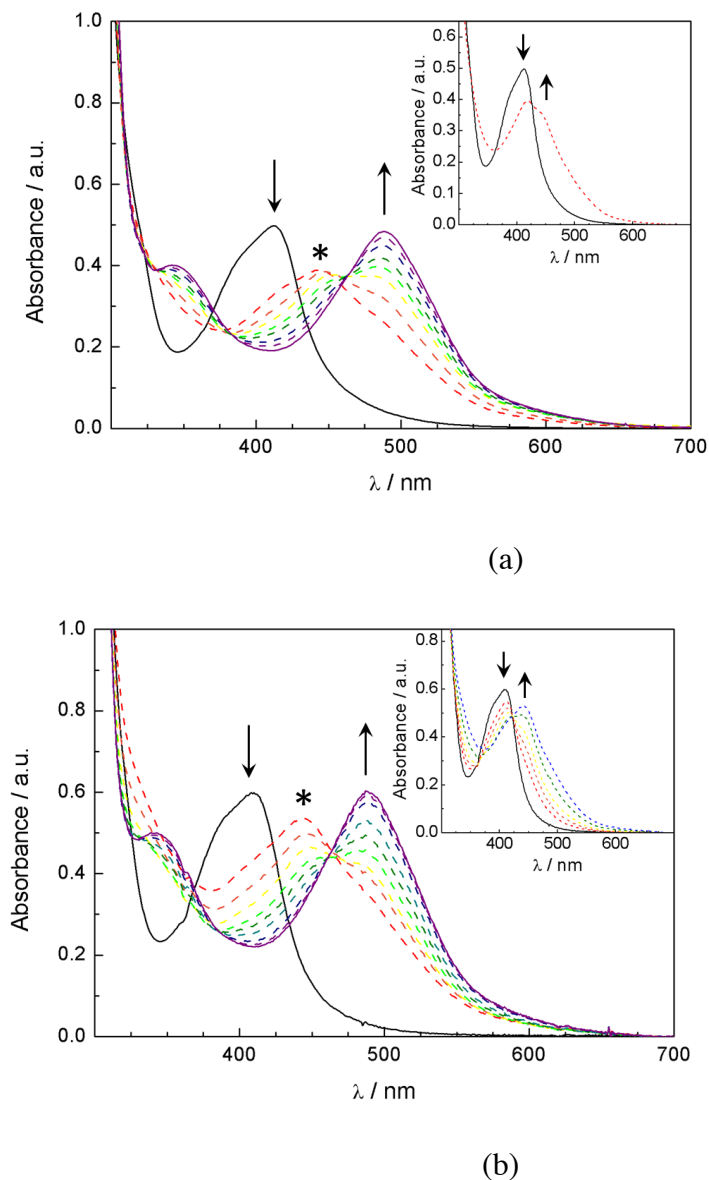
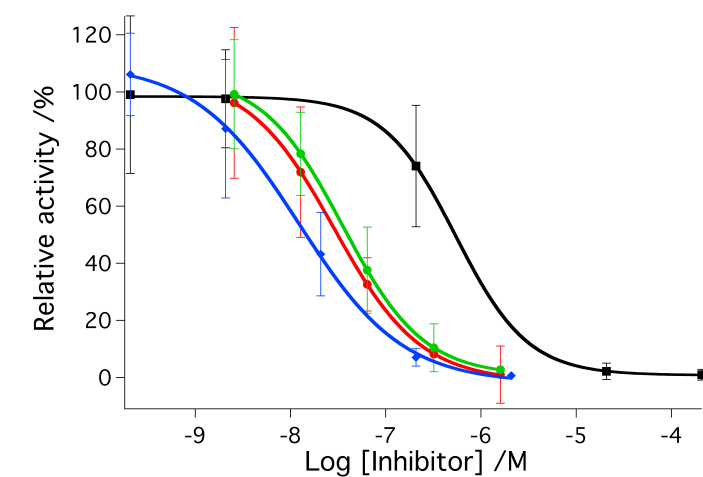


Figure 16: Changes to electronic absorption of (a) **62** (52 μ M) in a 1% DMSO aqueous solution irradiated at 0, 2, 3, 4, 5, 6, 7, 8, 10 and 15 min ($\lambda_{irr} \geq 395$ nm); inset 0 and 1 min; and (b) **63** (51 μ M) in a 2% acetone solution at irradiation times 0, 10, 13, 16, 20, 25, 30, 40, 50 and 60 min ($\lambda_{irr} \geq 395$ nm); inset 0, 1, 2, 3, 5 and 7 min. *Absorption maxima of the intermediate.

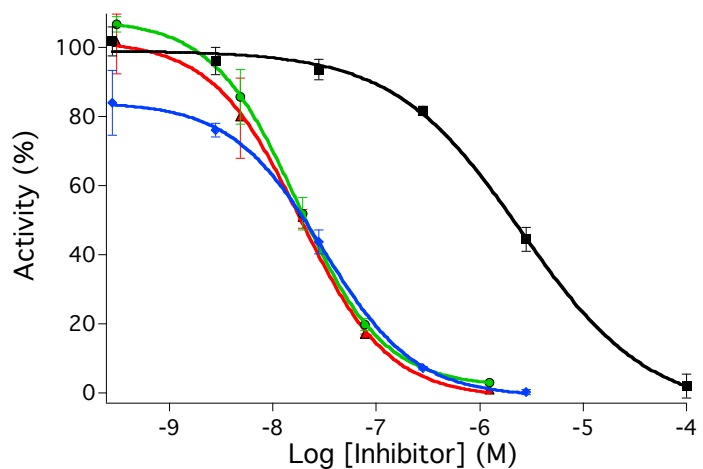
2.2.3 Light-activated inhibition of cathepsin K

To study the biological assays, first light-activated inhibition of cathepsin K was performed for parent inhibitors **60** and **61** against purified human cathepsin K under both light and dark conditions. Then we performed similar experiments for caged complexes **62** and **63** (Figure 17). Solutions of cathepsin K (2 nM) in assay buffer solutions (400 mM sodium acetate, pH 6.0, 4 mM EDTA, 8 mM DTT, 0.01% Triton X-100) were treated with varying amounts of **60** and **61**. Experiments were performed either in dark by leaving the solutions covered in aluminum foil or in light by irradiating with a tungsten halogen lamp (250 W, $\lambda_{\text{irr}} > 395$ nm, H₂O filter). Irradiation times were shorter for **60** and **62** ($t_{\text{irr}} = 15$ min) than **61** and **63** ($t_{\text{irr}} = 40$ min) because photolysis of **63** was much slower when compared to **62**. Z-Gly-Pro-Arg-AMC was the fluorogenic substrate used for measuring enzyme activity. Data indicate that **60** and **61** inhibit CTSK in the low nanomolar range under these conditions, giving IC₅₀ values of 36 nM and 28 nM, respectively. Data were identical within error under light vs. dark conditions for both of the parent inhibitors, suggesting that light had no effect on enzyme inhibition. In contrast, significant enhancements in cathepsin K inhibition were observed with **62** and **63** upon irradiation. IC₅₀ values for **62** under dark vs. light conditions were 560 nM and 16 nM respectively, which gives a dark to light IC₅₀ ratio of 35:1 (Figure 17a). Similarly, IC₅₀ values for **63** under dark vs. light conditions were 2.2 μ M and 25 nM, respectively, giving a dark to light IC₅₀ ratio of 88:1 (Figure 17b). As expected, when irradiated with light, **62** is more potent than the parent inhibitor **60**, because it carries 2 equivalents of the inhibitor molecule per ruthenium complex, and both are released upon irradiation. Enzyme inhibition data for **63** are consistent with results from the photochemical experiments, demonstrating that although 2 equivalents are available, release

of the second ligand is very slow, giving the same potency for **61** as for **63** under light conditions. Nonetheless, both compounds **62** and **63** show a considerable improvement over light-activated inhibition by our previous compound *cis*-[Ru(bpy)₂(**59**)₂](PF₆)₂, whose IC₅₀ value was only 5.4 μM under light conditions.¹⁴⁶



(a)



(b)

Figure 17: (a) IC₅₀ curves for inhibitor **60** (red = dark; green = light) and *cis*-[Ru(bpy)₂(**60**)₂]Cl₂ (**62**) (black = dark; blue = light) and (b) IC₅₀ curves for inhibitor **61** (red = dark; green = light) and *cis*-[Ru(bpy)₂(**61**)₂]Cl₂ (**63**) (black = dark; blue = light) against isolated cathepsin K.

2.2.4 Toxicity studies

One important goal with this project was to show that the caged molecules and their corresponding photolysis byproducts had no toxic effects on cell viability. In order to gain insight into the biological behavior of the caged inhibitor **62** and **63**, effects of the complexes and their photochemical byproducts on cell viability in murine BMM and human PC-3 cells were determined under light and dark conditions by the Podgorski group. The osteoclast cells could not be utilized for determination of viability because of their terminal nature. BMM or PC3 cells were treated with either *cis*-[Ru(bpy)₂(MeCN)₂](PF₆)₂ as a control, **62** or **63** (1 nM-100 mM), incubated for 30 min either in the dark or irradiated with a tungsten halogen lamp for light experiments. The irradiation times were different; complexes **62** and *cis*-[Ru(bpy)₂(MeCN)₂](PF₆)₂ were irradiated for 15 min, whereas complex **63** was irradiated for 40 min due to its slow photolysis rate. After 24 h, viabilities were determined using the MTT assay (Figure 18). To our delight compounds **62** and *cis*-[Ru(bpy)₂(MeCN)₂](PF₆)₂, which both release *cis*-[Ru(bpy)₂(H₂O)₂]²⁺ upon irradiation, showed no effects on viability within error over the full concentration range, up to 100 μM. Compound **63** showed no toxic effects at lower concentrations, but did start to affect cell viability at concentrations of 10 μM and higher.

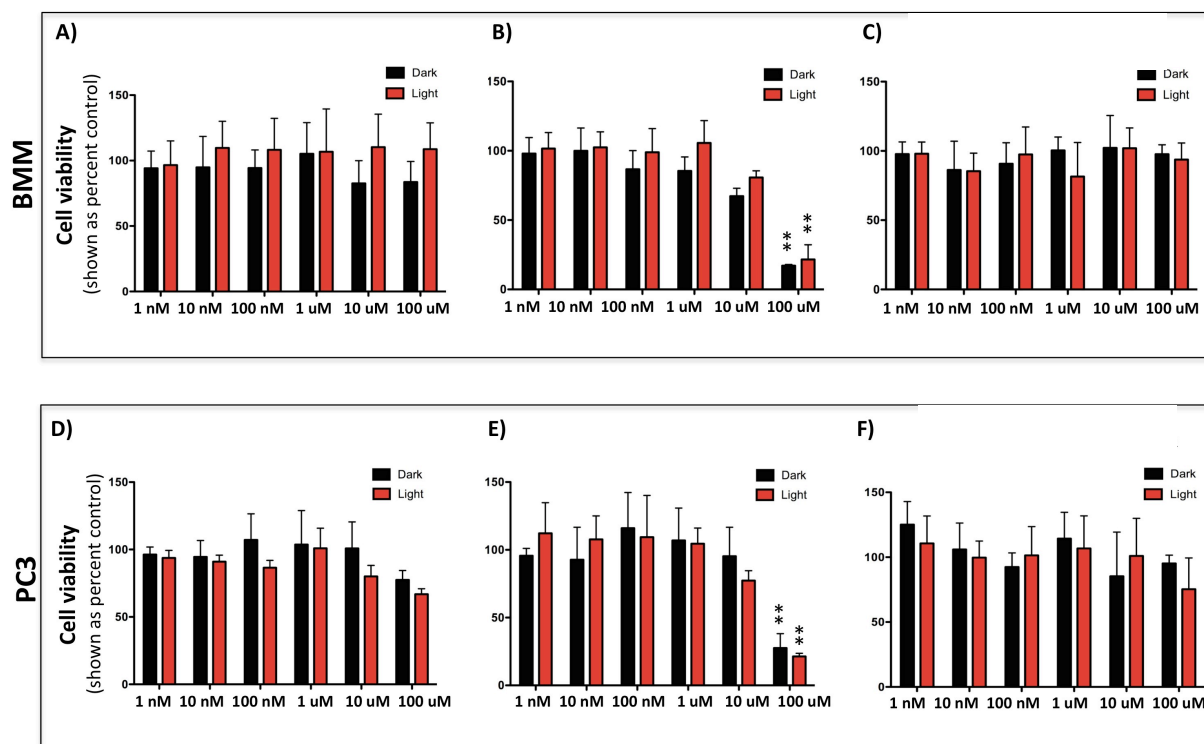


Figure 18: Cytotoxicity of *cis*-[Ru(bpy)₂(**60**)₂]Cl₂ (**62**) (A and D), *cis*-[Ru(bpy)₂(**61**)₂](BF₄)₂ (**63**) (B and E) and the control compound *cis*-[Ru(bpy)₂(MeCN)₂](PF₆)₂ (C and F) on BMM cells (A-C) and prostate cancer PC3 cells (D-F).

2.2.5 Light activated inhibition of cathepsin activity in cells.

To show the full potential of our caging strategy, we wanted to study the possibility of inhibiting CTSK activity in live cells along with isolated enzymes with caged inhibitor complexes. Compound **62** was chosen as the lead compound to evaluate in cell-based assays for light activated inhibition of cathepsin activity because **62** showed a lower IC₅₀ value under light conditions than **63**, required a shorter irradiation time and demonstrated no effects on cell viability. Bone marrow macrophage cells (BMM) express high levels of CTSK activity and their aberrant proteolysis is found to play an important role in inflammatory, osteolytic and tumor cell-driven processes in bone tumor microenvironments.¹²⁰ For this reason we initially decided to

use BMM cells for performing live cell assays. Results from Western blot analyses on murine BMM and BMM-derived osteoclast cells suggested that both the cell types are a significant source of CTSK and CTSB. Finally, we decided to use osteoclast cells, which had significantly higher levels of CTSK compared to BMM cells. Also, if cathepsin K inhibition were to be studied in BMM cells, the enzyme activity would be difficult to distinguish from noise in the presence of cathepsin B inhibitor CA-074Me because it is very close to the baseline.

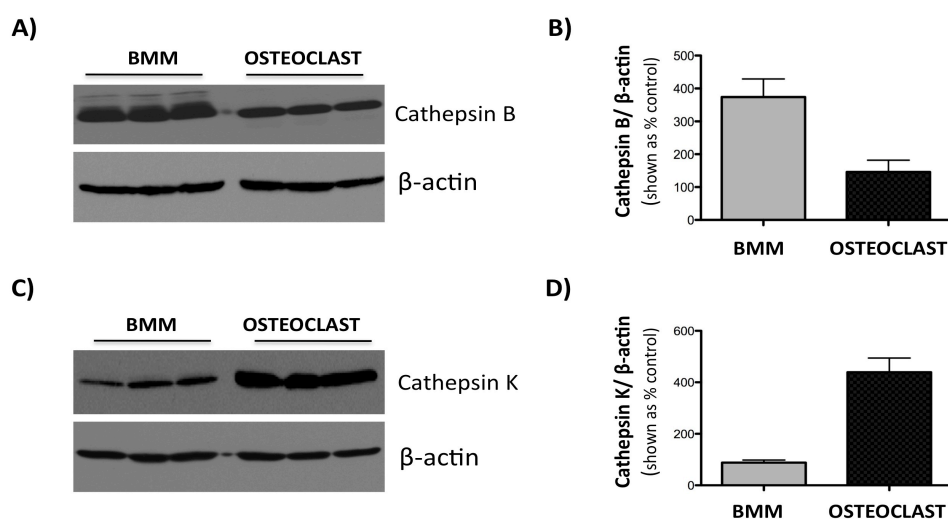


Figure 19: Expression of cathepsins B and K in BMM and BMM derived osteoclast cells. Western blots analysis (A and C) and densitometric analysis of CTSB (B) and CTSK (D) performed using Fuji Multimodal Imager.

Based on their cathepsin K expression pattern, osteoclasts were chosen as the cell line to examine the light activated inhibition of cathepsin activity in live cells in all subsequent experiments. First, the parent inhibitor **60** was studied for its ability to block proteolysis of two fluorescent cathepsin K substrates, Z-Gly-Pro-Arg-4-methoxy- β -naphthylamide (Z-GPR-4M β NA)¹⁵³ and Z-Leu-Arg-4-methoxy- β -naphthylamide (Z-LR-4M β NA).¹⁵⁹ In both cases 4-methoxy- β -naphthylamine is formed after hydrolysis. The formed 4-methoxy- β -naphthylamine

can then form a precipitate with nitrosalicylaldehyde that can be detected and quantified by fluorescence measurements. By following a literature protocol,¹²⁷ cells were preincubated with inhibitor **60** (1 nM to 1000 nM), in the presence of the selective CTSB inhibitor CA-074Me (1 μ M) to knock down CTSB activity, which is known to compete with cathepsin K for cleavage of these substrates.^{97,160} Confocal microscopy was used for visualizing enzyme activity and intensities of green fluorescence were integrated and averaged over 3 data sets in order to make a quantitative assessment of cathepsin inhibition. Results showed that hydrolysis of Z-LR-4M β NA were reduced up to 50% with **60** (10-1000 nM) in a dose dependent fashion (Figure 20). However, by further increasing the concentration no further reduction in substrate hydrolysis was observed, suggesting another protease, not inhibited by **60**, might be cleaving the same substrate. Although **60** also inhibited hydrolysis of Z-GPR-4M β NA, Z-LR-4M β NA was used as the substrate in following rounds of experiments because results were less pronounced and less consistent between independent experiments with Z-GPR-4M β NA.

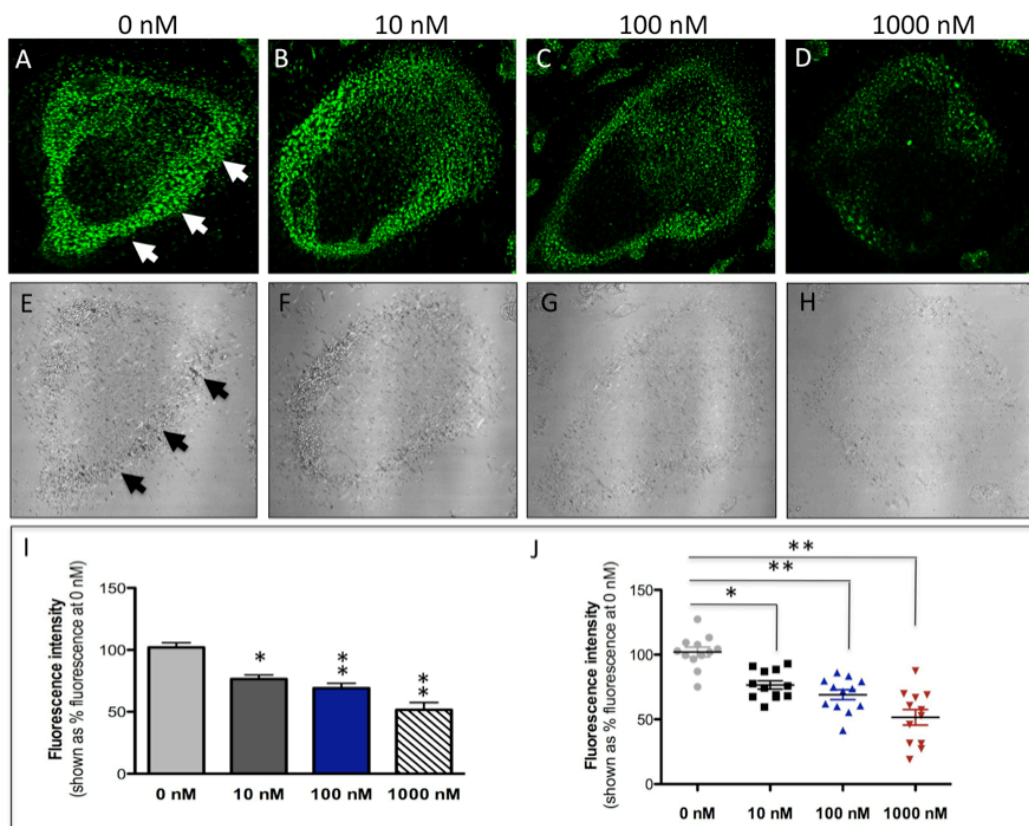
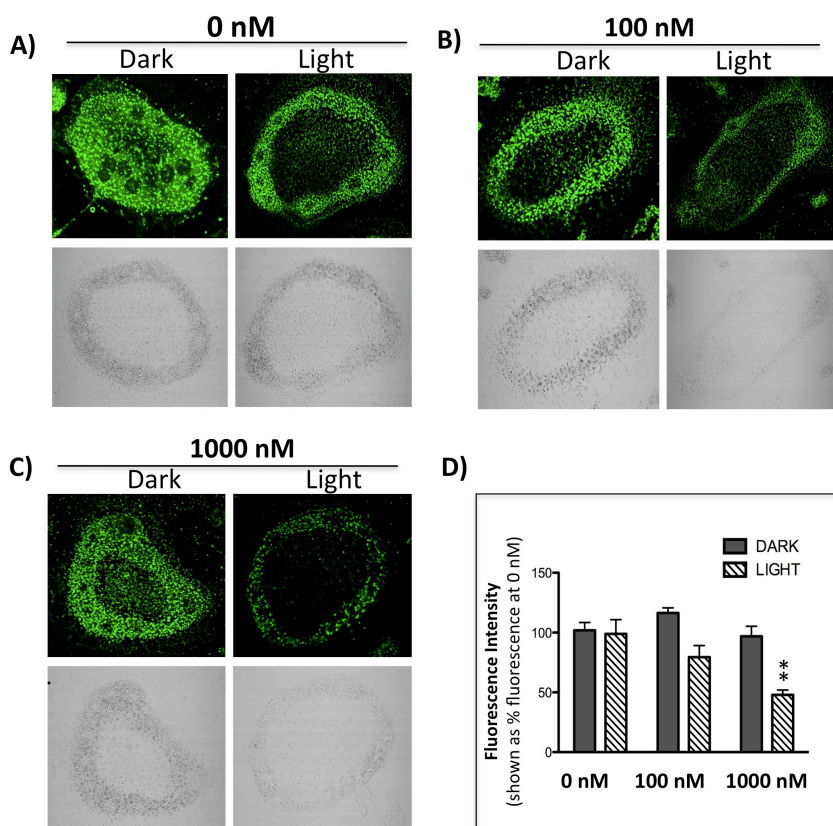


Figure 20: Confocal microscopy images of mouse osteoclast cells treated with **60** at different concentrations. The intensity of green fluorescence is a direct measure of the quantity of hydrolyzed and precipitated substrate (A-D) also visible on DIC images (E-H). The quantified data are shown as column (I) and dot (J) plots. * Indicates $p < 0.05$ and ** indicates $p < 0.001$.

Having performed live cell assays with the parent inhibitor and developed a method, experiments with the caged complex **62** were performed in dark and in the presence of light under similar conditions. Osteoclasts were treated with two concentrations of **62** over the same concentration range where **60** was active. Vehicle and *cis*-[Ru(bpy)₂(MeCN)₂](PF₆)₂ were used as controls. Results showed that **62** was able to produce the same response as **60** in the presence of light, but did not show inhibition in the dark, consistent with data against purified cathepsin K (Figure 21). Importantly, a strong, light-activated response at 1000 nM was observed with **62**. Also **62** showed a 25% reduction in activity at 100 nM under light conditions. No differences of

inhibition were observed with **62** when cells were washed between preincubation and irradiation, indicating that **62** might either be cell permeable or cell associated. Vehicle and *cis*-[Ru(bpy)₂(MeCN)₂](PF₆)₂ showed no difference in inhibition between light and dark experiments. A slight reduction in Z-LR-4MβNA hydrolysis was noted with *cis*-[Ru(bpy)₂(MeCN)₂](PF₆)₂ at high concentrations (1000 nM). However, these data were well outside the range of error for inhibition by **62** using light conditions, indicating that the release of **60** from the caged inhibitor **62** is responsible for the observed inhibition.



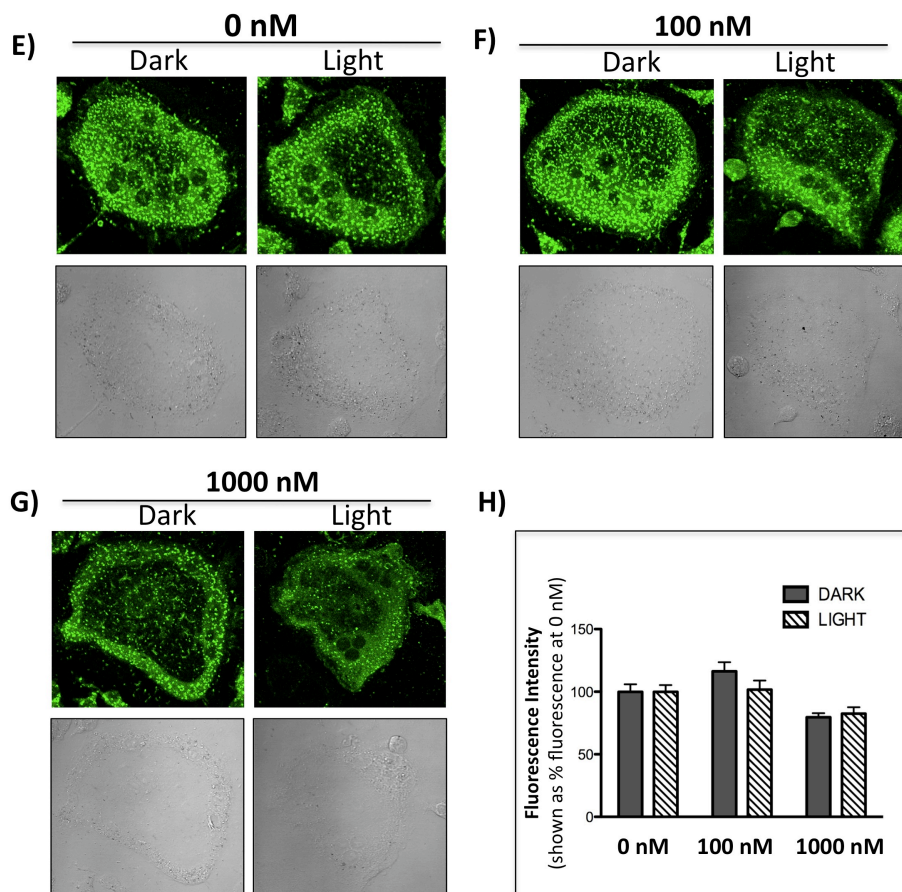


Figure 21: Confocal microscopy images of mouse osteoclasts cells treated with the ruthenium-caged inhibitor **62**(A-D) or *cis*-[Ru(bpy)₂(MeCN)₂](PF₆)₂ (E-H). Cells were preincubated with either complex (0-1000 nM) for 30 min at 37 °C in the presence of cathepsin B inhibitor CA-074Me (1 μM), then exposed to dark (no irradiation) or light (irradiation; 250W, 395-750 nm) conditions for 15 min. ** indicates p<0.001.

2.3 Discussions

In this study, we have shown that cathepsin activity in a cell-based assay can be controlled by compound **62**, which is a light-activated enzyme inhibitor. This approach was validated against cathepsin K in osteoclasts cells, one of the key sources of this proteolytic enzyme in the bone tumor microenvironment.¹²⁰ Given the availability of numerous potent and selective nitrile-based inhibitors developed for a range of cathepsin and caspase targets,^{127,133,135,139}

our method has great potential to control spatial aspects of many biological processes in cells, including apoptosis, inflammation and cell signaling.

Despite having the same caging group, compounds **62** and **63** showed a notable difference in photochemical behavior, indicating that not only the caging group but also the ligand structure plays a role in caged complex properties. The quantum yields for **62** were significantly lower than those reported for the photoaquation of the related complex $[\text{Ru}(\text{bpy})_2(\text{CH}_3\text{CN})_2]^{2+}$,⁷⁵ but are similar to those measured for *cis*- $[\text{Ru}(\text{bpy})_2(\mathbf{59})_2](\text{PF}_6)_2$. The quantum yields for **63** are significantly lower than both of these complexes. Because these steady-state measurements determine the overall yield of the reaction, it is possible that the initial dissociation of the ligand is relatively efficient, but that it quickly recombines with the metal before a water molecule is able to access the open coordination site. The steric bulk of the peptide-containing ligands may prevent water from quickly reaching the metal. Alternatively, the peptides may not be as water soluble as acetonitrile, such that solvation of the uncaged product may have a detrimental effect on the overall separation of the photoproducts, and therefore the overall reactivity. The significant decrease in efficiency for the photorelease of **61** from **63** may be due to the larger size and lower polarity of **61** compared to **59** and **60**.

One important result of this study is the lack of observed toxicity for **62**. Neither **62**, nor the control compound *cis*- $[\text{Ru}(\text{bpy})_2(\text{MeCN})_2](\text{PF}_6)_2$ caused growth inhibitory effects in BMM or PC3 cells under our experimental conditions. Compound **63**, however, did cause growth inhibitory effects at higher concentrations, confirming that the biological behavior of these ruthenium-caged compounds is not just dependent on the nature of the caging group, but on the overall structure of the complex. The caging group $\text{Ru}(\text{bpy})_2$ has been used successfully without causing deleterious side effects, as mentioned previously by others.^{37,38,161} Also, the effective

concentrations for light-activated inhibitors are dictated by the concentration of the target enzyme, as well as inhibitor potency, selectivity and cell permeability. Thus, toxicity may be prevented, because protease inhibitors are often effective in culture at low concentrations, typically below 5 μM ,^{118,162,163} where **63** caused no growth inhibitory effects. Taken together, **62** can be categorized as a caged nitrile-based inhibitor that, at the concentrations required for inhibition, employs a non-toxic metal center, rather than a bioactive ruthenium complex.

Our data confirm that the caged inhibitor complex **62** was able to produce the same results as the parent inhibitor **60** under light conditions, whereas in the dark **62** caused no inhibition. Thus spatial control over inhibition in a cell-based assay was realized, which was the goal of this study. Despite this achievement, neither compound **60** nor **62** were able to fully suppress hydrolysis of the substrate Z-LR-4M β NA in osteoclast cells, where a maximum inhibition of 50% was achieved. Given the nanomolar potencies measured against cathepsin K in purified enzyme assays, these data suggest that cathepsin K was fully inhibited and that another enzyme, not inhibited by **60**, was responsible for the remainder of Z-LR-4M β NA hydrolysis. Indeed, there are limitations with fluorescent substrates in detecting specific cathepsin activities.¹⁶² In addition to cathepsin K,¹⁵⁹ Z-LR-4M β NA is a substrate for other cathepsins, namely S and V. Although greater levels of inhibition were observed with Z-GPR-4M β NA, a substrate described to be selective for cathepsin K,¹⁶³ data were not as consistent between independent experiments. Another factor to consider is that nitrile-based inhibitors are less potent and selective against mouse cathepsins than human cathepsins, which provides an extra level of complexity in correlating pharmacological data from animal cells with human enzymes.¹⁶⁴ Unfortunately, human osteoclasts were not available for this study.

Confocal microscopy experiments indicated that intracellular inhibition was achieved with **62**. Previous studies have established that inhibitor **60** is highly cell permeable.¹⁶⁵ Washing cells after preincubation had no effect on the level of inhibition observed with **62**, suggesting that **62** is either cell permeable or membrane associated. Because **62** is not luminescent,¹⁶⁶ we are not currently able to understand its mode of action, which could either be **62** releasing **60** upon irradiation or **62** permeating the cell membrane and releasing inhibitor upon irradiation. Further studies will be needed to determine the exact mode of inhibitor uptake.

2.4 Conclusions

In conclusion, we demonstrated for the first time that the ruthenium caging approach can be used for intracellular light-activated enzyme inhibition. New photoactivated inhibitors of cathepsin K were reported that release inhibitors with potencies in the nanomolar range. Importantly, our studies confirm that the ruthenium caging approach can be carried out with no apparent toxicity. These data strongly support the translation of this technology to other enzyme targets and live cell systems.

2.5 Experimental procedures

2.5.1 General considerations

All reagents were purchased from commercial suppliers and used as received. Compounds **60**¹³⁹ and **61**¹²⁷ were prepared by literature procedures. NMR spectra were recorded on a Varian FT-NMR Mercury-400 Spectrometer. Mass spectra were recorded on a Waters ZQ2000 single quadrupole mass spectrometer using an electrospray ionization source. IR spectra were recorded on a Perkin Elmer Spectrum 2000 FT-IR Spectrometer. Enzymatic assays were conducted on a Tecan Infinite M200 or Tecan SPECTRAFluor Plus microplate reader. UV-vis spectra were recorded on a Varian Cary 50 spectrophotometer. The photolysis experiments were

conducted using a 250 W Tungsten Halogen lamp (Osram Xenophot HLX) powered by a 24 V power source. The irradiation wavelength was selected by placing a bandpass filter (395 nm cutoff) between the lamp and the sample, along with a 10 cm water cell to absorb infrared light. All reactions were performed under ambient atmosphere unless otherwise noted. The reaction solutions were purged with Ar or N₂ for performing anaerobic reactions.

2.5.2 Synthesis of Complexes and tabulated data

2.5.2.1 Δ - and Λ -cis [Ru(bpy)₂(**60**)₂]Cl₂ (**62**):

In the glove box, a sealable tube was charged with *cis*-Ru(bpy)₂Cl₂ (0.1 mmol, 48.4 mg), AgBF₄ (0.4 mmol, 77.9 mg) and (S)-benzyl (1-((cyanomethyl)amino)-4-methyl-1-oxopentan-2-yl)carbamate (**60**) (0.6 mmol, 91.0 mg) and of freshly distilled EtOH (20 mL). The resulting solution was wrapped in aluminum foil and heated to 80 °C for 5 h during which it turned from dark violet to bright orange. After cooling the crude solution to RT, it was placed in the freezer at -20 °C for 16 h. The precipitated silver salts were filtered off using celite and the filter cake was washed with cold EtOH. The solvents were removed under reduced pressure and the crude mixture was analyzed by ¹H NMR spectroscopy. The resulting yellow solid was dissolved in acetone (2 mL) and layered with Et₂O (10 mL) and placed in the freezer at -20 °C for 16 h. The reaction mixture was filtered and the filter cake washed with cold Et₂O. The resulting solid was dissolved in EtOAc (15 mL) and extracted 3 times with H₂O (15 mL). The organic layer was then precipitated with sat. *n*-Bu₄NCl in EtOAc (0.1 mL) at -20 °C. The resulting oily residue was isolated by centrifugation; the mixture was decanted and the residue was washed with cold EtOAc (3 × 5 mL), and then cold toluene (3 × 5 mL). The residue was dissolved in a minimum amount of acetone and layered with Et₂O. The resulting solid was washed with Et₂O. Layering and washing were repeated four times to give the title compound as an orange solid in

analytically pure form as a hydrate salt (21.0 mg, 0.019 mmol, 19%). ^1H NMR (400MHz $\text{CD}_2\text{Cl}_2\text{-d}_2$ δ) 9.93 (s, br, 2H), 9.54 (d, $J = 4.9$ Hz, 1H), 9.51 (d, $J = 4.9$ Hz, 1H), 8.53 (d, $J = 8.1$ Hz, 1H), 8.45 (d, $J = 8.1$ Hz, 2H), 8.36 (d, $J = 8.1$ Hz, 1H), 8.15 (m, 2H), 8.02 (m, 2H), 7.93 (m, 2H), 7.54 (d, $J = 5.9$ Hz, 2H), 7.32 (m, 8H), 7.25 (m, 2H), 6.86 (d, $J = 9.7$ Hz, 1H, NH), 6.74 (d, $J = 8.1$ Hz, 1H, NH), 5.04 (m, 3H), 4.16 (d, $J = 12.2$, 1H), 4.28 (m, 6H), 1.08 (under the H_2O peak, m, 4H), 0.91 (m, 12H); IR (KBr) ν_{max} (cm^{-1}): 3419, 3029, 2957, 2870, 2347, 2274, 1714, 1676, 1604, 1523, 1466, 1446, 1424, 1386, 1337, 1246, 1170, 1122, 1047, 917, 771, 731, 698, 670; LRMS (ESMS) calculated for $\text{C}_{52}\text{H}_{58}\text{N}_{10}\text{O}_6\text{Ru} [\text{M}]^{2+}$: 510.2, found: 510.1; Anal. Calculated for $\text{C}_{52}\text{H}_{65}\text{Cl}_2\text{N}_{10}\text{O}_{9.5}\text{Ru} ([\text{Ru}(\text{bpy})_2(\mathbf{60})_2]\text{Cl}_2 \cdot 3.5\text{H}_2\text{O})$: C, 54.12; H, 5.68; N, 12.14. Found: C, 54.16; H, 5.46; N, 12.13.¹⁶⁷

2.5.2.2 Δ - and Λ -cis $[\text{Ru}(\text{bpy})_2(\mathbf{61})_2](\text{BF}_4)_2$ (**63**):

In the glove box, a sealable tube was charged with *cis*- $\text{Ru}(\text{bpy})_2\text{Cl}_2$ (60 mg, 0.12 mmol), compound **61** (314.7 mg, 0.74 mmol), and AgBF_4 (96.6 mg, 0.49 mmol) in dry EtOH (28 mL) under inert atmosphere. The resulting solution was wrapped in aluminum foil and heated to 80 °C for 6 h during which it turned from dark violet to bright orange. After cooling the crude solution to RT, it was placed in the freezer at -20 °C for 16 h. The precipitated silver salts were filtered off using celite and the filter cake was washed with cold EtOH. The solvents were removed under reduced pressure and the crude mixture was analyzed by ^1H NMR spectroscopy. The reaction mixture was concentrated and the orange solid was stirred with Et_2O (3×20 mL) to remove excess **61**. The orange solid was purified using silica gel (acetone). Fractions were concentrated and the yellow solid was stirred with Et_2O (2×20 mL), filtered and dried under reduced pressure to get the caged complex as pale orange solid in analytically pure form (64 mg, 51%): Mp = 206 °C (decomp); ^1H NMR (400MHz $\text{C}_3\text{D}_6\text{O}$) δ 9.53 (d, 1H, $J = 5.2$ Hz), δ 9.49 (d,

1H, $J = 5.2$ Hz), δ 8.78-8.75 (m, 2H), δ 8.65 (t, 2H, $J = 8.8$ Hz), δ 8.36 (t, 2H, $J = 7.6$ Hz), δ 8.23 (t, 1H, $J = 7.2$ Hz, NH), δ 8.13-8.08 (m, 2H), δ 7.86 (t, 2H, $J = 6$ Hz), δ 7.81 (t, 1H, $J = 6.4$ Hz, NH), δ 7.46-7.22 (m, 14H, $J = 5.2$ Hz), δ 6.72 (d, 1H, $J = 7.6$ Hz, NH), δ 6.67 (d, 1H, $J = 7.6$ Hz), δ 9.53 (d, 1H, $J = 5.2$ Hz), δ 5.24-5.00 (m, 6H), δ 4.53-4.44 (m, 4H), δ 4.28-4.16 (m, 2H), δ 3.87-3.74 (m, 4H), δ 1.75-1.45 (m, 8H), δ 0.97-0.85 (m, 12H); IR (KBr) ν_{\max} (cm^{-1}) 3360, 3117, 3087, 3064, 3034, 2957, 2871, 2269, 1719, 1687, 1605, 1524, 1468, 1449, 1389, 1366, 1316, 1246, 1057, 769, 743, 732, 698; ESMS calculated for $\text{C}_{68}\text{H}_{74}\text{F}_4\text{N}_{10}\text{O}_8\text{BRu}$ (M^+) 1347.5, found 1347.9; UV-vis $\lambda_{\max} = 284$ nm ($\epsilon = 50,600 \text{ M}^{-1}\text{cm}^{-1}$) and 418 nm ($\epsilon = 9,810 \text{ M}^{-1}\text{cm}^{-1}$); Anal. Calculated for $\text{C}_{68}\text{H}_{74}\text{F}_8\text{N}_{10}\text{O}_{12}\text{B}_2\text{Ru}$ (**63**· 4 H_2O): C, 54.23; H, 5.49; N, 9.30. Found: C, 54.39; H, 5.22; N, 9.20.

2.5.3 Stability of **62** and **63**.

Solutions of **62** or **63** in 0.1 M pH 6.5 phosphate buffer (1.0% DMSO) were monitored by UV-Vis spectroscopy for 24 h. Ln A was plotted vs. time and the line was fit to give a first order reaction rate constant $k_{\text{obs}} = 1.0 \times 10^{-6} \text{ s}^{-1}$, corresponding to a half-life > 8.0 days ($t_{1/2} = -0.693/k_{\text{obs}}$) for **62** and $k_{\text{obs}} = 5.0 \times 10^{-9} \text{ s}^{-1}$ ($t_{1/2} > 1800$ days) for **63**.

2.5.4 Photochemical quantum yields.

Photosubstitution quantum yields were determined using ferrioxalate actinometry as previously described in detail.¹⁶⁸ A 150 W Xe lamp in a Milliarc compact arc lamp housing and powered by a PTI model LPS-220 power supply was used in the steady-state photolysis experiments; the wavelength of the light reaching the sample was controlled with colored glass long-pass and band-pass filters (Newport).

2.5.5 Cell assays and imaging.

The live-cell cathepsin K activity staining assays were performed following a method described previously.¹⁵³ Briefly, bone marrow macrophages (BMMs) were derived from FVBN mice as previously described and cultured on sterile petri dishes in MEM α media (Sigma) containing 20% fetal bovine serum (FBS) and 30% L929-conditioned media¹⁶⁹ as the source of macrophage colony stimulating factor (M-CSF). After 96 hours, cells had differentiated into BMMs, were washed with PBS (phosphate buffered saline), and gently scraped using osteoclast media (MEM α media containing 10% FBS, 10 ng/ml M-CSF (R&D Systems), and 10 ng/ml RANKL (R&D Systems)). Roughly 5×10^5 cells were plated per well into 24-well plates (Corning Costar) on acid-washed glass coverslips (Electron Microscope Sciences) re-treated after 48 hours, and cultured for additional 48 hours until visible osteoclasts are formed. For cathepsin inhibition assays, cells were incubated for 30 min at 37 °C with 200 μ L of reaction buffer (0.2 M sodium acetate, pH 6.0, 0.1 mM EDTA and 0.125 mM BME) containing **60**, **62**, or *cis*-[Ru(bpy)₂(MeCN)₂](PF₆)₂ control complex (1-1000 nM, +/- 1mM CA-074-Me, a cathepsin B inhibitor) in 2% DMSO. Cells were then treated with 100 μ L of substrate solution in reaction buffer (0.2 M sodium acetate, pH 6.0, 0.1 mM EDTA, 5% DMSO) containing either 1.0 mM Z-Gly-Pro-Arg-4M β NA or 0.25 mM Z-Leu-Arg-4M β NA (cathepsin K substrates), and 100 μ l of the precipitating agent, 1.0 mM nitrosalicylaldehyde, in reaction buffer. The reaction was allowed to occur for 30 min at 37 °C in the dark. Controls were incubated in the same manner but without substrate (with or without 1.0 μ M CA-074-Me). For assays involving photolysis of **62** or *cis*-[Ru(bpy)₂(MeCN)₂](PF₆)₂ control complex, prior to substrate addition, plates were wrapped in aluminum foil (“dark”) or exposed to visible light (“light”) for 15 min (with gentle shaking of the plate every 2-3 min). Photolysis was conducted with a 250W tungsten halogen

lamp (Osram Xenophot HLX) powered by a 24V power supply, using bandpass and water filters, as described previously.¹⁴⁶ Following the reaction with substrate and precipitating agent, cells were washed with PBS, fixed with 1% formaldehyde for 20 min at RT, washed again, and air-dried. Coverslips were mounted on microscope slides and viewed with a confocal laser-scanning microscope (Zeiss LSM 780) using a 40× oil immersion lens. Each image captured featured a mature osteoclast (minimum of 6 images/treatment). Intensity of green fluorescence per osteoclast area (indicative of the amount of hydrolyzed substrate) was analyzed using ImageJ software (NIH).

2.5.6 Cathepsin K inhibition studies.

Cathepsin enzyme activity was determined from kinetic measurements performed by fluorimetric detection of the hydrolysis product AMC at 37 °C every 2 min for 14 min (8 measures). The excitation and emission wavelengths were 360 and 485 nm respectively. The selective fluorescent substrate Z-Gly-Pro-Arg-AMC was used at a final concentration of 100 μM (obtained from Bachem, Torrance, CA). Enzyme activities are expressed as a percentage, with 100% equal to activity in the absence of inhibitor.

Recombinant cathepsin K (human) was obtained from Enzo Life Sciences (Farmingdale, NY). An 880 nM stock solution was prepared in 50 mM sodium acetate, pH 5.5, 50 mM NaCl, 0.5 mM EDTA and 5 mM DTT and kept at –80 °C. For each experiment the stock solution was diluted 440 times and activated for 15 min at 37 °C with a 400 mM sodium acetate, pH 5.5, 4 mM EDTA, 8 mM DTT assay buffer solution. The inhibitor was prepared as a 1% DMSO solution in the activated enzyme buffer solution and plated (Corning® 96 Well Flat Clear Bottom Black Polystyrene TC-Treated Microplates, 50 μL/well). Three experiments in triplicates (60-63, light or dark) were carried out on the different 96 well plates. The wells containing

“dark” were carefully wrapped in aluminum foil and the light plate was exposed to visible light. The photolysis was conducted for 15 min (**60** and **62**) or 40 min (**61** and **63**) (with gentle shaking of the plate every 2-3 min) using a 250W tungsten halogen lamp (Osram Xenophot HLX) powered by a 24V power supply. The irradiation wavelength was selected by placing a bandpass filter (395 nm cutoff) between the lamp and the sample, along with a 10 cm water cell to absorb infrared light. After photolysis, the reaction was initiated by addition of 50 μL of 200 μM Z-Phe-Arg-AMC solution in the assay buffer (final volume 100 μL , final enzyme concentration 1 nM). Cathepsin enzyme activity was determined from kinetic measurements performed by fluorimetric detection of the hydrolysis product AMC at 37 °C every 2 min for 14 min (8 measures) and MAX RFU slope values used for plotting.

2.5.7 Toxicity (cell viability) studies.

The cell viability of BMM and PC3 prostate carcinoma cells in the presence of **62**, **63** and the control compound *cis*-[Ru(bpy)₂(MeCN)₂](PF₆)₂ were measured using the MTT assay according to the manufacturer’s instructions (Invitrogen, Grand Island, NY). Briefly, the cells were grown in a 96 well plate for 48 h. After removing the media, the cells were treated with 50 μL solutions of **62**, **63** or *cis*-[Ru(bpy)₂(MeCN)₂](PF₆)₂ in the appropriate culture media and incubated for 30 min at 37 °C. The media was then removed, and the cells were washed 3 times and left in PBS buffer. The “dark” plate was wrapped in aluminum foil while the “light” plate was exposed to visible light. The photolysis was conducted for 15 min (with gentle shaking of the plate every 2-3 min) using a 250W tungsten halogen lamp (Osram Xenophot HLX) powered by a 24V power supply, using bandpass and water filters, as described previously. The cells were washed 6 times with PBS buffer. New media was then added and the cells were incubated for 24 h or 72 h in the dark under a 5% CO₂ atmosphere and 37 °C. After the incubation time, the media

was removed and 100 μL of new media was added. 10 μL of a 12 mM MTT stock solution (5 mg of MTT dissolved in 1.0 mL of sterile PBS) was then added to each well. The cells were covered and incubated for 4 h. A negative control consisting of 10 μL of stock MTT solution added to 100 μL media in empty wells was also prepared. 85 μL was then removed from each well and was replaced by 50 μL of DMSO, and thoroughly mixed. Absorbance measurements at 540 nm were collected on a microplate reader. Cell viabilities were expressed as a percentage, with 100% equal to activity in the absence of **62**, **63** and the control compound *cis*- $[\text{Ru}(\text{bpy})_2(\text{MeCN})_2](\text{PF}_6)_2$.

CHAPTER 3. IMAGING INHIBITION OF CATHEPSIN B ACTIVITY IN REAL-TIME IN SITU 3D MAME CULTURES

3.1 Introduction

Light can be controlled both spatially and temporally with great precision and can be used in numerous therapeutic applications.² One such application is cleavage of photocages that leads to targeted release of small molecules. Photocages, which release biologically active agents upon irradiation with light, can be used to garner spatial and temporal control over biological activity.^{42,148,149} This method is being explored for basic research applications *in vitro* and *in vivo*.¹⁷⁰ Photocaging also shows great potential in photochemotherapy, where therapeutically relevant compounds are released only in a desired location, reducing off target reactivity.⁵³ Amongst the numerous metal-based protecting groups, Ru(bpy)₂ has been widely used, due to its excellent visible light absorption and photoreactivity, to allow release of neurotransmitters,^{36,38,40,150,152} cytotoxic agents⁴⁷ and nitrile-based cysteine protease inhibitors.^{146,171}

The major focus of this dissertation is to develop Ru-based photocages for numerous biological applications. Initially we have utilized photocages for achieving spatio-temporal control over inhibition of cathepsin K. We have shown that nitrile-based CTSK enzyme inhibitors can be neutralized using Ru(bpy)₂ protecting group which can be photoactivated using light. To broaden the scope of photocages against proteases, we wanted to develop new caged inhibitors for other cathepsin enzymes.

Cathepsin B is one of the lysosomal proteases belonging to the papain family. These proteases, under normal physiological conditions, are tightly regulated by complex signaling pathways at multiple levels.¹⁷² In numerous pathological and oncogenic processes, aberrant CTSB activity has been reported. Cathepsin B has been causally linked to progression and

metastasis of numerous tumors. Studies have shown that aberrant CTSB activity leads to numerous cancers such as brain, prostate, lung and breast cancers.^{100,102,107,114,145} Cathepsin B plays an important role in tumor progression by degrading the extracellular matrix.¹¹¹ Apart from acting as a scavenger and neuro-protector, CTSB helps in maintenance of physiological functions under normal conditions.¹⁷³⁻¹⁷⁵ Although CTSB can be a viable target for chemotherapy, enzyme inhibition in normal cells could lead to serious side effects. Therefore, site-specific enzyme inhibition would be useful. This chapter is aimed at developing ruthenium-caged CTSB enzyme inhibitors as tools to achieve enzyme inhibition in specific locations, which could not be done using normal small molecule CTSB inhibitors.

In the previous chapters, we have shown that photocaged cathepsin inhibitors can be used in enzyme inhibition against purified enzymes and in tumor cells using 2D models. The tumor microenvironment, which is much more complex, has a major role in modulating the metastatic capacity of most cancers.¹⁷⁶ The *in vivo* characteristics of the tumor microenvironment are not represented in studies using purified enzymes or cancer cells cultured in two-dimensional (2D) monolayers. In contrast, three-dimensional (3D) cell cultures take into consideration interactions of cells with the extracellular matrix (ECM), cell polarity and cell-to-cell contacts, providing a more accurate context for evaluating compound activity and protease inhibition.¹⁷⁷⁻¹⁷⁹ Here we show the importance of studying enzyme inhibition using two distinct approaches (2D and 3D cell culture models), which demonstrates the value of evaluating compounds in more advanced cell culture models.

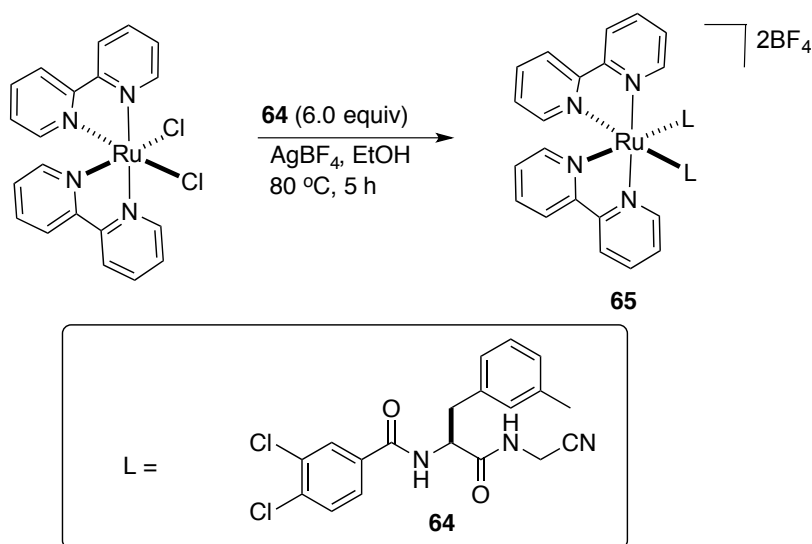
Herein, we describe inhibition of CTSB by a dipeptidyl nitrile-based inhibitor caged using a Ru(bpy)₂ fragment. We used a photoactivation strategy against activity assays of purified enzyme, human TNBC (triple negative breast cancer) cell lysates and live-cell proteolysis assay

of TNBC cell lines grown in 3D MAME (mammary architecture and microenvironment engineering) cultures.^{180,181} In MAME cultures, TNBC cells form structures resembling *in vivo* tumors¹⁸² and the live-cell proteolysis assay developed by the Sloane laboratory allows one to visualize, localize and quantify proteolysis in real time.¹⁸³ The ability to quantify and monitor with respect to time the proteolytic degradation of ECM (extracellular matrix) proteins by living tumor cells is important in designing protease inhibitors that will be efficacious in cancers.^{183,184} For the first time we demonstrate that photoactivation of a caged CTSB inhibitor can block proteolysis at the surface of living cancer cells. Living breast cancer cells grown in 3D MAME models used for the study recapitulate the *in vivo* microenvironment of human breast tumors.^{180,181}

3.2 Results and discussions

3.2.1 Synthesis and characterization of $[\text{Ru}(\text{bpy})_2(\text{L})_2](\text{BF}_4)_2$ (**65**)

Dipeptidyl nitrile **64** was chosen for caging in this study, because it was identified previously as a potent, selective and reversible inhibitor of recombinant human cathepsin B expressed in baculovirus (Scheme 7).¹³¹ Caging of inhibitor **64** was accomplished by treating **64** (6.0 equiv) with *cis*- $[\text{Ru}(\text{bpy})_2\text{Cl}_2]$ (1.0 equiv), and AgBF_4 (4.0 equiv) in EtOH at 80 °C, resulting in a color change from violet to orange. Cooling of the crude reaction mixture to -20 °C, followed by filtration and concentration gave crude **65**, which was obtained as the major ruthenium-based product, as judged by ¹H NMR spectroscopic analysis. Compound **65** was purified further by multiple cycles of stirring with diethyl ether to remove unreacted **65**, precipitation from a solution of acetone by diethyl ether vapor diffusion, treatment with QuadraSil® MP (a thiol-based Ag-scavenging silica gel) and washing with EtOAc and Et₂O, which provided **65** as a hydrate salt in an analytically pure form.



Scheme 7: Synthesis of ruthenium-based CTSB inhibitor **65** and structure of **64**

Caged inhibitor **65** was characterized by ^1H NMR, IR and UV-Vis spectroscopies, mass spectrometry and elemental analysis. Spectroscopic data were consistent with **65** being isolated as a 1:1 mixture of Δ - and Λ stereoisomers, consistent with other previously synthesized complexes.^{146,171} This was expected because *cis*-[Ru(bpy)₂Cl₂] was used as a racemic mixture of Δ - and Λ stereoisomers. The IR spectrum of **65** shows a ν_{CN} stretch at 2278 cm^{-1} , diagnostic of nitrile-binding to Ru(II). The electrospray ionization mass spectrum of **65** shows prominent peaks at $m/z = 1281.2$, along with a suitable isotopic pattern, consistent with a monocation of the formula [Ru(bpy)₂(**64**)₂](BF₄)⁺. The electronic absorption spectrum of **65** is highly consistent with other dications of the general formula *cis*-[Ru(bpy)₂(RCN)₂]²⁺, where RCN is MeCN, 5-cyanouracil, and protease inhibitors structurally related to **64**.^{42,148} Data for **65** in water containing 2 % acetone show a maximum at 420 nm ($\epsilon = 10,360 \text{ M}^{-1}\text{cm}^{-1}$) assigned to a singlet metal-to-ligand charge transfer ($^1\text{MLCT}$) transition.

3.2.2 Stability and photolysis of $[\text{Ru}(\text{bpy})_2(\text{L})_2](\text{BF}_4)_2$ (**65**)

The half-life for **65** in the dark was determined spectrophotometrically using the rate constant for decomposition, obtained from the slope of a $\ln A$ vs. t graph in DMSO ($k_{\text{obs}} = 1.6 \pm 0.1 \times 10^{-7} \text{ s}^{-1}$) and in phosphate buffered saline (PBS, pH 6.5, $k_{\text{obs}} = 1.2 \pm 0.1 \times 10^{-6} \text{ s}^{-1}$) as described previously,^{146,171} to be ~ 70 and ~ 10 days, respectively at $293 \pm 2 \text{ K}$.

The photochemical reactivity of ruthenium-caged complex **65** was evaluated by monitoring the changes to the electronic absorption spectrum of the complex as a function of irradiation time ($\lambda_{\text{irr}} \geq 395 \text{ nm}$) in a 2 % acetone aqueous solution (Figure 22). The Turro group performed the photolysis studies and quantum yield calculations for complex **65**. The changes to the absorption spectrum of **2** are consistent with those of the related $[\text{Ru}(\text{bpy})_2(\text{L})_2]^{2+}$ complexes.^{47,75,146,171} A decrease of the reactant ¹MLCT transition at 412 nm and evolution of a new transition at 446 nm at early irradiation times (up to 3 min) can be assigned as arising from the photoinduced substitution of one nitrile ligand, **64**, by a solvent H_2O molecule to form a mono-aqua intermediate, $[\text{Ru}(\text{bpy})_2(\text{64})(\text{H}_2\text{O})]^{2+}$ (I). This process exhibits an isosbestic point at 427 nm indicative that consumption of the reactant is directly correlated to intermediate formation. Further irradiation up to 15 min results in formation of the bis-aqua product, $[\text{Ru}(\text{bpy})_2(\text{H}_2\text{O})_2]^{2+}$ (P) via substitution of the remaining **64** ligand with H_2O . This process is indicated by a decrease of the peak of the intermediate at 446 nm, the appearance of a new transition at 487 nm, and isosbestic points at 383 and 460 nm. The quantum yield of ligand exchange for the first step, reactant R to intermediate I ($\Phi_{\text{R} \rightarrow \text{I}}$) was determined to be 0.026(4), while the second step, from intermediate I to product P ($\Phi_{\text{I} \rightarrow \text{P}}$) was measured to be 0.0045(9) in water ($\lambda_{\text{irr}} = 400 \text{ nm}$). The relatively low quantum yield values can be attributed to the low solubility of **64** in H_2O , such that following photoinduced nitrile dissociation, the ligand does not

exit the solvent cage efficiently and recombines with the pentacoordinate ruthenium fragment to regenerate the starting material. Because **64** is more soluble in acetone, the photosubstitution reaction was repeated in an acetone solution containing 0.25 M tetrabutylammonium chloride (TBACl). In this system, irradiation of **65** forms the intermediate $[\text{Ru}(\text{bpy})_2(\mathbf{64})\text{Cl}]^+$ followed by a second ligand substitution to form $[\text{Ru}(\text{bpy})_2\text{Cl}_2]$. The quantum yields in this solvent are greatly enhanced, with $\Phi_{\text{R}\rightarrow\text{I}}$ and $\Phi_{\text{I}\rightarrow\text{P}}$ of 0.056(9) and 0.032, respectively. This experiment clearly shows that increasing the water solubility of the nitrile inhibitor can enhance ligand exchange quantum yields of caged compounds, such as **65**.

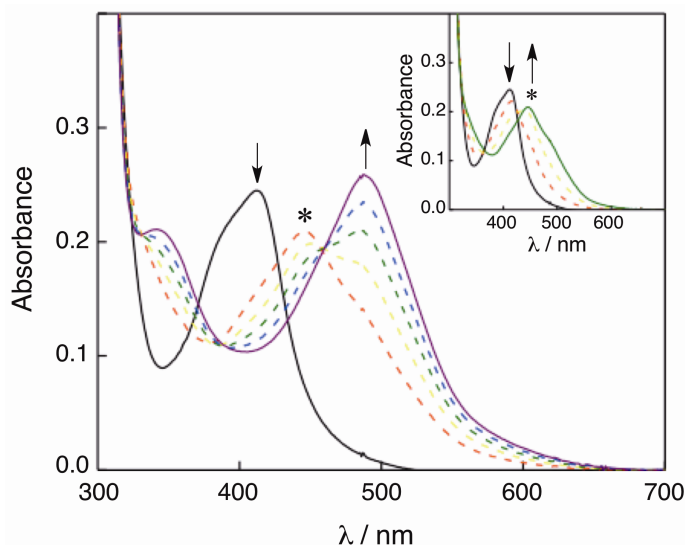


Figure 22: Changes to the electronic absorption of **65** (25 μm) in a 2 % acetone aqueous solution at irradiation times, t_{irr} , of 0, 3, 5, 7, 10, and 15 min ($\lambda_{\text{irr}} \geq 395$ nm); the * denotes the mono-aqua intermediate. Inset: $t_{\text{irr}} = 0.0, 0.5, 1.5,$ and 3.0 min.

3.2.3 Evaluation of **64** and **65** on purified CTSB and breast tumor cell lysates

The dipeptidyl nitrile cathepsin B inhibitor (**64**) and its caged version $[\text{Ru}(\text{bpy})_2(\mathbf{64})_2](\text{BF}_4)_2$ (**65**) were evaluated against CTSB purified from human liver and IC_{50} values were determined by the Sloane group. Compound **64** showed IC_{50} value of 0.33 μM ,

consistent with literature data reported for inhibition of recombinant human cathepsin B expressed in baculovirus.¹³¹ The IC_{50} values for the caged variant **65** under light ($\lambda_{irr} > 395$ nm) vs. dark conditions were 0.28 and 3.4 μ M, respectively, corresponding to a dark/light IC_{50} ratio of 12 (Table 1). As expected, caged **65** became more active under irradiation than in the dark, consistent with the dissociation of the dipeptidyl nitrile molecules from the ruthenium photocage. The potency of the uncaged **64** was very similar to that of **65** under light, i.e., 0.33 and 0.28 μ M, respectively. The strong similarity between the IC_{50} values for the uncaged and caged inhibitors in light could be related to the lower efficiency for the release of the second molecule of inhibitor from **65** (evident from its low $\Phi_{I \rightarrow P}$), as shown previously for caged inhibitors of cathepsin K.^{146,171}

We evaluated the ability of compounds **64** and **65** to inhibit proteolytic activity in lysates of two TNBC cell lines grown in monolayer cultures on plastic dishes: MDA-MB-231 and Hs578T. The substrate used was Z-Arg-Arg-AMC, a substrate that under the conditions of our assay is highly selective for CTSB.^{182,185} In MDA-MB-231 cell lysates the photocaged compound **65** was significantly more potent when irradiated than it was in the dark with a dark/light ratio of 80 (Table 1). Similar results were obtained with Hs578T cell lysates although the dark/light ratio was lower, which was 13. Besides the fact that both cell lines are TNBC, they present different behavior and express different amount of proteases, which could be related with the higher ratio for MDA-MB-231 cell lysates. The IC_{50} values for inhibitor **64** and for light-activated inhibitor **65** were comparable in each cell line. These analyses of both cell lysates and purified human CTSB confirmed the efficiency of light activation of the photocaged inhibitor.

Experiment	64 (μM)	65 dark (μM)	65 light (μM)	Dark/light ratio
Purified cat B	0.33	3.40	0.28	12
MDA-MB 231 lysate	1.54	126	1.58	80
Hs578T lysate	0.91	11.2	0.89	13

Table 1: IC₅₀ values (μM) for **64** and **65** and dark/light ratio (with and without irradiation) against human cathepsin B, MDA-MB 231 lysate and Hs578T lysate.

3.2.4 3D MAME cell culture assay for Breast Cancer Cell Lines

We tested the ability of the inhibitors to reduce cathepsin B activity in intact human TNBC cells grown in 3D MAME cultures. The Sloane group performed these 3D assays. Studies using 3D human pathomimetic models have demonstrated the importance of evaluating molecular and cellular function in a model that mimics disease progression by approximating organ structure. Such models encompass cell–cell and cell–matrix interactions.^{177,184} According to Schmeichel and Bissell, 3D models have the potential when used for drug screening to identify and validate molecules that will sustain efficacy in clinical trials.¹⁸⁴ We employed a live-cell proteolysis assay developed in the Sloane laboratory¹⁸⁶ in which dye quenched fluorescent proteins are the proteolytic substrates (Figure 23). The fluorescent signal in this gain-of-function assay allows us to localize the site of degradation and is proportional to the proteolytic activity.¹⁸⁶ The protein substrate can be cleaved by many proteases allowing the analysis of proteolytic networks rather than a single protease or protease class as is the case with assays employing selective synthetic small molecule substrates. We grew MDA-MB-231 and Hs578T TNBC breast cancer cells in 3D MAME cultures containing DQ-collagen IV¹⁸² and assessed the formation of degradation products of DQ-collagen IV (green fluorescence) in real-time. We found that the uncaged inhibitor **64** reduced degradation of DQ-collagen IV (Figure 23A and B). Quantification of the intensity of fluorescent degradation products per cell in the entire 3D

volume of TNBC structures revealed significantly less degradation of DQ-collagen IV in the presence of uncaged inhibitor **64** (Figure 23C). As a positive control, we confirmed that a mixture of highly selective cathepsin B inhibitors (CA-074 and CA-074Me)¹⁸⁷ resulted in a reduction in degradation of DQ-collagen IV comparable to that observed with uncaged inhibitor **64** (Figure 23). In breast carcinoma cells, cysteine cathepsins degrade collagen IV and this process can be suppressed by selective cysteine cathepsin inhibitors CA-074 and CA-074Me, described as non-permeable and cell permeable, respectively. CA-074Me can also inhibit cathepsin L activity,¹⁸⁷ which is considered a target for treatment of cancer.¹⁸⁸

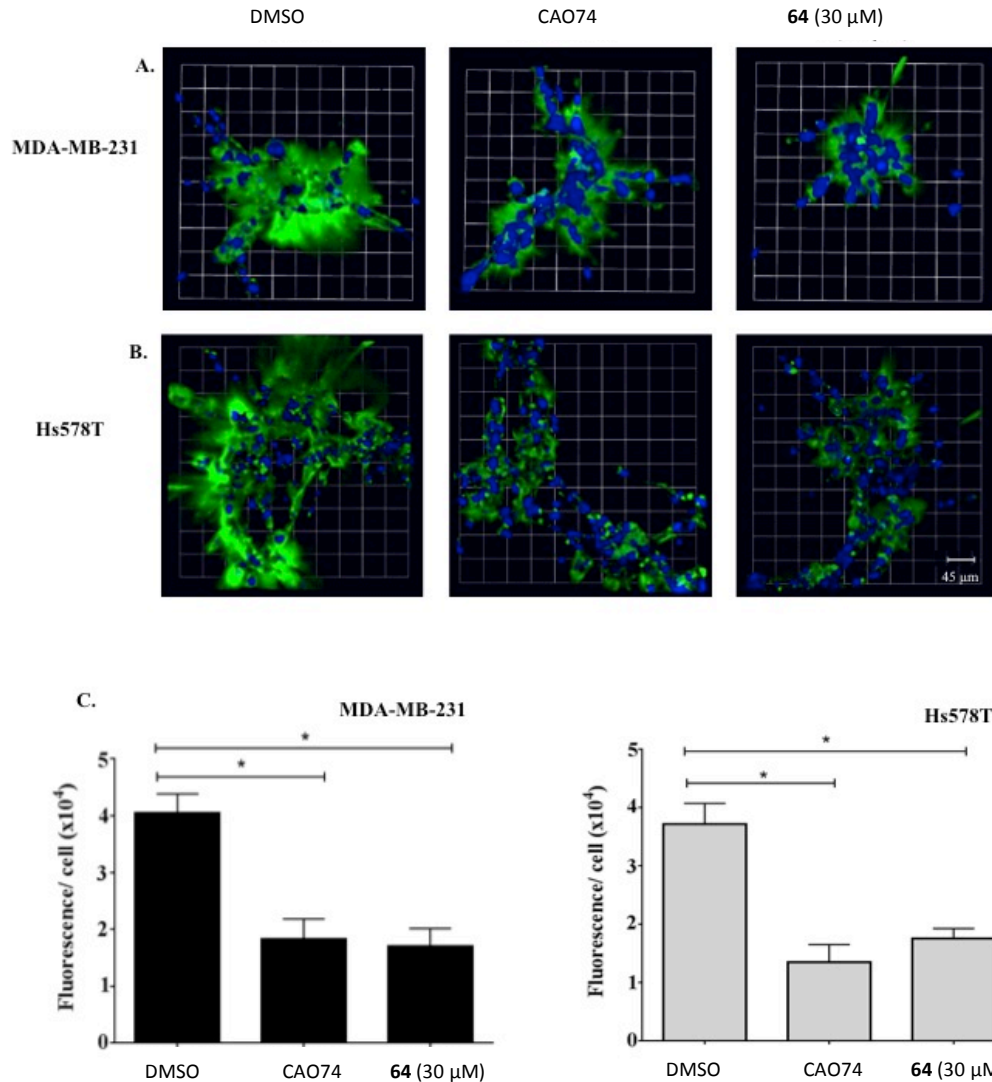


Figure 23. The uncaged inhibitor **64** (30 μM) reduces degradation of DQ-collagen IV (green) by MAME cultures of MDA-MB-231 (A) and Hs578T (B) breast carcinoma cells. Top views at 4 days of culture were reconstructed in 3D with Volocity software from optical sections of 16 contiguous fields acquired on a Zeiss LSM780. Fluorescent intensity per cell (C) was quantified in the entire volume; nuclei were stained with Hoechst 33342 (blue) at the time of imaging and counted. DMSO and CA-074/CA-074Me (5 μM each) are negative and positive controls, respectively. Data shown are from 3 independent experiments; * ≤ 0.05; mean ± SD

In cancers, the cellular localization of cathepsin B is often altered such that the enzyme is redistributed to the cell surface or secreted rather than being in lysosomes.^{83,92,99} Processes associated with malignancy such as acidosis accelerate this redistribution and result in increases

in pericellular proteolysis. Thus, when assessing the efficacy of protease inhibitors it is important to determine the site at which a protease is inhibited.^{114,182} This is an advantage of the live-cell proteolysis assay used here, i.e., degradation fragments can be localized to pericellular or intracellular compartments.^{182,186,189} This allowed us to determine potential differences in the ability of the uncaged inhibitor **64** to reduce total, pericellular or intracellular proteolysis by the MDA-MB-231 and Hs578T 3D MAME cultures. We observed significant reductions in total proteolysis and pericellular proteolysis, but not in intracellular proteolysis, in the presence of the uncaged inhibitor **64** and comparable results with highly selective cathepsin B inhibitors (Figure 24). These results are consistent with the uncaged inhibitor **64** acting through inhibition of pericellular cathepsin B.

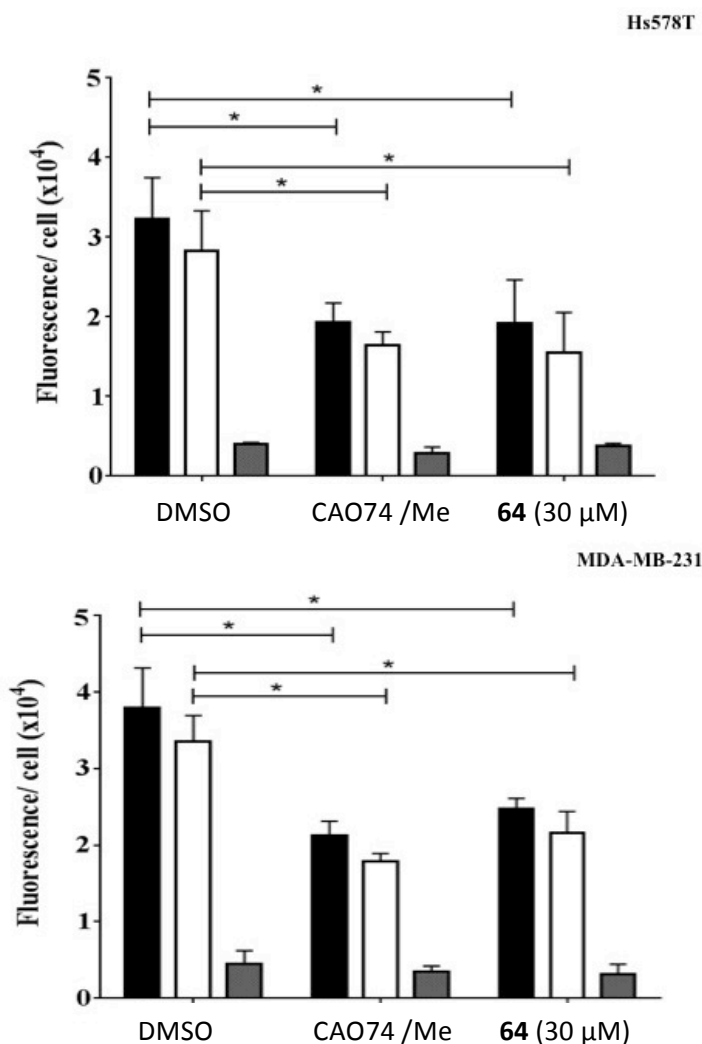


Figure 24: The uncaged inhibitor **64** (30 μM) reduces total and pericellular degradation, but not intracellular degradation of DQ-collagen IV by 3D MAME cultures of MDA-MB-231 and Hs578T breast carcinoma cells imaged at 4 days of culture. Quantification of total proteolytic fragments (black bars) and segmentation into pericellular (open bars) and intracellular (gray bars) fragments were performed by image arithmetic in Volocity software. DMSO was used as negative control and CA-074/CA-074Me (5 μM each) were used as positive controls. Data shown are from 3 independent experiments; * $p < 0.05$; mean \pm SD.

In order to prove the efficacy of the caging strategy, the caged compound **65**, a light-activated enzyme inhibitor, was evaluated in live-cell proteolysis assays in the dark and the light (Figure 25). At a concentration of 1 μM , photoactivated compound **65** significantly reduced the degradation of DQ-collagen IV (green fluorescence) in 3D MAME cultures of TNBC cells

exposed to visible light. Initially the assay was carried out with higher concentrations of compound **65**; however, significant inhibition of proteolysis was observed in the dark (data not shown). Reducing the concentration of compound **65** resulted in an increase in the dark/light ratio. Inhibition by **65** in the dark likely indicates that inhibitor **64** is partially released over the timescale of the experiment (4 days), consistent with the shorter half-life of **65** ($t_{1/2} \sim 10$ days) as compared to other $\text{Ru}^{\text{II}}(\text{bpy})_2$ caged inhibitors we have examined thus far.^{146,171} Therefore, further optimization of the caging group and/or inhibitor may be necessary to achieve higher dark to light ratios in these assays. Nonetheless, the live-cell proteolysis assay demonstrated that the caged inhibitor was more potent than the uncaged inhibitor and can be used at a much lower concentration, an advantage for use of the caged inhibitor *in vivo*.

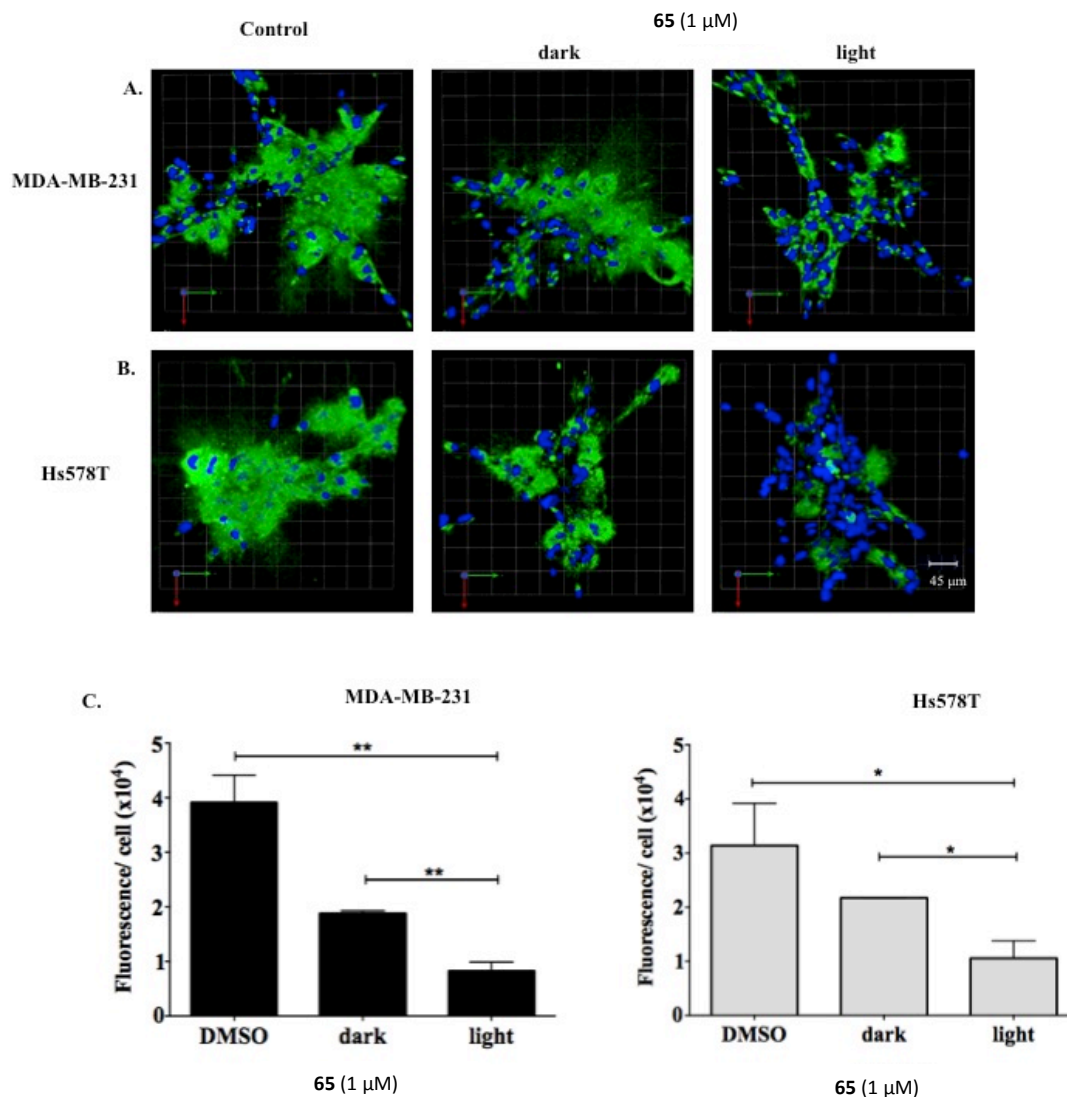


Figure 25. The caged inhibitor **65** (ruthenium-caged compound, 1 μM) when uncaged by light exposure reduces degradation of DQ-collagen IV (*green*) by MAME cultures of MDA-MB-231 and Hs578T breast carcinoma cells. Structures treated with **65** were incubated in the dark (no irradiation) or light ($\lambda_{\text{irr}} = 395\text{-}750\text{ nm}$) for 45 min. Top views at 4 days of culture were reconstructed in 3D. Fluorescent intensity per cell (C) was quantified in the entire volume; nuclei were stained with Hoechst 33342 (*blue*) at the time of imaging and counted. DMSO was used as a negative control. Data shown are from 3 independent experiments; * $p \leq 0.05$; ** $p \leq 0.005$; mean \pm SD.

Having established that caged inhibitor **65** was able to block proteolysis in a light activated fashion, experiments with only the ruthenium caging group, i.e., *cis*- $[\text{Ru}(\text{bpy})_2(\text{MeCN})_2](\text{PF}_6)_2$, were carried out in the absence and presence of light to determine the

ability of *cis*-[Ru(bpy)₂(MeCN)₂](PF₆)₂ to reduce proteolysis. Control experiments on 3D MAME cultures with a 1 μM concentration of inhibitor under light vs. dark conditions proved that *cis*-[Ru(bpy)₂(MeCN)₂](PF₆)₂ did not inhibit proteolysis (Figure 26A and B) as no differences on fluorescence were observed in the images. Furthermore, quantification established that the amount of green fluorescence per cell was the same as in the vehicle control (1% DMSO) (Figure 26C). Previous studies had described the successful use of caged-ruthenium compounds of the inhibitory neurotransmitter GABA³⁷ and a cathepsin K inhibitor.^{146,171} We did not observe any toxicity of compound **65** as determined by cell viability assays of MDA-MB-231 and Hs578T 3D MAME cultures in the dark or the light. Our results are consistent with data from the literature demonstrating that the caging fragment Ru(bpy)₂ does not exhibit side effects or toxicity.^{38,146,171}

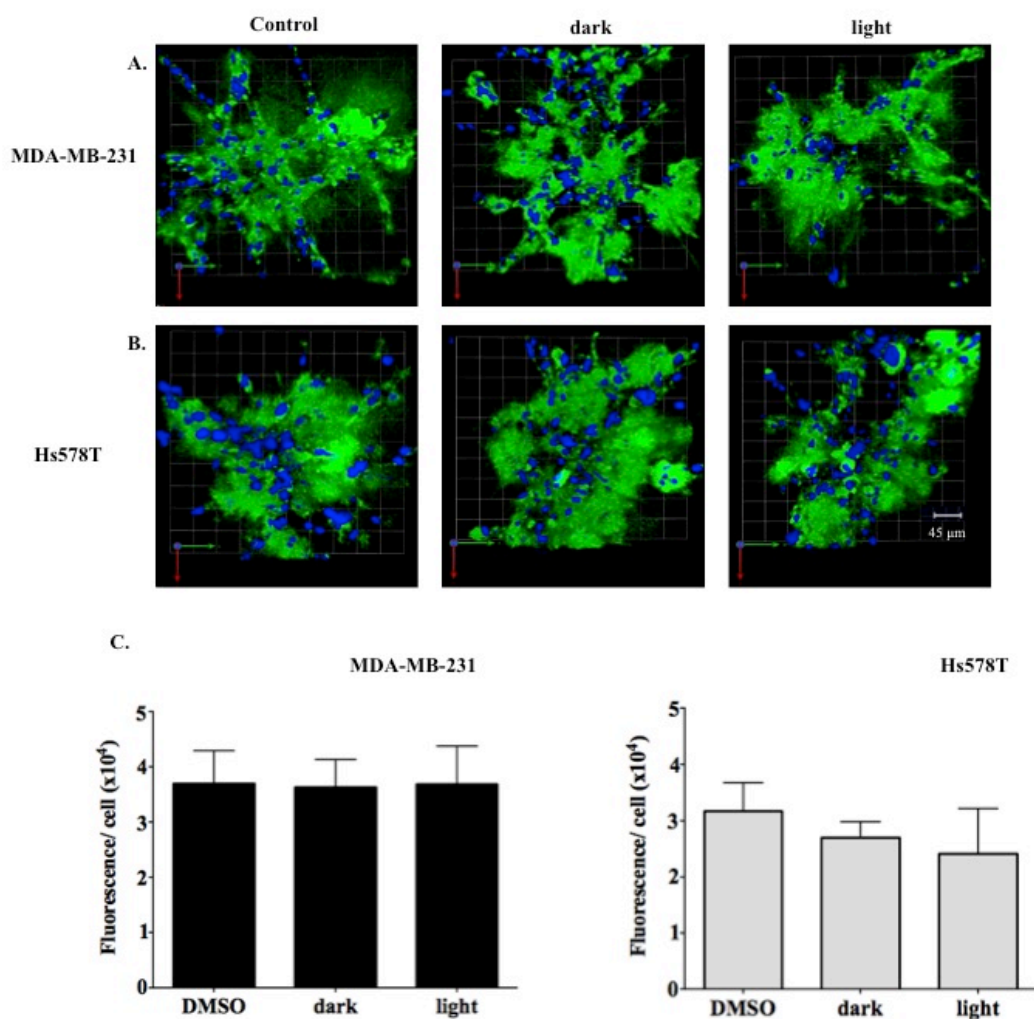


Figure 26. The ruthenium complex $cis\text{-}[\text{Ru}(\text{bpy})_2(\text{MeCN})_2](\text{PF}_6)_2$ used to cage the inhibitor did not affect degradation of DQ-collagen IV (green) by 3D MAME cultures of MDA-MB-231 and Hs578T breast carcinoma cells. Top views at 4 days of culture were reconstructed in 3D. Structures were incubated in the dark (no irradiation) and light ($\lambda_{\text{irr}} = 395\text{-}750\text{ nm}$) for 45 min. Fluorescent intensity per cell (C) was quantified in the entire volume; nuclei were stained with Hoechst 33342 (blue) at the time of imaging and counted. DMSO was used as a negative control. Data shown are from 3 independent experiments; mean \pm SD.

3.3 Discussions and Conclusions

Cathepsin B, one of the most abundant cysteine cathepsins, is upregulated in breast and other cancers and considered to be an attractive molecular target for cancer therapy. Though a potential chemotherapy target, no small molecule CTSB inhibitor has been FDA approved due to many off target toxicity profiles. Here we report the successful application of a photoactivated cathepsin B inhibitor (**65**) to block proteolysis not only in 2D assays but also in live-cell assays of 3D MAME TNBC models, which offer a unique system for dynamic imaging of proteolysis. These models mimic the *in vivo* microenvironment of human breast cancers and allow us to visualize, localize and quantify collagen IV degradation in real time. Our data indicate that compound **64** is as effective as the highly selective cathepsin B inhibitor CA-074 at blocking pericellular proteolysis. Positive results were also obtained in activity assays of purified cathepsin B and lysates of the 3D MAME TNBC models. These data also provide evidence that the ruthenium caging strategy can be used to garner control over inhibition with light. Although further optimization of caged inhibitors will be necessary to afford compounds with high stability and better dark to light ratios, our complexes were not toxic and the caging group did not inhibit proteolysis. Importantly, this example serves as a prototype for development of biochemical tools for further analysis of proteases in cancer and clinically relevant, photoactivated inhibitors of cathepsin B with red-shifted absorbance to facilitate tissue penetration by low energy light for *in vivo* applications. Also, by increasing our understanding of the role played by ECM components in the tumor microenvironment and their potential impact on protease inhibition, we can provide more reliable and better data for further assays. This is the first report to demonstrate proteolysis inhibition of TNBC cell lines grown in 3D MAME models by a strategy using photoactivation of a caged CTSB inhibitor.

3.4 Experimental procedures

3.4.1 Cathepsin B activity assay

Purified human liver cathepsin B was purchased from Athens Research & Technology (Athens, GA, USA). The enzyme activity was determined from kinetic measurements performed by fluorimetric detection of the hydrolysis product AMC at 37 °C for 30 min at one-minute intervals using a Tecan SpectraFluor Plus plate-reader. The excitation and emission wavelengths were 360 and 485 nm, respectively. The fluorescent substrate Z-Arg-Arg-AMC (Bachem, Torrance, CA, USA) was used at a final concentration of 150 μ M.

The enzyme was activated for 15 minutes with activator buffer (100 μ l) containing 5 mM EDTA, 10 mM DTT (pH 5.2) at 37 °C. The sample (1 μ l) was added and the reaction mixtures were conducted during 45 min under dark (no irradiation) and light (irradiation at 250 W, 395-750 nm) conditions with a tungsten halogen lamp and H₂O filter on separate plated. The plate containing dark compound was wrapped in aluminum foil, and the other plate was exposed to visible light for the same time period. The irradiation wavelength was selected by placing a 395 long-pass filter between the lamp and the sample, along with a 10 cm water cell to absorb infrared light. After photolysis, the reaction was initiated by addition of 200 μ l of assay buffer (0.6 mM CaCl₂, 0.6 mM MgCl₂, 25 mM piperazin-N-N'-bis[2-ethanosulfonic acid] (disodium salt)), pH 7.3 containing 150 μ M Z-Arg-Arg-AMC substrate solution. Enzyme concentration was 10 nM. The experiments were carried out in triplicate in 96-well flat bottom black plates at pH 6.0. Enzyme activities are expressed as a percentage, with 100% equal to activity in the absence of inhibitor. IC₅₀ values were determined by plotting percent activity vs. log (inhibitor concentration).

3.4.2 Inhibition of cellular cathepsin activity.

Cell lines purchased from American type culture collection (Rockville, MD, USA) were cultured in basal medium supplemented with 10 % fetal bovine serum (MDA-MB-231, DMEM; Hs578T, DMEM + 10 $\mu\text{g/ml}$ bovine insulin). To prepare cell lysates, cells were grown on 100 mm dishes to ~80 % confluency, washed twice with PBS (phosphate buffered saline), scraped and lysed in SME buffer (250 mM sucrose, 25 mM MES, 1 mM EDTA, pH 6.5, and 0.1 % Triton X-100) and then sonicated on ice three times for 10 sec each. Cathepsin B activity was measured as previously described.¹⁸⁵ Briefly, 50 μl of cell lysate was incubated with 300 μl of activator buffer (5 mM EDTA, 10 mM DTT (pH 5.2) at 37 °C during 15 min. The sample (1 μl) was added to 100 μl of the activator buffer containing cell lysate and the reaction mixtures were conducted during 45 min under dark (no irradiation) and light (irradiation at 250 W, 395-750 nm) conditions with a tungsten halogen lamp and H₂O filter on separate plates as described above. The experiments were carried out in triplicate (on 96-well flat bottom black plates) at pH 6.0.

3.4.3 Live-cell proteolysis assay.

Proteolytic cleavage of DQ-collagen IV substrate (Invitrogen, Carlsbad, CA, USA) by live TNBC cells was imaged in real time and quantified as previously described.^{186,190,191} Briefly, glass coverslips were coated with 50 μl of 16.4 mg/ml Cultrex™ containing 25 $\mu\text{g/ml}$ DQ-collagen IV and incubated for 15 min at 37 °C to solidify. TNBC cells (1.0×10^4) were seeded onto coated glass coverslips and incubated for 60 min. Medium containing 2 % Cultrex™ was added to the cells. The sample was added every 48 h. After 4 days of culture, proteolysis of DQ-collagen IV (green fluorescence) was observed in live cells with a Zeiss LSM 780 confocal

microscope with a 20X water immersion objective. Where indicated, assays were performed in the presence of CA-074 and CA-074Me (5 μ M each) (Peptides International, Louisville, KY, USA), compound **64** or compound **65**.

For experiments with the caged inhibitor, cells were exposed to dark (no irradiation) and light (irradiation at 250 W, 395-750 nm) conditions for 45 min with a tungsten halogen lamp and H₂O filter on separate plates. After 4 day of culture, optical sections through the entire depth of the 3D structures were acquired on a confocal microscope, reconstructed in 3D and quantified using Volocity software.

3.4.4 Cell viability assay.

3D cultures of TNBC cells were established, grown and treated with compound **65** as described above. After 4 days, a cell viability assay was performed to assess the cytotoxic effects of compound **65**. The assay has two components: Calcein AM that fluoresces green when cleaved by intracellular esterases, thereby labeling live cells, and Ethidium Homodimer-1 that fluoresces red when incorporated in the DNA of dead cells. A solution of 4 μ M Ethidium Homodimer-1 and 2 μ M Calcein AM was prepared in sterile PBS. Cultures were incubated for 30 minutes at 37 °C, washed once with warm PBS and replenished with warm MEGM media for live cell imaging. The samples were then imaged at 10X magnification using a Zeiss 510 META confocal microscope. Tiled 16-panel images and z-stacks through the depth of structures were captured. The images were processed to show top views using Volocity software. Statistics were performed using the data analysis package within GraphPad Prism 6.0 (GraphPad Software, San Diego, CA, USA). Unless otherwise stated, tests comparing two means are Student's t-test, with equal variance assumed.

3.4.5 Synthesis of Δ - and Λ -cis-[Ru(bpy)₂(**64**)₂](BF₄)₂ (**65**):

In the glove box, a sealable tube was charged with *cis*-Ru(bpy)₂Cl₂ (0.062 mmol, 30 mg), AgBF₄ (0.24 mmol, 47.9 mg) and (S)-3,4-dichloro-N-(1-((cyanomethyl)amino)-1-oxo-3-(*m*-tolyl)propan-2-yl)benzamide¹³¹ (**64**) (0.37 mmol, 145.3 mg) and freshly distilled EtOH (15 mL). The resulting solution was wrapped in aluminum foil and refluxed for 6 h during which time it turned from dark violet to bright orange. After cooling the crude solution to RT, it was placed in the freezer at -20 °C for 16 h. The precipitated silver salts were filtered off using celite and the filter cake was washed with cold EtOH (190 proof). The solvents were removed under reduced pressure and the crude mixture was analyzed by ¹H NMR spectroscopy. The resulting yellow solid was dissolved in acetone (2 mL) and layered with Et₂O (10 mL) and placed in the freezer at -20 °C for 16 h. The solution was decanted, and the solid was suspended in acetone (5 mL), then treated with Ag-scavenging silica gel (QuadraSil® MP, 20 mg). After 15 min, the suspension was filtered and the solution was concentrated. The resulting solid was stirred with EtOAc (15 mL) for 4 h. The orange solid was centrifuged and the resulting filtered cake was washed with Et₂O (3 ×15 mL) and dried under reduced pressure to give the title compound **65** as a yellow solid in analytically pure form as a hydrate salt (47 mg, 55 %). Mp = 178 °C (decomp); ¹H NMR (400MHz C₃D₆O) δ 9.51 (m, 2H), 8.79-8.75 (m, 2H), 8.66 (d, 2H, J = 8.4 Hz), 8.37-8.20 (m, 6H), 8.08 (t, 2H, J = 7.2 Hz), 7.89-7.70 (m, 8H), 7.62-7.61(m, 2H), 7.41-7.40 (m, 2H), 7.12-7.06 (m, 6H), 6.98 (t, 2H, J = 7.2 Hz), 4.80-4.75 (m, 2H), 4.58-4.55 (m, 1H), 4.47-4.44 (m, 3H), 3.21-3.18 (m, 2H), 3.07-3.00 (m, 2H), 2.22 (s, 3H), 2.19 (s, 3H); IR (KBr) ν_{\max} (cm⁻¹) 3618, 3567, 3374, 3083, 2921, 2278, 1664, 1606, 1591, 1526, 1467, 1447, 1426, 1379, 1340, 1312, 1276, 1242, 1161, 1125, 1009, 1062, 1032, 895, 834, 767, 731, 701, 675. ESMS calculated for C₅₈H₅₀BCl₄F₄N₁₀O₄Ru (M⁺¹ **65**-BF₄) 1281.18, found 1281.23; UV-Vis λ_{\max} = 420 nm (ϵ = 10,360

$M^{-1}cm^{-1}$); Anal. Calculated for $C_{58}H_{60}B_2Cl_4F_8N_{10}O_9Ru$ (**65**·5H₂O): C, 47.79; H, 4.15; N, 9.61. Found: C, 47.45; H, 4.20; N, 9.62, water content was confirmed by ¹H NMR spectroscopy.

3.4.6 Photoinduced ligand exchange.

Electronic absorption spectra were measured with a Hewlett-Packard 8453 diode array spectrophotometer. The ligand exchange quantum yield experiments were performed with a 150 W Xe arc lamp (USHIO) in a Milliarc lamp housing unit with an LPS-220 power supply and an LPS-221 igniter (PTI). A bandpass filter (Thorlabs) and long-pass filter (CVI Melles Griot) were used to select the appropriate irradiation wavelengths.

The photolysis experiments were performed in H₂O with 2 % acetone and in an acetone solution containing 0.25 M tetrabutylammonium chloride (TBACl) in a 1 × 1 cm quartz cuvette, and the irradiation wavelengths were selected with a 395 nm long-pass filter. The photon flux of the arc lamp with a 335 nm long-pass filter and a 400 nm bandpass filter was determined to be $4.30 \pm 0.25 \times 10^{-8}$ mol photons/min by ferrioxalate actinometry as previously described in detail.¹⁶⁸ The quantum yields (Φ) for ligand dissociation of **65** were determined in each of the solvent systems in a 1 × 1 cm quartz cuvette. The decrease in the MLCT absorption maximum of the reactant with $\epsilon = 10,360 M^{-1}cm^{-1}$ at 412 nm as a function of time was monitored at early irradiation times to calculate the rate of moles of reactant converted to intermediate, I. The increase of the MLCT absorption maximum of the product at 490 nm ($\epsilon = 9,300 M^{-1}cm^{-1}$)¹⁵⁸ was monitored at irradiation times after the formation of the intermediate to determine the rate of moles of product P formed. These rates along with the photon flux were used to calculate the quantum yields for the first and second steps, $\Phi_{R \rightarrow I}$ and $\Phi_{I \rightarrow P}$, respectively.

CHAPTER 4. CAGED NITRILE-BASED CA-074 ANALOG FOR INHIBITION OF CATHEPSIN B ACTIVITY

4.1 Introduction

Proteases play a dynamic role in tumor invasion and metastasis.¹⁸⁰ The role of proteases in tumors changes with the type of tumor and also by stages of tumor growth. The interactions of normal cells with cancer cells also have an effect on protease expression.^{85,192,193} Cathepsin B, one of the eleven-cysteine proteases found in humans, is an intracellular lysosomal protease. CTSB acts as both an exo- and endo-peptidase and is associated with the degradation and processing of proteins.^{194,195} Normal functions of CTSB include antigen processing, apoptosis and proenzyme activation.¹⁹⁶ Aberrant CTSB activity is related to numerous human diseases such as tumors, neurodegenerative disorders and rheumatoid arthritis.^{197,198} Thus, CTSB is considered as an important therapeutic target in tumors, arthritic conditions and other pathological disease states.

Specific inhibitors of CTSB would serve as a powerful tool in studying their role in cancer, and in this context numerous research articles are dedicated towards developing selective inhibitors of CTSB.^{102,106,107,114,131,132,138,145,199,200} A new type of irreversible inhibitor of cysteine proteases i.e. E-64 was first reported in 1977.²⁰¹ E-64 is a thiol protease inhibitor consisting of an active *trans*-epoxysuccinyl moiety, which selectively binds to an active thiol group found in many cysteine proteases, generating a thioether bond.²⁰² But E-64 and its derivatives lack selectivity both *in vitro* and *in vivo* among different types of cathepsins. For developing selective CTSB inhibitors, X-ray structure analysis of cathepsin enzymes and a cathepsin-E-64 complex showed that *L-trans*-epoxy-succinic acid group is useful for distinguishing cathepsin B from other relative enzymes.¹⁹⁹ Based on this study, CA-074 (**43** Figure 11, Chapter 1) (N-(L-3*trans*-propylcarbamoyloxirane-2-carbonyl)-L-isoleucyl-L-proline), a selective CTSB inhibitor, was

developed.¹⁹⁹ CA-074 showed an IC_{50} value of 2.24 nM for cathepsin B and the relative IC_{50} ratio for cathepsin B: L: H was 1: 77000: 188000.¹⁹⁹ As stated in the previous chapters, CA-074, like other cathepsin inhibitors, lacks the ability to specifically target cathepsin activity in the tumor microenvironment and cannot be used as therapeutic agent. So new compounds may be useful for specific delivery of CA-074 in the tumor region.

Controlled delivery of drugs can be achieved by using one of the numerous external stimulation methods.⁴³ Photoexcitation is one such method where light is used as external stimulation for controlled cleavage of prodrugs. Photocaging provides a unique mechanism that allows control over drug release. Numerous photolabile molecules based on organic and inorganic caging groups are routinely developed and used for biomedical release applications.^{43,203,204} In the previous chapters we have caged numerous nitrile based cathepsin inhibitors and we envisioned that a nitrile-based analog of CA-074 (**66**) (Figure 27) could be used in photocaging application using $Ru(bpy)_2$ caging groups. The nitrile functionality was not introduced as a warhead towards CTSB; instead it was a molecular replacement for the methyl group that can be used for caging applications.

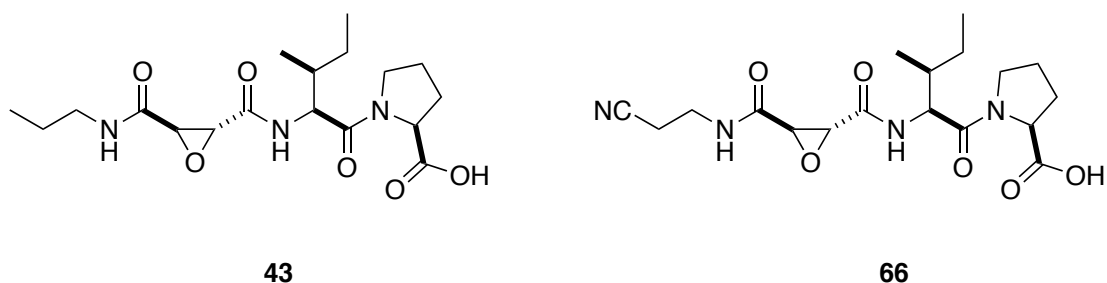
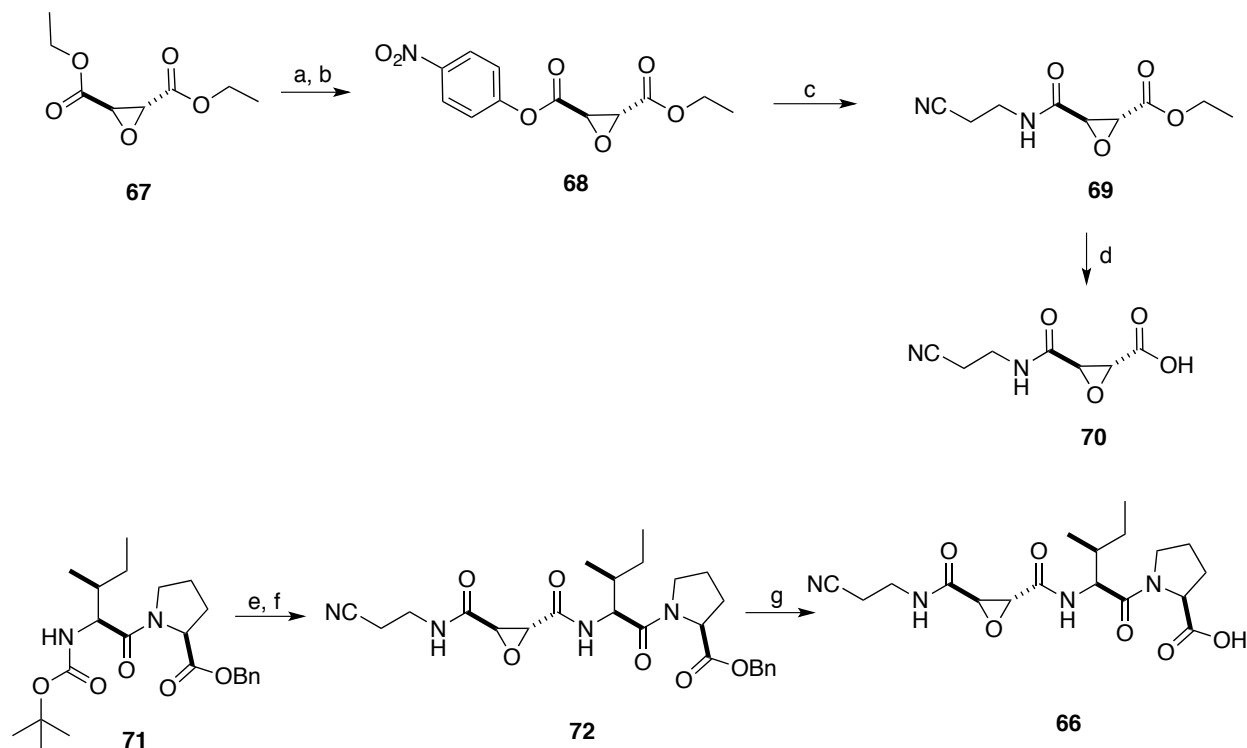


Figure 27: Structure of CA-074 (**43**) and its corresponding nitrile-based analog (**66**).

4.2 Results and discussions

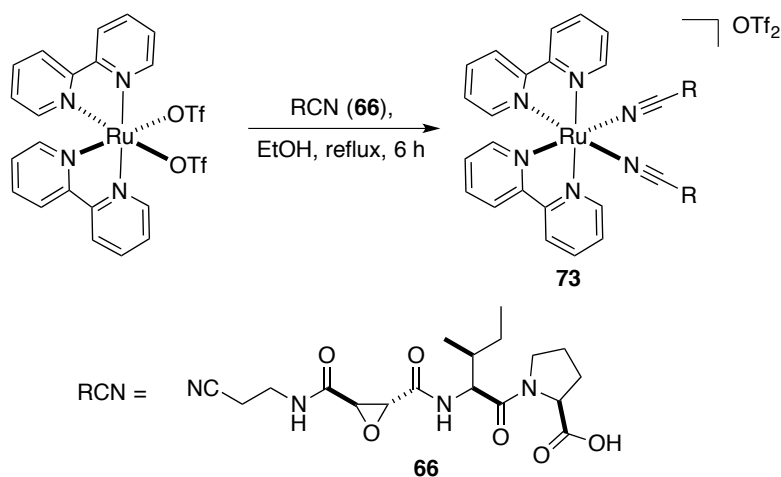
4.2.1 Synthesis of nitrile-based CA-074 analog (**66**) and its Ru(bpy)₂ caged complex (**73**)

Conditions: a) KOH, EtOH, RT, ON; b) *p*-nitrophenol, DCC, EtOAc, RT, ON; c) 3-aminopropionitrile, DCM, RT, 2 h; d) KOH, EtOH, THF, 3 h; e) TFA, DCM, RT, ON; f) **70**, HBTU, DIPEA, DMF, 0 °C, RT; g) LiOH, MeOH, THF, 0 °C, 5 h

Scheme 8: Synthesis of nitrile-based analog of CA-074 (**66**)

Synthesis of **66** started from a diester (**67**), which was synthesized from *D*-Tartaric acid using a literature protocol.²¹⁴ The diester was then converted into the activated ester (**68**) in 2 steps using standard KOH saponification followed by DCC coupling. The activated ester was reacted with 3-aminopropionitrile to give an amide compound (**69**). The ethyl ester of **69** was cleaved using KOH saponification to give the free acid (**70**). Boc-Ile-Pro-OBn²⁰⁵ **71** was subjected to Boc-deprotection using a 1:1 mixture of TFA: DCM. The formed free amine was

used without further purification and was coupled with **70** using HBTU to give compound **72**, which upon LiOH saponification gave the final nitrile-based analog **66** (Scheme 8).



Scheme 9: Synthesis of $Ru(bpy)_2$ -based caged complex (**73**).

Complex **73** was synthesized as an orange solid by refluxing $[Ru(bpy)_2(OTf)_2]^{206}$ in EtOH in the presence of 6 equiv. of the nitrile-based CA-074 analog **66** (Scheme 9). The reaction mixture was cooled to room temperature and concentrated under reduced pressure to obtain an orange solid. Spectroscopic analysis of the crude reaction mixture confirmed that **66** was bound to ruthenium with high conversion, as there was no metal-based byproducts. To remove excess of **66** and purify the complex, the crude product was washed with ethyl acetate and diethyl ether multiple times. Subsequent precipitation (layering) from acetone and diethyl ether, followed by drying in vacuum, gave the caged inhibitor **73** in pure form. Caged inhibitor **73** was characterized by 1H NMR, IR and UV-Vis spectroscopies and mass spectrometry. Spectroscopic data were consistent with **73** being isolated as a 1:1 mixture of Δ - and Λ stereoisomers; consistent with other previously synthesized complexes.^{146,171} The IR spectrum of **73** shows a ν_{CN} stretch at 2278 cm^{-1} , diagnostic of nitrile binding to Ru(II). The electrospray ionization mass spectrum of **73** shows prominent peaks at $m/z = 1201.3$, along with a suitable isotopic pattern,

consistent with a monocation of the formula $[M -(\text{HOTf} + \text{OTf})]^+$. The electronic absorption spectrum of **73** is highly consistent with other dications of the general formula $\text{cis-}[\text{Ru}(\text{bpy})_2(\text{RCN})_2]^{2+}$, where RCN is MeCN, 5-cyanouracil, and protease inhibitors structurally related to **73**.^{42,148} Data for **73** in water containing 2 % acetone show a maximum at 423 nm ($\epsilon = 9,800 \text{ M}^{-1}\text{cm}^{-1}$) assigned to a singlet metal-to-ligand charge transfer ($^1\text{MLCT}$) transition.

4.2.2 Stability and photolysis of $[\text{Ru}(\text{bpy})_2(\mathbf{66})_2](\text{OTf})_2$ (**73**)

The half-life for **73** in the dark was determined spectrophotometrically using the rate constant for decomposition, obtained from the slope of a $\ln A$ vs. t graph in DMSO ($k_{\text{obs}} = 1.6 \pm 0.1 \times 10^{-7} \text{ s}^{-1}$) and in phosphate buffered saline (PBS, pH 6.5, $k_{\text{obs}} = 7.5 \pm 0.1 \times 10^{-7} \text{ s}^{-1}$) as described previously,^{146,171} to be ~ 50 and ~ 11 days, respectively at $293 \pm 2 \text{ K}$.

The photochemical reactivity of the ruthenium-caged complex **73** was evaluated by monitoring the changes to the electronic absorption spectrum of the complex as a function of irradiation time ($\lambda_{\text{irr}} \geq 395 \text{ nm}$) in a 2 % acetone aqueous solution (Figure 28). The changes to the absorption spectrum of **73** are consistent with those of the related $[\text{Ru}(\text{bpy})_2(\text{L})_2]^{2+}$ complexes.^{47,75,146,171} A decrease of the reactant $^1\text{MLCT}$ transition at 410 nm and evolution of a new transition at 446 nm at early irradiation times (up to 3 min) can be assigned as arising from the photoinduced substitution of one nitrile ligand, **66**, by a solvent H_2O molecule to form a mono-aqua intermediate, $[\text{Ru}(\text{bpy})_2(\mathbf{66})(\text{H}_2\text{O})]^{2+}$ (I). This process exhibits an isosbestic point at 427 nm indicative that consumption of the reactant is directly correlated to intermediate formation. Further irradiation up to 15 min results in formation of the bis-aqua product, $[\text{Ru}(\text{bpy})_2(\text{H}_2\text{O})_2]^{2+}$ (P) via substitution of the remaining **66** ligand with H_2O . This process is indicated by a decrease of the peak of the intermediate at 446 nm, the appearance of a new transition at 487 nm, and isosbestic points at 383 and 460 nm. The quantum yield of ligand

exchange for the first step, reactant R to intermediate I ($\Phi_{R \rightarrow I}$) and second step i.e., from intermediate I to product P ($\Phi_{I \rightarrow P}$) will be measured by the Turro group.

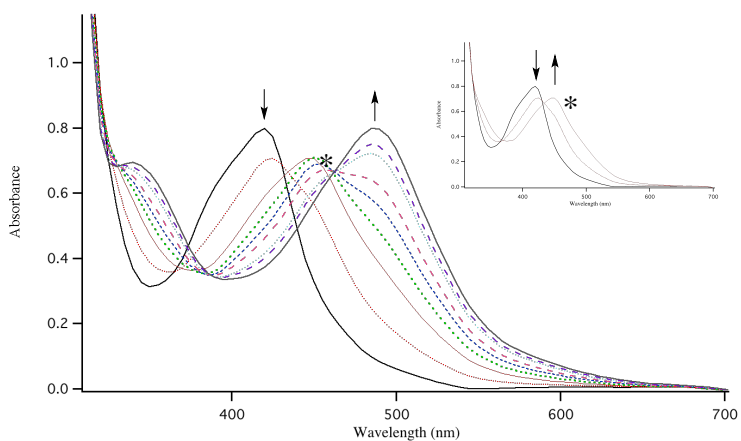


Figure 28: Changes to the electronic absorption of **73** in a 2 % acetone aqueous solution at irradiation times, t_{irr} , of 0, 1, 3, 5, 7, 10, and 15 min ($\lambda_{\text{irr}} \geq 395$ nm); the * denotes the mono-aqua intermediate. Inset: $t_{\text{irr}} = 0, 1,$ and 3 min.

4.2.3 Isolated CTSB enzyme inhibition by **66** and **73**.

Compound **66** acts as a potent CTSB inhibitor and complex **73** acts as a potent, photoactivated inhibitor of human cathepsin B. IC_{50} values were determined for **66** and **73** under dark and light conditions and upon irradiation with >395 nm light (Figure 29).

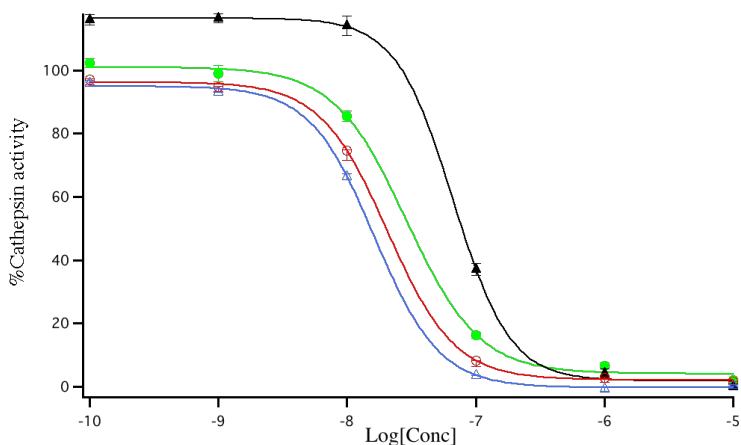


Figure 29: IC_{50} curves for ruthenium-caged inhibitor **73** (blue with irradiation and black without) and uncaged inhibitor **66** (red with irradiation and green without) against human cathepsin B.

Enzyme inhibition for **73** was enhanced by a factor of 5 upon exposure to light with IC_{50} values of 15 nM and 78 nM, for light and dark conditions respectively. In contrast, inhibition by the free inhibitor **66** was identical under light and dark conditions, 21 nM and 30 nM, respectively; confirming that irradiation with 395 nm light has no effect on inhibition under the assay conditions.

4.3 Discussions and conclusions

Cathepsin B, one of the most abundant cysteine cathepsins, is upregulated in numerous diseases and is considered to be an attractive molecular target for cancer therapy.¹⁰⁶ Though a potential chemotherapy target, no small molecule CTSB inhibitor such as CA-074 has been FDA approved due to many off target toxicity profiles. Thus new methods for drug delivery are needed for selective inhibition of enzymes in specific locations. Here we report the synthesis of a new nitrile-based CA-074 analog (**66**) and its corresponding $Ru(bpy)_2$ caged complex which could be used for light activated inhibition of CTSB. Upon 15 min of visible light irradiation (>395 nm) the caged complex **73** releases 2 molecules of **66**. Our data indicate that enzyme inhibition decreased by 7 fold upon introduction of nitrile group in CA-074 with the IC_{50} values of 3 nM and 21 nM for **43** and **66** respectively. Also a 5-fold increase of enzyme inhibition was observed when light was used for photoactivation of complex **73** with IC_{50} values of 15 nM and 78 nM under light and dark respectively. The stability data of complex **73** and the previously performed SAR studies on CA-074 and its analogs¹⁹⁹ indicate that complex **73** can itself act as CTSB inhibitor leading to high enzyme inhibition even in the dark conditions. New analogs of **43** and new caging groups for **66** should be developed for reducing the enzyme inhibition by the caged complex in dark.

4.3 Experimental procedures

4.4.1 Synthesis of CA-O74 analog (**66**)

Compound **68** (4.20 g, 14.9 mmol) was dissolved in DCM (80 mL) at RT and to the flask 3-aminopropionitrile (1.56 g, 22.4 mmol) was added dropwise over a period of 15 min. The reaction mixture was stirred for an additional 2 h at RT and then concentrated under reduced pressure to give crude yellow oil. The compound was then purified by silica gel flash chromatography ($R_f = 0.4$ with 50% EtOAc:Hexane) to give **69** as a white solid (2.8 g, 91%). M.p = 128 °C; ^1H NMR (400 MHz, Chloroform-*d*) δ 6.60 (s, 1H), 4.35-4.18 (m, 2H), 3.73-3.42 (m, 4H), 2.74-2.53 (m, 2H), 1.37-1.26 (m, 3H). ^{13}C NMR (400 MHz, Chloroform-*d*) δ 166.0, 166.3, 117.5, 62.5, 53.7, 53.0, 35.1, 18.2, 14.0. HRMS calculated for $(\text{M}+\text{Na})^+$ 235.0695, found 235.0696.

Compound **69** (2.6 g, 12.3 mmol) was subjected to saponification. Compound **69** was dissolved in THF (25 mL) and EtOH (13 mL) at 0 °C. To this a suspension of KOH (0.69 g, 12.6 mmol) in EtOH (12 mL) was added dropwise and the reaction mixture was allowed to stir at 0 °C for an additional 1 h. The reaction mixture was then concentrated under reduced pressure, dissolved in water (30 mL) and acidified to pH 3 using 1M HCl solution. The aqueous layer was then extracted with EtOAc (3 \times 30 mL) and the combined organic layer was dried over Na_2SO_4 and concentrated under reduced pressure to give compound **70** as a white solid which was used without further purification.

In a flask, compound **71**²⁰⁵ (1.3 g, 3.1 mmol) was dissolved in DCM (2.4 mL) at RT and to this TFA (2.4 mL, 3.54 g, 31.1 mmol) was added slowly and reaction mixture was stirred overnight. The reaction mixture was concentrated under reduced pressure to give the corresponding free amine as a colorless oil which was used without further purification and was

dissolved in DMF (30 mL) at 0 °C under inert atmosphere. To the flask, compound **70** (0.6 g, 3.1 mmol), HBTU (1.4 g, 3.7 mmol) and DIPEA (0.8 g, 6.2 mmol) was added and stirred for 12 h at 0 °C. The reaction mixture was diluted with EtOAc (300 mL) and the organic layer was washed with 10% NH₄Cl (2 × 100 mL), 10% NaHCO₃ (2 × 100 mL), water (2 × 100 mL) and brine (2 × 100 mL). The organic layer was dried over Na₂SO₄ and concentrated under reduced pressure to obtain the crude compound as a colorless oil. The crude was purified by silica gel flash chromatography ($R_f = 0.45$ in 100% EtOAc) to give compound **72** as a colorless oil (1.0 g, 64%). ¹H NMR (400 MHz, Chloroform-*d*) δ 7.39-7.32 (m, 5H), 7.05 (t, $J = 6.2$ Hz, 1H), 5.21-5.08 (m, 2H), 4.60 (t, $J = 8.8$ Hz, 1H), 4.51-4.47 (m, 1H), 3.88-3.82 (m, 1H), 3.70-3.60 (m, 1H), 3.61-3.36 (m, 4H), 2.62-2.51 (m, 2H), 2.26-2.22 (m, 1H), 2.05-1.93 (m, 3H), 1.82 (d, $J = 11.4$ Hz, 2H), 1.51-1.41 (m, 1H), 1.11-1.03 (m, 1H), 0.92 (d, $J = 6.7$ Hz, 3H), 0.84 (t, 3H). ¹³C NMR (400 MHz, Chloroform-*d*) δ 171.5, 170.6, 166.9, 165.5, 135.3, 128.6, 128.5, 128.3, 117.6, 77.2, 67.0, 59.2, 54.7, 54.5, 47.6, 45.1, 37.5, 35.1, 29.1, 28.5, 24.8, 24.5, 17.9, 14.9, 10.8. HRMS calculated for (M+Na)⁺ 507.2220, found 507.2216.

Compound **72** (1.0 g, 2.1 mmol) was dissolved in THF (10 mL) MeOH (10 mL) at 0 °C and to this LiOH (0.25 g, 10.3 mmol) aqueous solution (10 mL) was added dropwise over a period of 30 min and the reaction mixture was allowed to stir at 0 °C for an additional 5 h. The reaction mixture was then concentrated under reduced pressure and diluted with water (50 mL). The aqueous layer was acidified to pH = 3 using a 10% KHSO₄ solution and extracted with EtOAc (3 × 50 mL). The combined organic layer was dried over Na₂SO₄ and concentrated under reduced pressure to give a colorless oil which was purified using silica gel flash chromatography ($R_f = 0.3$ with 90:9:1 DCM:MeOH:AcOH) to give the compound **66** as a colorless oil (0.60 g, 74 %). ¹H NMR (400 MHz, Chloroform-*d*) δ 9.49 (s, 1H), 7.85 (d, $J = 8.9$ Hz, 1H), 7.30 (t, $J = 6.2$

Hz, 1H), 4.60 (t, $J = 8.8$ Hz, 1H), 4.54-4.42 (m, 1H), 3.92-3.86 (m, 1H), 3.73-3.59 (m, 3H), 3.54-3.45 (m, 2H), 2.68-2.56 (m, 2H), 2.30-2.21 (m, 1H), 1.85-1.81 (m, 1H), 1.55-1.43 (m, 1H), 1.14-1.03 (m, 1H), 0.96 (d, $J = 6.7$ Hz, 3H), 0.84 (t, $J = 7.3$ Hz, 3H). ^{13}C NMR (101 MHz, Chloroform-*d*) δ 176.74, 175.32, 171.19, 167.38, 166.16, 117.96, 59.31, 54.89, 54.43, 54.24, 47.84, 37.27, 35.27, 28.94, 24.87, 24.52, 20.80, 17.98, 14.90, 10.76. HRMS calculated for $(\text{M}+\text{Na})^+$ 417.1750, found 417.1764.

4.4.2. Synthesis of caged complex **73**

In the glove box, a sealable tube was charged with *cis*-Ru(bpy)₂(OTf)₂ (0.042 mmol, 30 mg), and **66** (0.252 mmol, 99.6 mg) and freshly distilled EtOH (15 mL). The resulting solution was wrapped in aluminum foil and refluxed for 6 h during which time it turned from dark red to bright orange. After cooling the crude solution to RT, the solvents were removed under reduced pressure and the crude mixture was analyzed by ^1H NMR spectroscopy. The resulting yellow solid was dissolved in acetone (2 mL) and layered with Et₂O (10 mL) and placed in the freezer at -20 °C for 16 h. The solution was decanted the resulting solid was stirred with EtOAc (15 mL) for 4 h. The orange solid was centrifuged and the resulting filter cake was washed with Et₂O (3 \times 15 mL) and dried under reduced pressure to give the title compound **73** as a yellow solid in analytically pure form (31 mg, 49 %). Mp = 184 °C (decomp); ^1H NMR (600 MHz, Acetone-*d*₆) δ 11.14 (s, 1H), 9.53 (d, $J = 5.5$ Hz, 1H), 8.78 (d, $J = 7.9$ Hz, 2H), 8.65 (t, $J = 7.3$ Hz, 2H), 8.10-8.02 (m, 2H), 8.00-7.91 (m, 2H), 7.90 (q, $J = 6.8, 6.1$ Hz, 2H), 7.81 (q, $J = 10.2, 8.1$ Hz, 3H), 7.40 (tdd, $J = 5.9, 4.8, 4.1, 2.5$ Hz, 2H), 4.62 (dt, $J = 21.9, 7.9$ Hz, 1H), 4.48-4.41 (m, 2H), 4.00-3.87 (m, 2H), 3.75-3.63 (m, 3H), 3.60-3.53 (m, 1H), 3.39 (qd, $J = 6.9, 1.6$ Hz, 2H), 3.14-3.06 (m, 2H), 2.26 (q, $J = 12.2, 9.9$ Hz, 2H), 2.08 (d, $J = 1.7$ Hz, 32H), 2.05-1.95 (m, 5H), 1.64 (s, 2H), 1.10 (td, $J = 7.0, 1.6$ Hz, 2H), 1.02 (dd, $J = 8.7, 6.9, 1.7$ Hz, 5H), 0.95-0.83 (m, 5H).; IR (KBr)

ν_{\max} (cm^{-1}) 3618, 3567, 3374, 3083, 2921, 2278, 1664, 1606, 1591, 1526, 1467, 1447, 1426, 1379, 1340, 1312, 1276, 1242, 1161, 1125, 1009, 1062, 1032, 895, 834, 767, 731, 701, 675. ESMS calculated for $\text{C}_{56}\text{H}_{67}\text{N}_{12}\text{O}_{12}\text{Ru}$ $[\text{M} - (\text{HOTf} + \text{OTf})]^+$ 1201.40, found 1201.3; UV-Vis λ_{\max} = 423 nm ($\epsilon = 9,800 \text{ M}^{-1}\text{cm}^{-1}$).

4.4.3 Isolated CTSB enzyme inhibition by **66** and **73**

Purified human cathepsin B was purchased from Athens Research & Technology (Athens, GA, USA). Cathepsin enzyme activity was determined from kinetic measurements performed by fluorimetric detection of the hydrolysis product AMC at 37 °C every 2 min for 14 min (8 measures). The excitation and emission wavelengths were 360 and 485 nm respectively. The selective fluorescent substrate Z-Arg-Arg-AMC was used at a final concentration of 100 μM (obtained from Bachem, Torrance, CA). Enzyme activities are expressed as a percentage, with 100% equal to activity in the absence of inhibitor.

Recombinant cathepsin B (human) was obtained from Enzo Life Sciences (Farmingdale, NY). For each experiment the stock solution 5 μM was diluted 625 times and activated for 15 min at 37 °C with a 400 mM sodium acetate, pH 5.5, 4 mM EDTA, 8 mM DTT assay buffer solution. The inhibitor was prepared as a 1% DMSO solution in the buffer solution (400 mM sodium acetate, pH 5.5, 4 mM EDTA, 0.01 % Triton X -100) and plated (Corning® 96 Well Flat Clear Bottom Black Polystyrene TC-Treated Microplates, 50 μL /well). Three experiments in triplicates (**66** and **73**, light or dark) were carried out on the different 96 well plates. The wells containing “dark” were carefully wrapped in aluminum foil for 15 min and the light plate was exposed to 365 nm light (8W) for the same time period. The photolysis was conducted for 15 min (with gentle shaking of the plate every 2-3 min) using a 250W tungsten halogen lamp (Osram Xenophot HLX) powered by a 24V power supply, using bandpass and water filters, as

described in the previous chapters. Both the plates were then left in dark for additional 30 min as the inhibitor is irreversible inhibitor. After photolysis, the reaction was initiated by addition of 50 μL of 200 μM Z-Arg-Arg-AMC solution in the assay buffer (final volume 100 μL , final enzyme concentration 2 nM). Cathepsin enzyme activity was determined from kinetic measurements performed by fluorimetric detection of the hydrolysis product AMC at 37 °C every 2 min for 14 min (8 measures) and MAX RFU slope values used for plotting.

CHAPTER 5. RUTHENIUM TRIS(2-PYRIDYLMETHYL)AMINE AS AN EFFECTIVE PHOTOCAGING GROUP FOR NITRILES²

5.1 Introduction

Caged small molecules with photolabile groups are being developed as remotely controllable tools for understanding the spatial and temporal aspects of biological activity.¹⁴⁹ Light-activated Ru-based compounds have been used in numerous biological applications. Ruthenium compounds are used both as caging groups for small molecules^{36,37,40,146,151,171} and also as biomolecules. The photodissociation generates open coordination sites on the metal center, which can be used in DNA binding.^{15,77,207} First examples of Ru-caged protease inhibitors are discussed in the previous chapters of this dissertation where we have used Ru(bpy)₂ caging group for nitriles.^{146,171}

Uncaging of metal-based compounds involves two important transformations; i) excitation of the caged molecule by absorption of light and ii) conversion of the ¹MLCT state to a ligand dissociation excited state. Ligand structure plays an important role in both of these steps. Despite numerous applications, ligands used for developing Ru-based photocages have focused mainly on bi- or tri-dentate planar heteroaromatic groups such as bpy or terpy. To date, Ru(bpy)₂ is the most widely used inorganic photolabile protecting group used for caging neurotransmitters,^{38,151} anticancer agents⁴⁷ and enzyme inhibitors.^{146,171} Classical photodissociation of Ru(bpy)₃⁺² and more recent examples of dissociation of bidentate ligands from the Ru-based photocages^{147,208} (Figure 30) guided us in developing ligands of greater denticity to prevent possible *in vivo* photo-degradation of the caging group. Past

² Portions of the text in this chapter were reprinted and adapted with permission from Sharma, R.; Knoll, J. D.; Martin, P. D.; Podgorski, I.; Turro, C.; Kodanko, J. J. *Inorg. Chem.* **2014**, 53, 3273.

research from our group has shown that these tertiary amine-based ligands can be used in peptide ligand conjugates. They can also be attached to drug delivering vectors such as LHRH, where their distribution could also be controlled.^{209,210} Also we wanted to study the effects of ligand structure on the properties of the caged complex.

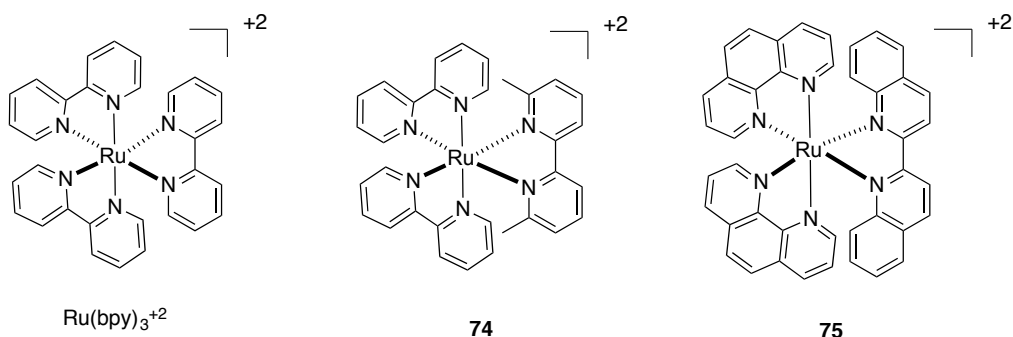


Figure 30: Structures of complexes releasing bidentate ligands on photolysis.

This chapter describes a new caging group Ru(TPA) for caging nitriles distinct from the established Ru(bpy)₂, where we have used a tertiary amine based tetradentate tri(2-pyridylmethyl)amine (TPA) ligand. Two caged nitriles of the general formula [Ru(TPA)(RCN)₂](PF₆)₂ were prepared for this study (Figure 31). The complex [Ru(TPA)(MeCN)₂](PF₆)₂ (**76**) contains two caged MeCN ligands, whereas the complex [Ru(TPA)(**60**)₂](PF₆)₂ (**77**) contains 2 equiv. of the cysteine protease inhibitor Cbz-Leu-NHCH₂CN (**60**), a potent and selective inhibitor of human cathepsin K.¹²⁷

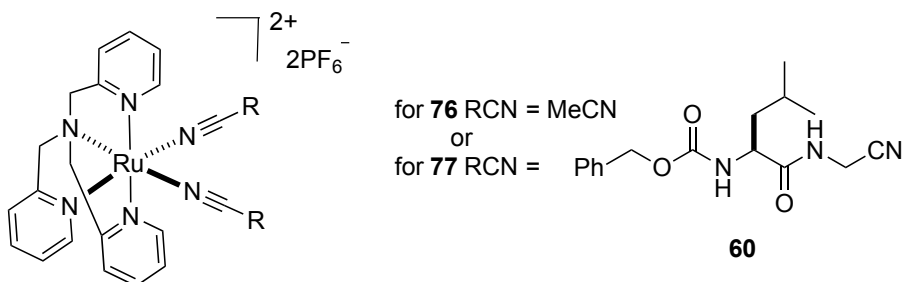
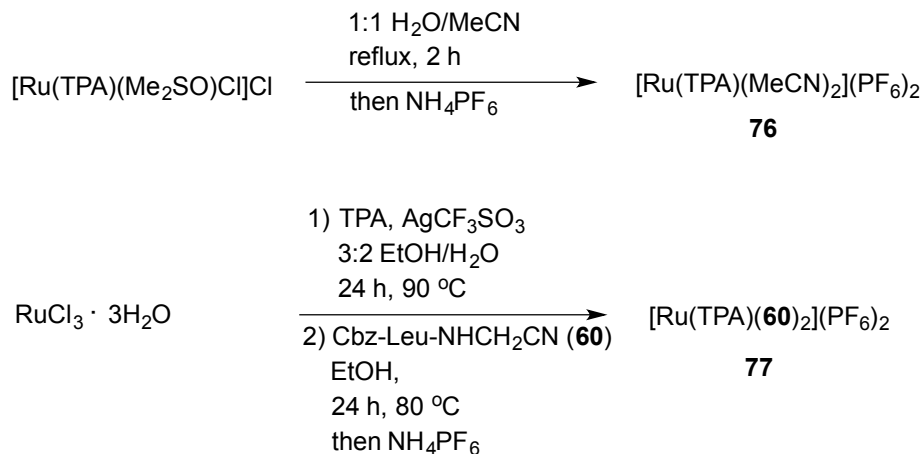


Figure 31: Structures of new nitrile-based Ru(TPA) complexes **76** and **77**.

5.2 Results and discussions

5.2.1 Synthesis and characterization of [Ru(TPA)(RCN)₂](PF₆)₂ (**76** and **77**).**Scheme 10:** Synthesis of nitrile-based Ru(TPA) complexes **76** and **77**.

Complex **76** was synthesized as a yellow solid by heating [Ru(TPA)(Me₂SO)Cl]Cl^{211,212} in 1:1 H₂O/MeCN, followed by precipitation with NH₄PF₆ (Scheme 10). UV-vis spectra of **76** showed peak maxima at 380 nm ($\epsilon = 11,200 \text{ M}^{-1} \text{ cm}^{-1}$) associated with metal-to-ligand charge transfer (MLCT) transition. ¹H NMR spectroscopic analysis indicated the presence of two distinct MeCN ligands, with singlets at 2.88 and 2.47 ppm, separated by approximately 0.4 ppm, consistent with the expected structure with one of the MeCN ligand *trans* to the basic nitrogen and other in *cis* position. IR spectroscopy of complex **76** showed at ν_{CN} stretch at 2276 cm⁻¹ consistent with nitriles bound to ruthenium. Mass spectra of **76** showed a prominent peak at *m/z* 619.1, along with a suitable isotopic pattern, consistent with the monocation of the formula [Ru(TPA)(MeCN)₂](PF₆)⁺. Based on COSY and NOESY spectroscopic analysis, the peak at 2.88 ppm was assigned to *trans*-MeCN where as the peak at 2.47 corresponded to the *cis*-MeCN. Complex **76** was further characterized by X-ray crystallography. Diffusing Et₂O into a solution of **76** in MeCN

yielded small yellow blocks of **76** suitable for crystallographic analysis. The structural parameters of **76** were similar to those of $[\text{Ru}(\text{TPA})(\text{MeCN})_2](\text{SbF}_6)_2$ which was reported while our studies were underway.²¹¹

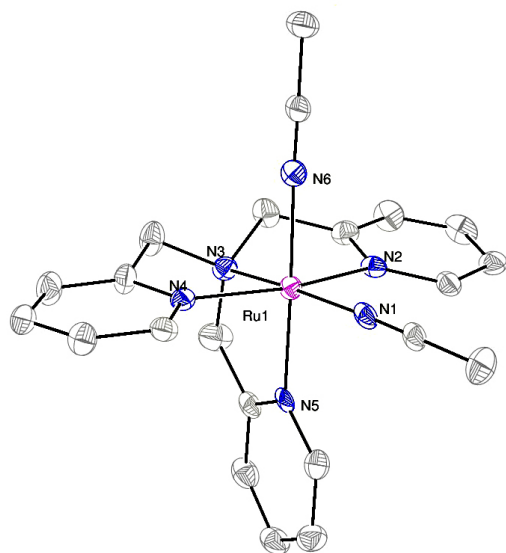


Figure 32: ORTEP diagram of dication $[\text{Ru}(\text{TPA})(\text{MeCN})_2]^{+2}$. Thermal ellipsoids are shown at 50% probability. Hydrogen atoms are omitted for clarity.

Complex **77** was synthesized by heating $[\text{Ru}(\text{TPA})(\text{H}_2\text{O})_2](\text{OTf})_2$ ²¹³ in the presence of 5 equiv. of the protease inhibitor **60** in EtOH (Scheme 10). UV-vis spectra of **77** showed peak maxima at 375 nm ($\epsilon = 12,000 \text{ M}^{-1} \text{ cm}^{-1}$) consistent with a metal-to-ligand charge transfer (MLCT) transition. ¹H NMR spectroscopic analysis indicated the presence of inhibitor in two distinct environments, with α -CN methylene unit multiplets at 4.9 and 4.5 ppm, separated by approximately 0.5 ppm, consistent with the expected structure with one of the inhibitor ligand *trans* to the basic nitrogen and other in *cis* position. IR spectrum of complex **77** showed at ν_{CN} stretch at 2269 cm^{-1} consistent with nitrile binding to Ru(II). Mass spectra of **70** showed a prominent peak at m/z 1143, along with a suitable isotopic pattern, consistent with the monocation of the formula $[\text{Ru}(\text{TPA})(\mathbf{60})_2](\text{PF}_6)^+$. Based on COSY and NOESY spectroscopic analysis, the multiplet at 4.9 ppm was assigned to the α -CN

methylene unit of *trans*-inhibitor whereas the peak at 4.5 corresponded to the α -CN methylene unit of *cis*-inhibitor molecule.

5.2.2 Photolysis studies of **76** and **77**

Complexes **76** and **77** show the release of a single nitrile upon relatively short irradiation times with 365 nm light.²¹⁴ A decrease in the absorption peak at 370 and 365 nm for **76** (Figure 33A) and **77** (Figure 33B) respectively, is observed within 10-15 min of irradiation with $\lambda > 345$ nm in 2% acetone in H₂O solutions, with the concomitant appearance of a new band at 395 and 390 nm, respectively (Figure 33). The quantum yields for decomposition of **76** and **77** are 0.012(1) and 0.011(1) respectively ($\lambda_{\text{irr}} = 350$ nm) and were determined by the Turro group.

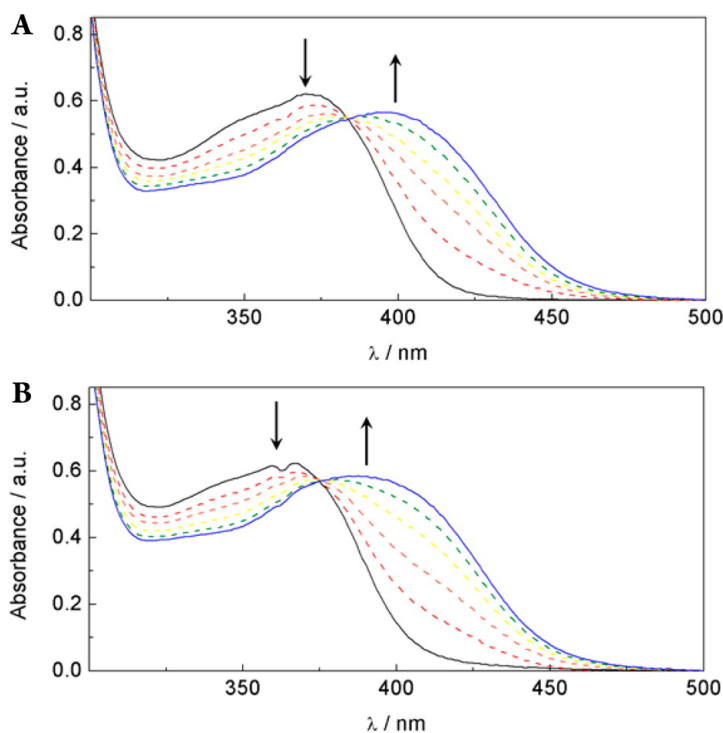


Figure 33: Changes in the electronic absorption spectra upon irradiation with $\lambda > 350$ nm in H₂O (2% acetone) of **76** (A) for 0, 1, 2, 3, 5, and 10 min and **77** (B) for 0, 1, 3, 7, 10, and 15 min.

To better understand the photochemical changes, the same reactions were followed in deuterated solvents by ^1H NMR spectroscopy. Experiments suggested exchange of only one nitrile-based ligand with solvent molecules from **76** (Figure 34) and **77** (Figure 35). The intensities of upfield resonances, assigned to methyl and methylene protons of $\alpha\text{-CN}$ of **76** and **77**, decreases as the peaks associated with free MeCN (2.05 ppm) and free **60** (4.16 ppm) increase. Released nitriles are assigned as *cis* to the basic nitrogen based on COSY and NOESY spectroscopic analysis data. This structural assignment is further supported by the fact that upfield shifts for resonances of $\alpha\text{-CN}$ protons in **76** and **77** would be expected because of shielding by two *cis*-pyridine rings of the TPA ligand, whose π systems are orthogonal to the Ru-N vector of the nitrile that is released upon photolysis.

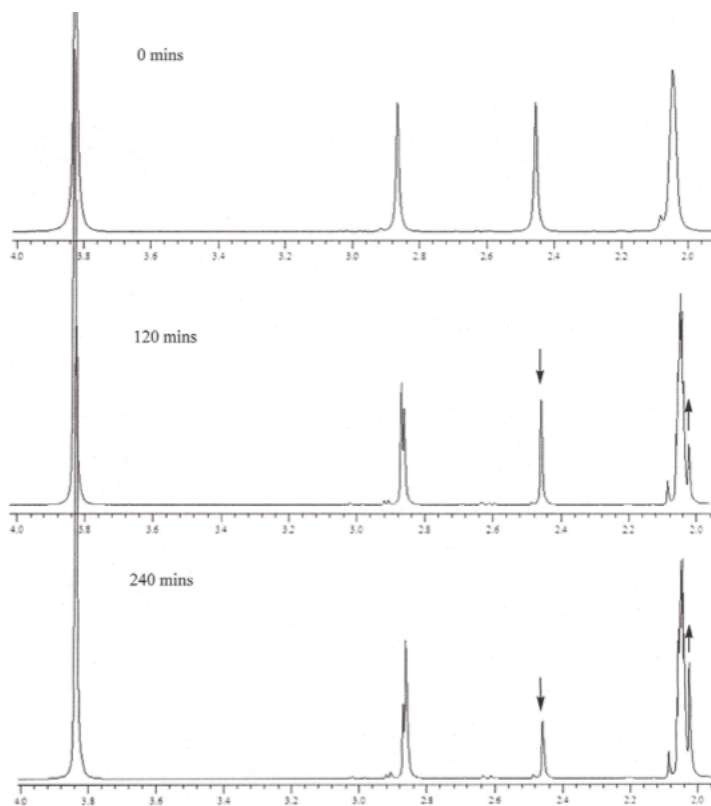


Figure 34: Photochemical reaction of **76** (0, 120 and 240 min) in $C_6D_6O: D_2O - 9: 1$ showing the release of *cis*-MeCN (2.47 ppm) and formation of free MeCN (2.05 ppm).

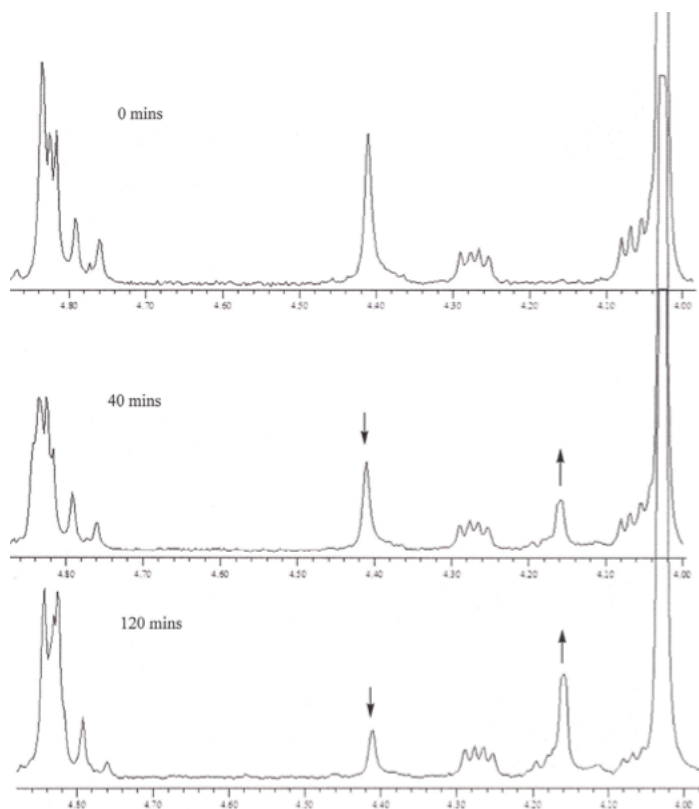


Figure 35: Photochemical reaction of **77** (0, 120 and 240 min) in $C_6D_6O: D_2O - 9: 1$ showing the release of *cis*-**60** (4.40 ppm) and formation of free **60** (4.16 ppm).

5.2.3 Stability studies of **76** and **77**

Complexes **76** and **77** showed excellent stability in solution in the dark. The decomposition rates for **76** and **77** in DMSO and phosphate-buffered saline (pH = 6.5) were determined spectrophotometrically. The rate constants were calculated from linear $\ln A$ vs t plots and ranged from $1.1(3) \times 10^{-8}$ to $6(2) \times 10^{-9} \text{ s}^{-1}$. These values correspond to half-lives of >730 days in solution, confirming that **76** and **77** are stable towards the release of their bound nitrile ligands in aqueous media.

5.2.4 Isolated CTSK enzyme inhibition by **77**

Complex **77** acts as a potent, photoactivated inhibitor of human cathepsin K. IC_{50} values were determined for **60** and **77** under dark and light conditions and upon irradiation with 365 nm light (Figure 36).

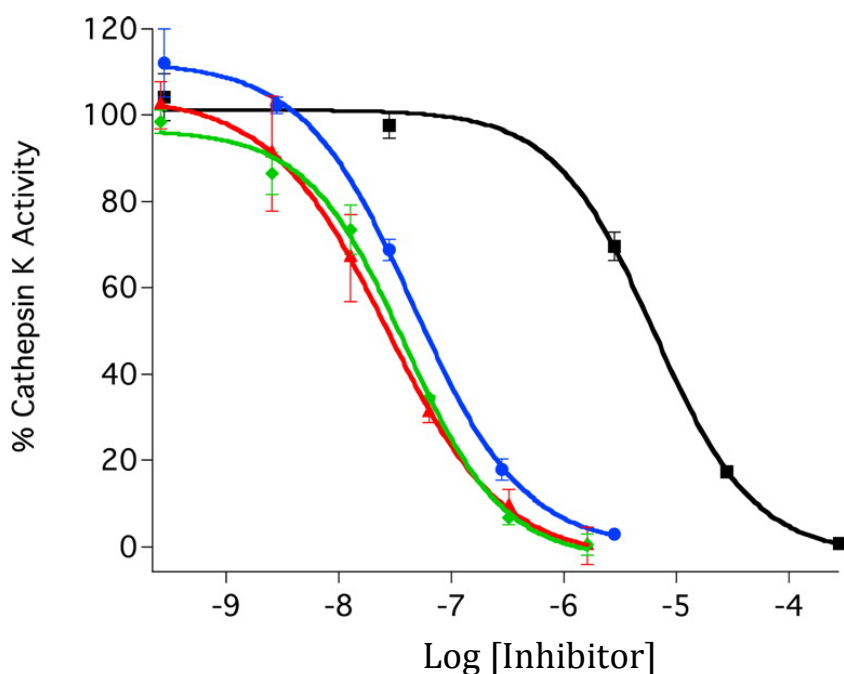


Figure 36: IC_{50} curves for ruthenium-caged inhibitor **77** (blue with irradiation and black without) and uncaged inhibitor **60** (red with irradiation and green without) against human cathepsin K.

Enzyme inhibition for **77** was enhanced by a factor of 89 upon exposure to light with IC_{50} values of 63 nM and 5.6 μ M, respectively. In contrast, inhibition by the free inhibitor **60** was identical under light and dark conditions, 27 nM and 34 nM, respectively; confirming that irradiation with 365 nm light has no effect on inhibition under the assay conditions. Also complex **77** is as potent as **60** in light conditions indicating the release of only one nitrile ligands on exposure to light. Control experiments with **76** showed no inhibition of CTSK under light and dark conditions at 500 μ M, the highest concentration surveyed for **77**, confirming that neither the ruthenium complex nor its byproducts is responsible for CTSK inhibition observed for **77** upon irradiation.

5.2.5 Discussions and conclusions

This study establishes Ru(TPA) as a new caging group for bioactive nitriles distant from standard planar, heteroaromatic caging groups such as Ru(bpy)₂ which are mostly used for photocaging purposes. Two new complexes were synthesized using the Ru(TPA) caging group. Both the complexes showed release of only one nitrile ligand on photolysis by UV light. This study also shows that ligand structure plays an important in photochemical properties of the complex. We have demonstrated that caged inhibitor complex **77** can be used for efficient photoactivated enzyme inhibition against human CTSK.

5.3 Experimental procedures

5.3.1 Synthesis and characterization of [Ru(TPA)(RCN)₂](PF₆)₂ (**76** and **77**).

Synthesis of [Ru(TPA)(CH₃CN)₂](PF₆)₂ (**76**): [Ru(TPA)(DMSO)Cl]Cl (200.0 mg, 0.370 mmol) as a 2:1 mixture of stereoisomers, was dissolved in a 1:1 mixture of H₂O and CH₃CN (20 mL) under argon atmosphere and the resulting solution was refluxed for 2 h under inert atmosphere. Ice cold water (20 mL) was added to the reaction mixture followed by a saturated solution of aqueous NH₄PF₆ (5 mL), resulting in a pale yellow precipitate that was isolated by filtration, washed with ice-cold H₂O and dried under reduced pressure to get the title complex as a yellow solid (136 mg, 48%). Crystals suitable for X-ray crystallographic analysis were obtained by diffusing Et₂O into a solution of **76** in MeCN: Mp = 190 °C (decomp); ¹H NMR (400MHz C₃D₆O:D₂O - 9:1) δ 9.18 (d, 1H, *J* = 5.9 Hz), 8.83 (d, 2H, *J* = 5.9 Hz), 7.85 (t, 2H, *J* = 7.8 Hz), 7.68-7.56 (m, 3H), 7.41 (t, 2H, *J* = 6.8 Hz), 7.25 (t, 1H, *J* = 6.8 Hz), 7.18 (d, 1H, *J* = 7.8 Hz), 5.25 (d, 2H, *J* = 15.6 Hz), 5.15 (d, 2H, *J* = 15.6 Hz), 4.86 (s, 2H), 2.88 (s, 3H), 2.47 (s, 3H); IR (KBr) ν_{max} (cm⁻¹) 3666, 3592, 3418, 3119, 2935, 2856, 2276, 1729, 1609, 1481, 1461, 1448, 1311, 1289, 1160, 992, 838, 767, 739. ESMS calculated for C₂₂H₂₄F₆N₆PRu (M⁺) 619.1, found 619.3; UV-vis λ_{max} = 380 (ε = 11,200 M⁻¹cm⁻¹); Anal. Calculated for C₂₂H₂₄F₁₂N₆P₂Ru: C, 34.61; H, 3.17; N, 11.01. Found: C, 34.70; H, 3.20; N, 10.82.

Synthesis of [Ru(TPA)(RCN)₂](PF₆)₂ (**77**): A solution of [Ru(TPA)(H₂O)₂](CF₃SO₃)₂²¹³ (540 mg, 0.72 mmol) and dry EtOH (40 mL) was deoxygenated by bubbling Ar through a submerged needle for 10 min. Cbz-Leu-NHCH₂CN (1.09 g, 3.6 mmol) was added and the reaction mixture was refluxed for 24 h at 80 °C under Ar atmosphere. The reaction mixture was cooled to room temperature and concentrated under reduced pressure. The green oil was extracted with Et₂O (3 × 20 mL) to get a dark green solid, which was dissolved in minimum

amount of CH_2Cl_2 and washed with water (3×30 mL). The organic layer was dried (NaSO_4) and concentrated under reduced pressure to get a dark green solid (501 mg). The dark green solid was dissolved in MeOH (10 mL) and H_2O (10 mL) was added. The insoluble green oil was removed by centrifugation. A saturated solution aqueous solution of NH_4PF_6 (2 mL) was added to the clear pale green supernatant solution, resulting in formation of a precipitate that was isolated by filtration, washed with water (3×20 mL) and dried under reduced pressure to get the title compound as a pale yellow solid in analytically pure form (290 mg, 53%): $\text{Mp} = 210$ °C (decomp); $^1\text{H NMR}$ (400MHz $\text{C}_3\text{D}_6\text{O}$) δ 9.19 (d, 1H, $J = 5.6$ Hz), 8.85 (d, 1H, $J = 6.1$ Hz), 8.84 (d, 1H, $J = 6.1$ Hz), 8.50 (t, 1H, $J = 5.1$ Hz), 8.16 (t, 1H, $J = 4.7$ Hz), 7.92-7.87 (m, 2H), 7.71-7.62 (m, 3H), 7.43-7.22 (m, 14H), 6.96 (d, 1H, $J = 7.3$ Hz), 6.79 (d, 1H, $J = 7.1$ Hz), 5.32 (d, 1H, $J = 15.7$ Hz), 5.31 (d, 1H, $J = 15.7$ Hz), 5.20-5.14 (m, 3H), 5.07-4.96 (m, 4H), 4.90-4.88 (m, 2H), 4.81 (d, 1H, $J = 12.7$ Hz), 4.57-4.45 (m, 2H), 4.36-4.32 (m, 1H), 4.16-4.11 (m, 1H), 1.86-1.65 (m, 3H), 1.61-1.42 (m, 3H), 0.97-0.84 (m, 12H); IR (KBr) ν_{max} (cm^{-1}) 3417, 3319, 2959, 2873, 2265, 1717, 1684, 1608, 1519, 1451, 1406, 1340, 1312, 1254, 1160, 1121, 1044, 844, 769, 740, 699; ESMS calculated for $\text{C}_{50}\text{H}_{60}\text{F}_6\text{N}_{10}\text{O}_6\text{PRu}$ (M^{+1}) 1143.3, found 1143.9; UV-vis $\lambda_{\text{max}} = 375$ ($\epsilon = 12,000 \text{ M}^{-1}\text{cm}^{-1}$); Anal. Calculated for $\text{C}_{50}\text{H}_{61}\text{F}_{12}\text{N}_{10}\text{O}_{6.5}\text{P}_2\text{Ru}$ ($77 \cdot 0.5 \text{ H}_2\text{O}$): C, 46.30; H, 4.74; N, 10.80. Found: C, 46.21; H, 4.79; N, 10.78.

5.3.2 Photochemical quantum yields of **76** and **77**

The Turro group, using ferrioxalate actinometry as previously described in detail determined photosubstitution quantum yields.¹⁶⁸ A 150 W Xe lamp housed in a Milliarc compact arc lamp housing (PTI) and powered by a PTI model LPS-220 power supply was used in the steady-state photolysis experiments; the wavelength of the light reaching the sample was controlled with colored glass long-pass (295 nm) and band-pass (350 nm) filters (Newport).

5.3.3 Stability studies of **76** and **77**

Solutions of **76** and **77** in 0.1 M pH 6.5 phosphate buffer (1.0% DMSO) were monitored by UV-Vis spectroscopy for 24 h. Ln A was plotted vs time and the line was fit to give a first order reaction rate constants.

Compound and condition	76 (DMSO)	76 (PBS)	77 (DMSO)	77 (PBS)
Rate constant k (s ⁻¹)	$8(2) \times 10^{-9}$	$6(2) \times 10^{-9}$	$7(3) \times 10^{-9}$	$1.2(2) \times 10^{-8}$
t _{1/2} (days)	1.07×10^3	1.33×10^3	1.25×10^3	7.35×10^3

Table 2: Observed rate constants for decomposition of **76** and **77** in 100% DMSO or pH 6.5 phosphate buffer (1.0% DMSO) at 298±2K.

5.3.4 Cathepsin K inhibition studies

Cathepsin enzyme activity was determined from kinetic measurements performed by fluorimetric detection of the hydrolysis product AMC at 37 °C every 2 min for 14 min (8 measures). The excitation and emission wavelengths were 360 and 485 nm respectively. The selective fluorescent substrate Z-Gly-Pro-Arg-AMC was used at a final concentration of 100 μM (obtained from Bachem, Torrance, CA). Enzyme activities are expressed as a percentage, with 100% equal to activity in the absence of inhibitor **60**.

Recombinant cathepsin K (human) was obtained from Enzo Life Sciences (Farmingdale, NY). An 880 nM stock solution was prepared in 50 mM sodium acetate, pH 5.5, 50 mM NaCl, 0.5 mM EDTA and 5 mM DTT and kept at -80 °C. For each experiment the stock solution was diluted 440 times and activated for 15 min at 37 °C with a 400 mM sodium acetate, pH 5.5, 4 mM EDTA, 8 mM DTT assay buffer solution. The inhibitor was prepared as a 1% DMSO solution in the buffer solution (400 mM sodium acetate, pH 5.5, 4 mM EDTA, 0.01 % Triton X -

100) and plated (Corning® 96 Well Flat Clear Bottom Black Polystyrene TC-Treated Microplates, 50 μL /well). Three experiments in triplicates (**60** and **77**, light or dark) were carried out on the different 96 well plates. The wells containing “dark” were carefully wrapped in aluminum foil for 15 min and the light plate was exposed to 365 nm light (8W) for the same time period. The photolysis was conducted for 15 min (with gentle shaking of the plate every 2-3 min) using a long wavelength (UV-365 nm) Black Ray Lamp (8W) held at distance of 18 cm from the plate. After photolysis, the reaction was initiated by addition of 50 μL of 200 μM Z-Gly-Pro-Arg-AMC solution in the assay buffer (final volume 100 μL , final enzyme concentration 2 nM). Cathepsin enzyme activity was determined from kinetic measurements performed by fluorimetric detection of the hydrolysis product AMC at 37 °C every 2 min for 14 min (8 measures) and MAX RFU slope values used for plotting.

5.3.5 X-ray Crystallographic analysis of **76**

A specimen of $\text{C}_{49.50}\text{H}_{57}\text{F}_{24}\text{N}_{15.50}\text{P}_4\text{Ru}_2$ was used for the X-ray crystallographic analysis. The X-ray intensity data were measured. The total exposure time was 56.65 hours. The frames were integrated with the Bruker SAINT software package using a narrow-frame algorithm. The integration of the data using a triclinic unit cell yielded a total of 65934 reflections to a maximum θ angle of 26.37° (0.80 Å resolution), of which 12628 were independent (average redundancy 5.221, completeness = 95.9%, $R_{\text{int}} = 3.66\%$) and 10076 (79.79%) were greater than $2\sigma(F^2)$. The final cell constants of $a = 12.1129(8)$ Å, $b = 12.2928(8)$ Å, $c = 21.8490(15)$ Å, $\alpha = 94.436(3)^\circ$, $\beta = 97.000(3)^\circ$, $\gamma = 91.324(3)^\circ$, volume = 3217.7(4) Å³, are based upon the refinement of the XYZ-centroids of 9922 reflections above $20 \sigma(I)$ with $4.669^\circ < 2\theta < 58.65^\circ$. Data were corrected for absorption effects using the multi-scan method (SADABS). The ratio of minimum to maximum apparent transmission was 0.923.

The final anisotropic full-matrix least-squares refinement on F^2 with 863 variables converged at $R1 = 5.79\%$, for the observed data and $wR2 = 19.52\%$ for all data. The goodness-of-fit was 1.413. The largest peak in the final difference electron density synthesis was $1.728 e^-/\text{\AA}^3$ and the largest hole was $-1.368 e^-/\text{\AA}^3$ with an RMS deviation of $0.130 e^-/\text{\AA}^3$. On the basis of the final model, the calculated density was 1.704 g/cm^3 and $F(000)$, 1653 e^- .

Table 3: Crystal data and structure refinement for $[\text{Ru}^{\text{II}}(\text{TPA})(\text{CH}_3\text{CN})_2](\text{PF}_6)_2$. (76)

Identification code	rs01147_rework	
Chemical formula	$\text{C}_{49.50}\text{H}_{57}\text{F}_{24}\text{N}_{15.50}\text{P}_4\text{Ru}_2$	
Formula weight	1651.12	
Temperature	100(2) K	
Wavelength	0.71073 \AA	
Crystal system	triclinic	
Space group	P -1	
Unit cell dimensions	$a = 12.1129(8) \text{\AA}$	$\alpha = 94.436(3)^\circ$
	$b = 12.2928(8) \text{\AA}$	$\beta = 97.000(3)^\circ$
	$c = 21.8490(15) \text{\AA}$	$\gamma = 91.324(3)^\circ$
Volume	$3217.7(4) \text{\AA}^3$	
Z	2	
Density (calculated)	1.704 g/cm^3	
Absorption coefficient	0.688 mm^{-1}	
$F(000)$	1653	
Theta range for data collection	0.94 to 26.37°	
Index ranges	$-15 \leq h \leq 15, -15 \leq k \leq 15, -26 \leq l \leq 27$	
Reflections collected	65934	
Independent reflections	12628 [$R(\text{int}) = 0.0366$]	
Coverage of independent reflections	95.9%	
Absorption correction	multi-scan	
Refinement method	Full-matrix least-squares on F^2	
Refinement program	SHELXL-2013 (Sheldrick, 2013)	
Function minimized	$\sum w(\text{Fo}^2 - \text{Fc}^2)^2$	
Data / restraints / parameters	12628 / 0 / 863	
Goodness-of-fit on F^2	1.413	
$\Delta/\sigma_{\text{max}}$	0.001	

Final R indices	10076 data; $I > 2\sigma(I)$ R1 = 0.0579, wR2 = 0.1853
	all data R1 = 0.0771, wR2 = 0.1952
Weighting scheme	$w = 1/[\sigma^2(F_o^2) + (0.1000P)^2 + 0.5098P]$ where $P = (F_o^2 + 2F_c^2)/3$
Largest diff. peak and hole	1.728 and -1.368 eÅ ⁻³
R.M.S. deviation from mean	0.130 eÅ ⁻³

Table 4: Atomic coordinates and equivalent isotropic atomic displacement parameters (Å²)
U(eq) is defined as one third of the trace of the orthogonalized U_{ij} tensor.

	x/a	y/b	z/c	U(eq)
Ru1	0.34193(3)	0.02767(3)	0.71876(2)	0.01620(14)
Ru2	0.12463(3)	0.48193(3)	0.22502(2)	0.01489(13)
P1	0.37972(15)	0.73310(15)	0.44715(8)	0.0404(4)
P2	0.28898(12)	0.70587(12)	0.94526(7)	0.0277(4)
P3	0.88862(12)	0.78405(12)	0.06745(7)	0.0257(3)
P4	0.93103(12)	0.79375(12)	0.55563(7)	0.0264(3)
F1	0.4210(4)	0.8474(4)	0.4811(2)	0.0693(14)
F2	0.4994(4)	0.7224(4)	0.4218(3)	0.0834(17)
F3	0.3461(5)	0.6162(4)	0.4136(3)	0.0880(18)
F4	0.3476(6)	0.7906(4)	0.3881(3)	0.115(3)
F5	0.4298(7)	0.6761(5)	0.5073(3)	0.120(3)
F6	0.2729(5)	0.7372(6)	0.4762(4)	0.148(4)
F7	0.3609(3)	0.7878(3)	0.99661(16)	0.0380(9)
F8	0.1842(3)	0.7210(3)	0.98206(18)	0.0399(9)
F9	0.2158(3)	0.6253(3)	0.89461(18)	0.0459(10)
F10	0.3934(3)	0.6912(3)	0.9086(2)	0.0549(11)
F11	0.3242(3)	0.6056(3)	0.98446(19)	0.0448(10)
F12	0.2524(3)	0.8083(3)	0.90713(18)	0.0468(10)
F13	0.8923(4)	0.9144(3)	0.0769(2)	0.0526(11)
F14	0.9894(3)	0.7860(4)	0.02752(19)	0.0589(13)
F15	0.9728(3)	0.7802(3)	0.12922(17)	0.0486(10)

F16	0.7868(3)	0.7824(3)	0.10735(17)	0.0429(9)
F17	0.8828(3)	0.6543(3)	0.05812(19)	0.0463(10)
F18	0.8035(3)	0.7885(3)	0.00615(16)	0.0327(8)
F19	0.0131(3)	0.6939(3)	0.5556(2)	0.0549(11)
F20	0.0171(3)	0.8643(4)	0.52577(17)	0.0530(11)
F21	0.9894(3)	0.8369(3)	0.62285(16)	0.0383(9)
F22	0.8449(3)	0.7215(3)	0.58718(18)	0.0445(9)
F23	0.8496(3)	0.8925(3)	0.55660(19)	0.0499(10)
F24	0.8735(3)	0.7499(3)	0.48833(16)	0.0354(8)
N1	0.3677(3)	0.0445(3)	0.8127(2)	0.0181(9)
N2	0.4968(3)	0.9698(3)	0.7064(2)	0.0175(9)
N3	0.3176(3)	0.9989(4)	0.6242(2)	0.0197(9)
N4	0.1820(3)	0.0846(3)	0.7047(2)	0.0180(9)
N5	0.2782(3)	0.8705(3)	0.7151(2)	0.0172(9)
N6	0.4043(3)	0.1828(4)	0.7180(2)	0.0199(10)
N7	0.0664(3)	0.3229(3)	0.2107(2)	0.0171(9)
N8	0.1535(4)	0.4530(4)	0.1348(2)	0.0215(10)
N9	0.1947(3)	0.6320(3)	0.2138(2)	0.0152(9)
C57	0.2406(4)	0.7078(5)	0.2576(3)	0.0242(12)
N11	0.2788(3)	0.4218(3)	0.2439(2)	0.0171(9)
N12	0.9689(3)	0.5378(3)	0.2050(2)	0.0197(9)
N13	0.0982(3)	0.5129(3)	0.3146(2)	0.0185(9)
N14	0.7548(6)	0.5979(6)	0.3667(4)	0.0591(18)
N15	0.5099(5)	0.4123(6)	0.8779(3)	0.0523(17)
N16	0.3473(5)	0.0853(6)	0.1038(3)	0.0565(18)
C1	0.3849(4)	0.0464(4)	0.8657(3)	0.0184(11)
C2	0.4082(5)	0.0460(5)	0.9327(3)	0.0284(13)
C3	0.5182(4)	0.9722(4)	0.6470(3)	0.0241(12)
C4	0.4302(4)	0.0213(5)	0.6038(3)	0.0260(12)
C5	0.2341(5)	0.0768(5)	0.6002(3)	0.0291(13)
C6	0.1449(4)	0.0898(5)	0.6437(3)	0.0233(12)
C7	0.1134(4)	0.1090(4)	0.7464(2)	0.0202(11)
C8	0.0048(4)	0.1401(5)	0.7293(3)	0.0245(12)
C9	0.9645(5)	0.1411(4)	0.6673(3)	0.0273(13)
C10	0.0393(5)	0.1152(5)	0.6237(3)	0.0298(13)
C11	0.2795(5)	0.8834(5)	0.6044(3)	0.0337(14)
C12	0.2610(4)	0.8206(4)	0.6585(3)	0.0211(12)
C13	0.2592(4)	0.8185(4)	0.7643(3)	0.0242(12)

C14	0.2195(4)	0.7095(5)	0.7570(3)	0.0289(13)
C15	0.2006(4)	0.6559(5)	0.6994(3)	0.0282(13)
C16	0.2232(4)	0.7115(5)	0.6488(3)	0.0280(13)
C17	0.6185(5)	0.9368(5)	0.6295(3)	0.0299(13)
C18	0.6991(5)	0.9016(5)	0.6724(3)	0.0297(14)
C19	0.6775(5)	0.8995(4)	0.7324(3)	0.0250(12)
C20	0.5748(4)	0.9316(4)	0.7483(3)	0.0212(11)
C21	0.4421(4)	0.2689(4)	0.7190(3)	0.0221(12)
C22	0.4892(5)	0.3799(5)	0.7204(3)	0.0290(13)
C23	0.0531(4)	0.2511(4)	0.2533(3)	0.0183(11)
C24	0.0232(4)	0.1414(4)	0.2366(3)	0.0222(12)
C25	0.0051(4)	0.1065(4)	0.1745(3)	0.0246(12)
C26	0.0160(4)	0.1805(4)	0.1305(3)	0.0244(12)
C27	0.0481(4)	0.2893(4)	0.1499(2)	0.0203(11)
C28	0.0636(4)	0.3730(4)	0.1051(3)	0.0235(12)
C29	0.1466(4)	0.5599(4)	0.1070(2)	0.0233(12)
C30	0.2047(4)	0.6462(4)	0.1536(3)	0.0211(11)
C31	0.2941(4)	0.8008(4)	0.2436(3)	0.0220(12)
C32	0.3064(5)	0.8149(5)	0.1823(3)	0.0298(13)
C33	0.2608(5)	0.7364(4)	0.1368(3)	0.0262(13)
C34	0.2675(4)	0.4052(5)	0.1313(3)	0.0254(13)
C35	0.3290(4)	0.3898(4)	0.1937(3)	0.0175(11)
C36	0.3316(4)	0.4090(4)	0.3009(3)	0.0226(12)
C37	0.4346(4)	0.3636(4)	0.3093(3)	0.0289(14)
C38	0.4865(5)	0.3319(4)	0.2583(3)	0.0301(14)
C39	0.4331(4)	0.3445(4)	0.1999(3)	0.0288(14)
C40	0.8781(4)	0.5651(5)	0.2009(3)	0.0251(12)
C41	0.7630(5)	0.5956(5)	0.1984(3)	0.0395(17)
C42	0.0771(4)	0.5367(4)	0.3638(3)	0.0217(12)
C43	0.0503(5)	0.5689(6)	0.4250(3)	0.0357(15)
C44	0.6871(7)	0.5614(7)	0.4713(4)	0.063(2)
C45	0.7249(6)	0.5799(6)	0.4128(4)	0.050(2)
C46	0.4140(5)	0.3682(5)	0.9730(3)	0.0404(16)
C47	0.4678(5)	0.3930(5)	0.9197(4)	0.0400(16)
C48	0.1739(5)	0.9740(5)	0.0515(3)	0.0364(15)
C49	0.2709(5)	0.0371(5)	0.0807(3)	0.0335(14)

Table 5: Bond lengths (Å).

Ru1-N1	2.031(5)	Ru1-N6	2.037(5)
Ru1-N3	2.053(4)	Ru1-N5	2.056(4)
Ru1-N2	2.062(4)	Ru1-N4	2.071(4)
Ru2-N13	2.030(5)	Ru2-N12	2.031(4)
Ru2-N11	2.032(4)	Ru2-N8	2.048(4)
Ru2-N7	2.051(4)	Ru2-N9	2.057(4)
P1-F6	1.510(5)	P1-F4	1.532(6)
P1-F1	1.579(4)	P1-F3	1.583(5)
P1-F5	1.599(6)	P1-F2	1.618(5)
P2-F10	1.583(4)	P2-F8	1.590(4)
P2-F11	1.592(4)	P2-F9	1.594(4)
P2-F12	1.604(4)	P2-F7	1.605(4)
P3-F14	1.585(4)	P3-F17	1.591(4)
P3-F18	1.593(4)	P3-F15	1.594(4)
P3-F16	1.595(4)	P3-F13	1.598(4)
P4-F20	1.574(4)	P4-F23	1.582(4)
P4-F21	1.596(4)	P4-F24	1.596(4)
P4-F19	1.597(4)	P4-F22	1.606(4)
N1-C1	1.151(7)	N2-C20	1.353(7)
N2-C3	1.357(7)	N3-C5	1.487(7)
N3-C11	1.498(7)	N3-C4	1.511(6)
N4-C7	1.327(7)	N4-C6	1.360(7)
N5-C12	1.328(7)	N5-C13	1.333(7)
N6-C21	1.141(7)	N7-C23	1.351(7)
N7-C27	1.352(7)	N8-C29	1.490(7)
N8-C28	1.501(7)	N8-C34	1.521(7)
N9-C57	1.342(7)	N9-C30	1.359(7)
C57-C31	1.375(8)	C57-H57	0.95
N11-C36	1.350(7)	N11-C35	1.355(7)
N12-C40	1.152(7)	N13-C42	1.152(7)
N14-C45	1.146(11)	N15-C47	1.137(9)
N16-C49	1.130(8)	C1-C2	1.456(7)
C2-H1	0.98	C2-H3	0.98
C2-H2	0.98	C3-C17	1.387(7)

C3-C4	1.503(8)	C4-H17	0.99
C4-H16	0.99	C5-C6	1.526(7)
C5-H8	0.99	C5-H9	0.99
C6-C10	1.352(7)	C7-C8	1.393(7)
C7-H7	0.95	C8-C9	1.384(8)
C8-H4	0.95	C9-C10	1.417(8)
C9-H5	0.95	C10-H6	0.95
C11-C12	1.498(8)	C11-H14	0.99
C11-H15	0.99	C12-C16	1.398(8)
C13-C14	1.404(8)	C13-H13	0.95
C14-C15	1.365(8)	C14-H10	0.95
C15-C16	1.396(9)	C15-H11	0.95
C16-H12	0.95	C17-C18	1.371(8)
C17-H21	0.95	C18-C19	1.370(8)
C18-H20	0.95	C19-C20	1.389(7)
C19-H19	0.95	C20-H18	0.95
C21-C22	1.463(8)	C22-H24	0.98
C22-H23	0.98	C22-H22	0.98
C23-C24	1.397(7)	C23-H25	0.95
C24-C25	1.381(8)	C24-H26	0.95
C25-C26	1.389(8)	C25-H42	0.95
C26-C27	1.402(8)	C26-H41	0.95
C27-C28	1.498(7)	C28-H39	0.99
C28-H40	0.99	C29-C30	1.511(8)
C29-H27	0.99	C29-H32	0.99
C30-C33	1.383(8)	C31-C32	1.388(8)
C31-H28	0.95	C32-C33	1.385(8)
C32-H30	0.95	C33-H29	0.95
C34-C35	1.500(8)	C34-H37	0.99
C34-H38	0.99	C35-C39	1.386(7)
C36-C37	1.377(7)	C36-H36	0.95
C37-C38	1.379(9)	C37-H33	0.95
C38-C39	1.380(9)	C38-H35	0.95
C39-H34	0.95	C40-C41	1.448(7)
C41-H43	0.98	C41-H44	0.98
C41-H45	0.98	C42-C43	1.442(8)
C43-H47	0.98	C43-H46	0.98

C43-H48	0.98	C44-C45	1.442(13)
C44-H49	0.98	C44-H51	0.98
C44-H50	0.98	C46-C47	1.450(10)
C46-H52	0.98	C46-H53	0.98
C46-H54	0.98	C48-C49	1.446(9)
C48-H58	0.98	C48-H55	0.98
C48-H56	0.98		

Table 6: Bond angles (°)

N1-Ru1-N6	88.80(17)	N1-Ru1-N3	175.88(16)
N6-Ru1-N3	94.79(17)	N1-Ru1-N5	93.86(17)
N6-Ru1-N5	177.34(17)	N3-Ru1-N5	82.55(17)
N1-Ru1-N2	96.35(16)	N6-Ru1-N2	89.14(16)
N3-Ru1-N2	81.70(17)	N5-Ru1-N2	90.43(16)
N1-Ru1-N4	99.50(16)	N6-Ru1-N4	89.73(16)
N3-Ru1-N4	82.57(17)	N5-Ru1-N4	89.96(15)
N2-Ru1-N4	164.09(18)	N13-Ru2-N12	84.79(17)
N13-Ru2-N11	95.87(17)	N12-Ru2-N11	178.38(17)
N13-Ru2-N8	178.94(17)	N12-Ru2-N8	95.59(17)
N11-Ru2-N8	83.77(18)	N13-Ru2-N7	99.34(17)
N12-Ru2-N7	91.47(16)	N11-Ru2-N7	86.96(16)
N8-Ru2-N7	81.64(17)	N13-Ru2-N9	97.26(17)
N12-Ru2-N9	91.30(16)	N11-Ru2-N9	90.08(15)
N8-Ru2-N9	81.75(17)	N7-Ru2-N9	163.35(17)
F6-P1-F4	101.5(5)	F6-P1-F1	91.4(3)
F4-P1-F1	88.6(3)	F6-P1-F3	91.5(3)
F4-P1-F3	92.8(3)	F1-P1-F3	176.4(3)
F6-P1-F5	85.7(5)	F4-P1-F5	172.5(4)
F1-P1-F5	89.0(3)	F3-P1-F5	89.2(3)
F6-P1-F2	174.3(5)	F4-P1-F2	84.2(4)
F1-P1-F2	88.8(3)	F3-P1-F2	88.1(3)
F5-P1-F2	88.6(4)	F10-P2-F8	179.8(2)
F10-P2-F11	90.9(2)	F8-P2-F11	89.2(2)
F10-P2-F9	90.5(2)	F8-P2-F9	89.5(2)
F11-P2-F9	90.2(2)	F10-P2-F12	90.2(2)
F8-P2-F12	89.7(2)	F11-P2-F12	178.7(2)

F9-P2-F12	90.5(2)	F10-P2-F7	90.3(2)
F8-P2-F7	89.6(2)	F11-P2-F7	90.1(2)
F9-P2-F7	179.1(2)	F12-P2-F7	89.2(2)
F14-P3-F17	89.7(2)	F14-P3-F18	89.9(2)
F17-P3-F18	89.6(2)	F14-P3-F15	90.7(2)
F17-P3-F15	90.7(2)	F18-P3-F15	179.4(2)
F14-P3-F16	179.7(3)	F17-P3-F16	90.5(2)
F18-P3-F16	89.9(2)	F15-P3-F16	89.6(2)
F14-P3-F13	91.1(3)	F17-P3-F13	179.1(2)
F18-P3-F13	90.0(2)	F15-P3-F13	89.7(2)
F16-P3-F13	88.7(2)	F20-P4-F23	90.5(2)
F20-P4-F21	89.8(2)	F23-P4-F21	89.8(2)
F20-P4-F24	90.1(2)	F23-P4-F24	90.6(2)
F21-P4-F24	179.5(2)	F20-P4-F19	90.0(3)
F23-P4-F19	179.2(2)	F21-P4-F19	89.6(2)
F24-P4-F19	90.0(2)	F20-P4-F22	178.9(2)
F23-P4-F22	90.1(2)	F21-P4-F22	89.3(2)
F24-P4-F22	90.8(2)	F19-P4-F22	89.5(2)
C1-N1-Ru1	175.1(4)	C20-N2-C3	118.8(4)
C20-N2-Ru1	129.1(4)	C3-N2-Ru1	112.1(3)
C5-N3-C11	111.0(4)	C5-N3-C4	111.8(4)
C11-N3-C4	109.9(4)	C5-N3-Ru1	107.2(3)
C11-N3-Ru1	111.9(3)	C4-N3-Ru1	104.8(3)
C7-N4-C6	119.0(4)	C7-N4-Ru1	128.4(4)
C6-N4-Ru1	112.4(3)	C12-N5-C13	121.1(5)
C12-N5-Ru1	114.2(3)	C13-N5-Ru1	124.7(4)
C21-N6-Ru1	177.7(4)	C23-N7-C27	119.6(4)
C23-N7-Ru2	128.4(4)	C27-N7-Ru2	111.8(3)
C29-N8-C28	112.1(4)	C29-N8-C34	110.7(4)
C28-N8-C34	110.3(4)	C29-N8-Ru2	106.8(3)
C28-N8-Ru2	106.0(3)	C34-N8-Ru2	110.7(3)
C57-N9-C30	118.7(5)	C57-N9-Ru2	128.4(4)
C30-N9-Ru2	112.5(3)	N9-C57-C31	122.3(5)
N9-C57-H57	118.8	C31-C57-H57	118.8
C36-N11-C35	119.1(4)	C36-N11-Ru2	125.8(4)
C35-N11-Ru2	115.1(3)	C40-N12-Ru2	171.3(4)
C42-N13-Ru2	174.4(4)	N1-C1-C2	178.4(6)
C1-C2-H1	109.5	C1-C2-H3	109.5

H1-C2-H3	109.5	C1-C2-H2	109.5
H1-C2-H2	109.5	H3-C2-H2	109.5
N2-C3-C17	120.7(5)	N2-C3-C4	115.7(5)
C17-C3-C4	123.4(5)	C3-C4-N3	109.0(4)
C3-C4-H17	109.9	N3-C4-H17	109.9
C3-C4-H16	109.9	N3-C4-H16	109.9
H17-C4-H16	108.3	N3-C5-C6	109.6(4)
N3-C5-H8	109.8	C6-C5-H8	109.8
N3-C5-H9	109.8	C6-C5-H9	109.8
H8-C5-H9	108.2	C10-C6-N4	122.4(5)
C10-C6-C5	122.2(5)	N4-C6-C5	115.1(4)
N4-C7-C8	121.8(5)	N4-C7-H7	119.1
C8-C7-H7	119.1	C9-C8-C7	119.8(5)
C9-C8-H4	120.1	C7-C8-H4	120.1
C8-C9-C10	117.4(5)	C8-C9-H5	121.3
C10-C9-H5	121.3	C6-C10-C9	119.5(5)
C6-C10-H6	120.2	C9-C10-H6	120.2
N3-C11-C12	111.7(5)	N3-C11-H14	109.3
C12-C11-H14	109.3	N3-C11-H15	109.3
C12-C11-H15	109.3	H14-C11-H15	107.9
N5-C12-C16	121.0(5)	N5-C12-C11	119.2(5)
C16-C12-C11	119.8(5)	N5-C13-C14	120.2(6)
N5-C13-H13	119.9	C14-C13-H13	119.9
C15-C14-C13	120.2(5)	C15-C14-H10	119.9
C13-C14-H10	119.9	C14-C15-C16	118.5(5)
C14-C15-H11	120.8	C16-C15-H11	120.8
C15-C16-C12	119.1(6)	C15-C16-H12	120.5
C12-C16-H12	120.5	C18-C17-C3	120.5(6)
C18-C17-H21	119.8	C3-C17-H21	119.8
C19-C18-C17	118.7(5)	C19-C18-H20	120.6
C17-C18-H20	120.6	C18-C19-C20	119.7(5)
C18-C19-H19	120.2	C20-C19-H19	120.2
N2-C20-C19	121.5(5)	N2-C20-H18	119.3
C19-C20-H18	119.3	N6-C21-C22	179.2(6)
C21-C22-H24	109.5	C21-C22-H23	109.5
H24-C22-H23	109.5	C21-C22-H22	109.5
H24-C22-H22	109.5	H23-C22-H22	109.5
N7-C23-C24	122.1(5)	N7-C23-H25	118.9

C24-C23-H25	118.9	C25-C24-C23	118.4(5)
C25-C24-H26	120.8	C23-C24-H26	120.8
C24-C25-C26	119.7(5)	C24-C25-H42	120.1
C26-C25-H42	120.1	C25-C26-C27	119.4(5)
C25-C26-H41	120.3	C27-C26-H41	120.3
N7-C27-C26	120.6(5)	N7-C27-C28	117.0(5)
C26-C27-C28	122.4(5)	C27-C28-N8	107.9(4)
C27-C28-H39	110.1	N8-C28-H39	110.1
C27-C28-H40	110.1	N8-C28-H40	110.1
H39-C28-H40	108.4	N8-C29-C30	108.2(4)
N8-C29-H27	110.1	C30-C29-H27	110.1
N8-C29-H32	110.1	C30-C29-H32	110.1
H27-C29-H32	108.4	N9-C30-C33	121.6(5)
N9-C30-C29	115.5(5)	C33-C30-C29	122.9(5)
C57-C31-C32	119.2(5)	C57-C31-H28	120.4
C32-C31-H28	120.4	C33-C32-C31	118.8(5)
C33-C32-H30	120.6	C31-C32-H30	120.6
C30-C33-C32	119.3(5)	C30-C33-H29	120.4
C32-C33-H29	120.4	C35-C34-N8	112.9(4)
C35-C34-H37	109.0	N8-C34-H37	109.0
C35-C34-H38	109.0	N8-C34-H38	109.0
H37-C34-H38	107.8	N11-C35-C39	121.1(5)
N11-C35-C34	117.4(4)	C39-C35-C34	121.4(5)
N11-C36-C37	121.8(5)	N11-C36-H36	119.1
C37-C36-H36	119.1	C36-C37-C38	119.3(6)
C36-C37-H33	120.4	C38-C37-H33	120.4
C37-C38-C39	119.3(5)	C37-C38-H35	120.3
C39-C38-H35	120.3	C38-C39-C35	119.3(5)
C38-C39-H34	120.3	C35-C39-H34	120.3
N12-C40-C41	176.8(6)	C40-C41-H43	109.5
C40-C41-H44	109.5	H43-C41-H44	109.5
C40-C41-H45	109.5	H43-C41-H45	109.5
H44-C41-H45	109.5	N13-C42-C43	178.7(6)
C42-C43-H47	109.5	C42-C43-H46	109.5
H47-C43-H46	109.5	C42-C43-H48	109.5
H47-C43-H48	109.5	H46-C43-H48	109.5
C45-C44-H49	109.5	C45-C44-H51	109.5
H49-C44-H51	109.5	C45-C44-H50	109.5

H49-C44-H50	109.5	H51-C44-H50	109.5
N14-C45-C44	178.0(9)	C47-C46-H52	109.5
C47-C46-H53	109.5	H52-C46-H53	109.5
C47-C46-H54	109.5	H52-C46-H54	109.5
H53-C46-H54	109.5	N15-C47-C46	179.9(10)
C49-C48-H58	109.5	C49-C48-H55	109.5
H58-C48-H55	109.5	C49-C48-H56	109.5
H58-C48-H56	109.5	H55-C48-H56	109.5
N16-C49-C48	179.1(7)		

Table 7: Anisotropic displacement parameters (\AA^2).

The anisotropic atomic displacement factor exponent takes the form: $-2\pi^2 [h^2 a^{*2} U_{11} + \dots + 2 h k a^* b^* U_{12}]$

	U11	U22	U33	U23	U13	U12
Ru1	0.0147(2)	0.0168(2)	0.0175(3)	0.00155(18)	0.00313(15)	0.00220(16)
Ru2	0.0125(2)	0.0153(2)	0.0171(2)	-0.00021(17)	0.00365(15)	0.00086(16)
P1	0.0521(11)	0.0404(10)	0.0282(10)	-0.0096(8)	0.0145(8)	-0.0165(8)
P2	0.0273(8)	0.0273(8)	0.0293(9)	0.0024(7)	0.0063(6)	0.0020(6)
P3	0.0241(8)	0.0286(8)	0.0239(8)	-0.0033(7)	0.0036(6)	0.0044(6)
P4	0.0287(8)	0.0282(8)	0.0229(8)	0.0020(7)	0.0056(6)	0.0038(6)
F1	0.099(4)	0.059(3)	0.050(3)	-0.023(2)	0.037(3)	-0.035(3)
F2	0.076(3)	0.059(3)	0.126(5)	0.012(3)	0.051(3)	0.010(3)
F3	0.150(5)	0.043(3)	0.075(4)	-0.026(3)	0.054(3)	-0.034(3)
F4	0.214(7)	0.061(3)	0.054(4)	0.003(3)	-0.046(4)	-0.007(4)
F5	0.199(7)	0.086(4)	0.071(4)	0.032(4)	-0.001(4)	-0.046(5)
F6	0.087(4)	0.148(6)	0.209(9)	-0.104(6)	0.102(5)	-0.070(4)
F7	0.033(2)	0.046(2)	0.033(2)	0.0027(17)	-0.0022(15)	-0.0098(16)
F8	0.0267(19)	0.046(2)	0.049(2)	0.0016(19)	0.0120(16)	-0.0003(16)
F9	0.055(2)	0.045(2)	0.036(2)	-0.0081(18)	0.0052(17)	-0.0148(18)
F10	0.035(2)	0.065(3)	0.069(3)	-0.004(2)	0.028(2)	-0.0010(19)
F11	0.043(2)	0.029(2)	0.062(3)	0.0117(19)	-0.0014(18)	0.0074(16)
F12	0.063(3)	0.034(2)	0.043(3)	0.0136(19)	-0.0018(19)	0.0001(18)
F13	0.073(3)	0.030(2)	0.048(3)	-0.0107(19)	-0.007(2)	-0.0065(19)
F14	0.029(2)	0.099(3)	0.045(3)	-0.028(2)	0.0174(17)	-0.023(2)
F15	0.042(2)	0.068(3)	0.032(2)	-0.007(2)	-0.0090(16)	0.0236(19)

F16	0.036(2)	0.056(2)	0.039(2)	0.0004(19)	0.0152(16)	0.0021(17)
F17	0.054(2)	0.0281(19)	0.056(3)	0.0042(19)	-0.0013(19)	0.0150(17)
F18	0.041(2)	0.0268(18)	0.028(2)	-0.0003(15)	-0.0015(14)	-0.0050(15)
F19	0.052(2)	0.057(3)	0.051(3)	-0.011(2)	-0.0071(19)	0.028(2)
F20	0.054(2)	0.079(3)	0.025(2)	0.006(2)	0.0051(17)	-0.022(2)
F21	0.054(2)	0.037(2)	0.023(2)	-0.0015(16)	0.0051(16)	-0.0046(17)
F22	0.049(2)	0.047(2)	0.038(2)	0.0033(18)	0.0114(17)	-0.0122(18)
F23	0.064(3)	0.041(2)	0.047(3)	0.0077(19)	0.0077(19)	0.0254(19)
F24	0.0323(19)	0.043(2)	0.032(2)	0.0049(17)	0.0033(14)	0.0038(15)
N1	0.010(2)	0.017(2)	0.027(3)	-0.001(2)	0.0022(17)	0.0018(17)
N2	0.015(2)	0.014(2)	0.024(3)	0.0007(19)	0.0070(17)	0.0009(17)
N3	0.019(2)	0.021(2)	0.020(2)	0.004(2)	0.0058(17)	0.0017(18)
N4	0.018(2)	0.013(2)	0.023(3)	0.0029(19)	0.0027(17)	0.0010(17)
N5	0.0050(19)	0.019(2)	0.028(3)	0.002(2)	0.0018(16)	0.0027(16)
N6	0.017(2)	0.022(3)	0.021(3)	0.002(2)	0.0059(17)	0.0027(19)
N7	0.013(2)	0.017(2)	0.021(3)	-0.0020(19)	0.0028(16)	-0.0004(17)
N8	0.029(3)	0.019(2)	0.017(2)	0.0022(19)	0.0024(18)	0.0007(19)
N9	0.013(2)	0.012(2)	0.021(2)	-0.0004(18)	0.0028(16)	0.0036(16)
C57	0.021(3)	0.031(3)	0.020(3)	-0.001(3)	0.000(2)	0.007(2)
N11	0.014(2)	0.010(2)	0.027(3)	0.0013(19)	0.0048(17)	0.0006(16)
N12	0.020(2)	0.020(2)	0.020(3)	0.0003(19)	0.0041(17)	0.0003(18)
N13	0.016(2)	0.016(2)	0.024(3)	0.0009(19)	0.0022(18)	-0.0012(17)
N14	0.058(4)	0.053(4)	0.062(5)	-0.008(4)	-0.004(3)	0.015(3)
N15	0.027(3)	0.069(5)	0.062(5)	0.012(4)	0.000(3)	0.014(3)
N16	0.060(4)	0.070(5)	0.036(4)	0.019(3)	-0.015(3)	-0.012(3)
C1	0.011(2)	0.020(3)	0.024(3)	0.001(2)	0.002(2)	0.003(2)
C2	0.035(3)	0.032(3)	0.017(3)	0.003(3)	0.000(2)	0.005(3)
C3	0.026(3)	0.020(3)	0.027(3)	0.002(2)	0.006(2)	0.001(2)
C4	0.019(3)	0.037(3)	0.024(3)	0.002(3)	0.010(2)	0.002(2)
C5	0.026(3)	0.042(4)	0.020(3)	0.007(3)	0.004(2)	0.010(3)
C6	0.020(3)	0.028(3)	0.022(3)	0.006(2)	0.001(2)	0.006(2)
C7	0.022(3)	0.020(3)	0.018(3)	0.002(2)	0.002(2)	-0.004(2)
C8	0.023(3)	0.026(3)	0.026(3)	0.000(3)	0.006(2)	0.006(2)
C9	0.020(3)	0.023(3)	0.040(4)	0.008(3)	0.003(2)	0.007(2)
C10	0.028(3)	0.041(4)	0.021(3)	0.008(3)	-0.003(2)	0.002(3)
C11	0.044(4)	0.035(3)	0.023(3)	0.001(3)	0.005(3)	-0.010(3)
C12	0.010(2)	0.025(3)	0.027(3)	0.001(3)	0.003(2)	0.002(2)
C13	0.018(3)	0.022(3)	0.033(3)	0.005(3)	0.003(2)	0.008(2)

C14	0.024(3)	0.030(3)	0.035(4)	0.013(3)	0.010(2)	0.003(2)
C15	0.021(3)	0.018(3)	0.045(4)	0.001(3)	0.004(2)	0.000(2)
C16	0.024(3)	0.025(3)	0.033(4)	-0.005(3)	0.000(2)	-0.001(2)
C17	0.025(3)	0.034(3)	0.033(4)	0.001(3)	0.014(2)	0.008(3)
C18	0.023(3)	0.028(3)	0.039(4)	-0.007(3)	0.014(2)	0.004(2)
C19	0.023(3)	0.017(3)	0.035(4)	0.005(2)	0.005(2)	0.002(2)
C20	0.016(3)	0.019(3)	0.028(3)	0.001(2)	0.002(2)	0.000(2)
C21	0.015(3)	0.020(3)	0.032(3)	0.002(2)	0.004(2)	0.005(2)
C22	0.025(3)	0.022(3)	0.040(4)	0.002(3)	0.006(2)	-0.002(2)
C23	0.016(3)	0.016(3)	0.024(3)	0.002(2)	0.005(2)	0.002(2)
C24	0.022(3)	0.020(3)	0.025(3)	0.001(2)	0.005(2)	-0.001(2)
C25	0.025(3)	0.017(3)	0.031(3)	-0.006(3)	0.005(2)	0.000(2)
C26	0.026(3)	0.024(3)	0.022(3)	-0.002(2)	0.001(2)	0.000(2)
C27	0.015(3)	0.027(3)	0.018(3)	0.001(2)	0.0034(19)	0.002(2)
C28	0.024(3)	0.023(3)	0.023(3)	-0.003(2)	0.004(2)	-0.003(2)
C29	0.029(3)	0.024(3)	0.017(3)	0.004(2)	0.003(2)	0.001(2)
C30	0.019(3)	0.019(3)	0.026(3)	0.002(2)	0.006(2)	0.006(2)
C31	0.024(3)	0.014(3)	0.027(3)	0.000(2)	0.000(2)	0.000(2)
C32	0.033(3)	0.026(3)	0.029(4)	-0.004(3)	0.005(2)	-0.003(2)
C33	0.034(3)	0.021(3)	0.026(3)	0.011(3)	0.010(2)	-0.001(2)
C34	0.018(3)	0.032(3)	0.028(3)	-0.003(3)	0.012(2)	-0.001(2)
C35	0.016(3)	0.006(2)	0.033(3)	0.003(2)	0.008(2)	-0.0014(19)
C36	0.021(3)	0.015(3)	0.031(3)	0.002(2)	0.000(2)	0.000(2)
C37	0.020(3)	0.018(3)	0.047(4)	0.007(3)	-0.002(3)	-0.003(2)
C38	0.018(3)	0.010(3)	0.063(5)	0.005(3)	0.004(3)	0.004(2)
C39	0.022(3)	0.017(3)	0.050(4)	0.000(3)	0.016(3)	-0.001(2)
C40	0.022(3)	0.027(3)	0.028(3)	0.008(3)	0.005(2)	0.007(2)
C41	0.015(3)	0.044(4)	0.062(5)	0.023(4)	0.004(3)	0.008(3)
C42	0.012(3)	0.024(3)	0.029(3)	0.000(3)	0.005(2)	-0.001(2)
C43	0.035(3)	0.048(4)	0.025(4)	-0.006(3)	0.011(3)	-0.003(3)
C44	0.055(5)	0.050(5)	0.081(7)	0.016(5)	-0.007(4)	-0.010(4)
C45	0.037(4)	0.041(4)	0.066(6)	-0.001(4)	-0.016(4)	0.002(3)
C46	0.020(3)	0.038(4)	0.062(5)	-0.001(3)	0.002(3)	-0.003(3)
C47	0.029(4)	0.035(4)	0.052(5)	-0.003(3)	-0.005(3)	0.005(3)
C48	0.034(3)	0.029(3)	0.046(4)	0.003(3)	0.004(3)	0.005(3)
C49	0.036(4)	0.031(3)	0.035(4)	0.015(3)	0.001(3)	0.003(3)

Table 8: Hydrogen coordinates (x) and isotropic atomic displacement parameters (\AA^2).

	x	y	z	U(eq)
H57	0.2359	0.6968	0.2998	0.029
H1	0.3901	-0.0266	0.9451	0.043
H3	0.3631	0.1002	0.9525	0.043
H2	0.4873	0.0639	0.9456	0.043
H17	0.4318	-0.0111	0.5610	0.031
H16	0.4446	0.1010	0.6045	0.031
H8	0.1993	0.0494	0.5584	0.035
H9	0.2710	0.1486	0.5972	0.035
H7	0.1391	0.1052	0.7890	0.024
H4	-0.0414	0.1605	0.7602	0.029
H5	-0.1104	0.1584	0.6545	0.033
H6	0.0154	0.1157	0.5807	0.036
H14	0.3361	-0.1529	0.5816	0.04
H15	0.2094	-0.1168	0.5759	0.04
H13	0.2725	-0.1446	0.8045	0.029
H10	0.2057	-0.3271	0.7922	0.035
H11	0.1727	-0.4175	0.6939	0.034
H12	0.2131	-0.3242	0.6083	0.034
H21	0.6314	-0.0631	0.5875	0.036
H20	0.7686	-0.1209	0.6608	0.036
H19	0.7325	-0.1238	0.7630	0.03
H18	0.5591	-0.0734	0.7896	0.025
H24	0.4315	0.4280	0.7038	0.044
H23	0.5507	0.3799	0.6952	0.044
H22	0.5168	0.4061	0.7631	0.044
H25	0.0645	0.2760	0.2959	0.022
H26	0.0156	0.0920	0.2673	0.027
H42	-0.0148	0.0323	0.1619	0.03
H41	0.0019	0.1576	0.0877	0.029
H39	-0.0066	0.4111	0.0951	0.028
H40	0.0853	0.3375	0.0663	0.028
H27	0.0677	0.5781	0.0963	0.028
H32	0.1828	0.5562	0.0687	0.028

H28	0.3223	0.8549	0.2754	0.026
H30	0.3454	0.8774	0.1718	0.036
H29	0.2679	0.7443	0.0946	0.031
H37	0.2582	0.3338	0.1067	0.031
H38	0.3124	0.4542	0.1095	0.031
H36	0.2968	0.4321	0.3361	0.027
H33	0.4696	0.3540	0.3498	0.035
H35	0.5583	0.3018	0.2633	0.036
H34	0.4674	0.3224	0.1643	0.035
H43	-0.2849	0.5379	0.1747	0.059
H44	-0.2467	0.6639	0.1783	0.059
H45	-0.2572	0.6058	0.2405	0.059
H47	0.1035	0.6262	0.4447	0.054
H46	0.0545	0.5057	0.4498	0.054
H48	-0.0251	0.5968	0.4221	0.054
H49	0.6848	0.6312	0.4959	0.094
H51	0.7384	0.5135	0.4938	0.094
H50	0.6125	0.5267	0.4641	0.094
H52	0.4131	0.2892	0.9765	0.061
H53	0.3375	0.3933	0.9680	0.061
H54	0.4551	0.4053	1.0105	0.061
H58	0.1974	0.9098	0.0276	0.055
H55	0.1282	1.0189	0.0239	0.055
H56	0.1302	0.9503	0.0833	0.055

CHAPTER 6. SOLID PHASE SYNTHESIS AS A PLATFORM FOR DEVELOPING NEW CAGING GROUPS³

6.1 Introduction

Numerous inorganic complexes have been developed as therapeutics and tools for chemical biology after the discovery and success of cisplatin.^{18,28,53} Despite their success in these two arenas, our ability to rapidly synthesize, screen and identify metal complexes with desired properties has not evolved at the same pace as organic molecules, which are synthesized routinely by solid phase in large libraries and screened in high throughput assays.²¹⁵ Notwithstanding a few notable exceptions, metal complexes for biological applications are mostly synthesized and evaluated one molecule at a time.²¹⁶⁻²¹⁹ Thus new methods of synthesizing and screening of metal-based compounds are to be developed if they are to compete with their organic counterparts as tool compounds and therapeutics. Given the fact that structure activity relationships are notoriously difficult to predict, more rapid methods are clearly needed to access diverse libraries of metal complexes.

One area of biology where metal complexes have made an important impact is photocaging.^{42,148,220} Photocaging has revolutionized our ability to study living systems, by allowing researchers to control spatial and temporal aspects of biological activity.¹⁴⁹ Metal complexes have emerged more recently as an important class of photocaging groups. They are attractive because they bind to a variety of different functional groups, including groups that can't be protected with organic-based cages such as nitriles,^{47,48,75,146,171,221} nitrogen-containing heteroaromatics³⁸ or thioethers.⁴⁹ Metal-based caging groups also carry the advantage of being

³ Portions of the text in this chapter were reprinted and adapted with permission from Sharma, R.; Ancona, N.; Kodanko, J. J. *Inorg. Chem.* **2015**, 54, 1901

labile with visible light under single-photon excitation,¹⁵¹ which is rare for organic photolabile protecting groups that are usually cleaved with UV light.^{222,223}

Of the various classes of metal-based photocaging groups, ruthenium complexes based on planar, heteroaromatic ligands have been the most widely used (Figure 37). Pioneering work in the neuroscience area showed that Ru(bpy)₂ can be used to achieve high spatial and temporal control over receptor activity in live neuronal cells. Importantly, no toxic effects were observed from the caged neurotransmitters or their metal-based byproducts. Later work showed that Ru(bpy)₂ and similar congeners can also be used to cage cytotoxic agents and protease inhibitors for cell-based assays.^{36,38,56,146,171}

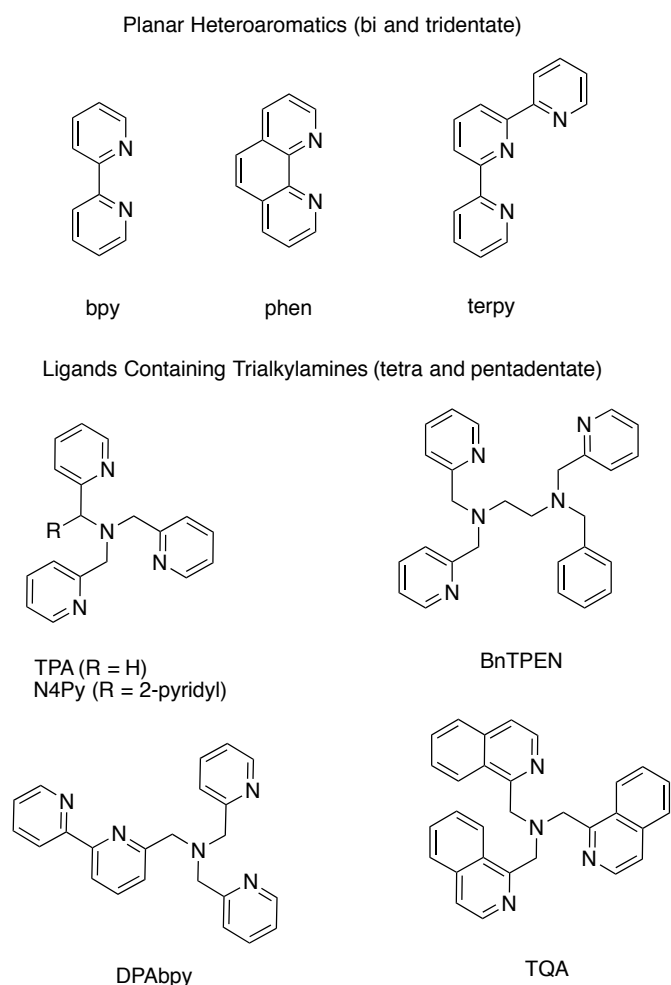


Figure 37: Ligands used in Ru(II)-based caging groups

In the previous chapter we showed that ruthenium tris(2-pyridylmethyl)amine, Ru(TPA), is an effective caging group for bioactive nitriles which is distinct from previously developed photolabile protecting groups.²²¹ Although complexes of the general formula $[\text{Ru}(\text{TPA})(\text{RCN})_2]^{2+}$ showed promising activity, including excellent stability in the dark and high levels of selectivity for enzyme inhibition under dark vs. light conditions, the potential for improvement remained. Most notably, UV light is required for rapid release of nitrile because singlet metal-to-ligand charge transfer (¹MLCT) bands for these complexes occur at < 400 nm. Moreover, only one of the two potentially labile nitrile molecules was released upon irradiation.

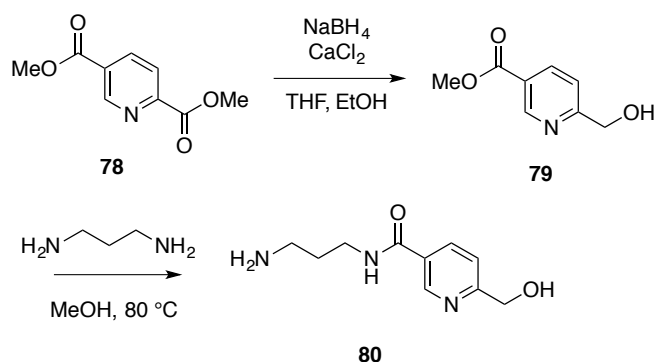
This chapter is dedicated towards developing a library approach for accessing ruthenium complexes by solid phase, one that provides rapid access to new derivatives for screening photochemical behavior. Ligands designed to tune spectral properties of the ruthenium-based photocaging group were synthesized in parallel fashion on resin. This library was processed to form caged ruthenium complexes bound to resin, then subsequently cleaved and analyzed for photochemical reactivity. To validate the screening protocol, three compounds identified from this screen were synthesized by solution phase and fully characterized. Data were in good agreement with compounds from solid phase, thus validating the predictive power of our library approach. Data from solid phase screening indicate a surprisingly wide range of spectral tuning and reactivity with light, demonstrating the utility of this screening technology, as well as the power it has to identify lead caging groups.

6.2 Results and discussions

6.2.1 Synthesis of ligand library

The strategy for synthesis of the ligand library was based on previous work from our laboratory, where a single pyridine precursor bound to resin could be functionalized with two

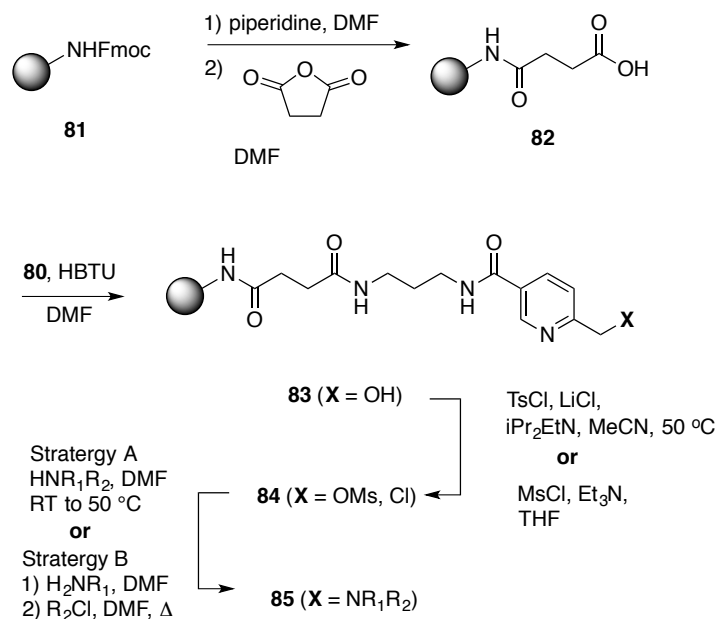
components (R_1 and R_2) to create a library of polypyridyl ligands.^{209,210} The pyridine precursor chosen for this study was derived from commercially available dimethyl pyridine-2,5-dicarboxylate (**78**, Scheme 11). Following a literature protocol, selective reduction of the ester in the 2-position furnishes alcohol **79**. Amidation of **79** with excess 1,3-propanediamine by heating in MeOH at 80 °C provided amine **80** in quantitative yield. Excess of 1,3-propanediamine was removed by simple azeotropic distillation using toluene.



Scheme 11. Synthesis of pyridine precursor **80**

To begin our studies with solid phase, Fmoc-protected Rink amide MBHA resin derived from polystyrene (**81**, Scheme 12) was chosen for attachment of pyridine precursor **80**. The Fmoc group was cleaved from **81** using 1:1 piperidine:DMF, then treatment with succinic anhydride in DMF, which furnished acid **82**. Acid **82** was coupled to amine **80** using HBTU in DMF, giving pyridylmethyl alcohol **83**, containing a 10-atom spacer between the pyridine group and the amide nitrogen bound to resin. Activation of alcohol **83** was accomplished by either mesylation or chlorination using conditions shown in Scheme 12. Mesylation with MsCl and Et_3N proceeded smoothly at RT with 100 mg or less of resin to furnish **84** ($X = \text{OMs}$). However, upon further scale up, it was difficult to observe full consumption of alcohol **83**, as judged by ^1H NMR and ESMS analysis of product cleaved from resin. Optimal conditions developed later

involved heating resin to 50 °C in the presence of excess TsCl, LiCl, *i*Pr₂EtN and MeCN, which worked routinely on scales of up to 1 g of resin, providing **84** (X = Cl).



Scheme 12. Solid phase synthesis of the polypyridyl ligand library (**85a-j**)

A library of ten polypyridyl derivatives (**85a-j**) was accessed in 1-2 steps from monopyridine **84** (X = Cl or OMs) using straightforward alkylation chemistry (Scheme 12). Full structures of the ligands are shown in Figure 38. In some cases, delivery of the appropriate secondary amine resulted in nucleophilic displacement of the leaving group (X = Cl or OMs), providing derivatives of **85** in one step (*Strategy A*). Alternatively, reaction with a primary amine (R₁NH₂) was used to attach one group to the ligand (R₁), with a second alkylation reaction with R₂Cl to complete synthesis of the tertiary amine ligand (*Strategy B*).

After ligand syntheses were completed, the library was evaluated by cleaving a small amount of each derivative from the resin using 95% TFA in H₂O (Figure 38), providing terminal amides **86a-j** that were characterized by LCMS and ¹H NMR spectroscopy. LCMS analysis indicated each of the 10 derivatives was furnished in >90% purity, with a few exceptions.

Compound **86g**, a derivative of the known ligand N4Py, which was produced in <20% purity, with the remainder being unreacted **84** (X = Cl).

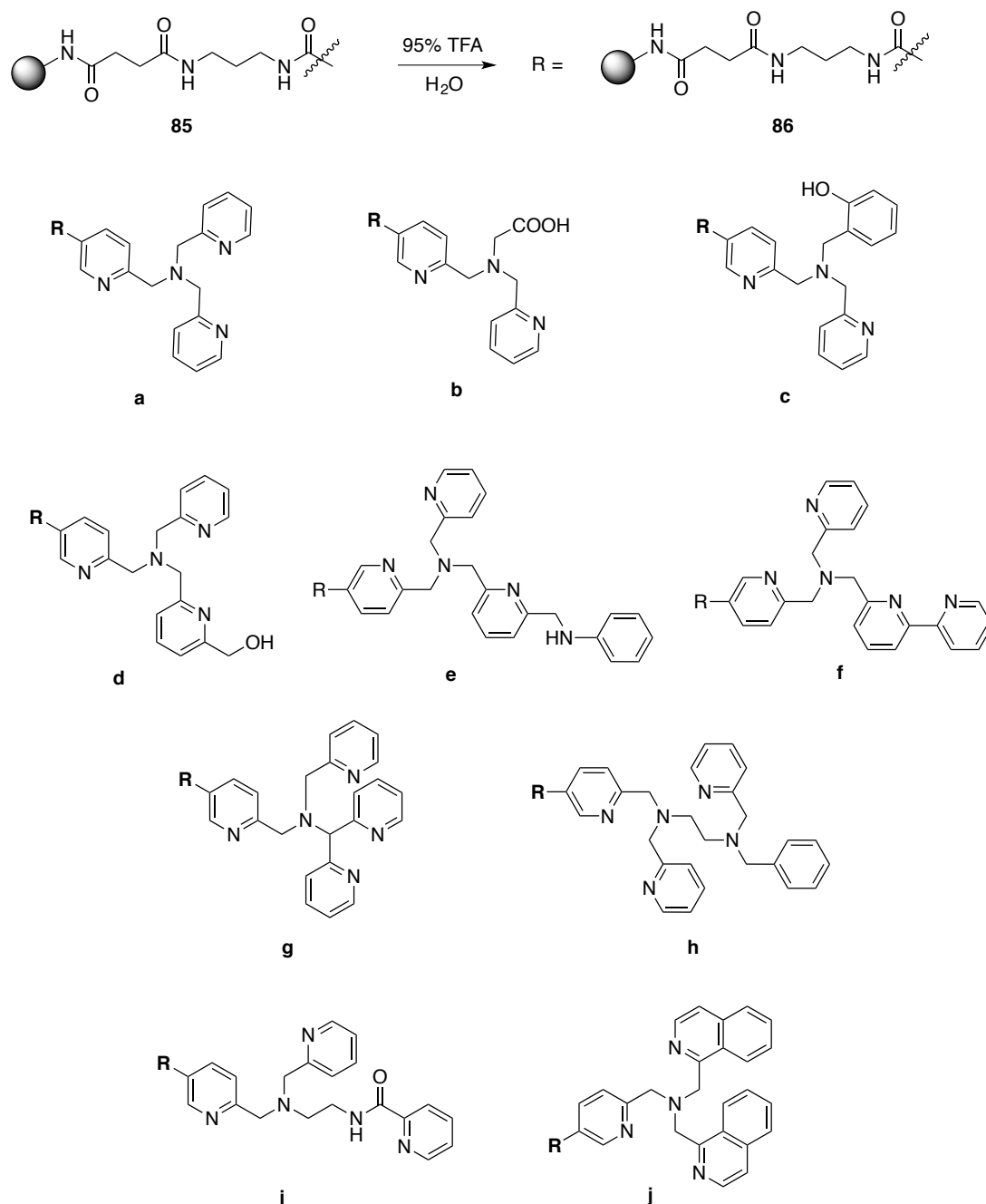


Figure 38. Structures of polypyridyl ligand library bound to resin (**85a-j**) and cleaved for analysis (**86a-j**)

In this case, the secondary amine used to synthesize **86g**, 1,1-di(pyridin-2-yl)-N-(pyridin-2-ylmethyl)methanamine, is a hindered nucleophile.^{209,224} Optimized reaction conditions were developed using NaI as a catalyst, MeCN as solvent and iPr_2EtN , which raised the level of purity of **86g** to 88%. Synthesis of compound **86e** proceeded smoothly in the first alkylation of **84** (X = Cl) with 2-pyridylmethylamine. Subsequent alkylation with 2,6-bis(bromomethyl)pyridine followed by aniline proved challenging, resulting in lower conversion to product **86e** (52% purity) under a variety of conditions, and was not optimized further.

6.2.2 Synthesis of metal complexes on solid phase.

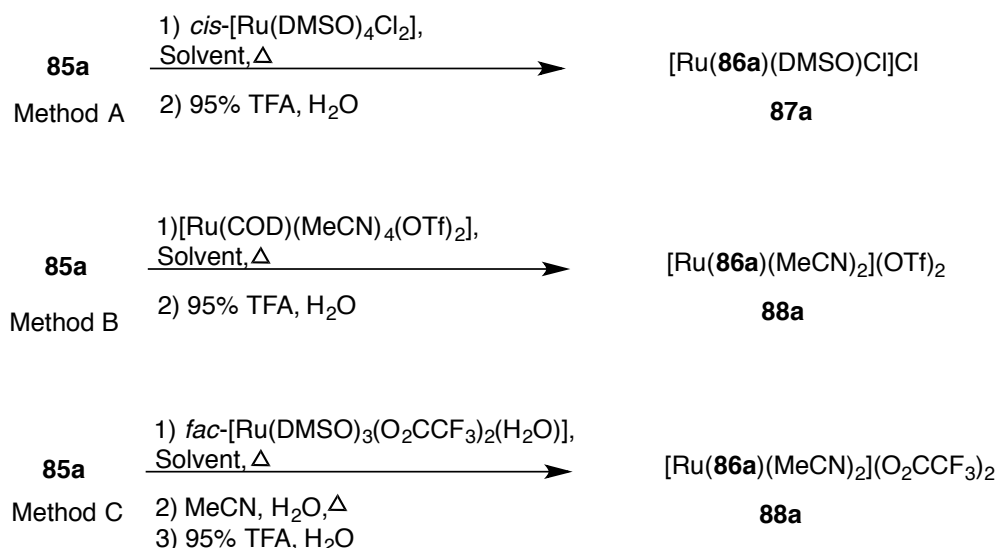
With a library of resin-bound polypyridyl ligands **85a-j** in hand, conditions were developed to generate ruthenium complexes with bound MeCN groups to be released photochemically. Ligands **85a-c** and **85j** contain four donor atoms and were expected to furnish complexes of the general formula $[Ru(L)(MeCN)_2]^{n+}$ ($n = 1,2$) with two molecules of MeCN coordinated to the metal. Ligands **85d-i** each carry five potential donor atoms, and were expected to result in complexes of the general formula $[Ru(L)(MeCN)]^{n+}$ ($n = 1,2$) with only one bound nitrile. A mixture of neutral and anionic ligands were incorporated that were expected to furnish ruthenium (II) complexes as mono- or dicationic species.

Optimization efforts began by surveying a number of conditions and ruthenium(II) precursors for metalation of the resin-bound ligands (Scheme 13, Table 9). Compound **85a**, a derivative of TPA, was used to develop the protocol because data for ruthenium(II) TPA complexes were available to use as benchmarks.^{211,212,221} Two ruthenium(II) starting materials were surveyed initially, $cis-[Ru(DMSO)_4Cl_2]$, which was expected to give a mixture of complexes of the general formula $[Ru(\mathbf{85a})(DMSO)Cl]^+$ that could later be converted into $[Ru(\mathbf{85a})(MeCN)_2]^{2+}$, and $[Ru(COD)(MeCN)_4](OTf)_2$,²²⁵ which could potentially give access to

the desired complex $[\text{Ru}(\mathbf{85a})(\text{MeCN})_2]^{2+}$ directly in one step. Combining resin-bound **85a** with 2-10 equiv. of these ruthenium salts in the presence of solvent (DMF, EtOH or MeCN) and heat (50-80 °C) led to metallation, as judged by UV-vis spectroscopic and ESMS analysis of products cleaved from resin using 95% TFA in H₂O. Relative yields were approximated by absorbance using extinction coefficients of the species $[\text{Ru}(\mathbf{86a})(\text{DMSO})\text{Cl}]^+$ and $[\text{Ru}(\mathbf{86a})(\text{MeCN})_2]^{2+}$. Importantly, both species were shown to be stable for > 24 h in the TFA cleavage cocktail in the absence of irradiation, indicating decomposition does not occur to a measurable extent during 15 min cleavage from resin.

Data indicated a wide range of yields for metallation conditions surveyed. Relative to *cis*- $[\text{Ru}(\text{DMSO})_4\text{Cl}_2]$ (Table 9, entries 1-3), $[\text{Ru}(\text{COD})(\text{MeCN})_4](\text{OTf})_2$ is a sluggish ruthenium(II) starting material, giving <5% yield after 18 h at 50 °C in MeCN. The choice of solvent was also important. DMF, which shows superior swelling of polystyrene resin compared to MeCN, MeOH or EtOH, actually showed much lower yields for metallation (entries 1, 2 and 7). We considered at this stage that swelling properties could play a key role in optimizing formation of the ruthenium complex bound to resin, so compound **85a** was also prepared bound to Tenta-Gel resin, which shows better swelling properties than polystyrene in protic solvents, where yields for binding to Ru(II) were higher. However, use of Tenta-Gel resin did not enhance yields for metallation with EtOH (entry 8). Optimal conditions using conventional heating methods were identified using polystyrene-based **85a**, 4 equiv. of *cis*- $[\text{Ru}(\text{DMSO})_4\text{Cl}_2]$, EtOH as the solvent and heating at 80 °C for 18 h (entry 6). By using microwave heating, reaction timescales were cut down from 18 h to 30 min (entry 7). Raising the amount of Ru(II) source to 10 equiv. and heating at 120 °C for 1 h in the microwave reactor did not enhance the yield relative to 4 equiv. and 80 °C (entry 9). Thus, *cis*- $[\text{Ru}(\text{DMSO})_4\text{Cl}_2]$ (4 equiv.), EtOH as the solvent and heating at 80

°C for 30 min with microwave irradiation were deemed optimal for formation of the intermediate $[\text{Ru}(\mathbf{85a})(\text{DMSO})\text{Cl}]^+$.



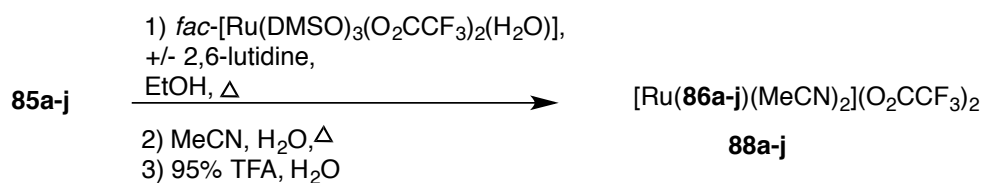
Scheme 13: Three methods (A-C) explored for synthesis of Ru(II) complexes $[\text{Ru}(\mathbf{86a})(\text{DMSO})\text{Cl}]\text{Cl}$ (**87a**) and $[\text{Ru}(\mathbf{86a})(\text{MeCN})_2]\text{X}_2$ (**88a**, X = OTf, O_2CCF_3).

A number of conditions were also surveyed for conversion of the resin-bound $[\text{Ru}(\mathbf{85a})(\text{DMSO})\text{Cl}]^+$ to the caged nitrile species $[\text{Ru}(\mathbf{85a})(\text{MeCN})_2]^{2+}$. Heating the resin in MeCN solvent lead to poor conversion to $[\text{Ru}(\mathbf{85a})(\text{MeCN})_2]^{2+}$ as judged by UV-vis spectroscopic and determined by absorbance at $\lambda_{\text{max}} = 348 \text{ nm}$ ($\epsilon = 9,040 \text{ M}^{-1} \text{ cm}^{-1}$) after cleavage from resin with 95% TFA in H_2O .

Addition of H_2O to the MeCN medium did enhance conversion to $[\text{Ru}(\mathbf{85a})(\text{MeCN})_2]^{2+}$, however, full conversion was still not observed. We hypothesized at this stage that it could be difficult to obtain higher yields of $[\text{Ru}(\mathbf{85a})(\text{MeCN})_2]^{2+}$ because the chloride counteranions, which are highly polar, show limited ability to solubilize dications in organic media and may not be favorable for association of the dicationic complex with the polystyrene polymer. Therefore, additives were explored that could potentially exchange with chloride, including NaBF_4 , NaOAc , NaOTf and NH_4PF_6 . However, significant levels of decomposition with little to no formation of

product were observed. Considering these facts, an additional ruthenium (II) source was explored that already contained less polar anion than chloride. Gratifyingly, heating resin **85a** in the presence of *fac*-[Ru(DMSO)₃(O₂CCF₃)₂(H₂O)]²²⁶ (4 equiv.) in EtOH at 80 °C for 30 min under microwave irradiation, followed by microwave irradiation in MeCN:H₂O (1:1) for 30 min at 80 °C and cleavage from resin, resulted in good conversion and provided [Ru(**86a**)(MeCN)₂](O₂CCF₃)₂ (**88a**) in 81% yield (Table 9, entry 10).

With optimal conditions developed, the library of resin-bound ligands **85a-j** was processed to Ru(II) MeCN complexes (Scheme 14). Conditions for metallation employed *fac*-[Ru(DMSO)₃(O₂CCF₃)₂(H₂O)] (4.0 equiv.) in EtOH with microwave heating at 80 °C for 30 min, followed by replacement of the solvent with MeCN:H₂O and microwave heating at 80 °C for an additional 30 min. In the case of compounds **85b**, **85c**, **85d**, and **85i**, 2,6-lutidine (10 equiv.) was added during step 1 for deprotonation of acidic protons. Each member of the library was cleaved from resin and screened by UV-vis spectroscopy for reactivity with visible light (30 min irradiation, $\lambda_{\text{irr}} \geq 395$ nm) in H₂O, with the goal of identifying complexes that exchanged H₂O for MeCN upon irradiation (Figure 39a-j).



Scheme 14. Synthesis of Ru(II)-MeCN complex library (**88a-j**)

Condition ^{a,b}	Ru(II) source (equiv) ^c	Solvent	Temp (° C) ^{d,e}	Time (h)	% Yield ^{f,g}
1 ^a	A (2)	DMF	50 ^d	18	24 ^f
2 ^a	A (2)	MeOH	50 ^d	18	35 ^f
3 ^a	B (2)	MeCN	50 ^d	18	<5 ^g
4 ^a	B (4)	MeCN	80 ^e	0.5	<5 ^g
5 ^a	B (4)	EtOH	80 ^e	0.5	<5 ^g
6 ^a	A (4)	EtOH	80 ^d	18	70 ^f
7 ^a	A (4)	EtOH	80 ^e	0.5	57 ^f
8 ^b	A (4)	EtOH	80 ^e	0.5	68 ^f
9 ^a	A (10)	EtOH	120 ^e	1	51 ^f
10 ^a	C (4)	EtOH, then MeCN:H ₂ O	80 ^e	0.5 × 2	81 ^g

Table 9: Conditions and Ru(II) sources examined for conversion of resin-bound ligand **85a** to Ru(II) complexes [Ru(**86a**)(DMSO)Cl]Cl (**87a**) and [Ru(**86a**)(MeCN)₂]X₂ (**88a**, X = OTf, O₂CCF₃). ^a**85a** derived from polystyrene resin (0.75 mmol/g); ^b**85a** derived from Tenta-Gel resin (0.23 mmol/g); ^cRuthenium(II) sources are *cis*-[Ru(DMSO)₄Cl₂] (A), [Ru(COD)(MeCN)₄](OTf)₂ (B) and *fac*-[Ru(DMSO)₃(O₂CCF₃)₂(H₂O)] (C); ^dconventional heating; ^emicrowave heating (50 W); ^f% yield of [Ru(**86a**)(DMSO)Cl]⁺ as determined by absorbance at λ_{max} = 345 nm (ε = 10,500 M⁻¹ cm⁻¹) after cleavage from resin with 95% TFA in H₂O; ^g% yield of [Ru(**86a**)(MeCN)₂]²⁺ as determined by absorbance at λ_{max} = 348 nm (ε = 9,040 M⁻¹ cm⁻¹) after cleavage from resin with 95% TFA in H₂O.

Data from the photochemical screening indicate a range of spectral tuning, as well as reactivity with visible light. All of the complexes absorb strongly below 400 nm, with select examples showing significant absorbance from 400-500 nm (ex. **88f-g** and **88i-j**). As expected, most of the complexes are slow to react with visible light because their corresponding ¹MLCT

bands lie below 400 nm (**88a-e**, **88h**). However, absorbance above 400 nm did not guarantee reactivity with visible light. Complex **88f**, which absorbs strongly to almost 500 nm, did not react with visible light. The N4Py derivative **88g** did react slowly with visible light, but did not demonstrate the expected bathochromic shift for substitution of H₂O for MeCN. Complexes **88i** and **88j** did show the desired shift to longer wavelengths, with **88j** showing the most rapid spectral change upon irradiation with visible light.

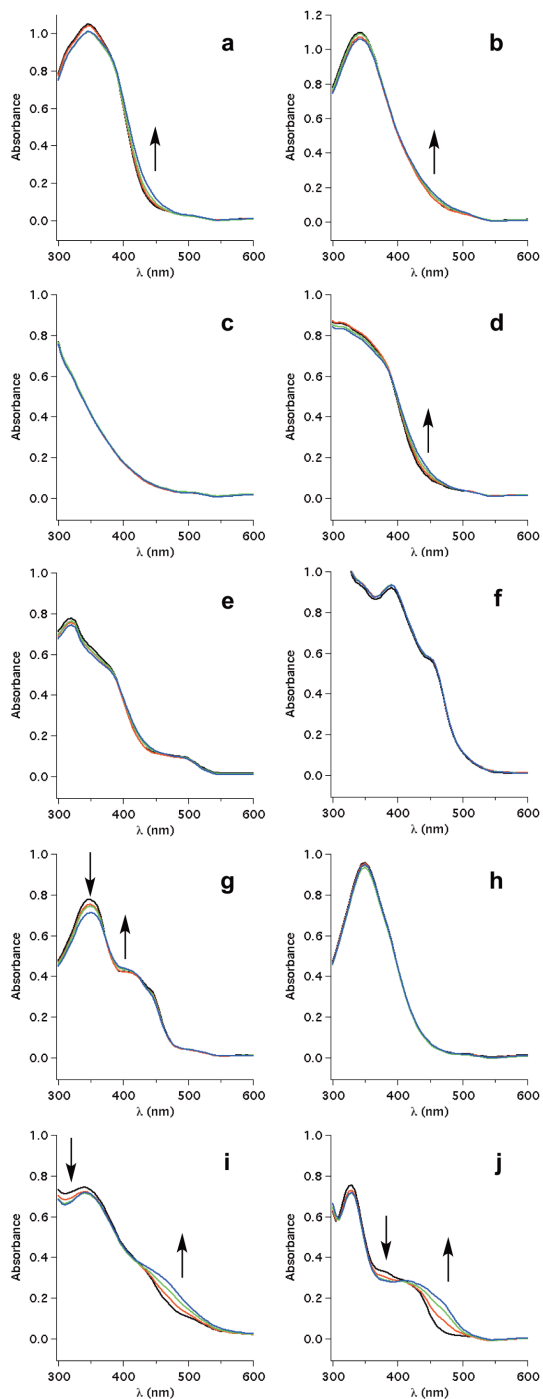


Figure 39: Changes in the electronic absorption spectra upon irradiation with visible light ($\lambda_{\text{irr}} > 400$ nm) in H_2O of complexes **88a-j** for 0 (black), 5 (red), 15 (green) and 30 (blue) min.

In addition to photochemical screening, each of the library members was analyzed by ESMS (Table 10). Major peaks were observed for each species, along with suitable isotope patterns, corresponding to calculated m/z values for dications. Compounds **88a**, **88c-e** and **88j** all showed m/z values consistent with two bound MeCN groups. Data for **88b** were consistent with three bound nitriles, suggesting that the carboxylic acid group of ligand **86b** was not bound to ruthenium. Complexes derived from the pentadentate ligands **88f-h** all showed major species corresponding to one bound MeCN group.

Compound ^{1,b}	m/z (obs)	Formula (calculated) ^c
88a ^a	337	[Ru(86a)(MeCN) ₂] ²⁺
88b ^a	340	[Ru(86b)(MeCN) ₃] ²⁺
88c ^a	344	[Ru(86c)(MeCN) ₂] ²⁺
88d ^a	351	[Ru(86d)(MeCN) ₂] ²⁺
88e ^a	389	[Ru(86e)(MeCN) ₂] ²⁺
88f ^a	355	[Ru(86f)(MeCN)] ²⁺
88g ^a	355	[Ru(86g)(MeCN)] ²⁺
88h ^b	382	[Ru(86h)(MeCN)] ²⁺
88i ^a	nd	nd
88j ^a	387	[Ru(86j)(MeCN) ₂] ²⁺

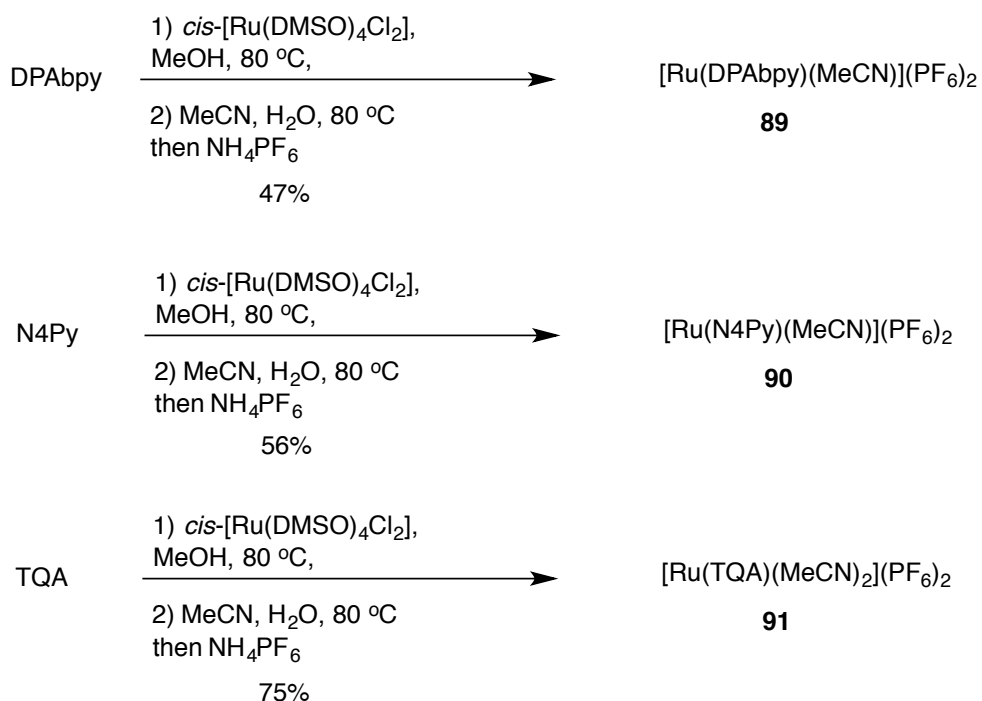
Table 10. ESMS data for compounds **88a-j** showing major m/z values observed and molecular formulas for dications consistent with the data (nd = not detected).

6.2.3 Synthesis and Characterization of Complexes by Solution Phase.

Based on results from our screening, three ligands were chosen for further evaluation in Ru(II) MeCN complexes. Ligand **85f**, a derivative of the known ligand DPAbpy, was chosen because its Ru(II) MeCN complex showed significant absorbance in the visual region, yet no reactivity with visible light, a surprising observation that needed to be verified by solution phase. Ligand **85g**, a derivative of the known ligand N4Py, was chosen because it also showed significant absorbance above 400 nm. Unlike **88f**, complex **88g** did show reactivity with visible light, but data were not consistent with substitution of H₂O for MeCN, because a bathochromic shift was not observed. Therefore a follow up study was warranted. Finally, ligand **85j**, which contains two isoquinoline donors, was identified as the lead ligand from this study. The UV-vis spectrum of **88j** showed a significant bathochromic shift in absorbance relative to **88a**, as well as rapid spectral changes upon irradiation with visible light that were consistent with substitution of H₂O for MeCN. However, instead of **86j**, we chose to examine the C₃ symmetric ligand TQA, which replaces the pyridine donor of **86j** with isoquinoline. This was expected to simplify our analysis, because only one isomer can be formed from TQA, unlike **86j**, where quinoline donors could adopt either a *cis* or *trans* configuration and lead to formation of two isomers.

Three Ru(II) complexes were synthesized by solution phase for evaluation against compounds from our library screen (Scheme 15). The ligands DPAbpy, N4Py and TQA were synthesized using literature procedures.^{213,227,228} Treating each ligand with one equiv. of *cis*-[Ru(DMSO)₄Cl₂] in MeOH at 80 °C led to rapid metallation. Concentration and heating in MeCN:H₂O (1:1), followed by precipitation with NH₄PF₆ produced [Ru(DPAbpy)(MeCN)](PF₆)₂ (**89**), [Ru(N4Py)(MeCN)₂](PF₆)₂ (**90**) and [Ru(TQA)(MeCN)₂](PF₆)₂ (**91**) in yields of 47-75%. Complexes **89-91** were characterized by ¹H NMR and IR spectroscopies and ESMS. X-ray

crystallographic data were collected for complexes **89** and **90** only, data for **91** were described previously in in the literature.²²⁹



Scheme 15: Synthesis of Ru(II) MeCN complexes **89-91** by solution phase methods.

X-ray crystallographic data were obtained for **89** and **91**. Diffusion of Et₂O into acetone solutions provided crystals of **89** and **91** suitable for X-ray crystallographic analysis. Select data for **89** and **91** are presented in Figure 40; full tables can be found at the end of Chapter 6.

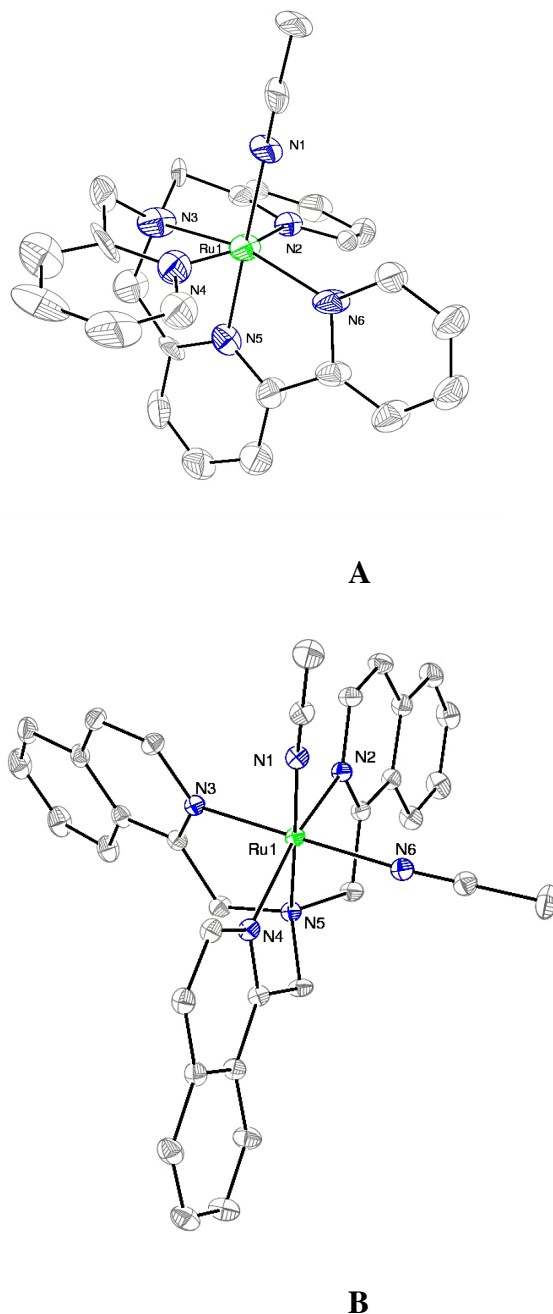


Figure 40: ORTEP diagrams of the dication $[\text{Ru}(\text{DPA}bpy)(\text{MeCN})]^{2+}$ (**A**) and $[\text{Ru}(\text{TQA})(\text{MeCN})_2]^{2+}$ (**B**) derived from **89** and **91**, respectively. Thermal ellipsoids are shown at 50% probability. Hydrogen atoms are omitted for clarity. Select bond lengths (\AA) and angles (deg) for $[\text{Ru}(\text{DPA}bpy)(\text{MeCN})]^{2+}$ (**A**); Ru–N1, 2.052(11); Ru–N2, 2.060(12); Ru–N3, 2.085(12); Ru–N4, 1.986(14); Ru–N5, 1.954(11); Ru–N6, 2.052(11); N1–Ru–N6, 97.6(4). Select bond lengths (\AA) and angles (deg) for $[\text{Ru}(\text{TQA})(\text{MeCN})_2]^{2+}$ (**B**); Ru–N1, 2.032(1); Ru–N2, 2.067(1); Ru–N3, 2.052(1); Ru–N4, 2.061(1); Ru–N5, 2.042(1); Ru–N6, 2.042(1); N1–Ru–N6, 87.50(4).

6.2.4 Photolysis of the metal complexes

The changes to the electronic absorption spectra of **89**, **90**, and **91** in H₂O at room temperature were monitored by the Turro group as a function of irradiation time to detect generation of any photochemical products. No change in the absorption spectrum of **89** was observed following irradiation ($\lambda \geq 395$ nm) for 1 h. The irradiation of **90** in H₂O with $\lambda \geq 395$ nm results in a shift in the absorption maximum from 348 nm to 361 nm, whereas the peak at 420 nm blue shifts to 408 nm with clear isosbestic points at 368 nm and 412 nm (Figure 41A). This process, occurring with $\Phi_{400} = 0.019(3)$, is not consistent with substitution of CH₃CN with H₂O because a shift of the MLCT band at 420 nm to lower energy is expected. Further irradiation causes a red shift of the 420 nm peak (Figure 41B), suggesting that substitution of CH₃CN may occur as a secondary process following the first photoinduced event. The first event is presumed to correspond to the substitution of one of the coordinated pyridyl substituents from the N4Py ligand with H₂O, a point that is explored by ¹H NMR spectroscopy with the results described below. Irradiation of **91** with $\lambda \geq 395$ nm, Figure 41C, causes a red shift of the absorption maximum from 418 nm to 425 nm with an isosbestic point at 420 nm and $\Phi_{400} = 0.027(1)$. This red shift of the MLCT band is consistent with formation of the corresponding mono-aqua complex upon substitution of one CH₃CN. Further irradiation results in a further red shift to 460 nm (Figure 41D), consistent with substitution of the second CH₃CN ligand with H₂O. Indeed, a second isosbestic point is apparent in Figure 41D for the changes to the absorption spectrum at longer irradiation time at 398 nm.

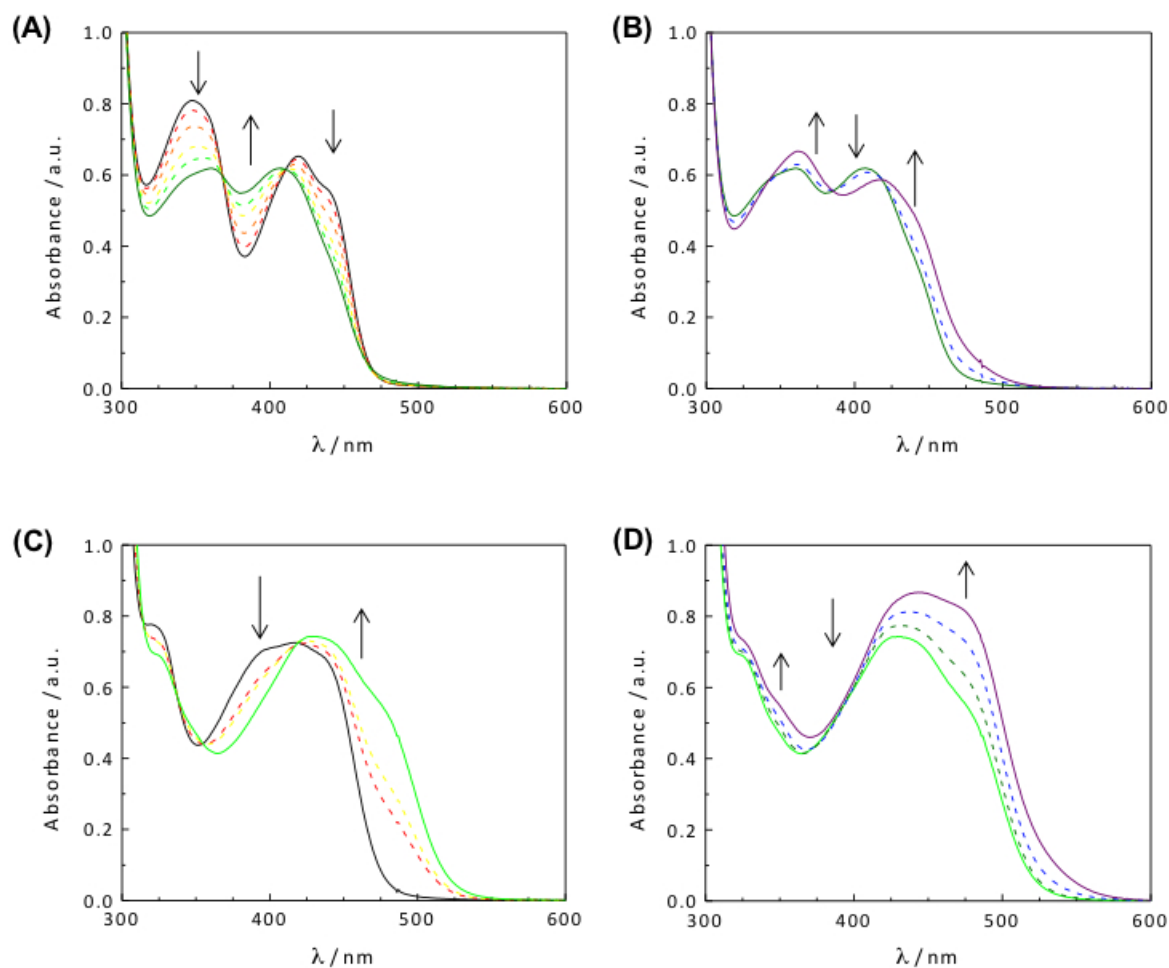


Figure 41: Electronic absorption spectra of **90** irradiated for 0, 0.5, 1, 4, 7, and 15 min (A) and 15, 40, and 85 min (B) and **91** irradiated for 0, 0.5, 1, and 2 min (C) and 2, 5, 20, and 60 min (D), in H₂O upon irradiation with $\lambda \geq 395$ nm.

To confirm the nature of the photoproducts formed during the photolysis of **90** and **91**, the changes to the ¹H NMR spectrum of each complex was monitored as a function of irradiation time in D₂O with $\lambda \geq 395$ nm. In D₂O in the dark, no changes were observed, confirming that the complexes are stable in solution in the absence of light. Figure 42A depicts the changes in the NMR spectrum of **91** upon irradiation in D₂O. In 180 min, a clean progression to a single photoproduct is observed, assigned to the mono-aqua species, labeled M in Figure 42A. Most

notably, the loss of the singlet at 2.32 ppm concurrent with the evolution of a singlet at 2.06 ppm (free CH₃CN) indicates substitution of bound CH₃CN with D₂O. By comparison with the previously reported [Ru(TPA)(CH₃CN)₂]²⁺ analogue,²²¹ the photosubstituted CH₃CN is assigned as the ligand *trans* to the quinoline group (N6, Figure 40B), as this CH₃CN chemical shift is more shielded than the CH₃CN *trans* to the amine (2.92 ppm). A schematic representation of this ligand exchange is shown in Figure 42B. This experiment confirms the ability of **91** to release a nitrile ligand and coordinate a solvent molecule when irradiated with visible light at early irradiation times. It should be noted that after 180 min of irradiation, the integration of the peak corresponding to remaining bound CH₃CN ligand begins to decrease, together with a continued increase in free CH₃CN. At 360 min of irradiation, peaks corresponding to the bis-aqua product are discerned in the ¹H NMR spectrum, labeled B in Figure 42A. This finding, together with the presence of an isosbestic point a longer irradiation times in the absorption spectra (Figure 41B), is indicative that the first step shown in Figure 42B is followed by the exchange of the second CH₃CN ligand with prolonged photolysis.

The photoproduct(s) formed upon irradiation of **90** in D₂O were also studied by ¹H NMR and the results are shown in Figure 43. Unlike **91**, the bound CH₃CN singlet at 2.81 ppm does not show a clear decrease concurrent with only free CH₃CN evolution; instead, as the singlet at 2.81 ppm decreases, a new peak at 2.86 ppm increases as well as a small increase of free CH₃CN at 2.06 ppm. Additionally, the singlet at 6.62 ppm, assigned as the methine proton, decreases and two new additional singlets at 6.08 and 6.35 ppm appear with irradiation. The aromatic region becomes more complicated with new peaks arising at 6.98, 7.80, 8.25, and 8.84 ppm. The shift is consistent with a small change in the environment around the CH₃CN protons upon exchange of one coordinated pyridyl ring for a solvent molecule. The ¹H NMR results are consistent with the

presence of multiple photoprocesses upon visible light irradiation, where the dominant pathway is the dissociation of a coordinated N4Py pyridyl ring from the ruthenium center, but with CH₃CN exchange for a solvent molecule also operative to a smaller extent, the methine proton singlet upfield is consistent with one of the pyridyl rings being released and replaced by solvent.

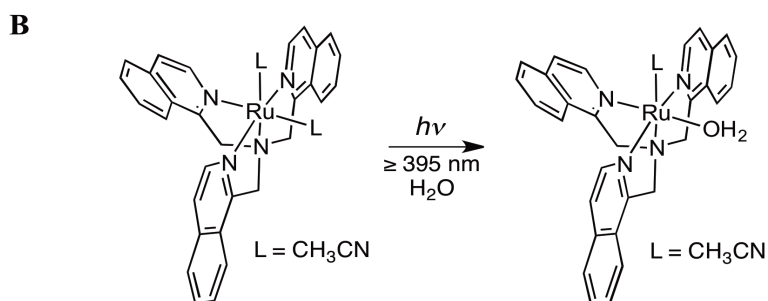
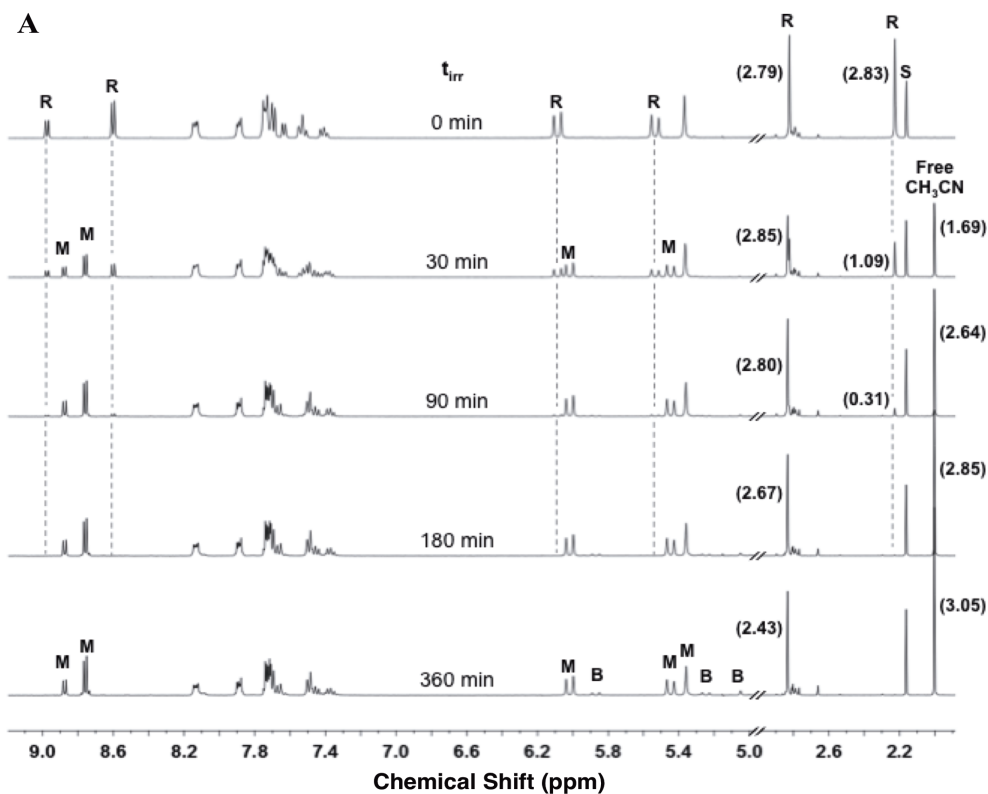


Figure 42: ¹H NMR spectra following irradiation of **91** in D₂O with $\lambda_{\text{irr}} \geq 395$ nm for 0, 15, 45, 90, and 180 min; the label M indicates signal from the mono-aqua intermediate and B from the bis-aqua product formed upon irradiation with selected integrations shown parentheses (A) and schematic representation of the first ligand exchange process of the complex (B).

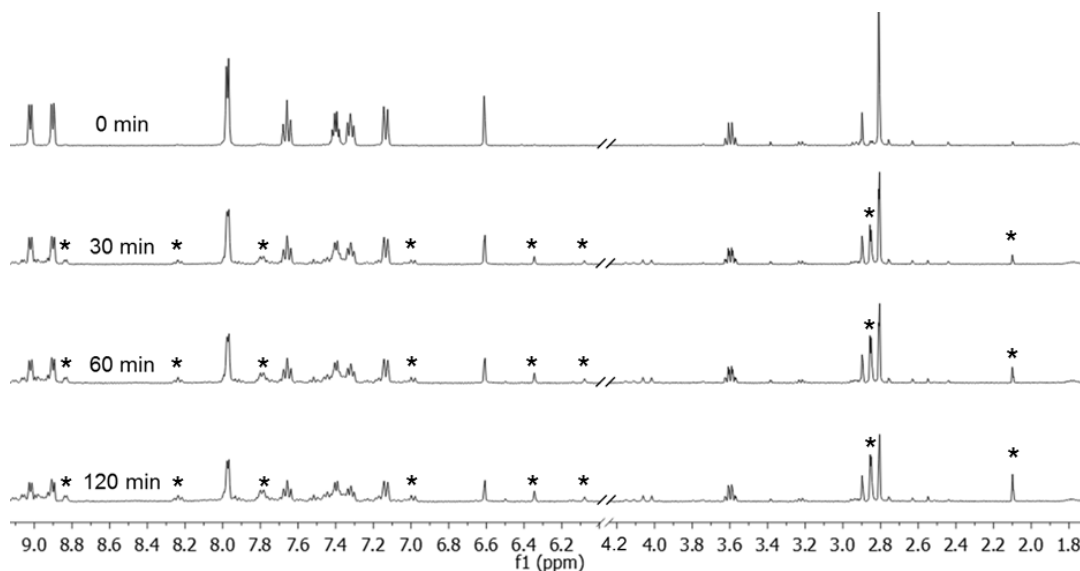


Figure 43: ^1H NMR spectra following irradiation of **90** in D_2O with $\lambda_{\text{irr}} \geq 395$ nm for 0, 30, 60, and 120 min. Stars indicate new signals evolved upon irradiation.

6.2.5 Discussions.

Combinatorial chemistry, diversity-oriented synthesis and other compound library approaches have made a major impact in chemical biology and drug discovery.²³⁰⁻²³⁶ Methods for synthesizing large libraries of organic compounds have advanced to the point where a single researcher can synthesize hundreds of thousands of compounds in a week.²¹⁵ In comparison to organic compounds, methods to synthesize libraries of inorganic compounds are grossly underdeveloped. Most attention has focused on the discovery of metal-based catalysts for organic reactions,²³⁷⁻²³⁹ selective metal-binding agents,²⁴⁰⁻²⁴² and new photosensitizers.²⁴³ Peptide- and oligonucleotide conjugates of metal complexes have been synthesized by solid phase for biological applications, and these compounds have enjoyed great success as biologically active agents and tool compounds.²⁴⁴⁻²⁵³ However, their synthesis often involves late-stage attachment of the complex (or ligand) to the biomolecule, where the coordination environment of the complex is preset. Surprisingly, even though there is an enormous amount of chemical space that

remains unexplored, studies that apply combinatorial chemistry to vary and tune the coordination sphere of biologically active inorganic compounds are rare. To the best of our knowledge, library approaches had not been applied yet towards discovery of new metal-based caging groups, a class of inorganic compounds with many important biological applications.^{36-38,40,56,76,146,150-}

152,171,221,254-266

The solid phase synthesis and screening platform described in this manuscript allowed us to rapidly identify complexes that release their ligands with visible light. Three examples with varied reactivity were synthesized and fully characterized, and the photochemical behavior of the complexes was in good agreement between solid- and solution-phase compounds. Thus, our library approach was validated as a method for identifying lead caging groups. Solid-phase synthesis carries numerous advantages over its solution-phase counterpart, including the ability to perform reactions on small scale, and isolate compounds by simple filtration, thereby avoiding time consuming and often tedious purifications of ligand precursors, ligands and metal complexes, which can all be challenging. Removing the need for compound isolation and chromatography is a major advantage, especially for researchers that do not carry a strong experimental skill set in synthesis. Key to this study, only 1-2 compounds out of the 10 surveyed actually reacted with visible light in the desired manner to release bound nitriles. Synthesizing and characterizing the photochemistry of each of these 10 complexes would have taken considerable effort. The synthesis and screening approach we adopted allowed us to direct our efforts in synthesis and full characterization toward the most promising compounds only.

The library members from this study displayed a wide range of reactivity with visible light. Many of the examples showed little if any photochemical activity, an observation easily explained by the fact that most compounds did not absorb strongly in the visible region. Indeed,

photochemistry is observed for many of the compounds surveyed when irradiated with in the MLCT bands with UV light.²⁶⁷ However, several of the compounds prepared absorb well in the visible range, and either do react when irradiated with visible light to follow a non-desired pathway, such as the pyridine release observed with complex **90**, or are not photoactive with visible light at all (ex. **89**). Thus, absorbing in the visible range did not guarantee nitrile release with visible light, an observation that has been reported with other caging strategies.²⁵⁷ The lead compound established from this study was complex **91**, which acts much like its congener $[\text{Ru}(\text{TPA})(\text{MeCN})_2]^{2+}$,²²¹ with the selective release the nitrile ligand positioned *trans* to quinoline upon irradiation with short irradiation times. Complex **91**, however, does provide numerous advantages over $[\text{Ru}(\text{TPA})(\text{MeCN})_2]^{2+}$, including efficient release of MeCN with visible light and larger quantum yield, $\Phi_{400} = 0.027(1)$ for **91** vs. $\Phi_{350} = 0.012(1)$ for $[\text{Ru}(\text{TPA})(\text{MeCN})_2]^{2+}$. In order to explain the wide range of reactivity with light, computations were carried out with compounds **89-91** and other examples.²⁶⁸ Time-dependent density functional theory (TD-DFT) calculations, performed by the Schlegel group have provided significant insight into the disparity of reactivity for these complexes, which are all derived from very similar ligands.²⁶⁹ These data have allowed us to assign many of the optical bands observed in absorption spectra of the complexes as ¹MLCT transitions, which fall in the UV to visible range. Preliminary assessment of the data indicates that the barrier for internal conversion between the lowest energy ³MLCT state and the dissociative triplet metal centered (³MC) states is a key factor that controls the outcome and selectivity of nitrile release with these complexes. Results of these studies in great detail are published and will not be discussed here further.²⁶⁹

6.2.6 Conclusions.

In conclusion, we have described a new platform for discovering metal-based caging groups that provides rapid access to new derivatives for screening photochemical behavior. A representative library of 10 compounds was produced that contained a range of different donors, denticities and coordination geometries. Absorption and photoreactivity with visible light was screened, resulting in the identification of several compounds that demonstrated interesting behavior worthy of further investigation. Three new analogs were synthesized by solution phase, and data for compounds were in good agreement with the corresponding complexes from solid phase, thus validating the predictive power of the library approach. The wide range of reactivity with visible light amongst the library of compounds illustrated the need to prescreen compounds for their photochemical behavior, before efforts were directed towards solution phase synthesis and full characterization, an inherently tedious but necessary process. In general terms, this study represents an important example of why combinatorial, library-based approaches should be applied towards the development of inorganic complexes for biological applications. Such studies are currently underway in our laboratory.

6.3 Experimental procedures for solid phase-based metal complexes

6.3.1 Synthesis of compound **80**

Compound **80** can be synthesized from compound **79**, which is prepared from dimethyl pyridine 2-5-dicarboxylate in two steps using a literature protocol.²⁷⁰ Compound **79** (2g, 11.9 mmol) was dissolved in 160 mL of dry MeOH under inert atmosphere. To this 1,3-propanediamine (10.6 g, 0.14 mol) was added and the reaction mixture was refluxed for 24 h under inert atmosphere. Reaction mixture was concentrated under reduced pressure and excess 1,3-propanediamine was removed by azeotropic distillation from toluene (3 × 100 mL) to give compound **80** as a white solid (2.4 g, 96%). Mp = 122 °C; ¹H NMR (400MHz, D₂O) δ 8.64 (s,

¹H), 8.02 (d, 1H, *J* = 8.8 Hz), 7.46 (d, 1H, *J* = 8.4 Hz), 3.30 (t, 2H, *J* = 6.8 Hz), 2.55 (t, 2H, *J* = 7.6 Hz), 1.62 (m, 2H, *J* = 7.2 Hz); ¹³C NMR (400MHz, D₂O) δ 168.2, 162.5, 146.9, 136.7, 128.8, 120.9, 63.6, 37.9, 37.5, 31.1; IR (KBr) ν_{max} (cm⁻¹) 3666, 3592, 3418, 3119, 2935, 2856, 2276, 1729, 1609, 1481, 1461, 1448, 1311, 1289, 1160, 992, 838, 767, 739. ESMS calculated for (M+H)⁺ 210.1243, found 210.1252.

6.3.2 Synthesis of resin bound pyridine precursor (**83** and **84**) and ligand library (**85a-j** and **86a-j**)

Commercially available rink amide MBHA resin **81** (Chem-impex, 0.75 mmol) was Fmoc deprotected by agitating the resin in a standard peptide synthesizer in the presence of 20% piperidine in DMF (20 mL) for 20 min at room temperature (2 cycle). After 2 cycles the resin was washed with DMF (3 × 20 mL), IPA (3 × 20 mL) and DCM (3 × 20 mL) and dried under reduced pressure. The deprotected resin (0.7 mmol) is then treated with succinic anhydride (2.8 mmol) in DMF (8 mL) in a peptide synthesizer and agitated for 2 h at RT. Amidation was done for two cycles to ensure complete consumption of the amine to give compound **82**. After 2 cycles the resin was washed with DMF (3 × 20 mL), IPA (3 × 20 mL) and DCM (3 × 20 mL) and dried under reduced pressure. Compound **82** (0.7 mmol) was then reacted with compound **80** (2.8 mmol) in the presence of HBTU (2.8 mmol), DIPEA (0.84 mmol) in DMF (20 mL) in a peptide synthesizer at RT for 16 h to give the coupling product **83**. Resin was then washed with DMF (3 × 20 mL), IPA (3 × 20 mL) and DCM (3 × 20 mL) and dried under reduced pressure. Small amount of resin can be cleaved using standard cleaving conditions described below and NMR was taken to ensure reaction completion.

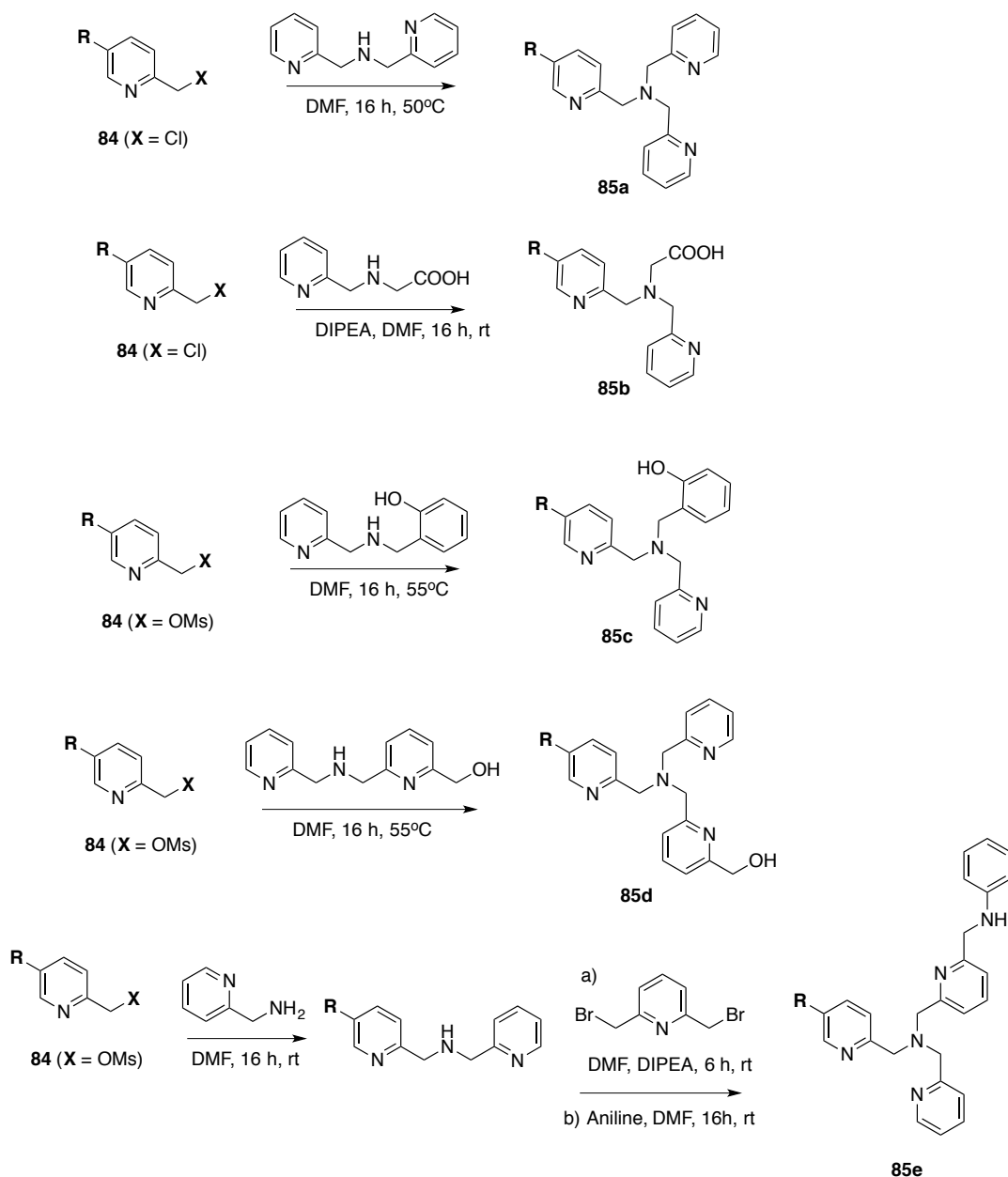
The alcohol group of compound **83** can be mesylated by treating compound **83** (0.21 mmol) with MsCl (0.84 mmol), TEA (1.05 mmol) in dry THF (12 mL) for 2h at RT in a peptide agitator for 2 cycles. Small amount of resin was cleaved by following standard cleaving procedure and NMR of the product was taken to ensure reaction completion.

Operation	Scale	Reagent	Vol	No of cycles	Time/Temp
Fmoc deprotection	0.7 mmol	20% piperidine in DMF	20 mL	2	20 min/ RT
Drain and wash	0.7 mmol	DMF, iPrOH, DCM	20 mL	3	2 min (each)/ RT
Amidation	0.7 mmol	Succinic anhydride (2.8 mmol)	8 mL DMF	2	2h / RT
Coupling with 80	0.7 mmol	Compound 3 (2.8 mmol), HBTU (2.8 mmol), DIPEA (0.84 mmol)	20 mL DMF	1	16 h / RT
Mesylation	0.21 mmol	MsCl (0.84 mmol), TEA (1.05 mmol)	12 mL dry THF	3	2 h / RT
Chlorination	0.7 mmol	TsCl (7 mmol), LiCl (35 mmol), DIPEA (10.5 mmol)	20 mL CH ₃ CN	1	16 h /50 °C

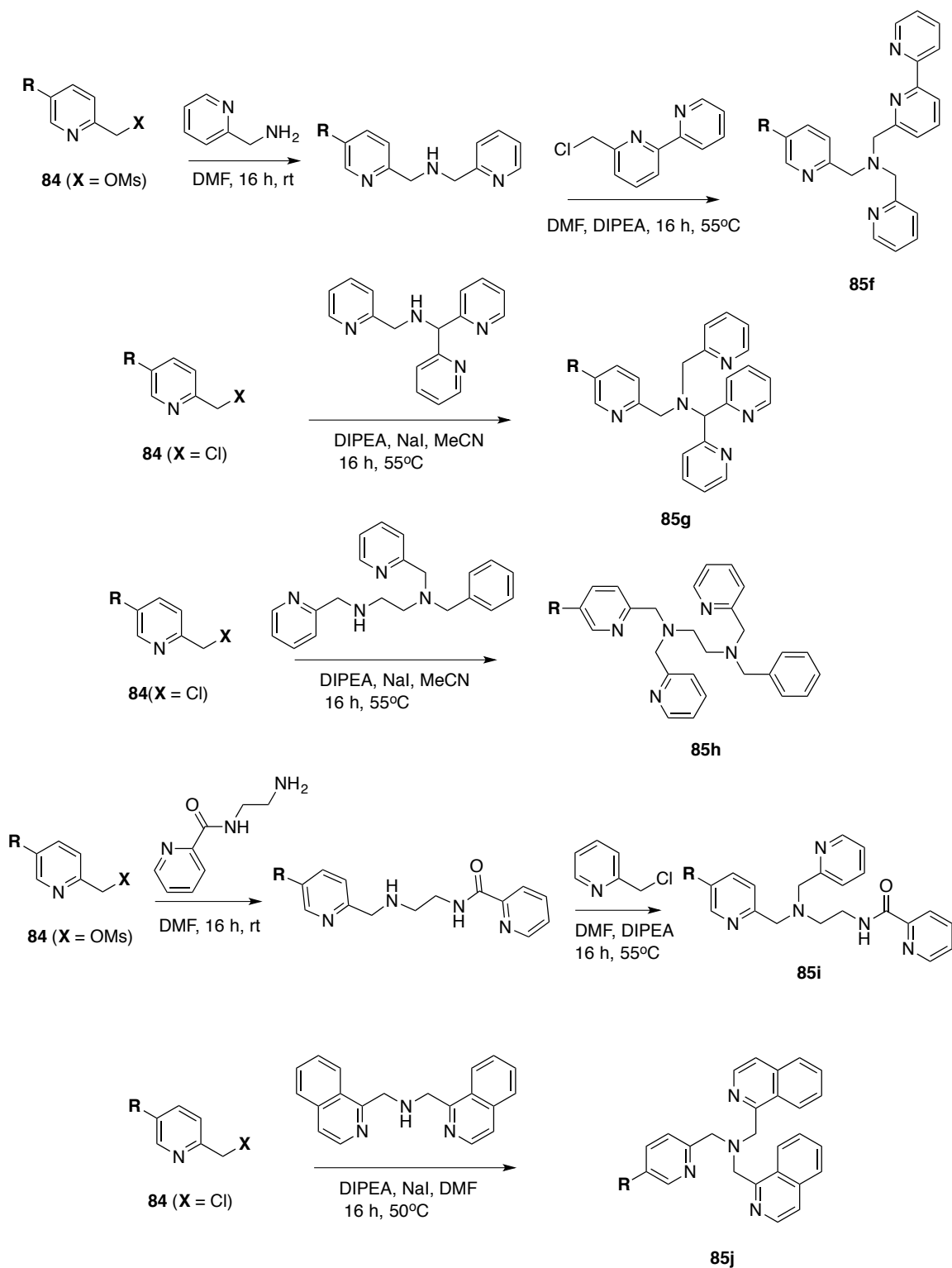
Table 11: Synthesis of compounds **83** and **84**

The alcohol group of compound **83** can be chlorinated by heating compound **83** (0.7 mmol) with TsCl (7 mmol), LiCl (35 mmol), DIPEA (10.5 mmol) in acetonitrile (20 mL) for 16

h at 50 °C in a vial equipped with slow stirring. After reaction completion, resin was washed with DMF (3 × 20 mL), IPA (3 × 20 mL) and DCM (3 × 20 mL) and dried under reduced pressure to give compound **84**. ¹H NMR spectroscopic analysis of product, obtained by cleavage of a small amount of resin, was used to measure reaction progress.



Scheme 16a: Synthesis of polypyridyl ligand library (**85a-85e**)



Scheme 16b: Synthesis of polypyridyl ligand library (**85f-85j**)

Standard procedure for resin cleavage is 10 mg of resin was suspended in 1 mL of 95% TFA in water and allowed to stand for 15 min at room temperature. The contents of the vial were filtered through a cotton plug and concentrated under reduced pressure. The resulting compound would be either dissolved in 1 mL D₂O for NMR (compounds **83** and **84** and polypyridyl ligands **86a-j**) or 1 mL of H₂O (metal complexes **88a-j**) for UV spectroscopy and mass spectrometry.

Synthesis of compound **86a** – Resin bound Compound **84** (X = Cl) (100 mg, 0.07 mmol) was heated at 50 °C for 16 h in the presence of bis(pyridine-2-ylmethyl)amine²⁷¹ (70 mg, 0.35 mmol) in 3 mL DMF under ambient atmosphere in a vial with slow stirring to get resin bound **85a** which was then washed with DMF (3 × 10 mL), IPA (3 × 10 mL) and DCM (3 × 10 mL) and dried under reduced pressure. 10 mg of resin was then cleaved using standard cleavage condition to get **86a** which was analyzed by NMR and HPLC; ¹H NMR (400MHz, D₂O) δ 8.75 (s, 1H), 8.66 (d, 2H, *J* = 6.0 Hz), 8.42 (t, 2H, *J* = 8 Hz), 8.05 (d, 1H, *J* = 8.4 Hz), 7.94 (d, 2H, *J* = 8 Hz) 7.86(t, 2H, *J* = 7.6 Hz) 7.46(d, 1H, *J* = 8.4 Hz) 4.40(s, 4H) 4.11(s, 2H), 3.39 (t, 2H, *J* = 6.8 Hz), 2.55 (m, 4H), 1.79 (m, 2H). Calculated mass for (M+H)⁺ 490.56, found 491.

Synthesis of compound **86b** – Resin bound Compound **84** (X = Cl) (100 mg, 0.07 mmol) was agitated in a standard solid phase peptide synthesizer at room temperature for 16 h in the presence of (pyridine-2-ylmethyl)glycine hydrochloride salt²⁷² (141 mg, 0.7 mmol) in 3 mL DMF along with DIPEA (90 mg, 0.7 mmol) under ambient atmosphere to get resin bound **85b** which was then washed with DMF (3 × 10 mL), IPA (3 × 10 mL) and DCM (3 × 10 mL) and dried under reduced pressure. 10 mg of resin was then cleaved using standard cleavage condition to get **86b** which was analyzed by NMR and HPLC; ¹H NMR (400MHz, D₂O) δ 8.93(s, 1H), 8.67(d, 1H, *J* = 5.6 Hz), 8.47(d, 1H, *J* = 8 Hz), 8.41(t, 1H, *J* = 8 Hz), 7.91-7.86(m, 3H), 4.44(s, 2H),

4.39(s, 2H), 3.72(s, 2H), 3.43(t, 2H, $J = 6.8$ Hz), 3.26(t, 2H, $J = 6.8$ Hz), 2.55-2.48(m, 4H), 1.81(t, 2H, $J = 6.8$ Hz). Calculated mass for $(M+H)^+$ 457.22, found 457.

Synthesis of compound **86c** – Resin bound Compound **84** (X = OMs) (100 mg, 0.07 mmol) was slowly stirred in a vial at 55 °C for 16 h in the presence of 2-(((pyridine-2-ylmethyl)amino)methyl)phenol²⁷³ (150 mg, 0.7 mmol) in 3 mL DMF under ambient atmosphere to get resin bound **85c** which was then washed with DMF (3 × 10 mL), IPA (3 × 10 mL) and DCM (3 × 10 mL) and dried under reduced pressure. 10 mg of resin was then cleaved using standard cleavage condition to get **86c** which was analyzed by NMR and HPLC; ¹H NMR (400MHz, D₂O) δ 8.91(s, 1H), 8.65(d, 1H, $J = 5.6$ Hz), 8.42(d, 2H, $J = 8.4$ Hz), 8.28(t, 1H, $J = 8.0$ Hz), 7.83(d, 1H, $J = 7.6$ Hz), 7.78-7.75(m, 2H), 7.21(d, 1H, $J = 8$ Hz), 7.10(t, 1H, $J = 7.6$ Hz), 6.81(t, 1H, $J = 7.6$ Hz), 6.60(d, 1H, $J = 8$ Hz), 4.57-4.56(m, 2H), 4.10(s, 2H), 3.47(t, 2H, $J = 6.8$ Hz), 3.30(t, 2H, $J = 6.4$ Hz), 2.59-2.51(m, 4H), 1.87-1.82(m, 2H). Calculated mass for $(M+Na)^+$ 527.24, found 527.

Synthesis of compound **86d** – Resin bound Compound **84** (X = OMs) (100 mg, 0.07 mmol) was slowly stirred in a vial at 55 °C for 16 h in the presence of (6-(((pyridine-2-ylmethyl)amino)methyl)pyridine-2-yl)methanol²⁷⁴ (160 mg, 0.7 mmol) in 3 mL DMF under ambient atmosphere to get resin bound **85d** which was then washed with DMF (3 × 10 mL), IPA (3 × 10 mL) and DCM (3 × 10 mL) and dried under reduced pressure. 10 mg of resin was then cleaved using standard cleavage condition to get **86d** which was analyzed by NMR and HPLC; ¹H NMR (400MHz, D₂O) δ 8.85(s, 1H), 8.68(d, 1H, (t, 2H, $J = 5.2$ Hz), 8.43(t, 1H, $J = 7.6$ Hz), 8.34(t, 1H, $J = 7.6$ Hz), 8.13(d, 1H, $J = 8.4$ Hz), 7.97(d, 1H, $J = 8$ Hz), 7.88(t, 1H, $J = 7.2$ Hz), 7.81(t, 2H, $J = 8.0$ Hz), 7.52(d, 1H, $J = 8.4$ Hz), 4.99(s, 2H), 4.43(s, 2H), 4.39(s, 2H), 4.19(s,

2H), 3.46-3.41(m, 2H), 3.30-3.25(m, 2H), 2.57-2.49(m, 4H), 1.86-1.79(m, 2H). Calculated mass for (M+H)⁺ 519.26, found 520.

Synthesis of compound **86e** – Resin bound Compound **84** (X = OMs) (100 mg, 0.07 mmol) was agitated in a standard solid phase peptide synthesizer at room temperature for 16 h in the presence of pyridine-2-yl-methanamine (2-picolylamine)²⁷⁰ (76 mg, 0.7 mmol) in 6 mL DMF under ambient atmosphere to get resin bound secondary amine which was washed with DMF (3 × 10 mL), IPA (3 × 10 mL) and DCM (3 × 10 mL) and dried under reduced pressure. The secondary amine was then alkylated using 2,6-bis(bromomethyl)pyridine²⁷⁴ (186 mg, 0.7 mmol) and DIPEA (90 mg, 0.7 mmol) in 6 mL DMF at room temperature for 6 h. The resin was washed using standard washing procedure with DMF, IPA and DCM and further subjected to third alkylation using aniline (65 mg, 0.7 mmol) in 3 mL DMF at room temperature for 16 h under ambient temperature to give resin bound **85e**, which was then washed with DMF (3 × 10 mL), IPA (3 × 10 mL) and DCM (3 × 10 mL) and dried under reduced pressure. 10 mg of resin was then cleaved using standard cleavage condition to get **86e** which was analyzed by NMR and HPLC; ¹H NMR (600MHz, D₂O) δ 8.70(s, 1H), 8.45(m, 1H), 8.21-8.18(m, 2H), 7.95-7.93(m, 1H), 7.73-7.66(m, 3H), 7.55-7.46 (Junk), 7.36-7.33(m, 1H), 7.22-7.21(m, 1H), 7.12-7.10(m, 2H), 6.87(t, 1H, J = 7.8 Hz), 6.77(d, 2H, J = 7.8 Hz), 4.58(s, 2H), 4.14(s, 2H), 4.05(m, 4H), 3.62(s, 1H, impurity), 3.26-3.24(m, 2H), 3.08-3.06(m, 2H), 2.36-2.33(m, 4H), 1.65-1.63(m, 2H). Calculated mass for (M+H)⁺ 594.31, found 595.

Synthesis of compound **86f** – Resin bound Compound **84** (X = OMs) (100 mg, 0.07 mmol) was agitated in a standard solid phase peptide synthesizer at room temperature for 16 h in the presence of pyridine-2-yl-methanamine (2-picolylamine) (76 mg, 0.7 mmol) in 6 mL DMF under ambient atmosphere to get a resin bound secondary amine, which was then washed with

DMF (3 × 10 mL), IPA (3 × 10 mL) and DCM (3 × 10 mL) and dried under reduced pressure. The secondary amine was then alkylated using 6-(chloromethyl)-2,2'-bipyridine²⁷⁵ (143 mg, 0.7 mmol) and DIPEA (90 mg, 0.7 mmol) in 3 mL DMF at 55 °C for 16 h in a vial with slow stirring. The resin was washed using standard washing procedure with DMF, IPA and DCM and dried under reduced pressure to get resin bound **85f**. 10 mg of resin was then cleaved using standard cleavage condition to get **86f** which was analyzed by NMR and HPLC; ¹H NMR (400MHz, D₂O) δ 8.91(d, 1H, *J* = 6.0 Hz), 8.82(s, 1H), 8.72-8.68(m, 1H), 8.64(d, 1H, *J* = 5.6 Hz), 8.57-8.55(m, 1H), 8.30(t, 1H, *J* = 6.4 Hz), 8.25(d, 1H, *J* = 8.0 Hz), 8.15-8.10(m, 2H), 8.04(t, 1H, *J* = 8.0 Hz), 7.90(d, 1H, *J* = 8.0 Hz), 7.78(t, 1H, *J* = 8.0 Hz), 7.73(d, 1H, *J* = 8.4 Hz), 7.66(d, 1H, *J* = 8.0 Hz), 4.58(s, 2H), 4.49(s, 2H), 4.38(s, 2H), 3.42(t, 2H, *J* = 6.8 Hz), 3.30-3.25(m, 2H), 2.58-2.52(m, 4H), 1.83-1.77(m, 2H). Calculated mass for (M+H)⁺ 566.28, found 567.

Synthesis of compound **86g** – Resin bound Compound **84** (X = Cl) (100 mg, 0.07 mmol) was heated at 55 °C for 16 h in the presence of 1,1-di(pyridine-2-yl)-N-(pyridine-2-ylmethyl)methanamine²⁷⁶ (193 mg, 0.7 mmol) and NaI (10.5 mg, 0.07 mmol) in 3 mL MeCN under ambient atmosphere in a vial with slow stirring to get resin bound **85g** which was then washed with DMF (3 × 10 mL), IPA (3 × 10 mL) and DCM (3 × 10 mL) and dried under reduced pressure. 10 mg of resin was then cleaved using standard cleavage condition to get **86g** which was analyzed by NMR and HPLC; ¹H NMR (400MHz, D₂O) δ 8.82(s, 1H), 8.55(d, 2H, *J* = 4.8 Hz), 8.48(d, 1H, *J* = 5.6 Hz), 8.17-8.14(m, 3H), 8.09(d, 1H, *J* = 8.0 Hz), 7.78(d, 2H, *J* = 8.0 Hz), 7.65-7.58(m, 4H), 7.36(d, 1H, *J* = 8.4 Hz), 4.30(s, 2H), 4.21(s, 1H), 4.14(s, 1H), 3.25-3.22(m, 2H), 3.09-3.06(m, 2H), 2.36-2.33(m, 4H), 1.64-1.61(m, 2H). Calculated mass for (M+H)⁺ 566.28, found 567.

Synthesis of compound **86h** – Resin bound Compound **84** (X = Cl) (100 mg, 0.07 mmol) was heated at 55 °C for 16 h in the presence of N¹-benzyl-N¹,N²-bis(pyridine-2-ylmethyl)ethane-1,2-diamine²⁷⁷ (232 mg, 0.7 mmol) and NaI (10.5 mg, 0.07 mmol) in 3 mL MeCN under ambient atmosphere in a vial with slow stirring to get resin bound **85h**, which was then washed with DMF (3 × 10 mL), IPA (3 × 10 mL) and DCM (3 × 10 mL) and dried under reduced pressure. 10 mg of resin was then cleaved using standard cleavage condition to get **86h** which was analyzed by NMR and HPLC; ¹H NMR (400MHz, D₂O) δ 8.95(s, 1H), 8.89(d, 1H, *J* = 6.4 Hz), 8.81(d, 1H, *J* = 5.2 Hz), 8.64(t, 1H, *J* = 8.0 Hz), 8.34(d, 1H, *J* = 8.4 Hz), 8.20-8.06(m, 3H), 7.56(t, 1H, *J* = 7.6 Hz), 7.69(t, 2H, *J* = 9.6 Hz), 7.61-7.50(m, 5H), 4.66(s, 2H), 4.51(s, 2H), 4.36(s, 2H), 4.18(s, 2H), 3.73-3.65(m, 4H), 3.51(t, 2H, *J* = 6.4 Hz), 3.45(t, 2H, *J* = 6.4 Hz), 2.80-2.74(m, 4H), 2.09-2.05(m, 2H). Calculated mass for (M+H)⁺ 622.34, found 623.

Synthesis of compound **86i** – Resin bound Compound **84** (X = OMs) (100 mg, 0.07 mmol) was agitated in a standard solid phase peptide synthesizer at room temperature for 16 h in the presence of N-(2-aminoethyl)picolinamide²⁷⁸ (115 mg, 0.7 mmol) in 6 mL DMF under ambient atmosphere to get resin bound secondary amine which was washed with DMF (3 × 10 mL), IPA (3 × 10 mL) and DCM (3 × 10 mL) and dried under reduced pressure. The secondary amine was then alkylated using 2-(chloromethyl)pyridine hydrochloride salt (115 mg, 0.7 mmol) and DIPEA (90 mg, 0.7 mmol) in 3 mL DMF at 55 °C for 16 h in a vial with slow stirring. The resin was washed using standard washing procedure with DMF, IPA and DCM and dried under reduced pressure to get resin bound **85i**. 10 mg of resin was then cleaved using standard cleavage condition to get **86i** which was analyzed by NMR and HPLC; ¹H NMR (400MHz, D₂O) δ 8.66-8.61(m, 3H), 8.34-8.30(m, 1H), 8.10-8.05(m, 2H), 7.98(d, 1H, *J* = 7.6 Hz), 7.90(d, 1H, *J* = 8.0 Hz), 7.79(t, 1H, *J* = 6.8 Hz), 7.69-7.67(m, 1H), 7.61(d, 1H, *J* = 8.4 Hz), 4.47(s, 2H), 4.24(s, 2H),

3.59-3.55(m, 2H), 3.42-3.48(m, 2H), 3.29-3.25(m, 2H), 3.20-3.18(m, 2H), 2.56-2.53(m, 4H), 1.84-1.80(m, 2H). Calculated mass for $(M+Na)^+$ 569.26, found 569.

Synthesis of compound **86j** – Resin bound Compound **84** (X = Cl) (100 mg, 0.07 mmol) was heated at 50 °C for 16 h in the presence of bis(isoquinolin-1-ylmethyl)amine (**94**) (209 mg, 0.7 mmol) and NaI (10.5 mg, 0.07 mmol) in 3 mL DMF under ambient atmosphere in a vial with slow stirring to get resin bound **85j**, which was then washed with DMF (3 × 10 mL), IPA (3 × 10 mL) and DCM (3 × 10 mL) and dried under reduced pressure. 10 mg of resin was then cleaved using standard cleavage condition to give **86j** which was analyzed by NMR and HPLC; ¹H NMR (600MHz, D₂O) δ 8.57(s, 1H), 8.50(d, 2H, *J* = 9.0 Hz), 8.19(d, 2H, *J* = 6.6 Hz), 8.16-8.13(m, 2H), 8.09(t, 4H, *J* = 8.4 Hz), 8.00(t, 2H, *J* = 8.4 Hz), 7.88(d, 2H, *J* = 7.2 Hz), 7.25(d, 1H, *J* = 8.4 Hz), 5.11(s, 4H), 4.39(s, 2H), 3.43-3.41(m, 2H), 3.30-3.28(m, 2H), 2.57-2.54(m, 4H), 1.83(t, 2H, *J* = 6.6 Hz). Calculated mass for $(M+H)^+$ 589.28, found 590.

6.3.3 Optimization studies for metallation and synthesis of **87** and **88**.

TPA based ligand attached to either polystyrene (^a**85a** - 0.7 mmol/g) or Tenta-gel resin (^b**85a** - 0.23 mmol/g) was used for optimization of metallation conditions. Both compound **84** (X = Cl) and compound **86a** on tentagel for the optimization steps can be prepared by following the same procedure reported for **84** and **86a** on polystyrene. Ruthenium starting materials which were used are (A) *cis*-[Ru(DMSO)₄Cl₂], (B) [Ru(COD)(MeCN)₄](BF₄)₂²⁷⁹ or (C) *fac*-[Ru(DMSO)₃(O₂CCF₃)₂(H₂O)]²⁸⁰. Different mole ratios of the ruthenium (II) were used for different reactions starting from 2 equiv. to 10-equiv. with respect to resin loading. Solvents used for the reactions were DMF or MeCN or MeOH or EtOH (1 mL). Reactions carried out by conventional heating were done in a vial under inert atmosphere in an oil bath at 50 °C for 18 h

with slow stirring of the resin in the solvent in the presence of ruthenium (II) source. The microwave reactions were performed in a 2 mL Biotage vial using Biotage microwave reactor (Initiator eight microwave system) at 80 °C or 100 °C for 0.5 h or 1 h reaction time. Metal complexes $[\text{Ru}(\mathbf{86a})(\text{DMSO})(\text{Cl})]^{1+}$ were then cleaved from the resins using standard cleavage procedure and yield was calculated using UV spectroscopy by determining the absorbance at $\lambda_{\text{max}} = 345 \text{ nm}$ ($\epsilon = 10,500 \text{ M}^{-1} \text{ cm}^{-1}$). For condition 10^a yield was calculated based on extinction coefficient of $[\text{Ru}(\mathbf{86a})(\text{MeCN})_2]^{2+}$ ($\epsilon = 9,040 \text{ M}^{-1} \text{ cm}^{-1}$).

All the solid phase based metallation reactions were carried out in 2 mL microwave glass reactors (Biotage). Each microwave vial was charged with 10 mg (0.007 mmol) ligand (**85a-j**). A stock solution of $[\text{Ru}(\text{DMSO})_3(\text{H}_2\text{O})(\text{OTFA})_2]$ was prepared by following a known literature protocol²⁸⁰ in dry EtOH inside the glove box and 17 mg (0.028 mmol) of the ruthenium complex was delivered to each vial inside the glove box. The final volume of EtOH was adjusted to 1 mL by adding additional dry EtOH. 2, 6 lutidine (7.5 mg, 0.07 mmol) was added to vials containing ligands **85b**, **85c**, and **85i**. All the glass vials were sealed inside the glove box and reacted on an Initiator eight microwave system (Biotage microwave reactor) for 30 min at 80 °C. The resin was then washed with EtOH (4 × 2 mL) followed by 1:1 MeCN: H₂O mixture (4 × 2 mL). Then 1 mL of 1:1 MeCN: H₂O solution was added to each vial and reacted on Initiator eight microwave system (Biotage microwave reactor) for 30 min at 80 °C. Resin was dried under reduced pressure and solid-state based metal complex was cleaved from resin using standard cleavage procedure to get complexes **88a-j**, which were analyzed, by UV spectroscopy and mass spectrometry.

6.3.4 Synthesis of metal complexes by solution phase **89-91**

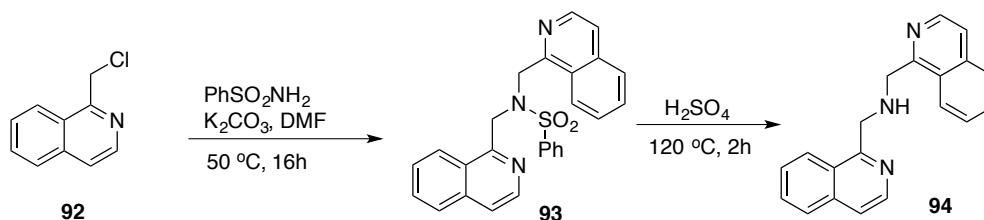
Synthesis of [Ru(DPAbpy)(MeCN)](PF₆)₂ (**89**) - DPAbpy (50 mg, 0.14 mmol) that was prepared by a known procedure²¹³ was dissolved in dry MeOH (12 mL) under inert atmosphere in a pressure flask. To this Ru(DMSO)₄Cl₂ (65 mg, 0.14 mmol) was added and the solution was purged with Ar for 10 min at room temperature. The reaction mixture was refluxed for 5 h under inert temperature. Color of the reaction mixture changes from pale yellow to dark red. The reaction mixture was cooled to room temperature and concentrated under reduced pressure. To the flask 1:1 mixture of MeCN: H₂O was added and the reaction mixture was refluxed for 16 h under inert atmosphere. Ice cold water (25 mL) was then added to the reaction mixture followed by a saturated solution of aqueous NH₄PF₆ (5 mL), which resulted in the formation of dark red precipitate that was filtered, washed with ice cold water (150 mL) and dried under reduced pressure to give title complex as a dark red solid (51 mg, 47%). Crystals for X-ray crystallographic analysis were obtained by diffusing Et₂O into a solution of **89** in acetone: Mp = 194 °C (decomp); ¹H NMR (400MHz C₃D₆O) δ 9.54(d, 1H, J = 5.6 Hz), 8.86(d, 1H, J = 8.0 Hz), 8.59(d, 1H, J = 8.8 Hz), 8.43(t, 1H, J = 7.6 Hz), 8.05(t, 1H, J = 6.4 Hz), 8.00(t, 1H, J = 8.0 Hz), 7.95(t, 2H, J = 7.6 Hz), 7.75(d, 2H, J = 8.0 Hz), 7.61(d, 2H, J = 5.6 Hz), 7.55(d, 1H, J = 8.0 Hz), 7.29(t, 2H, J = 6.4 Hz), 5.49(s, 4H), 5.43(s, 2H), 2.73(s, 3H); IR (KBr) ν_{max} (cm⁻¹) 3687, 3401, 3257, 3082, 3005, 2945, 2273, 1983, 1709, 1607, 1568, 1477, 1450, 1408, 1355, 1309, 1295, 1247, 1162, 1128, 1115, 1092, 1073, 1062, 990, 963, 939, 832, 768, 739, 670, 650, 557, 511, 465, 450, 425, 391, 353, 337, 330, 313. ESMS calculated for C₂₅H₂₄F₆N₆PRu (M⁺) 655.07, found 655.00; UV-vis λ_{max} = 371 nm (ε = 10,200 M⁻¹cm⁻¹), 462 nm (ε = 5,850 M⁻¹cm⁻¹); Anal. Calculated for C₂₅H₂₄F₁₂N₆P₂Ru: C, 37.56; H, 3.03; N, 10.51. Found: C, 37.64; H, 3.19; N, 10.42.

Synthesis of $[\text{Ru}(\text{N4py})(\text{MeCN})](\text{PF}_6)_2$ (**90**) - N4py (200 mg, 0.54 mmol) that was prepared by a known procedure²⁸¹ was dissolved in dry MeOH (50 mL) under inert atmosphere in a pressure flask. To this $\text{Ru}(\text{DMSO})_4\text{Cl}_2$ (263 mg, 0.54 mmol) was added and the solution was purged with Ar for 10 min at room temperature. The reaction mixture was refluxed for 5 h under inert temperature. Color of the reaction mixture changes from pale yellow to dark red. The reaction mixture was cooled to room temperature and concentrated under reduced pressure. To the flask 1:1 mixture of MeCN: H_2O was added and the reaction mixture was refluxed for 16 h under inert atmosphere. Ice cold water (30 mL) was then added to the reaction mixture followed by a saturated solution of aqueous NH_4PF_6 (20 mL) which resulted in the formation of pale green precipitate which was filtered, washed with ice cold water (400 mL) and dried under reduced pressure to give title complex as a dark red solid (243 mg, 56%): Mp = 191 °C (decomp); ^1H NMR (400MHz $\text{C}_3\text{D}_6\text{O}$) δ 9.22(d, 2H, J = 5.6 Hz), 9.11(d, 2H, J = 5.6 Hz), 8.18-8.08(m, 4H), 7.76(t, 2H, J = 7.2 Hz), 7.52(t, 2H, J = 6.4 Hz), 7.41(t, 2H, J = 6.4 Hz), 7.26(d, 2H, J = 8.0 Hz), 6.97(s, 1H), 4.89(m, 4H), 2.93(s, 3H); IR (KBr) ν_{max} (cm^{-1}) 3692, 3420, 3224, 3113, 3082, 2919, 2851, 2275, 1991, 1708, 1604, 1564, 1463, 1447, 1358, 1336, 1308, 1289, 1262, 1238, 1199, 1160, 1076, 1053, 1026, 970, 931, 907, 822, 765, 750, 740, 722, 653, 644, 620, 581, 556, 532, 514, 426, 373, 353, 337, 331, 313. ESMS calculated for $\text{C}_{25}\text{H}_{24}\text{F}_6\text{N}_6\text{PRu}$ (M^+) 655.07, found 655.00; UV-vis λ_{max} = 355 nm ($\epsilon = 11,900 \text{ M}^{-1}\text{cm}^{-1}$) 425 nm ($\epsilon = 9,880 \text{ M}^{-1}\text{cm}^{-1}$).

Synthesis of $[\text{Ru}(\text{TQA})(\text{MeCN})_2](\text{PF}_6)_2$ (**91**) - TQA (110 mg, 0.25 mmol), which was prepared by a known procedure²²⁷ was dissolved in dry MeOH (28 mL) under inert atmosphere in a pressure flask. To this $\text{Ru}(\text{DMSO})_4\text{Cl}_2$ (121 mg, 0.25 mmol) was added and the solution was purged with Ar for 10 min at room temperature. The reaction mixture was refluxed for 5 h under inert temperature. Color of the reaction mixture changes from pale yellow to dark red. The

reaction mixture was cooled to room temperature and concentrated under reduced pressure. To the flask a 1:1 mixture of MeCN: H₂O was added and the reaction mixture was refluxed for 16 h under inert atmosphere. Ice cold water (20 mL) was then added to the reaction mixture followed by a saturated solution of aqueous NH₄PF₆ (15 mL), which resulted in the formation of pale yellow precipitate which was filtered, washed with ice cold water (300 mL) and dried under reduced pressure to give title complex as a dark red solid (170 mg, 75%) Crystals for X-ray crystallographic analysis were obtained by diffusing Et₂O into a solution of **91** in acetone: Mp = 187 °C (decomp); ¹H NMR (600MHz C₃D₆O) δ 9.26(d, 1H, *J* = 6.6 Hz), 8.86(d, 2H, *J* = 6.0 Hz), 8.25(d, 2H, *J* = 8.4 Hz), 8.04(d, 2H, *J* = 7.2 Hz), 7.90-7.82(m, 8H), 7.69(d, 1H, *J* = 9.0 Hz), 7.65(t, 1H, *J* = 7.8 Hz), 7.50(t, 1H, *J* = 7.8 Hz), 6.40(d, 2H, *J* = 15.6 Hz), 5.88-5.86(m, 4H), 3.02(s, 3H), 2.42(s, 3H); IR (KBr) ν_{max} (cm⁻¹) 3665, 3590, 3423, 3222, 3065, 3007, 2942, 2275, 1922, 1707, 1626, 1596, 1556, 1509, 1456, 1430, 1398, 1378, 1321, 1271, 1239, 1202, 1167, 1149, 1098, 1081, 1036, 986, 952, 817, 748, 664, 556, 417, 391, 353, 337, 313. ESMS calculated for C₃₄H₃₀F₆N₆PRu (M⁺) 769.12, found 769.00; UV-vis λ_{max} = 424 nm (ε = 12,000 M⁻¹cm⁻¹); Anal. Calculated for C₃₄H₃₁F₁₂N₆O_{0.5}P₂Ru: (**91**·0.5 H₂O) C, 44.26; H, 3.39; N, 9.11. Found: C, 44.16; H, 3.40; N, 9.16.

6.3.5 Synthesis of secondary amine (**94**) for TQA ligand



Scheme 17: Synthesis of secondary amine (**94**) for the synthesis of TQA ligand

Compound **92**²⁸² (1.8 g, 10.2 mmol) was dissolved in DMF (12 mL) and to the flask benzene sulfonamide (0.8 g, 5.1 mmol) and K₂CO₃ (1.7 g, 12.2 mmol) were added and the reaction mixture was heated to 50 °C for 16 h. A white precipitate formed in the reaction mixture, which was cooled to RT and then dumped in 10% NaCl (30 mL) solution. The solid was then filtered, washed with water (30 mL), EtOAc (20 mL) and dried under reduced pressure to get **93** as a white solid (1.8 g, 94%), which was characterized by NMR. ¹H NMR (600MHz CD₆O₃) δ 8.30 (d, 2H, *J* = 8.4 Hz), 8.04 (d, 2H, *J* = 5.4 Hz), 7.96 (d, 2H, *J* = 7.2 Hz), 7.79 (d, 2H, *J* = 8.4 Hz), 7.69 (t, 1H, *J* = 7.8 Hz), 7.64 (t, 2H, *J* = 6.6 Hz), 7.59(t, 2H, *J* = 8.4 Hz), 7.48(d, 2H, *J* = 6.0 Hz), 7.44(t, 2H, *J* = 7.2 Hz), 5.14 (s, 4H), ¹³ C NMR (600MHz CD₆O₃) 154.8, 141.2, 136.0, 132.6, 129.8, 128.8, 127.8, 127.0, 126.8, 126.6, 125.0, 120.3, 52.2.

Compound **93** (1.8 g, 4.8 mmol) was then dissolved in conc H₂SO₄ (30 mL) and heated to 120 °C for 2 h under inert atmosphere. The reaction mixture was then cooled and pH was adjusted to 11. The amine was then extracted with DCM (3 × 20 mL), dried with Na₂SO₄ and concentrated to get secondary amine **94** as green oil (1.1 g, 78%): ¹H NMR (600MHz CDCl₃) δ 8.45 (d, 2H, *J* = 6.0 Hz), 8.22 (d, 2H, *J* = 8.4 Hz), 7.80 (d, 2H, *J* = 8.4 Hz), 7.65 (t, 2H, *J* = 7.8 Hz), 7.56 (t, 2H, *J* = 7.5 Hz), 7.53 (d, 2H, *J* = 6.0 Hz), 4.61 (s, 4H), ¹³ C NMR (600MHz CDCl₃) 158.4, 141.7, 136.1, 129.9, 127.3, 127.2, 126.7, 124.8, 120.0, 52.4. HRMS calculated for (M+H)⁺ 300.1501, found 300.1508.

6.3.6 X-ray crystallographic analysis of **89****Table 12:** Sample and crystal data for [Ru^{II}(DPAby)(MeCN)](PF₆)₂ (**89**)

Identification code	rs350	
Chemical formula	C ₂₈ H ₃₅ F ₁₃ N ₆ O ₃ P ₂ Ru	
Formula weight	913.63	
Temperature	100(2) K	
Wavelength	0.71073 Å	
Crystal system	triclinic	
Space group	P -1	
Unit cell dimensions	a = 8.819(3) Å	α = 72.241(13)°
	b = 13.035(5) Å	β = 83.765(15)°
	c = 17.450(7) Å	γ = 77.201(15)°
Volume	1861.1(12) Å ³	
Z	2	
Density (calculated)	1.630 g/cm ³	
Absorption coefficient	0.611 mm ⁻¹	
F(000)	920	

Table 13. Data collection and structure refinement

Theta range for data collection	1.23 to 23.57°	
Index ranges	-9<=h<=9, -14<=k<=14, -19<=l<=19	
Reflections collected	18648	
Independent reflections	5276 [R(int) = 0.1206]	
Coverage of independent reflections	95.3%	
Absorption correction	multi-scan	
Refinement method	Full-matrix least-squares on F ²	
Refinement program	SHELXL-2013 (Sheldrick, 2013)	
Function minimized	$\Sigma w(F_o^2 - F_c^2)^2$	
Data / restraints / parameters	5276 / 0 / 483	
Goodness-of-fit on F ²	1.071	
Final R indices	3014 data; I>2σ(I)	R1 = 0.1116, wR2 = 0.2732
	all data	R1 = 0.1801, wR2 = 0.3116
Weighting scheme	$w=1/[\sigma^2(F_o^2)+(0.1395P)^2+20.0036P]$	
	where $P=(F_o^2+2F_c^2)/3$	
Extinction coefficient	0.0076(17)	
Largest diff. peak and hole	1.972 and -1.544 eÅ ⁻³	
R.M.S. deviation from mean	0.179 eÅ ⁻³	

Table 14. Atomic coordinates and equivalent isotropic atomic displacement parameters

($^{\circ}\text{A}^2$) $U(\text{eq})$ is defined as one third of the trace of the orthogonalized U_{ij} tensor.

	x/a	y/b	z/c	$U(\text{eq})$
Ru1	0.92632(18)	0.77245(9)	0.75269(7)	0.0413(6)
P1	0.1309(6)	0.7521(3)	0.4314(3)	0.0548(15)
P2	0.7412(6)	0.8805(3)	0.1070(3)	0.0538(15)
O4	0.6248(16)	0.7733(10)	0.5144(8)	0.070(4)
F2	0.0221(16)	0.8376(13)	0.4704(12)	0.145(7)
F3	0.0301(17)	0.7960(8)	0.3556(8)	0.107(5)
F4	0.2346(13)	0.8401(7)	0.3926(6)	0.066(3)
F5	0.2385(14)	0.6655(8)	0.3944(7)	0.087(4)
F6	0.0266(17)	0.6647(10)	0.4691(7)	0.094(4)
F7	0.2267(19)	0.7097(11)	0.5094(6)	0.116(5)
F8	0.9058(15)	0.8360(12)	0.0752(7)	0.115(5)
F9	0.8059(14)	0.8225(7)	0.1950(5)	0.074(3)
F10	0.6943(15)	0.7688(8)	0.1074(9)	0.106(5)
F11	0.7878(13)	0.9913(8)	0.1075(6)	0.067(3)
F12	0.6831(14)	0.9376(8)	0.0197(6)	0.081(4)
F13	0.5762(14)	0.9201(8)	0.1453(8)	0.098(5)
N3	0.0278(14)	0.6699(9)	0.8485(6)	0.032(3)

	x/a	y/b	z/c	U(eq)
N4	0.9667(16)	0.6299(9)	0.7201(7)	0.045(4)
O3	0.3392(16)	0.5975(8)	0.1271(6)	0.066(4)
N1	0.7154(14)	0.7535(8)	0.8129(6)	0.028(3)
N2	0.9099(17)	0.8858(10)	0.8170(7)	0.045(4)
C11B	0.0778(19)	0.5618(11)	0.8502(8)	0.038(4)
C17B	0.0411(18)	0.5364(11)	0.7776(8)	0.036(4)
N5	0.1279(15)	0.8178(9)	0.7123(7)	0.040(3)
N6	0.8283(16)	0.8767(9)	0.6485(7)	0.042(4)
C1	0.627(4)	0.6088(17)	0.4906(19)	0.143(13)
C2	0.626(2)	0.7208(14)	0.4669(12)	0.066(6)
C3	0.639(2)	0.6712(11)	0.8278(9)	0.039(4)
C4	0.510(2)	0.6586(11)	0.8817(9)	0.047(5)
C5	0.461(2)	0.7368(12)	0.9239(9)	0.049(5)
C6	0.5358(19)	0.8246(11)	0.9078(9)	0.038(4)
C7	0.6618(19)	0.8349(10)	0.8521(8)	0.035(4)
C8	0.7433(17)	0.9290(10)	0.8270(9)	0.035(4)
C9	0.987(2)	0.8273(12)	0.8964(9)	0.051(5)
C10	0.0502(17)	0.7076(11)	0.9085(7)	0.030(3)
C11	0.162(2)	0.4891(12)	0.9147(9)	0.047(4)
C12	0.182(2)	0.5291(13)	0.9780(9)	0.050(5)

	x/a	y/b	z/c	U(eq)
C13	0.123(2)	0.6366(12)	0.9763(9)	0.047(4)
C14	0.925(2)	0.6108(12)	0.6533(9)	0.049(5)
C15	0.953(2)	0.5080(12)	0.6424(10)	0.058(5)
C16	0.020(2)	0.4188(12)	0.7006(9)	0.052(5)
C17	0.063(2)	0.4344(12)	0.7687(9)	0.046(4)
C18	0.995(2)	0.9720(13)	0.7666(9)	0.048(5)
C19	0.143(2)	0.9097(16)	0.7347(10)	0.061(6)
C20	0.254(2)	0.7666(13)	0.6805(9)	0.046(4)
C21	0.396(3)	0.8041(16)	0.6670(9)	0.068(6)
C22	0.413(3)	0.8963(19)	0.6879(10)	0.083(7)
C23	0.277(3)	0.9509(16)	0.7206(9)	0.060(5)
C24	0.787(2)	0.9320(12)	0.5889(9)	0.042(4)
C25	0.737(2)	0.0001(12)	0.5078(8)	0.051(5)
C26	0.278(3)	0.7609(15)	0.1668(14)	0.086(7)
C27	0.359(2)	0.6461(12)	0.1725(9)	0.047(4)
C28	0.471(3)	0.5916(17)	0.2395(11)	0.084(7)
C2B	0.617(3)	0.775(2)	0.3785(13)	0.104(8)

Table 15. Bond lengths ($^{\circ}\text{A}^2$)

Ru1-N3	1.954(11)	Ru1-N5	1.986(14)
Ru1-N4	2.052(11)	Ru1-N6	2.052(11)
Ru1-N1	2.060(12)	Ru1-N2	2.085(12)
P1-F5	1.559(11)	P1-F3	1.562(11)
P1-F6	1.566(13)	P1-F7	1.567(11)
P1-F2	1.571(11)	P1-F4	1.571(12)
P2-F8	1.550(12)	P2-F12	1.563(9)
P2-F13	1.580(12)	P2-F11	1.589(10)
P2-F9	1.595(9)	P2-F10	1.597(11)
O4-C2	1.22(2)	N3-C10	1.334(17)
N3-C11B	1.371(17)	N4-C14	1.368(18)
N4-C17B	1.401(16)	O3-C27	1.203(17)
N1-C3	1.339(19)	N1-C7	1.403(16)
N2-C8	1.464(19)	N2-C18	1.49(2)
N2-C9	1.515(17)	C11B-C11	1.391(19)
C11B-C17B	1.488(19)	C17B-C17	1.35(2)
N5-C20	1.327(19)	N5-C19	1.40(2)
N6-C24	1.116(17)	C1-C2	1.39(3)
C1-H4	0.98	C1-H1	0.98

C1-H3	0.98	C2-C2B	1.49(3)
C3-C4	1.39(2)	C3-H6	0.95
C4-C5	1.40(2)	C4-H26	0.95
C5-C6	1.39(2)	C5-H7	0.95
C6-C7	1.40(2)	C6-H8	0.95
C7-C8	1.49(2)	C8-H25	0.99
C8-H24	0.99	C9-C10	1.493(19)
C9-H9	0.99	C9-H17	0.99
C10-C13	1.379(18)	C11-C12	1.40(2)
C11-H10	0.95	C12-C13	1.37(2)
C12-H12	0.95	C13-H11	0.95
C14-C15	1.38(2)	C14-H13	0.95
C15-C16	1.35(2)	C15-H16	0.95
C16-C17	1.37(2)	C16-H15	0.95
C17-H14	0.95	C18-C19	1.52(3)
C18-H22	0.99	C18-H23	0.99
C19-C23	1.37(3)	C20-C21	1.41(3)
C20-H21	0.95	C21-C22	1.40(3)
C21-H20	0.95	C22-C23	1.41(3)
C22-H19	0.95	C23-H18	0.95
C24-C25	1.475(19)	C25-H29	0.98

C25-H27	0.98	C25-H28	0.98
C26-C27	1.49(2)	C26-H30	0.98
C26-H33	0.98	C26-H34	0.98
C27-C28	1.51(2)	C28-H31	0.98
C28-H32	0.98	C28-H35	0.98
C2B-H2B1	0.98	C2B-H2B2	0.98
C2B-H2B3	0.98		

Table 16. Bond angles (°)

N3-Ru1-N5	89.2(5)	N3-Ru1-N4	80.3(4)
N5-Ru1-N4	98.3(5)	N3-Ru1-N6	177.1(5)
N5-Ru1-N6	89.1(5)	N4-Ru1-N6	97.6(4)
N3-Ru1-N1	88.1(4)	N5-Ru1-N1	164.6(4)
N4-Ru1-N1	96.1(5)	N6-Ru1-N1	94.2(5)
N3-Ru1-N2	83.1(4)	N5-Ru1-N2	83.0(5)
N4-Ru1-N2	163.4(4)	N6-Ru1-N2	98.9(4)
N1-Ru1-N2	81.6(5)	F5-P1-F3	90.5(7)
F5-P1-F6	87.4(7)	F3-P1-F6	88.9(7)
F5-P1-F7	91.4(8)	F3-P1-F7	177.9(9)

F6-P1-F7	90.4(7)	F5-P1-F2	178.9(9)
F3-P1-F2	90.2(9)	F6-P1-F2	91.8(8)
F7-P1-F2	87.9(9)	F5-P1-F4	92.4(6)
F3-P1-F4	90.4(6)	F6-P1-F4	179.2(6)
F7-P1-F4	90.4(7)	F2-P1-F4	88.4(7)
F8-P2-F12	92.2(7)	F8-P2-F13	176.0(7)
F12-P2-F13	91.7(7)	F8-P2-F11	92.4(8)
F12-P2-F11	89.6(5)	F13-P2-F11	88.6(7)
F8-P2-F9	86.2(6)	F12-P2-F9	178.2(8)
F13-P2-F9	89.9(7)	F11-P2-F9	89.7(5)
F8-P2-F10	87.8(8)	F12-P2-F10	91.0(6)
F13-P2-F10	91.1(8)	F11-P2-F10	179.4(7)
F9-P2-F10	89.8(6)	C10-N3-C11B	122.5(11)
C10-N3-Ru1	119.2(9)	C11B-N3-Ru1	118.3(9)
C14-N4-C17B	115.1(12)	C14-N4-Ru1	130.1(9)
C17B-N4-Ru1	114.7(9)	C3-N1-C7	118.3(13)
C3-N1-Ru1	130.3(10)	C7-N1-Ru1	110.7(10)
C8-N2-C18	112.5(11)	C8-N2-C9	113.0(12)
C18-N2-C9	110.5(13)	C8-N2-Ru1	105.8(9)
C18-N2-Ru1	106.2(8)	C9-N2-Ru1	108.5(8)
N3-C11B-C11	119.4(13)	N3-C11B-C17B	114.2(11)

C11-C11B-C17B	126.4(13)	C17-C17B-N4	122.0(13)
C17-C17B-C11B	125.3(12)	N4-C17B-C11B	112.5(12)
C20-N5-C19	116.7(16)	C20-N5-Ru1	130.5(12)
C19-N5-Ru1	111.8(12)	C24-N6-Ru1	174.4(14)
C2-C1-H4	109.5	C2-C1-H1	109.5
H4-C1-H1	109.5	C2-C1-H3	109.5
H4-C1-H3	109.5	H1-C1-H3	109.5
O4-C2-C1	123.(2)	O4-C2-C2B	121.6(17)
C1-C2-C2B	115.(2)	N1-C3-C4	124.5(13)
N1-C3-H6	117.7	C4-C3-H6	117.7
C3-C4-C5	117.3(16)	C3-C4-H26	121.3
C5-C4-H26	121.3	C6-C5-C4	119.2(17)
C6-C5-H7	120.4	C4-C5-H7	120.4
C5-C6-C7	121.3(14)	C5-C6-H8	119.3
C7-C6-H8	119.3	C6-C7-N1	119.2(14)
C6-C7-C8	125.4(13)	N1-C7-C8	115.4(14)
N2-C8-C7	108.2(11)	N2-C8-H25	110.1
C7-C8-H25	110.1	N2-C8-H24	110.1
C7-C8-H24	110.1	H25-C8-H24	108.4
C10-C9-N2	114.1(11)	C10-C9-H9	108.7
N2-C9-H9	108.7	C10-C9-H17	108.7

N2-C9-H17	108.7	H9-C9-H17	107.6
N3-C10-C13	120.0(13)	N3-C10-C9	115.0(11)
C13-C10-C9	125.0(13)	C11B-C11-C12	117.5(14)
C11B-C11-H10	121.2	C12-C11-H10	121.2
C13-C12-C11	121.4(14)	C13-C12-H12	119.3
C11-C12-H12	119.3	C12-C13-C10	118.9(14)
C12-C13-H11	120.5	C10-C13-H11	120.5
N4-C14-C15	122.9(13)	N4-C14-H13	118.5
C15-C14-H13	118.5	C16-C15-C14	120.4(15)
C16-C15-H16	119.8	C14-C15-H16	119.8
C15-C16-C17	118.3(14)	C15-C16-H15	120.8
C17-C16-H15	120.8	C17B-C17-C16	121.1(14)
C17B-C17-H14	119.4	C16-C17-H14	119.4
N2-C18-C19	105.4(13)	N2-C18-H22	110.7
C19-C18-H22	110.7	N2-C18-H23	110.7
C19-C18-H23	110.7	H22-C18-H23	108.8
C23-C19-N5	123.1(19)	C23-C19-C18	120.0(17)
N5-C19-C18	116.4(15)	N5-C20-C21	122.1(16)
N5-C20-H21	119.0	C21-C20-H21	119.0
C22-C21-C20	122.(2)	C22-C21-H20	118.9
C20-C21-H20	118.9	C21-C22-C23	115.(2)

C21-C22-H19	122.5	C23-C22-H19	122.5
C19-C23-C22	121.(2)	C19-C23-H18	119.6
C22-C23-H18	119.6	N6-C24-C25	176.5(15)
C24-C25-H29	109.5	C24-C25-H27	109.5
H29-C25-H27	109.5	C24-C25-H28	109.5
H29-C25-H28	109.5	H27-C25-H28	109.5
C27-C26-H30	109.5	C27-C26-H33	109.5
H30-C26-H33	109.5	C27-C26-H34	109.5
H30-C26-H34	109.5	H33-C26-H34	109.5
O3-C27-C26	123.1(16)	O3-C27-C28	120.5(14)
C26-C27-C28	116.4(15)	C27-C28-H31	109.5
C27-C28-H32	109.5	H31-C28-H32	109.5
C27-C28-H35	109.5	H31-C28-H35	109.5
H32-C28-H35	109.5	C2-C2B-H2B1	109.5
C2-C2B-H2B2	109.5	H2B1-C2B-H2B2	109.5
C2-C2B-H2B3	109.5	H2B1-C2B-H2B3	109.5
H2B2-C2B-H2B3	109.5		

Table 17. Anisotropic atomic displacement parameters ($^{\circ}\text{A}^2$)

The anisotropic atomic displacement factor exponent takes the form: $-2\pi^2 [h^2 a^{*2} U_{11} + \dots + 2 h k a^* b^* U_{12}]$

	U_{11}	U_{22}	U_{33}	U_{23}	U_{13}	U_{12}
Ru1	0.0735(12)	0.0293(7)	0.0225(7)	-0.0119(5)	-0.0260(6)	0.0047(6)
P1	0.085(4)	0.044(2)	0.041(2)	-0.023(2)	-0.022(3)	0.000(3)
P2	0.081(4)	0.040(2)	0.045(2)	-0.0234(19)	-0.029(3)	0.008(2)
O4	0.087(11)	0.067(8)	0.077(9)	-0.053(7)	0.010(8)	-0.020(7)
F2	0.077(10)	0.163(13)	0.27(2)	-0.192(15)	0.028(11)	-0.020(9)
F3	0.155(13)	0.055(6)	0.119(10)	-0.005(6)	-0.101(10)	-0.018(7)
F4	0.081(8)	0.045(5)	0.077(7)	-0.027(5)	-0.021(6)	-0.001(5)
F5	0.096(10)	0.057(6)	0.103(9)	-0.037(6)	0.008(7)	0.006(6)
F6	0.148(12)	0.102(9)	0.067(7)	-0.054(7)	0.014(8)	-0.064(9)
F7	0.174(14)	0.134(11)	0.050(7)	-0.002(7)	-0.057(8)	-0.060(10)
F8	0.084(10)	0.167(13)	0.066(8)	-0.040(8)	-0.018(7)	0.050(9)
F9	0.115(9)	0.048(5)	0.043(5)	-0.011(4)	-0.027(6)	0.023(6)
F10	0.114(11)	0.035(5)	0.177(13)	-0.027(7)	-0.103(10)	0.013(6)
F11	0.092(8)	0.064(6)	0.062(6)	-0.016(5)	-0.035(6)	-0.038(6)
F12	0.131(10)	0.061(6)	0.056(6)	-0.024(5)	-0.062(7)	0.011(6)
F13	0.075(9)	0.045(6)	0.132(11)	0.010(6)	0.008(8)	0.018(6)

	U_{11}	U_{22}	U_{33}	U_{23}	U_{13}	U_{12}
N3	0.031(8)	0.044(7)	0.025(6)	-0.016(5)	0.001(5)	-0.006(6)
N4	0.070(10)	0.033(6)	0.025(6)	-0.008(5)	-0.025(6)	0.013(6)
O3	0.117(11)	0.039(6)	0.048(7)	-0.020(5)	-0.053(7)	0.008(6)
N1	0.042(8)	0.028(6)	0.015(5)	-0.012(4)	-0.007(5)	0.005(6)
N2	0.066(11)	0.044(7)	0.021(6)	-0.013(5)	-0.009(6)	0.006(7)
C11B	0.055(11)	0.035(8)	0.028(7)	-0.015(6)	-0.009(7)	-0.003(8)
C17B	0.045(11)	0.033(8)	0.024(7)	-0.005(6)	-0.007(7)	0.006(7)
N6	0.069(10)	0.040(7)	0.022(6)	-0.015(6)	-0.028(7)	0.005(7)
C1	0.16(3)	0.055(14)	0.21(3)	-0.001(17)	-0.10(3)	-0.024(16)
C2	0.082(16)	0.040(10)	0.082(14)	-0.027(10)	-0.002(12)	-0.010(10)
C3	0.064(13)	0.020(7)	0.035(8)	-0.007(6)	-0.036(9)	0.000(8)
C4	0.084(15)	0.029(8)	0.029(8)	0.000(6)	-0.021(9)	-0.016(8)
C5	0.058(12)	0.049(10)	0.039(9)	-0.024(7)	-0.011(8)	0.013(9)
C6	0.049(12)	0.025(8)	0.042(9)	-0.008(6)	-0.032(9)	0.002(7)
C7	0.050(11)	0.026(7)	0.027(8)	-0.006(6)	-0.022(8)	0.002(7)
C8	0.032(10)	0.026(7)	0.056(9)	-0.015(7)	-0.016(8)	-0.012(7)
C9	0.076(14)	0.049(9)	0.031(8)	-0.021(7)	-0.015(8)	-0.001(9)
C10	0.030(9)	0.039(8)	0.019(7)	0.000(6)	-0.016(6)	-0.008(7)
C11	0.063(13)	0.042(9)	0.036(9)	-0.006(7)	-0.013(8)	-0.010(8)
C12	0.058(13)	0.049(10)	0.038(9)	0.001(7)	-0.022(8)	-0.012(9)

	U_{11}	U_{22}	U_{33}	U_{23}	U_{13}	U_{12}
C13	0.063(13)	0.050(10)	0.039(9)	-0.007(7)	-0.012(8)	-0.035(9)
C14	0.072(13)	0.037(8)	0.040(9)	-0.018(7)	-0.028(9)	0.004(8)
C15	0.093(16)	0.033(8)	0.050(10)	-0.019(7)	-0.023(10)	0.005(9)
C16	0.078(14)	0.033(8)	0.047(10)	-0.022(7)	-0.013(9)	0.004(9)
C17	0.063(13)	0.031(8)	0.038(9)	-0.004(7)	-0.003(8)	-0.003(8)
C18	0.068(14)	0.047(9)	0.039(9)	-0.017(8)	-0.021(9)	-0.018(9)
C19	0.056(14)	0.079(13)	0.052(11)	0.004(9)	-0.040(10)	-0.038(12)
C21	0.097(18)	0.072(12)	0.021(8)	-0.002(8)	-0.024(9)	0.009(12)
C22	0.092(18)	0.102(17)	0.036(10)	0.009(11)	-0.050(11)	0.002(14)
C23	0.076(16)	0.083(13)	0.030(9)	-0.028(9)	-0.006(9)	-0.013(12)
C24	0.054(12)	0.039(8)	0.046(10)	-0.030(8)	-0.016(9)	-0.006(8)
C25	0.082(14)	0.041(8)	0.029(8)	-0.012(7)	-0.039(9)	0.009(9)
C26	0.100(19)	0.054(11)	0.111(18)	-0.039(12)	0.004(14)	-0.009(12)
C27	0.064(13)	0.039(8)	0.044(9)	-0.022(7)	-0.015(9)	-0.007(8)
C28	0.12(2)	0.094(15)	0.053(11)	-0.041(11)	-0.031(12)	-0.016(14)
C2B	0.13(2)	0.13(2)	0.067(15)	-0.031(14)	0.000(15)	-0.051(18)

Table 18. Hydrogen coordinates and isotropic atomic displacement parameters (\AA^2).

	x/a	y/b	z/c	U(eq)
H4	0.7351	0.5679	0.4959	0.215
H1	0.5779	0.5906	0.4500	0.215
H3	0.5699	0.5888	0.5425	0.215
H6	0.6737	0.6176	0.7997	0.046
H26	0.4586	0.5993	0.8895	0.057
H7	0.3775	0.7298	0.9631	0.059
H8	0.5005	0.8789	0.9352	0.046
H25	0.7033	0.9811	0.7756	0.042
H24	0.7251	0.9685	0.8684	0.042
H9	1.0734	0.8631	0.8994	0.061
H17	0.9105	0.8362	0.9409	0.061
H10	1.2040	0.4150	0.9158	0.057
H12	1.2382	0.4810	1.0231	0.059
H11	1.1324	0.6616	1.0210	0.057
H13	0.8733	0.6714	0.6125	0.058
H16	0.9264	0.4995	0.5938	0.07
H15	1.0369	0.3472	0.6943	0.063
H14	1.1084	0.3727	0.8104	0.056

	x/a	y/b	z/c	U(eq)
H22	1.0210	1.0154	0.7994	0.058
H23	0.9317	1.0225	0.7216	0.058
H21	1.2495	0.7026	0.6664	0.056
H20	1.4825	0.7655	0.6429	0.082
H19	1.5089	0.9204	0.6806	0.1
H18	1.2777	1.0168	0.7329	0.072
H29	0.8140	1.0454	0.4820	0.076
H27	0.6357	1.0479	0.5123	0.076
H28	0.7285	0.9524	0.4753	0.076
H30	0.1931	0.7825	0.1294	0.13
H33	0.3514	0.8104	0.1470	0.13
H34	0.2344	0.7653	0.2201	0.13
H31	0.4137	0.5832	0.2916	0.126
H32	0.5482	0.6371	0.2353	0.126
H35	0.5243	0.5191	0.2349	0.126
H2B1	0.5788	0.8542	0.3685	0.155
H2B2	0.5462	0.7444	0.3562	0.155
H2B3	0.7211	0.7618	0.3525	0.155

6.3.7 X-ray crystallographic analysis of **91****Table 19.** Sample and crystal data for $[\text{Ru}^{\text{II}}(\text{TQA})(\text{MeCN})_2](\text{PF}_6)_2$ (**91**)

Identification code	rs337	
Chemical formula	$\text{C}_{22}\text{H}_{27}\text{F}_6\text{N}_3\text{O}_2\text{PRu}_{0.50}$	
Formula weight	572.98	
Temperature	100(2) K	
Wavelength	0.71073 Å	
Crystal size	0.302 x 0.442 x 0.708 mm	
Crystal system	triclinic	
Space group	P -1	
Unit cell dimensions	$a = 12.0377(11)$ Å	$\alpha = 91.125(5)^\circ$
	$b = 14.0264(13)$ Å	$\beta = 90.825(5)^\circ$
	$c = 16.2856(16)$ Å	$\gamma = 113.890(4)^\circ$
Volume	$2512.9(4)$ Å ³	
Z	4	
Density (calculated)	1.514 g/cm ³	
Absorption coefficient	0.469 mm ⁻¹	
F(000)	1172	

Table 20. Data collection and structure refinement

Theta range for data collection	1.25 to 35.66°
Index ranges	-18<=h<=19, -22<=k<=22, -26<=l<=26
Reflections collected	121269
Independent reflections	23019 [R(int) = 0.0695]
Max. and min. transmission	0.8710 and 0.7330
Absorption correction	multi-scan
Refinement method	Full-matrix least-squares on F ²
Refinement program	SHELXL-2013 (Sheldrick, 2013)
Function minimized	$\Sigma w(F_o^2 - F_c^2)^2$
Data / restraints / parameters	23019 / 4 / 653
Goodness-of-fit on F ²	0.916
Final R indices	18642 data; I>2σ(I) R1 = 0.0385, wR2 = 0.0999
	all data R1 = 0.0510, wR2 = 0.1054
Weighting scheme	w=1/[σ ² (F _o ²)+(0.0647P) ² +0.7003P] where P=(F _o ² +2F _c ²)/3
Largest diff. peak and hole	1.779 and -1.007 eÅ ⁻³
R.M.S. deviation from mean	0.092 eÅ ⁻³

Table 21. Atomic coordinates and equivalent isotropic atomic displacement parameters

($^{\circ}\text{A}^2$) $U(\text{eq})$ is defined as one third of the trace of the orthogonalized U_{ij} tensor.

	x/a	y/b	z/c	$U(\text{eq})$
C1R	0.89797(11)	0.02036(10)	0.88758(8)	0.0146(2)
Ru1	0.84333(2)	0.74608(2)	0.74645(2)	0.01102(3)
N2	0.71452(9)	0.62034(8)	0.68304(7)	0.01360(18)
P2	0.0	0.5	0.0	0.02257(10)
P3	0.40262(3)	0.94040(3)	0.77823(2)	0.02251(7)
P4	0.0	0.5	0.5	0.02738(12)
N4	0.93183(9)	0.88462(8)	0.81235(6)	0.01314(18)
F1	0.27282(9)	0.88622(8)	0.73211(6)	0.0311(2)
F2	0.12186(12)	0.60359(10)	0.00258(10)	0.0575(4)
F3	0.13674(11)	0.56013(10)	0.47228(9)	0.0530(4)
F4	0.38419(11)	0.04658(9)	0.78632(8)	0.0402(3)
F5	0.53202(9)	0.99375(9)	0.82541(7)	0.0370(2)
F6	0.33779(10)	0.90357(10)	0.86389(7)	0.0400(3)
F7	0.94677(13)	0.54733(11)	0.92919(7)	0.0493(3)
F8	0.42150(10)	0.83323(8)	0.76933(7)	0.0350(2)
F9	0.95786(13)	0.46352(11)	0.40702(7)	0.0505(3)
F10	0.05788(11)	0.44965(9)	0.93254(7)	0.0362(2)

F11	0.46651(10)	0.97495(9)	0.69209(7)	0.0378(2)
F12	0.97588(11)	0.60281(9)	0.48825(9)	0.0488(3)
O1	0.15567(15)	0.86795(12)	0.29928(12)	0.0536(4)
O2	0.46163(12)	0.76937(11)	0.55022(9)	0.0377(3)
O3	0.38894(14)	0.24063(14)	0.99355(10)	0.0484(4)
N1	0.97765(10)	0.69264(8)	0.75360(7)	0.01478(18)
N6	0.77973(10)	0.67193(8)	0.85277(7)	0.01521(19)
C00	0.41939(13)	0.37880(11)	0.56177(9)	0.0225(3)
C01	0.85695(11)	0.92796(9)	0.83781(7)	0.0133(2)
C02	0.81997(12)	0.88737(10)	0.52262(8)	0.0157(2)
C03	0.91005(12)	0.87812(10)	0.47197(8)	0.0173(2)
C04	0.72333(11)	0.86768(10)	0.81498(8)	0.0157(2)
C05	0.59202(11)	0.70872(10)	0.73364(8)	0.0164(2)
C06	0.73613(13)	0.92463(11)	0.48861(9)	0.0214(3)
C07	0.63929(13)	0.46268(10)	0.60087(9)	0.0196(2)
C08	0.1364(2)	0.78328(16)	0.26870(14)	0.0403(4)
C09	0.06772(13)	0.15964(10)	0.96099(9)	0.0195(2)
C0E	0.72659(12)	0.86803(10)	0.66416(8)	0.0165(2)
C0M	0.69216(15)	0.56411(13)	0.98184(10)	0.0273(3)
C0F	0.73224(12)	0.54235(10)	0.64072(8)	0.0167(2)
C0Q	0.81467(11)	0.85499(9)	0.60509(8)	0.0136(2)

C0O	0.50197(11)	0.54238(10)	0.64339(8)	0.0149(2)
C0N	0.86389(14)	0.15324(11)	0.96742(9)	0.0227(3)
C0I	0.81901(13)	0.06531(11)	0.91787(9)	0.0194(2)
C0B	0.91452(14)	0.90578(11)	0.38828(9)	0.0231(3)
C0H	0.38510(17)	0.79403(15)	0.52015(12)	0.0357(4)
C0G	0.05173(12)	0.66194(10)	0.76277(8)	0.0166(2)
C0R	0.98988(12)	0.83776(10)	0.50665(8)	0.0183(2)
C011	0.05329(11)	0.93206(10)	0.83323(8)	0.0146(2)
C0J	0.58124(19)	0.30478(15)	0.06161(13)	0.0380(4)
C0D	0.97662(11)	0.80641(10)	0.58562(8)	0.0161(2)
C0S	0.02412(11)	0.06840(10)	0.90961(8)	0.0152(2)
C0K	0.98941(14)	0.20084(11)	0.98922(9)	0.0219(3)
C0T	0.52002(12)	0.45974(10)	0.60165(8)	0.0171(2)
C0C	0.10075(11)	0.02173(10)	0.88014(8)	0.0163(2)
C0L	0.38348(12)	0.54163(11)	0.64437(9)	0.0196(2)
C0P	0.14637(13)	0.62365(12)	0.77496(10)	0.0231(3)
C0V	0.48237(16)	0.22910(14)	0.00895(10)	0.0298(3)
C0A	0.60410(11)	0.62183(9)	0.68332(8)	0.0140(2)
C2AN	0.74097(12)	0.62443(10)	0.90945(8)	0.0177(2)
C10E	0.6929(3)	0.6821(2)	0.20338(15)	0.0675(9)
C11E	0.3976(4)	0.8345(5)	0.4360(3)	0.160(3)

C14E	0.2339(3)	0.7583(2)	0.22979(19)	0.0649(7)
C15E	0.0133(3)	0.6978(2)	0.2657(2)	0.0809(11)
C55E	0.4719(3)	0.6640(3)	0.20157(17)	0.0749(9)
C17E	0.4992(2)	0.13563(18)	0.97648(13)	0.0472(5)
C18E	0.5627(2)	0.61741(16)	0.18346(11)	0.0392(4)
C19E	0.27234(19)	0.78177(18)	0.56234(15)	0.0455(5)
N5	0.71088(9)	0.80262(8)	0.73864(6)	0.01228(17)
N3	0.88878(9)	0.81392(8)	0.63509(6)	0.01279(17)
O1S	0.52988(14)	0.53087(12)	0.15400(9)	0.0437(3)
C56E	0.83057(16)	0.93920(12)	0.35704(10)	0.0280(3)
C57E	0.74118(15)	0.94824(12)	0.40715(10)	0.0269(3)
C58E	0.28849(13)	0.46209(12)	0.60532(10)	0.0240(3)
C59E	0.30700(13)	0.38067(11)	0.56363(10)	0.0239(3)

Table 22. Bond lengths ($^{\circ}\text{A}^2$)

C1R-C01	1.4175(17)	C1R-C0I	1.4252(18)
C1R-C0S	1.4265(17)	Ru1-N6	2.0321(12)
Ru1-N3	2.0418(11)	Ru1-N1	2.0420(11)

Ru1-N5	2.0516(10)	Ru1-N2	2.0612(11)
Ru1-N4	2.0666(11)	N2-C0A	1.3378(16)
N2-C0F	1.3715(16)	P2-F2	1.5919(13)
P2-F2	1.5920(13)	P2-F7	1.5920(11)
P2-F7	1.5920(11)	P2-F10	1.6067(10)
P2-F10	1.6067(10)	P3-F4	1.5953(11)
P3-F11	1.5970(11)	P3-F6	1.5984(11)
P3-F1	1.6016(11)	P3-F5	1.6048(11)
P3-F8	1.6129(11)	P4-F3	1.5927(12)
P4-F3	1.5927(12)	P4-F12	1.5964(11)
P4-F12	1.5965(11)	P4-F9	1.5967(11)
P4-F9	1.5967(11)	N4-C01	1.3412(15)
N4-C011	1.3729(16)	O1-C08	1.209(2)
O2-C0H	1.208(2)	O3-C0V	1.223(2)
N1-C0G	1.1457(16)	N6-C2AN	1.1394(17)
C00-C59E	1.364(2)	C00-C0T	1.4187(19)
C00-H00	0.95	C01-C04	1.5196(17)
C02-C03	1.4173(19)	C02-C0Q	1.4201(18)
C02-C06	1.4217(19)	C03-C0R	1.414(2)
C03-C0B	1.4201(19)	C04-N5	1.4969(16)
C04-H04A	0.99	C04-H04B	0.99

C05-N5	1.5015(16)	C05-C0A	1.5119(17)
C05-H05A	0.99	C05-H05B	0.99
C06-C57E	1.370(2)	C06-H06	0.95
C07-C0F	1.3638(19)	C07-C0T	1.4198(19)
C07-H07	0.95	C08-C15E	1.481(3)
C08-C14E	1.499(3)	C09-C0K	1.370(2)
C09-C0S	1.4193(18)	C09-H09	0.95
C0E-N5	1.5028(17)	C0E-C0Q	1.5042(18)
C0E-H0E1	0.99	C0E-H0E2	0.99
C0M-C2AN	1.452(2)	C0M-H0M1	0.98
C0M-H0M2	0.98	C0M-H0M3	0.98
C0F-H0F	0.95	C0Q-N3	1.3345(16)
C0O-C0A	1.4195(17)	C0O-C0L	1.4224(18)
C0O-C0T	1.4249(18)	C0N-C0I	1.3684(19)
C0N-C0K	1.419(2)	C0N-H0N	0.95
C0I-H0I	0.95	C0B-C56E	1.370(2)
C0B-H0B	0.95	C0H-C19E	1.479(3)
C0H-C11E	1.480(4)	C0G-C0P	1.4557(18)
C0R-C0D	1.3581(19)	C0R-H0R	0.95
C011-C0C	1.3637(18)	C011-H011	0.95
C0J-C0V	1.480(3)	C0J-H0J1	0.98

C0J-H0J2	0.98	C0J-H0J3	0.98
C0D-N3	1.3746(16)	C0D-H0D	0.95
C0S-C0C	1.4140(18)	C0K-H0K	0.95
C0C-H0C	0.95	C0L-C58E	1.3691(19)
C0L-H0L	0.95	C0P-H0P1	0.98
C0P-H0P2	0.98	C0P-H0P3	0.98
C0V-C17E	1.493(3)	C10E-C18E	1.485(3)
C10E-H10A	0.98	C10E-H10B	0.98
C10E-H10C	0.98	C11E-H11A	0.98
C11E-H11B	0.98	C11E-H11C	0.98
C14E-H14A	0.98	C14E-H14B	0.98
C14E-H14C	0.98	C15E-H15A	0.98
C15E-H15B	0.98	C15E-H15C	0.98
C55E-C18E	1.514(3)	C55E-H55A	0.98
C55E-H55B	0.98	C55E-H55C	0.98
C17E-H17A	0.98	C17E-H17B	0.98
C17E-H17C	0.98	C18E-O1S	1.201(2)
C19E-H19A	0.98	C19E-H19B	0.98
C19E-H19C	0.98	C56E-C57E	1.404(3)
C56E-H56E	0.95	C57E-H57E	0.95
C58E-C59E	1.413(2)	C58E-H58E	0.95

C59E-H59E 0.95

Table 23. Bond angles (°)

C01-C1R-C0I	123.18(11)	C01-C1R-C0S	117.77(11)
C0I-C1R-C0S	119.03(11)	N6-Ru1-N3	173.98(4)
N6-Ru1-N1	87.50(4)	N3-Ru1-N1	96.67(4)
N6-Ru1-N5	93.32(4)	N3-Ru1-N5	82.56(4)
N1-Ru1-N5	178.86(4)	N6-Ru1-N2	88.64(4)
N3-Ru1-N2	86.47(4)	N1-Ru1-N2	98.28(4)
N5-Ru1-N2	82.53(4)	N6-Ru1-N4	89.81(4)
N3-Ru1-N4	93.90(4)	N1-Ru1-N4	97.81(4)
N5-Ru1-N4	81.41(4)	N2-Ru1-N4	163.76(4)
C0A-N2-C0F	119.84(11)	C0A-N2-Ru1	112.70(8)
C0F-N2-Ru1	127.41(9)	F2-P2-F2	180.0
F2-P2-F7	90.36(8)	F2-P2-F7	89.64(8)
F2-P2-F7	89.64(8)	F2-P2-F7	90.36(8)
F7-P2-F7	180.00(9)	F2-P2-F10	89.68(7)
F2-P2-F10	90.32(7)	F7-P2-F10	89.57(6)
F7-P2-F10	90.44(6)	F2-P2-F10	90.32(7)

F2-P2-F10	89.68(7)	F7-P2-F10	90.43(6)
F7-P2-F10	89.56(6)	F10-P2-F10	180.0
F4-P3-F11	90.45(7)	F4-P3-F6	90.49(7)
F11-P3-F6	178.92(7)	F4-P3-F1	89.67(6)
F11-P3-F1	90.22(6)	F6-P3-F1	89.26(6)
F4-P3-F5	90.61(6)	F11-P3-F5	90.44(6)
F6-P3-F5	90.08(6)	F1-P3-F5	179.28(7)
F4-P3-F8	179.57(7)	F11-P3-F8	89.12(6)
F6-P3-F8	89.94(6)	F1-P3-F8	90.23(6)
F5-P3-F8	89.49(6)	F3-P4-F3	180.0
F3-P4-F12	90.43(7)	F3-P4-F12	89.58(7)
F3-P4-F12	89.57(7)	F3-P4-F12	90.42(7)
F12-P4-F12	180.0	F3-P4-F9	90.35(7)
F3-P4-F9	89.65(8)	F12-P4-F9	90.71(7)
F12-P4-F9	89.29(7)	F3-P4-F9	89.65(8)
F3-P4-F9	90.34(7)	F12-P4-F9	89.29(7)
F12-P4-F9	90.71(7)	F9-P4-F9	180.0
C01-N4-C011	119.37(11)	C01-N4-Ru1	113.20(8)
C011-N4-Ru1	127.40(8)	C0G-N1-Ru1	175.72(11)
C2AN-N6-Ru1	175.55(11)	C59E-C00-C0T	120.04(13)
C59E-C00-H00	120.0	C0T-C00-H00	120.0

N4-C01-C1R	122.37(11)	N4-C01-C04	115.74(10)
C1R-C01-C04	121.75(10)	C03-C02-C0Q	118.09(11)
C03-C02-C06	119.23(12)	C0Q-C02-C06	122.63(12)
C0R-C03-C02	118.08(12)	C0R-C03-C0B	122.43(13)
C02-C03-C0B	119.45(13)	N5-C04-C01	109.85(10)
N5-C04-H04A	109.7	C01-C04-H04A	109.7
N5-C04-H04B	109.7	C01-C04-H04B	109.7
H04A-C04-H04B	108.2	N5-C05-C0A	110.51(10)
N5-C05-H05A	109.5	C0A-C05-H05A	109.5
N5-C05-H05B	109.5	C0A-C05-H05B	109.5
H05A-C05-H05B	108.1	C57E-C06-C02	119.79(14)
C57E-C06-H06	120.1	C02-C06-H06	120.1
C0F-C07-C0T	119.80(12)	C0F-C07-H07	120.1
C0T-C07-H07	120.1	O1-C08-C15E	121.7(2)
O1-C08-C14E	122.7(2)	C15E-C08-C14E	115.5(2)
C0K-C09-C0S	120.33(13)	C0K-C09-H09	119.8
C0S-C09-H09	119.8	N5-C0E-C0Q	112.19(10)
N5-C0E-H0E1	109.2	C0Q-C0E-H0E1	109.2
N5-C0E-H0E2	109.2	C0Q-C0E-H0E2	109.2
H0E1-C0E-H0E2	107.9	C2AN-C0M-H0M1	109.5
C2AN-C0M-H0M2	109.5	H0M1-C0M-H0M2	109.5

C2AN-C0M-H0M3	109.5	H0M1-C0M-H0M3	109.5
H0M2-C0M-H0M3	109.5	C07-C0F-N2	122.10(12)
C07-C0F-H0F	119.0	N2-C0F-H0F	119.0
N3-C0Q-C02	122.30(11)	N3-C0Q-C0E	116.33(11)
C02-C0Q-C0E	121.35(11)	C0A-C0O-C0L	122.78(12)
C0A-C0O-C0T	117.95(11)	C0L-C0O-C0T	119.27(12)
C0I-C0N-C0K	120.52(13)	C0I-C0N-H0N	119.7
C0K-C0N-H0N	119.7	C0N-C0I-C1R	120.31(13)
C0N-C0I-H0I	119.8	C1R-C0I-H0I	119.8
C56E-C0B-C03	119.77(14)	C56E-C0B-H0B	120.1
C03-C0B-H0B	120.1	O2-C0H-C19E	123.02(19)
O2-C0H-C11E	120.8(2)	C19E-C0H-C11E	116.1(2)
N1-C0G-C0P	179.50(16)	C0D-C0R-C03	119.95(12)
C0D-C0R-H0R	120.0	C03-C0R-H0R	120.0
C0C-C011-N4	122.15(11)	C0C-C011-H011	118.9
N4-C011-H011	118.9	C0V-C0J-H0J1	109.5
C0V-C0J-H0J2	109.5	H0J1-C0J-H0J2	109.5
C0V-C0J-H0J3	109.5	H0J1-C0J-H0J3	109.5
H0J2-C0J-H0J3	109.5	C0R-C0D-N3	122.49(12)
C0R-C0D-H0D	118.8	N3-C0D-H0D	118.8
C0C-C0S-C09	122.51(12)	C0C-C0S-C1R	118.26(11)

C09-C0S-C1R	119.22(12)	C09-C0K-C0N	120.59(13)
C09-C0K-H0K	119.7	C0N-C0K-H0K	119.7
C00-C0T-C07	122.56(12)	C00-C0T-C0O	119.19(12)
C07-C0T-C0O	118.25(12)	C011-C0C-C0S	120.06(12)
C011-C0C-H0C	120.0	C0S-C0C-H0C	120.0
C58E-C0L-C0O	119.90(13)	C58E-C0L-H0L	120.1
C0O-C0L-H0L	120.1	C0G-C0P-H0P1	109.5
C0G-C0P-H0P2	109.5	H0P1-C0P-H0P2	109.5
C0G-C0P-H0P3	109.5	H0P1-C0P-H0P3	109.5
H0P2-C0P-H0P3	109.5	O3-C0V-C0J	121.88(18)
O3-C0V-C17E	120.63(19)	C0J-C0V-C17E	117.47(16)
N2-C0A-C0O	122.00(11)	N2-C0A-C05	116.26(11)
C0O-C0A-C05	121.60(11)	N6-C2AN-C0M	179.72(15)
C18E-C10E-H10A	109.5	C18E-C10E-H10B	109.5
H10A-C10E-H10B	109.5	C18E-C10E-H10C	109.5
H10A-C10E-H10C	109.5	H10B-C10E-H10C	109.5
C0H-C11E-H11A	109.5	C0H-C11E-H11B	109.5
H11A-C11E-H11B	109.5	C0H-C11E-H11C	109.5
H11A-C11E-H11C	109.5	H11B-C11E-H11C	109.5
C08-C14E-H14A	109.5	C08-C14E-H14B	109.5
H14A-C14E-H14B	109.5	C08-C14E-H14C	109.5

H14A-C14E-H14C	109.5	H14B-C14E-H14C	109.5
C08-C15E-H15A	109.5	C08-C15E-H15B	109.5
H15A-C15E-H15B	109.5	C08-C15E-H15C	109.5
H15A-C15E-H15C	109.5	H15B-C15E-H15C	109.5
C18E-C55E-H55A	109.5	C18E-C55E-H55B	109.5
H55A-C55E-H55B	109.5	C18E-C55E-H55C	109.5
H55A-C55E-H55C	109.5	H55B-C55E-H55C	109.5
C0V-C17E-H17A	109.5	C0V-C17E-H17B	109.5
H17A-C17E-H17B	109.5	C0V-C17E-H17C	109.5
H17A-C17E-H17C	109.5	H17B-C17E-H17C	109.5
O1S-C18E-C10E	121.5(2)	O1S-C18E-C55E	120.7(2)
C10E-C18E-C55E	117.8(2)	C0H-C19E-H19A	109.5
C0H-C19E-H19B	109.5	H19A-C19E-H19B	109.5
C0H-C19E-H19C	109.5	H19A-C19E-H19C	109.5
H19B-C19E-H19C	109.5	C04-N5-C05	112.21(10)
C04-N5-C0E	110.00(10)	C05-N5-C0E	110.82(10)
C04-N5-Ru1	106.64(7)	C05-N5-Ru1	106.01(7)
C0E-N5-Ru1	111.02(7)	C0Q-N3-C0D	119.02(11)
C0Q-N3-Ru1	115.49(8)	C0D-N3-Ru1	124.76(8)
C0B-C56E-C57E	120.80(14)	C0B-C56E-H56E	119.6
C57E-C56E-H56E	119.6	C06-C57E-C56E	120.91(15)

C06-C57E-H57E	119.5	C56E-C57E-H57E	119.5
C0L-C58E-C59E	120.61(13)	C0L-C58E-H58E	119.7
C59E-C58E-H58E	119.7	C00-C59E-C58E	120.99(13)
C00-C59E-H59E	119.5	C58E-C59E-H59E	119.5

Table 24. Anisotropic atomic displacement parameters ($^{\circ}\text{A}^2$)

The anisotropic atomic displacement factor exponent takes the form: $-2\pi^2[h^2 a^{*2} U_{11} + \dots + 2 h k a^* b^* U_{12}]$

	U_{11}	U_{22}	U_{33}	U_{23}	U_{13}	U_{12}
C1R	0.0140(5)	0.0149(5)	0.0147(5)	-0.0009(4)	-0.0013(4)	0.0057(4)
Ru1	0.00887(4)	0.01258(4)	0.01167(5)	-0.00078(3)	-0.00064(3)	0.00450(3)
N2	0.0120(4)	0.0135(4)	0.0147(5)	-0.0011(3)	-0.0002(3)	0.0046(4)
P2	0.0247(2)	0.0219(2)	0.0265(3)	0.00645(19)	0.0061(2)	0.0145(2)
P3	0.01966(17)	0.02716(18)	0.02462(18)	0.00682(14)	0.00073(14)	0.01326(15)
P4	0.0216(2)	0.0354(3)	0.0312(3)	-0.0175(2)	-0.0075(2)	0.0189(2)
N4	0.0108(4)	0.0152(4)	0.0129(4)	-0.0002(3)	-0.0007(3)	0.0048(4)
F1	0.0207(4)	0.0382(5)	0.0336(5)	0.0028(4)	-0.0022(4)	0.0113(4)
F2	0.0399(7)	0.0344(6)	0.0872(11)	-0.0022(6)	0.0180(7)	0.0034(5)
F3	0.0282(6)	0.0511(7)	0.0765(9)	-0.0264(7)	0.0087(6)	0.0139(5)
F4	0.0423(6)	0.0342(5)	0.0530(7)	-0.0030(5)	-0.0121(5)	0.0253(5)

	U_{11}	U_{22}	U_{33}	U_{23}	U_{13}	U_{12}
F5	0.0253(5)	0.0464(6)	0.0422(6)	-0.0027(5)	-0.0100(4)	0.0179(5)
F6	0.0369(6)	0.0636(7)	0.0275(5)	0.0139(5)	0.0089(4)	0.0280(6)
F7	0.0677(8)	0.0747(9)	0.0341(6)	0.0146(6)	0.0085(6)	0.0574(8)
F8	0.0338(5)	0.0310(5)	0.0472(6)	0.0061(4)	0.0027(5)	0.0202(4)
F9	0.0610(8)	0.0573(8)	0.0347(6)	-0.0237(6)	-0.0170(6)	0.0272(7)
F10	0.0494(6)	0.0418(6)	0.0316(5)	0.0058(4)	0.0118(5)	0.0327(5)
F11	0.0309(5)	0.0485(6)	0.0314(5)	0.0164(5)	0.0088(4)	0.0124(5)
F12	0.0449(7)	0.0403(6)	0.0710(9)	-0.0219(6)	-0.0248(6)	0.0293(6)
O1	0.0404(8)	0.0352(7)	0.0811(12)	-0.0084(8)	0.0113(8)	0.0112(6)
O2	0.0315(6)	0.0399(7)	0.0434(8)	0.0008(6)	-0.0042(6)	0.0164(6)
O3	0.0433(8)	0.0724(11)	0.0463(8)	0.0127(8)	0.0089(7)	0.0402(8)
N1	0.0133(4)	0.0161(4)	0.0148(5)	0.0001(4)	-0.0008(4)	0.0060(4)
N6	0.0128(4)	0.0156(4)	0.0163(5)	-0.0014(4)	-0.0006(4)	0.0048(4)
C00	0.0223(6)	0.0169(6)	0.0225(7)	-0.0042(5)	-0.0041(5)	0.0022(5)
C01	0.0120(5)	0.0150(5)	0.0133(5)	-0.0005(4)	-0.0008(4)	0.0058(4)
C02	0.0157(5)	0.0126(5)	0.0160(5)	0.0002(4)	-0.0026(4)	0.0030(4)
C03	0.0181(6)	0.0137(5)	0.0148(5)	-0.0002(4)	0.0000(4)	0.0011(4)
C04	0.0127(5)	0.0178(5)	0.0164(5)	-0.0061(4)	-0.0011(4)	0.0062(4)
C05	0.0095(5)	0.0168(5)	0.0215(6)	-0.0043(4)	0.0004(4)	0.0041(4)
C06	0.0218(6)	0.0198(6)	0.0218(6)	0.0045(5)	-0.0025(5)	0.0074(5)

	U_{11}	U_{22}	U_{33}	U_{23}	U_{13}	U_{12}
C07	0.0192(6)	0.0169(5)	0.0220(6)	-0.0046(5)	-0.0003(5)	0.0069(5)
C08	0.0418(10)	0.0348(9)	0.0465(11)	0.0041(8)	0.0092(9)	0.0174(8)
C09	0.0189(6)	0.0157(5)	0.0200(6)	-0.0022(4)	-0.0040(5)	0.0033(5)
C0E	0.0165(5)	0.0191(5)	0.0171(6)	0.0017(4)	0.0004(4)	0.0103(5)
C0M	0.0269(7)	0.0314(7)	0.0237(7)	0.0126(6)	0.0075(6)	0.0113(6)
C0F	0.0145(5)	0.0164(5)	0.0193(6)	-0.0036(4)	0.0002(4)	0.0065(4)
C0Q	0.0118(5)	0.0123(5)	0.0151(5)	-0.0011(4)	-0.0018(4)	0.0035(4)
C0O	0.0118(5)	0.0151(5)	0.0154(5)	-0.0005(4)	-0.0008(4)	0.0031(4)
C0N	0.0234(6)	0.0211(6)	0.0251(7)	-0.0069(5)	-0.0039(5)	0.0110(5)
C0I	0.0175(6)	0.0195(6)	0.0220(6)	-0.0050(5)	-0.0032(5)	0.0087(5)
C0B	0.0278(7)	0.0191(6)	0.0158(6)	0.0021(5)	0.0023(5)	0.0025(5)
C0H	0.0271(8)	0.0379(9)	0.0390(10)	0.0075(7)	-0.0011(7)	0.0096(7)
C0G	0.0151(5)	0.0186(5)	0.0168(6)	0.0002(4)	-0.0003(4)	0.0076(4)
C0R	0.0168(5)	0.0186(5)	0.0166(6)	-0.0008(4)	0.0040(4)	0.0042(5)
C011	0.0106(5)	0.0168(5)	0.0156(5)	0.0006(4)	-0.0002(4)	0.0046(4)
C0J	0.0425(10)	0.0324(9)	0.0392(10)	0.0116(7)	0.0057(8)	0.0146(8)
C0D	0.0136(5)	0.0189(5)	0.0156(5)	-0.0006(4)	0.0009(4)	0.0065(4)
C0S	0.0145(5)	0.0150(5)	0.0144(5)	0.0000(4)	-0.0018(4)	0.0042(4)
C0K	0.0242(7)	0.0163(5)	0.0230(7)	-0.0052(5)	-0.0050(5)	0.0063(5)
C0T	0.0162(5)	0.0157(5)	0.0161(6)	-0.0014(4)	-0.0015(4)	0.0032(4)

	U_{11}	U_{22}	U_{33}	U_{23}	U_{13}	U_{12}
C0C	0.0118(5)	0.0173(5)	0.0174(6)	0.0002(4)	-0.0015(4)	0.0035(4)
C0L	0.0127(5)	0.0193(6)	0.0246(7)	-0.0012(5)	-0.0030(5)	0.0044(4)
C0P	0.0195(6)	0.0279(7)	0.0279(7)	0.0036(6)	-0.0010(5)	0.0156(6)
C0V	0.0349(8)	0.0415(9)	0.0219(7)	0.0139(6)	0.0103(6)	0.0237(7)
C0A	0.0122(5)	0.0138(5)	0.0148(5)	-0.0006(4)	-0.0001(4)	0.0042(4)
C2AN	0.0157(5)	0.0187(5)	0.0185(6)	0.0003(4)	0.0006(4)	0.0068(5)
C10E	0.0713(18)	0.0615(16)	0.0332(11)	0.0052(11)	-0.0068(11)	-0.0105(13)
C11E	0.089(3)	0.300(7)	0.121(3)	0.154(4)	0.048(3)	0.103(4)
C14E	0.0674(17)	0.0621(16)	0.081(2)	0.0074(14)	0.0227(15)	0.0411(14)
C15E	0.0567(17)	0.0583(16)	0.102(3)	-0.0364(17)	0.0141(16)	-0.0015(13)
C55E	0.119(3)	0.091(2)	0.0461(14)	0.0252(14)	0.0357(16)	0.072(2)
C17E	0.0634(14)	0.0549(13)	0.0372(10)	-0.0096(9)	-0.0146(10)	0.0393(12)
C18E	0.0530(12)	0.0399(10)	0.0219(8)	0.0088(7)	0.0105(8)	0.0153(9)
C19E	0.0362(10)	0.0482(11)	0.0552(13)	-0.0120(10)	0.0047(9)	0.0207(9)
N5	0.0087(4)	0.0138(4)	0.0138(4)	-0.0010(3)	-0.0012(3)	0.0042(3)
N3	0.0109(4)	0.0137(4)	0.0130(4)	-0.0009(3)	-0.0006(3)	0.0043(3)
O1S	0.0447(8)	0.0430(8)	0.0351(7)	0.0000(6)	0.0050(6)	0.0091(7)
C56E	0.0372(8)	0.0240(7)	0.0175(6)	0.0057(5)	-0.0025(6)	0.0068(6)
C57E	0.0302(8)	0.0252(7)	0.0233(7)	0.0078(5)	-0.0053(6)	0.0090(6)
C58E	0.0132(6)	0.0226(6)	0.0314(8)	-0.0001(5)	-0.0046(5)	0.0025(5)

	U_{11}	U_{22}	U_{33}	U_{23}	U_{13}	U_{12}
C59E	0.0183(6)	0.0195(6)	0.0260(7)	-0.0025(5)	-0.0069(5)	-0.0002(5)

Table 25. Hydrogen coordinates and isotropic atomic displacement parameters (\AA^2).

	x/a	y/b	z/c	U(eq)
H00	0.4303	0.3233	0.5337	0.027
H04A	0.6815	0.8222	0.8605	0.019
H04B	0.6847	0.9170	0.8058	0.019
H05A	0.5290	0.7278	0.7081	0.02
H05B	0.5662	0.6845	0.7897	0.02
H06	0.6768	0.9331	0.5223	0.026
H07	0.6543	0.4093	0.5727	0.023
H09	1.1516	1.1923	0.9759	0.023
HOE1	0.7562	0.9423	0.6818	0.02
HOE2	0.6468	0.8482	0.6358	0.02
HOM1	0.7568	0.5518	1.0109	0.041
HOM2	0.6268	0.4971	0.9653	0.041
HOM3	0.6599	0.6027	1.0183	0.041
HOE	0.8118	0.5439	0.6391	0.02
HON	0.8106	1.1826	0.9874	0.027

	x/a	y/b	z/c	U(eq)
H0I	0.7348	1.0341	0.9036	0.023
H0B	0.9755	0.9011	0.3541	0.028
H0R	1.0527	0.8326	0.4747	0.022
H011	1.1060	0.9014	0.8144	0.018
H0J1	0.5626	0.3652	0.0747	0.057
H0J2	0.6580	0.3278	0.0325	0.057
H0J3	0.5886	0.2715	0.1126	0.057
H0D	1.0301	0.7782	0.6075	0.019
H0K	1.0194	1.2618	1.0237	0.026
H0C	1.1854	1.0529	0.8930	0.02
H0L	0.3703	0.5962	0.6721	0.024
H0P1	1.2261	0.6825	0.7760	0.035
H0P2	1.1421	0.5749	0.7299	0.035
H0P3	1.1345	0.5878	0.8272	0.035
H10A	0.7412	0.6422	0.1902	0.101
H10B	0.7028	0.7013	0.2620	0.101
H10C	0.7206	0.7454	0.1711	0.101
H11A	0.4140	0.9088	0.4387	0.239
H11B	0.3221	0.7963	0.4043	0.239
H11C	0.4650	0.8250	0.4092	0.239

	x/a	y/b	z/c	U(eq)
H14A	0.3105	0.8207	0.2315	0.097
H14B	0.2105	0.7352	0.1725	0.097
H14C	0.2446	0.7026	0.2599	0.097
H15A	-0.0448	0.7230	0.2890	0.121
H15B	0.0136	0.6393	0.2975	0.121
H15C	-0.0105	0.6745	0.2085	0.121
H55A	0.3899	0.6133	0.1863	0.112
H55B	0.4913	0.7272	0.1698	0.112
H55C	0.4758	0.6818	0.2603	0.112
H17A	0.4256	0.0896	-0.0541	0.071
H17B	0.5145	0.0980	0.0224	0.071
H17C	0.5685	0.1579	-0.0602	0.071
H19A	0.2732	0.7547	0.6172	0.068
H19B	0.2019	0.7329	0.5305	0.068
H19C	0.2672	0.8496	0.5672	0.068
H56E	0.8329	0.9565	0.3008	0.034
H57E	0.6834	0.9710	0.3842	0.032
H58E	0.2094	0.4617	0.6063	0.029
H59E	0.2402	0.3264	0.5365	0.029

6.3.8 HPLC conditions for analysis of purity of **86a-j**

Instrument conditions

Instrument – LCMS-MS (Schimadzu) Nexera X2 connected to LCMS-8040 mass spectrometry

Software for data processing – Labsolutions Version 5.55

LCMS conditions

Column – Kinetex (Phenomenex)

P/No – 00A-4496-YO

Description – Kinetex 2.6 μ XB – C18 100 $^{\circ}$ A

Size – 30 X 3.0 mm

Mobile phase A – 0.1% HCOOH in water

Mobile phase B – 0.1% HCOOH in acetonitrile

Gradient program

Time (min)	B conc (%)	Command
0.50	1	Pump B conc
5.50	90	Pump B conc
5.51	90	Pump B conc
8.00	90	Pump B conc
8.01	90	Pump B conc
12.0	-	Stop

Flow rate – 0.3 mL/min

Column temperature – 35 $^{\circ}$ C, sample temperature – 10 $^{\circ}$ C

Injection volume – 1 μ L

Analysis time – 12 min.

CHAPTER 7. TUNING EXCITED STATE LIFETIMES OF RUTHENIUM COMPLEXES

7.1 Introduction

Photosensitizers are compounds that absorb light (UV or visible) and transfer it to adjacent molecules, which then induce a chemical change in the neighboring molecule. These compounds have broad applications in chemistry, biology, materials and medicine.^{283,284} Triplet photosensitizers are the compounds that upon irradiation reach triplet states and then transfer their triplet energy to adjacent molecules. For instance, in photodynamic therapy, the triplet photosensitizers transfer their energy to triplet oxygen ($^3\text{O}_2$) to generate singlet dioxygen species ($^1\text{O}_2$) (Figure 9a, chapter 1).^{58,67,71,283,285} Triplet sensitizers are being used for numerous applications such as PDT,²⁸⁶⁻²⁸⁹ molecular sensing,²⁹⁰⁻²⁹² light-initiated polymerization, and electroluminescence.^{293,294} Photosensitizers are also used in redox catalysis, as excited states can act as strong oxidant or reductant.²⁹⁵⁻²⁹⁷ A good triplet photosensitizer should have a strong visible light absorption (high ϵ value), effective conversion of singlet excited state to triplet excited state (quantum yields) and long-lived triplet excited states.^{298,299} While transition metal complexes absorb visible light, their molar absorption coefficients (ϵ) and their triplet lifetimes are usually small, so most of the complexes are not useful as triplet photosensitizers.²⁸³

Ruthenium-based compounds are an important class of photosensitizers that have undergone decades of development to tune their excited state properties.^{10,284,300-304} The majority of the previous studies were largely focusing on ligands with denticities of three or below for the ruthenium complexes.³⁰⁵ Figure 44 shows a few examples of Ru-based photosensitizers, where **95** is considered as a gold standard which has a long-lived excited state of 0.890 μs in ambient

H₂O when the complex is excited at 452 nm. More recently developed complexes have their emission lifetimes in microsecond range.³⁰⁶⁻³⁰⁸

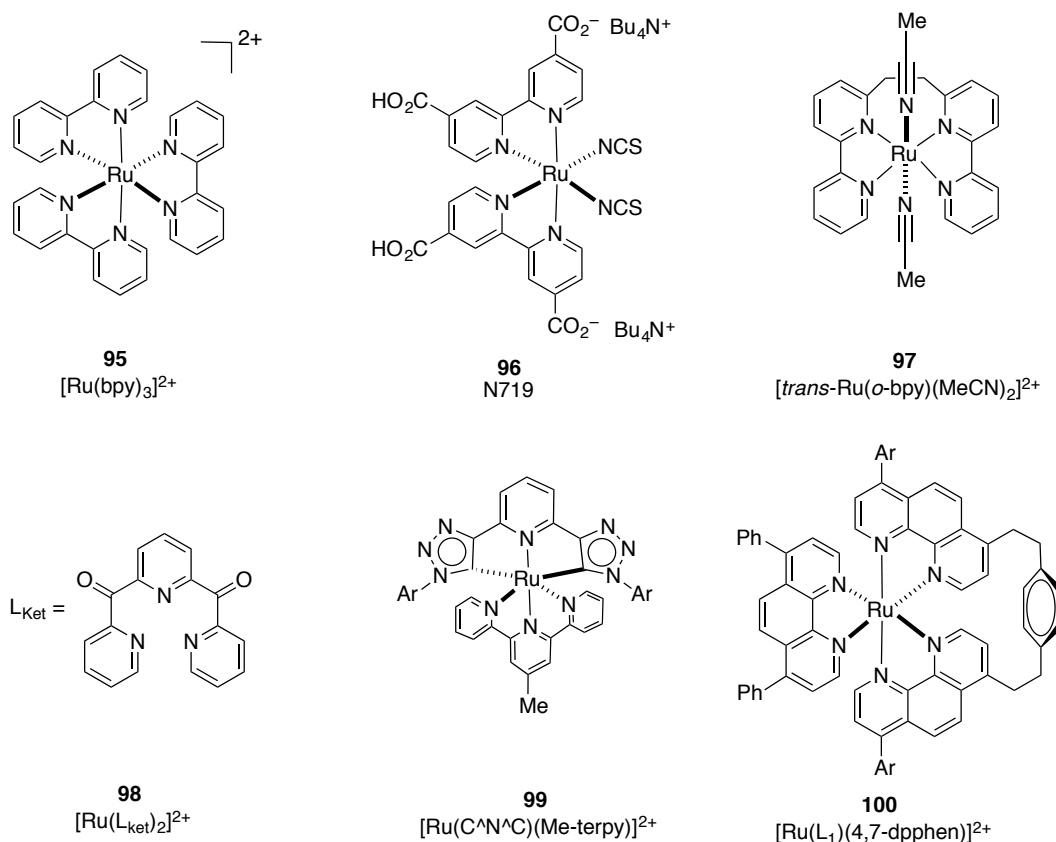


Figure 44: Examples of Ru-based photosensitizers

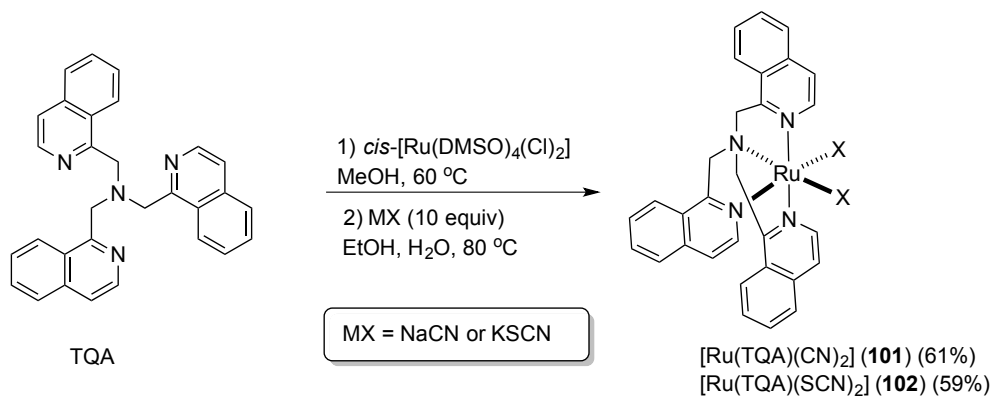
In this chapter, we report a new class of ruthenium-based photosensitizers derived from the chromophore Ru(TQA), where TQA (tris(isoquinolin-1-ylmethyl)amine) is a tetradentate ligand. The longer a molecule stays at the excited state, the greater is the likelihood of it undergoing an electron or energy transfer to its neighboring molecules. Thus excited state lifetime plays a key role in the use of compounds as photosensitizers. The $[Ru(TQA)(X)_2]^{m+}$ complexes described in this chapter have consistently longer lived emitting triplet metal to ligand charge transfer (³MLCT) excited states at 77 K than do their Ru-bipyridine analogs even though their lowest energy triplet metal centered (³MC) excited states have energies that are lower than

or comparable to the emitting MLCT excited state energies. These observations indicate that the longer $^3\text{MLCT}$ lifetimes found for these complexes are unique properties of the Ru-TQA chromophore and suggest that achieving long lived MLCT excited states depends on the optimization of some excited state electronic properties of the complexes and not just finding complexes for which the $^3\text{MLCT}$ excited state is lower in energy than any ^3MC excited state.

7.2 Results and discussions

7.2.1 Synthesis and characterization of complexes **101** and **102**

Three compounds were developed and examined in this study. Two new derivatives of Ru(TQA) were prepared (Scheme 18), along with a third compound reported in the previous chapter (**91**).³⁰⁹ Treating the ligand TQA²²⁷ with 1 equiv. of *cis*-[Ru(DMSO)₄(Cl)₂] in refluxing MeOH resulted in formation of [Ru(TQA)(DMSO)(Cl)]Cl, isolated as a mixture of stereoisomers. As described previously, treating this intermediate with 1:1 MeCN:H₂O at 80 °C, followed by precipitation with NH₄PF₆ provided [Ru(TQA)(MeCN)₂](PF₆)₂ (**91**).³⁰⁹ Alternatively, heating [Ru(TQA)(DMSO)(Cl)]Cl in 1:1 EtOH:H₂O at 80 °C in the presence of 10 equiv. of NaCN or KSCN provided [Ru(TQA)(CN)₂] (**101**) and [Ru(TQA)(SCN)₂] (**102**), respectively, in 59-61% yield.



Scheme 18. Synthesis of Ru(TQA) complexes **101** and **102**

Complexes **101** and **102** were characterized by ^1H NMR, UV-vis and IR spectroscopies. X-ray crystallographic data for **91** is at the end of the previous chapter. Spectroscopic data for the three complexes are highly consistent across the series. ^1H NMR spectra of all the three complexes show two distinct sets of resonances for the 3-isoquinoloyl CH groups, present in a 2:1 ratio at approximately 9.8-8.6 ppm. UV-vis data indicate strong absorbance in the visible region; with metal-to-ligand charge transfer (MLCT) bands occurring with λ_{max} values for MeCN ($\epsilon_{424} = 12,000 \text{ M}^{-1}\text{cm}^{-1}$), CN ($\epsilon_{470} = 9,600 \text{ M}^{-1}\text{cm}^{-1}$) and SCN ($\epsilon_{510} = 9,440 \text{ M}^{-1}\text{cm}^{-1}$). The IR spectrum of **101** shows diagnostic strong absorbances at 2063 and 2043 cm^{-1} , consistent with CN binding to Ru(II). Likewise, the IR spectrum of **102** shows a strong absorbance at 2102 cm^{-1} , consistent with N-bound thiocyanate.^{310,311}

7.2.2 Excited state lifetimes and quantum yield calculations

The efficiency of the photosensitization process generally depends on the properties of the lowest energy photosensitizer excited state (LEES). Since the photosensitized reactions of interest occur in competition with intra-sensitizer processes leading to excited state deactivation, the intrinsic LEES lifetime (τ_{in}) is a critical excited state property, which is inversely dependent on the sum of the rate constants for intra-sensitizer deactivation processes: $(\tau_{\text{in}})^{-1} = (k_{\text{RAD}} + k_{\text{NRD}} + k_{\text{IC}})$, where the most important deactivation processes are radiative decay (RAD), non-radiative population of ground state vibrational modes (NRD) and the population of a shorter lived excited state (typically ^3MC) with the same spin multiplicity (IC). The new class of ruthenium-quinoline based photosensitizers reported in this chapter has values of τ_{in} that are an order of magnitude larger than those of paradigmatic Ru-bipyridine chromophores (Table 26). Derivatives of Ru(TQA) show remarkably long-lived excited states and relatively high emission quantum yields with several different ancillary ligands, X, demonstrating that Ru-(TQA) is a special, highly

consistent chromophore with unique intrinsic properties. Furthermore, these long 77 K lifetimes are observed even though the $^3\text{MLCT}$ is not always the lowest energy excited state (contrary to Kasha's rule),³¹² presumably because of large reorganizational barriers to internal conversion.³¹³ Excited state lifetime and emission spectrum studies presented in this chapter were performed by the Endicott group.

Ligands	$h\nu_{\text{max}}$	τ_{in}	Φ_{em}	τ_{TQA}
$\text{L}(\text{X})_2$	$\text{cm}^{-1}/10^3$	μs		$/\tau_{\text{bpy}}$
$\text{TQA}(\text{MeCN})_2$	18.3	145	0.45	17
$(\text{bpy})_2(\text{MeCN})_2$	18.5	8.3	0.6	
$\text{TQA}(\text{CN})_2$	17.3	78	0.26	22
$(\text{bpy})_2(\text{CN})_2$	15.9	3.4	0.27	
$\text{TQA}(\text{NCS})_2^{\text{b}}$	16.0	17.6	0.50	31
$(\text{bpy})_2(\text{NCS})_2^{\text{b}}$	14.9	0.57	0.084	

Table 26. Excited state lifetimes (τ_{in}) and emission quantum yields (Φ_{em}) of some $[\text{RuL}(\text{X})_2]^{\text{m}+}$ complexes at 77 K^a. ^a Determined in ethanol/methanol ($v/v' = 4/1$) solvent except as indicated. ^b Butyronitrile.

The emission spectra of the $[\text{Ru}(\text{TQA})(\text{X})_2]^{\text{m}+}$ complexes in Figure 45 differ from those of the Ru-bpy analogs^{314,315} in Table 26 in that the dominant vibronic feature, the second highest energy peak in the spectra, is relatively more intense and suggestive of more configurational mixing between the $^3\text{MLCT}$ and aromatic ligand-based $\pi\pi^*$ excited state.³¹⁶

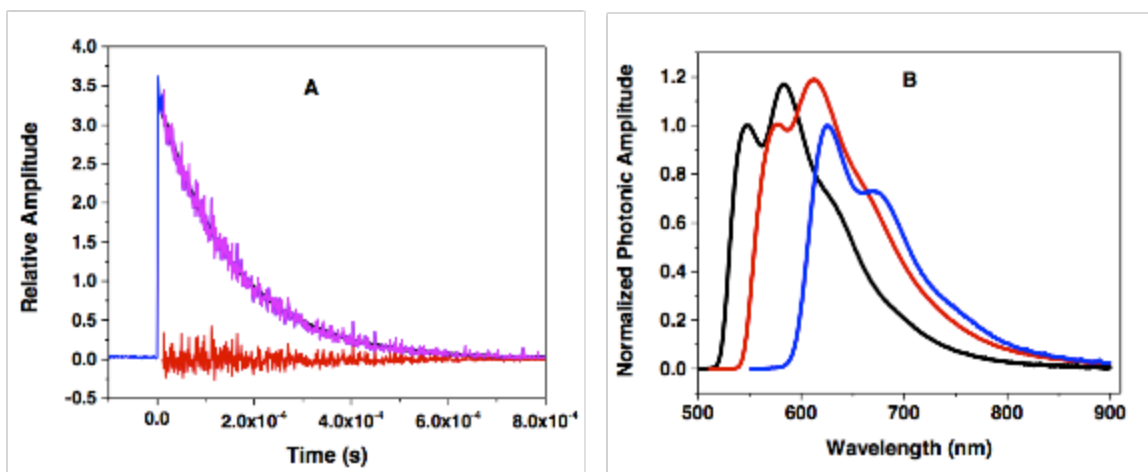


Figure 45. A) Lifetime determination for **91**; B) Emission spectra for $[\text{Ru}(\text{TQA})(\text{L})_2]^{m+}$ complexes **91** (L = MeCN, black), **101** (L = CN, red) and **102** (L = SCN, blue).

7.2.3 DFT calculations

DFT calculations were performed by the Schlegel group on the $^3\text{MLCT}$ states to understand the origins of the longer lifetimes of the Ru(TQA) complexes compared to the Ru(bpy) $_2$ species. The $^3\text{MLCT}$ state MOs of Ru(TQA) and Ru(bpy) $_2$ complexes (Figure 46) show that the metal-based singly occupied MOs (SOMOs) of Ru(TQA) complexes have significant contribution (35-54%) from the π orbital of one of the quinoline (Q) moieties and as a result, they exhibit significant π -delocalization between Ru d π and Q π orbitals. The $[\text{Ru}(\text{TQA})(\text{MeCN})_2]^{2+}$ (**91**) complex is particularly striking since the extent of delocalization is quite large (Ru d π and quinoline π 54%) and the Ru spin density of 0.54 is also unusually low. In contrast to the Ru(TQA) complexes, the Ru(bpy) $_2$ species show less contribution (11-19%) from the bpy ligand in the metal-centered SOMOs as illustrated in Figure 46. These results suggest that the emitting excited states of the Ru(TQA) complexes are not pure $^3\text{MLCT}$ states, but that they have significant contributions from the quinoline $^3\pi,\pi^*$ states. In contrast, the $^3\text{MLCT}$ states of Ru(bpy) $_2$ complexes have much less contribution from the π,π^* states. Since

the ${}^3\pi,\pi^*$ state is intrinsically longer-lived than a pure ${}^3\text{MLCT}$ state, this greater configurational mixing is very likely the origin of the longer excited state lifetimes for the Ru(TQA) species. Among the four complexes studied by DFT, $[\text{Ru}(\text{TQA})(\text{MeCN})_2]^{2+}$ displays the highest mixing. In a previous study of Ru-bpy chromophores³¹⁶ we showed that variations of the ancillary ligands results in variations in the ${}^3\text{MLCT}$ excited state energy and thereby “tunes” the ${}^3\text{MLCT}/{}^3\pi\pi^*(\text{bpy})$ mixing, and the same behavior is apparently the case for the TQA complexes.

Table 27 lists the relative energies of the ${}^3\text{MLCT}$ and the ${}^3\text{MC}$ states. The ${}^3\text{MC}$ energies calculated for the cyanide complexes are close to or slightly higher than those of the ${}^3\text{MLCT}$ states, while the MeCN complexes have significantly lower energy ${}^3\text{MC}$ states.

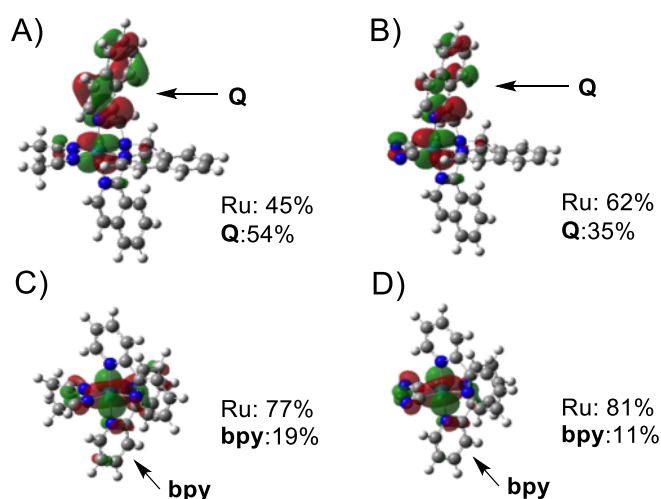


Figure 46. Metal-based SOMOs (corresponding orbitals with isovalue of 0.03 a.u.) and orbital contributions (%) of Ru and ligands for A) $[\text{Ru}(\text{TQA})(\text{MeCN})_2]^{2+}$ (**91**); B) $[\text{Ru}(\text{TQA})(\text{CN})_2]$ (**101**); C) $[\text{Ru}(\text{bpy})_2(\text{MeCN})_2]^{2+}$; D) $[\text{Ru}(\text{bpy})_2(\text{CN})_2]$ in the ${}^3\text{MLCT}$ optimized geometries.

		ΔE	SOMO(1)		SOMO(2)	
		$\text{cm}^{-1} \times 10^3$	Ru	Ligand	Ru	Ligand
A	$^3\text{MLCT} (T_3)$	0	45	54	3	97
	$^3\text{MC} (T_0)$	-4.5	78	17	77	17
	$^3\text{MC} (T_1)$	-3.3	77	18	91	8
	$^3\text{MC} (T_2)$	-2.8	75	22	86	9
B	$^3\text{MLCT} (T_1)$	0	62	35	3	97
	$^3\text{MC} (T_0)$	-1.2	75	17	81	8
C	$^3\text{MLCT} (T_1)$	0	78	19	2	98
	$^3\text{MC} (T_0)$	-3.7	92	6	74	16
D	$^3\text{MLCT} (T_0)$	0	81	11	2	98
	$^3\text{MC} (T_1)$	2.1	91	2	73	22

Table 27. Relative energies of the $^3\text{MLCT}$ and ^3MC states and orbital contributions (%) of Ru and ligands to the SOMOs of A) $[\text{Ru}(\text{TQA})(\text{MeCN})_2]^{2+}$ (**91**); B) $[\text{Ru}(\text{TQA})(\text{CN})_2]$ (**101**); C) $[\text{Ru}(\text{bpy})_2(\text{MeCN})_2]^{2+}$; D) $[\text{Ru}(\text{bpy})_2(\text{CN})_2]$. Energies of the $^3\text{MLCT}$ states are set to be zero. Energies of the ^3MC states are compared to those of the $^3\text{MLCT}$ states.

The energy barrier for the internal conversion is expected to be small enough so that the ^3MC states can be thermally accessed at ambient temperature in the case of MeCN complexes.³¹³ These results are in agreement with the difficulty in finding any ambient emission from these complexes and with our previous report of CH_3CN photodissociation from $[\text{Ru}(\text{TQA})(\text{MeCN})_2]^{2+}$ at room temperature.³⁰⁹

7.3 Discussions and conclusions

A new class of ruthenium-based photosensitizers was developed and their excited state life-times and DFT calculations were performed. Complexes which were part of the study had general formula $[\text{Ru}(\text{TQA})(\text{X}_2)]^{n+}$, where TQA is tris(isoquinoline-1-ylmethyl)amine, and X = MeCN (**91**), CN (**101**) or SCN (**102**) with $n = 0$ or 2. These complexes showed exceptionally long-lived excited states ($\tau_{\text{em}} = 78\text{-}145 \mu\text{s}$) and high emission quantum yields ($\phi_{\text{em}} = 0.26\text{-}0.50$) at 77 K. The chromophore Ru(TQA) furnishes complexes with extremely long-lived excited states. Although long lifetimes have been achieved before by appending aromatic acceptors (AA) on a Ru-(polypyridine) chromophore,^{306,308,317} such complexes take advantage of a reversible energy transfer equilibrium between a pendant AA moiety with a very long intrinsic lifetime and the shorter lived Ru-(polypyridine) $^3\text{MLCT}$ state. In marked contrast, the systems in the current chapter demonstrate that intrinsic long excited state lifetimes depend on the configurational mixing between the $^3\text{MLCT}$ excited state of the donor/acceptor complex and a acceptor/ligand localized excited state.

7.4 Experimental procedures

7.4.1 Synthesis and characterization of complexes **101** and **102**

Synthesis of **101** $[\text{Ru}(\text{TQA})(\text{CN})_2]$ - TQA (47.2 mg, 0.11 mmol), which was prepared by a known procedure²²⁷ was dissolved in 10 mL of dry MeOH under inert atmosphere in a pressure flask. To this, $\text{Ru}(\text{DMSO})_4\text{Cl}_2$ (52.0 mg, 0.11 mmol) was added and the solution was purged with Ar for 10 min at room temperature. The reaction mixture was refluxed for 5 h under inert temperature. Color of the reaction mixture changes from pale yellow to dark red. The reaction mixture was cooled to room temperature and concentrated under reduced pressure. To the flask,

NaCN (53.9 mg, 1.1 mmol) and a 1:1 mixture of EtOH: H₂O (10 mL) was added, and the reaction mixture was refluxed for 16 h under inert atmosphere. Ice cold water (20 mL) was then added to the reaction mixture which resulted in the formation of dark red precipitate, which was filtered and washed with ice cold water (300 mL) and dried under reduced pressure to give title complex as a dark red solid (39 mg, 61%): Mp = 194 °C (decomp); ¹H NMR (400MHz (CD₃)₂SO) δ 9.64(d, 1H, *J* = 6.0 Hz), 8.66(d, 2H, *J* = 6.4 Hz), 8.14-8.16(m, 2H), 7.90-7.82(m, 3Hz), 7.77-7.70(m, 6H), 7.65-7.62(m, 3H), 7.51(t, 1H, *J* = 8.0 Hz), 5.94(d, 2H, *J* = 15.6 Hz), 5.54-5.49(m, 4H); IR (KBr) ν_{max} (cm⁻¹) 3852, 3744, 3726, 3673, 3528, 3432, 3252, 2994, 2947, 2891, 2063, 2043, 1693, 1650, 1594, 1553, 1503, 1453, 1394, 1376, 1317, 1294, 1262, 1236, 1198, 1145, 1099, 955, 827, 748, 679, 668, 660; UV-vis λ_{max} = 470 nm (ε = 9,600 M⁻¹cm⁻¹); Anal. Calculated for C₁₀₀H₈₆N₁₈O₃Ru₃: (3 moles **101**·2 moles H₂O and 1 mole Et₂O) C, 63.51; H, 4.58; N, 13.33. Found: C, 63.49; H, 4.54; N, 13.29.

Synthesis of **102** [Ru(TQA)(SCN)₂] - TQA (27.3 mg, 0.06 mmol) was dissolved in 10 mL of dry MeOH under inert atmosphere in a pressure flask. To this, Ru(DMSO)₄Cl₂ (30.0 mg, 0.06 mmol) was added and the solution was purged with Ar for 10 min at room temperature. The reaction mixture was refluxed for 5 h under inert temperature. Color of the reaction mixture changes from pale yellow to dark red. The reaction mixture was cooled to room temperature and concentrated under reduced pressure. To the flask, KSCN (58.2 mg, 0.6 mmol) and a 1:1 mixture of EtOH: H₂O (10 mL) was added and the reaction mixture was refluxed for 16 h under inert atmosphere. Ice cold water (20 mL) was then added to the reaction mixture followed by saturated brine solution, which resulted in the formation of dark red precipitate that was filtered and washed with ice cold water (300 mL) and dried under reduced pressure to give title complex as a dark red solid (24 mg, 59%): Mp = 214 °C (decomp); ¹H NMR (400MHz (CD₃)₂SO) δ 9.03(d,

1H, $J = 6.4$ Hz), 8.55(d, 2H, $J = 6.4$ Hz), 8.19-8.17(m, 2H), 7.98-7.96(m, 2H), 7.84-7.82(m, 3H), 7.79-7.75(m, 5H), 7.62(t, 2H, $J = 6.4$ Hz), 7.50(t, 1H, $J = 8.0$ Hz), 5.92(d, 2H, $J = 15.6$ Hz), 5.46(s, 2H), 5.19(d, 2H, $J = 15.6$ Hz); IR (KBr) ν_{\max} (cm^{-1}) 3901, 3743, 3419, 3261, 2917, 2101, 1705, 1622, 1593, 1552, 1504, 1451, 1395, 1316, 1224, 1199, 1146, 1093, 1014, 949, 871, 827, 796, 749, 658, 641, 616; UV-vis $\lambda_{\max} = 510$ nm ($\epsilon = 9,440 \text{ M}^{-1}\text{cm}^{-1}$); Anal. Calculated for $\text{C}_{32}\text{H}_{32}\text{N}_6\text{O}_4\text{RuS}_2 \cdot (\mathbf{102} \cdot 4 \text{ H}_2\text{O})$ C, 52.65; H, 4.42; N, 11.52. Found: C, 52.68; H, 4.45; N, 11.49.

7.4.2 UV-Vis Spectra conditions

The UV-vis spectra were determined in ethanol-methanol ($[\text{Ru}(\text{TQA})(\text{NCCH}_3)_2]^{2+}$ (**91**) and $[\text{Ru}(\text{TQA})(\text{CN})_2]^0$ (**101**) and butyronitrile ($[\text{Ru}(\text{TQA})(\text{NCS})_2]^0$) (**102**) (Figures 46-48) glasses using a Quartz Tungsten Halogen (QTH) lamp as the light source for low-temperature spectroscopic measurements. An Oxford Instruments OptistatCF static exchange gas continuous-flow cryostat with liquid nitrogen as the cryogen was employed at 90 K with NSG Precision Cells, Inc. cryogenic square 1 cm quartz cuvettes. The detection system was an ANDOR Shamrock 500 spectrometer with dual exit ports and equipped with a 600 l/mm, 500 nm blaze grating. Light was collected with a lens and transmitted by means of Thorlabs 3 mm Core Liquid Light Guide LLG0338-4 (wavelength range 340 – 800 nm) to an Andor F/# matcher SR 500i to the spectrometers entrance slit. The ANDOR Newton detector and liquid light guide combination that was used for spectroscopic determinations has no response to light wavelengths less than ~ 400 nm. As a result, any response shown less than or equal to 400 nm is the result of partial 90 K absorption.

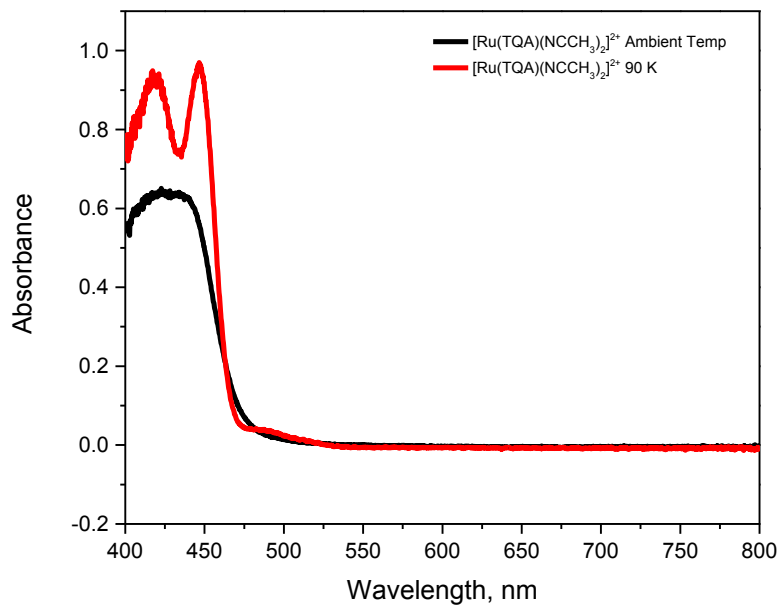


Figure 47- Absorption spectrum of **91** at RT (black) and at 90 K (red)

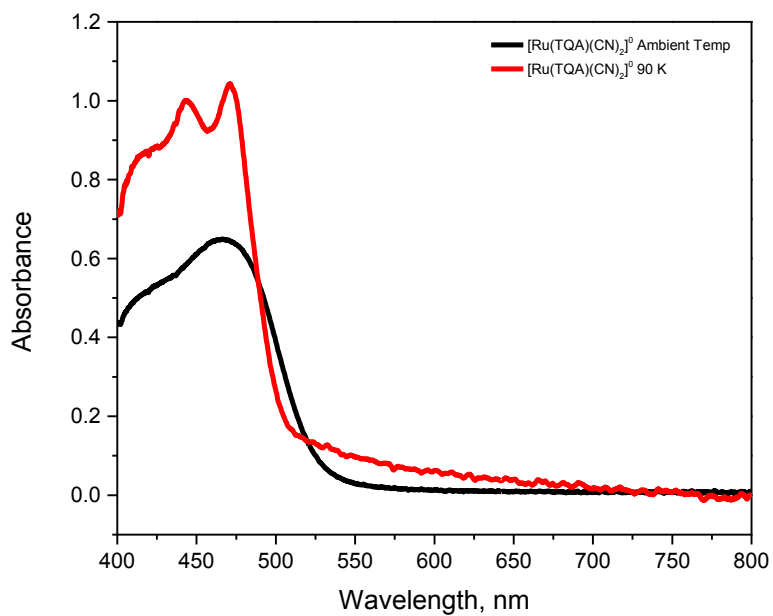


Figure 48- Absorption spectrum of **101** at RT (black) and at 90 K (red)

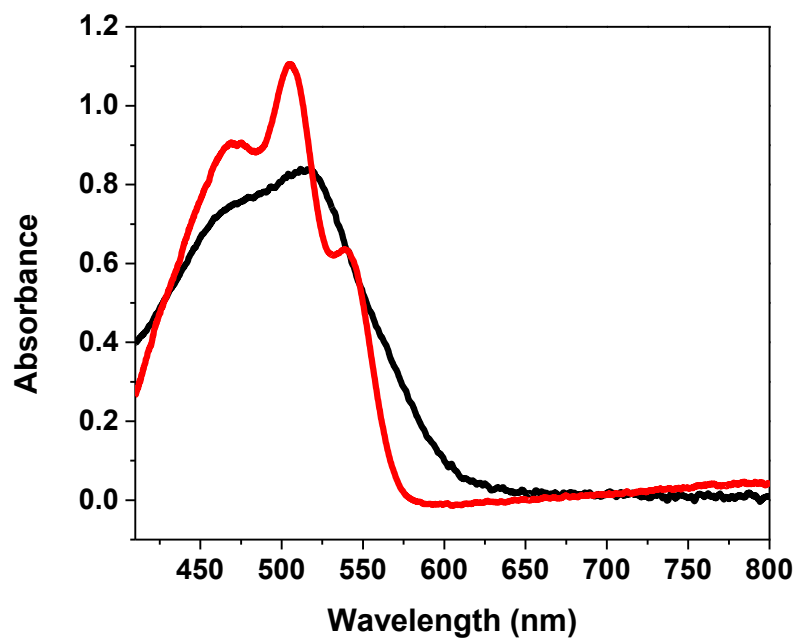


Figure 49- Absorption spectrum of **102** at RT (black) and at 90 K (red)

CHAPTER 8. CONCLUSIONS

8.1 Goals achieved and future directions

Light can be controlled both temporally and spatially and it can also be used in activation of numerous compounds through energy transfer.² This ability of light can be harnessed to develop new tools for solving problems in biology. Three different projects are discussed in this dissertation, so the goals achieved and their corresponding future directions are also discussed in three different sections.

8.1.1 Caging nitrile based inhibitors of cathepsin K and B using Ru(bpy)₂

caging group:

Light activated compounds can be used as tools for understanding and solving numerous biological problems.^{43,148} To develop metal-based photocages as tools for biology, we chose cathepsin enzymes as our initial targets. Cathepsins are required for normal cell growth and are involved in numerous physiological functions and are thus called housekeeping enzymes.^{85,93,95,129,196,318,319} Numerous results have shown that these enzymes are over expressed in numerous tumors and other pathological problems.^{83,92,94,99,105,106,109,320,321} These results suggest that cathepsins could be viable target for cancer chemotherapy and treatment of other disorders. Several academic and industrial research groups developed numerous inhibitors for targeting cathepsins.^{93,124,131,132,140,154,201,202,322-326} While these inhibitors were both potent and selective towards cathepsins, they could not reach the market due to their off-target reactivity and inhibition of cathepsins in normal cells. The photolabile group strategy we developed could be useful in achieving spatial control over the activation of these inhibitors. We envisioned that these inhibitors can be protected using photolabile-protecting groups and be specifically released at the target site. Towards this end, we have developed

nitrile-based caged cathepsin inhibitors, which can be released using light. Ru(bpy)₂ was used as a group for caging numerous nitrile-based cathepsin B and cathepsin K inhibitors. Initially we used known nitrile-based inhibitors of CTSK and CTSB for our photolabile caging strategy. Later we also synthesized an analog of a known CTSB inhibitor, which was caged successfully. These inhibitors are stable in the dark and release the active inhibitor when irradiated with light of suitable wavelength. In the first few chapters of this dissertation, we have shown that spatial and temporal control can be achieved for enzyme inhibitors using photolabile-caging groups. These caged molecules were shown to inhibit cathepsin activity in isolated enzyme assays and also in 2D and 3D assays.¹⁷¹ Moreover no toxic effects were seen from either the complexes or their corresponding photolysis byproducts, which makes us believe that this strategy would be extremely useful in studying aberrant proteolysis in tumor models.

The focus of this dissertation was only on nitrile-based cathepsin B and K inhibitors, and current research in our group is directed towards inhibition of other proteases, which are over expressed in numerous pathological states. New nitrile-based cathepsin inhibitors or their analogs with higher activity and selectivity can be synthesized and caged for developing the photocaging applications.

While only nitriles were used, other functionalities such as pyridines, imidazoles and thioethers can also be caged using various ruthenium-caging groups, thus increasing the applicability of this method across different inhibitor groups apart from nitriles. Stability of caged complexes in different mediums is an important factor that could determine the usefulness of our caging strategy. While caged nitriles were successful for preliminary studies, where they showed good stability profiles in DMSO, some lacked long-term stability

in other biological mediums. Pyridines on the other hand have greater affinity towards ruthenium when compared to nitriles, which could be useful for increasing the stability of the caged complex in dark.

Rate of photodissociation is also an important factor in photocaging strategy. The quantum yields for the complexes synthesized and studied were low and some compounds required a longer irradiation time. New methods could be developed to increase the rate of photodissociation. One strategy would be to increase the steric bulk on the metal complex, which could assist in ligand release. While the caged complexes are charged, the free inhibitors are hydrophobic. Our studies have also shown that the released inhibitors, due to their hydrophobic nature, are trapped in the solvent cage, which decreases the overall quantum yields. Water-soluble inhibitors with polar groups could increase the quantum yields by assisting in inhibitor solubility.

Enzymes have different functions in various locations of human body. While numerous research articles have been dedicated towards studying their functions and distribution; it is not completely understood. Photocaging can be used for understanding the role of enzymes and other biological molecules in the body. Small molecules can be caged and specifically delivered using photocages, and their effects on different physiological functions can be studied.

A combination strategy can also be developed where cathepsin inhibitors with different functionalities are caged using suitable metal complexes. Upon photolysis the caged complex acts as dual therapeutic agent where the inhibitors interact with the enzymes and the metal complex either generates singlet oxygen species through triplet sensitization or induces

DNA damage. Both oxygen sensitization and DNA damage can induce cell death, thus paving a way for dual strategy.

8.1.2 Developing new ligands for photocaging applications:

In the latter part of this dissertation, focus was laid towards developing new caging groups for nitriles. Traditionally small, flat heteroaromatic ligands are used as ancillary ligands for caging groups. Here we have shown that tertiary nitrogen-based tetra- and pentadentate ligands can also be used for caging nitrile groups.^{221,309} The ligands were developed for tuning the MLCT bands more towards the PDT region to decrease the damage caused to tissues by light. Also these tertiary amine-based ligands are known to be useful for attaching metal complexes to drug delivery vectors, which could provide an additional advantage to the caging strategy.^{209,210} We initially synthesized and studied TPA ligand-based acetonitrile-Ru complex and inhibitor-Ru complex. Both complexes showed ligand exchange with UV light irradiation where only one potential nitrile based ligand was released on photolysis.²²¹

Usually metal complexes are synthesized and screened one molecule at a time. This method is not practical if inorganic molecules are to compete with their organic counterparts as therapeutic agents and biochemical tools, which are usually synthesized and screened in a library fashion.^{215,218,231} Towards this end, a new platform for discovering metal-based caging groups was developed. We have shown that solid phase synthesis can be used for synthesis and screening of ligands and their corresponding metal complexes for the caging applications.³⁰⁹ Ten different ligands and their acetonitrile-ruthenium complexes were synthesized and their photochemistry was studied. Synthesizing and studying the complexes in solution phase verified the results from solid phase. The wide range of photochemical

reactivity of the synthesized complexes illustrated the need for prescreening compounds using the library approach, as solution phase synthesis is tedious. Several complexes showed no photochemical nitrile release, despite having their MLCT bands in the visible region, indicating that achieving ligand exchange is much more complex than irradiating into a MLCT band.

This solid phase synthesis approach can be used to screen for caging other functional groups such as pyridines, imidazoles and thioethers using the same library instead of making them through solution phase. The library can also be extended to study other ligands and metal complexes. Toxicity of ruthenium-based metal complexes depends on both the structure of the ligand and the structure of the inhibitor. Only photochemical studies were performed on the complexes made by solid phase during this dissertation period. Toxicity of complexes should also be studied on metal complexes synthesized from the library approach.

Photocaging provides spatial control over small molecules but current photocages cannot affect the distribution of the caged molecules to the target site. Drug delivery vectors can be used for achieving control over distribution.²⁰⁹ Ligands with attached delivery vectors should be used to synthesize and study metal-based caged complexes. This property would be useful if photocages are to be developed as drugs and prodrugs for tumors and other pathological conditions, as the overall dose of the inhibitor can be decreased using controlled delivery.

Metal complexes based on TPA and TQA have shown the release of only one nitrile group out of the two potential bound nitriles. The released nitriles were assigned *cis* to the basic nitrogen. The non-labile *trans* nitriles can be replaced by strong sigma-donating groups, which could increase the quantum yields for exchange of *cis* nitriles. Also new complexes

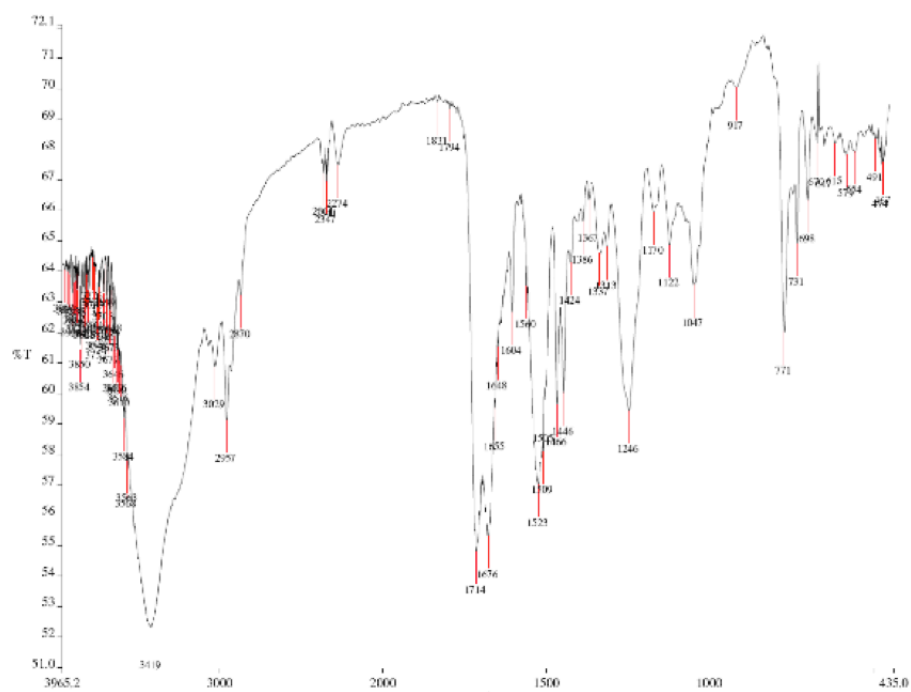
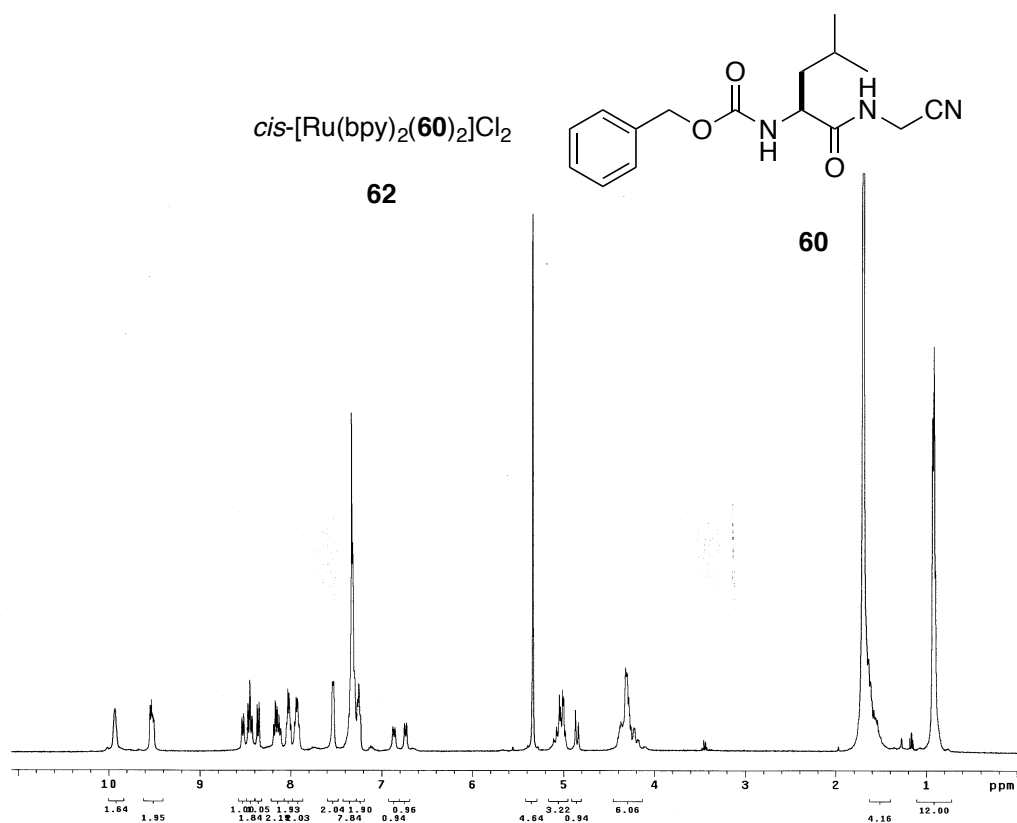
with more sterically crowded tetra- and penta-dentate ligands should be used, as steric bulk on ligands can accelerate ligand dissociation.

Energy transfer FRET chemistry can be utilized for inducing ligand dissociation using less energetic light. In FRET chemistry, a donor chromophore absorbs light and transfers its energy through nonradiative coupling to the acceptor chromophore. While FRET chemistry is used in numerous other energy transfer reactions, it has not been applied for caged cathepsin inhibitor complexes. Ruthenium complexes with attached organic chromophores such as Resorufin, Ampliflu Red and Resazurin can be developed which can absorb less energetic light and transfer it to the metal center to induce ligand exchange.

8.1.3 Developing new ruthenium complexes as photosensitizers:

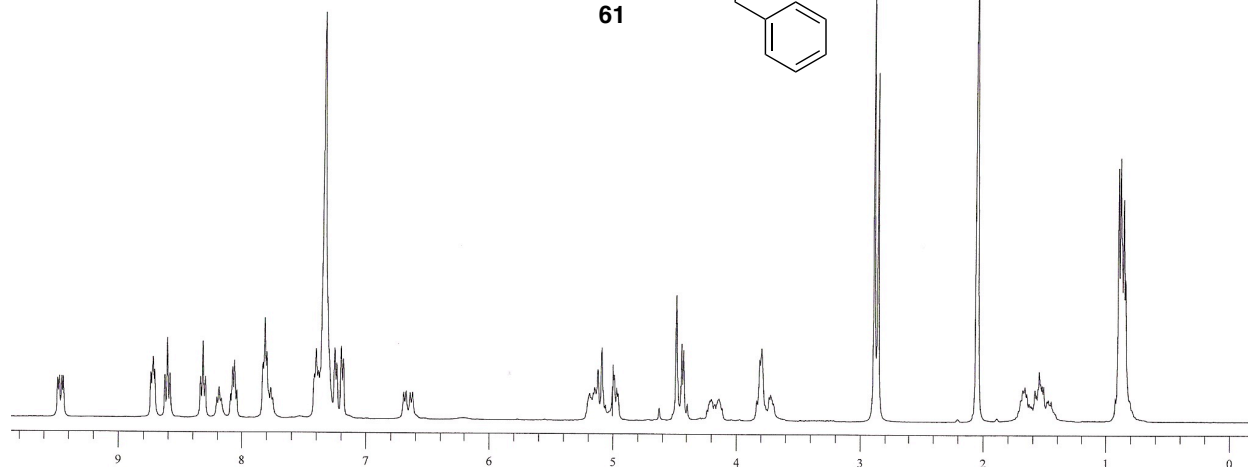
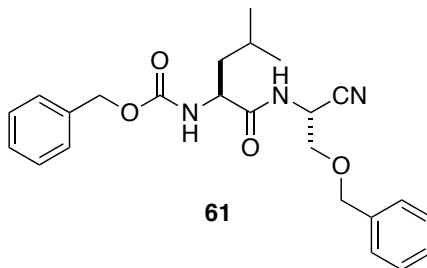
In the final part of this dissertation ruthenium complexes were developed as triplet sensitizers, which could be used in solar cell applications. We developed ruthenium complexes based on the TQA ligand with exceptionally long triplet-excited lifetimes at 77K, which can be used for energy transfer reactions. Three complexes with general formula $[\text{Ru}(\text{TQA})(\text{X})_2]^n$ were synthesized and studied where X was an ancillary ligand (X = MeCN or CN or SCN). Experimental and DFT calculation results suggest that achieving long lived MLCT excited states depends on the optimization of some excited state electronic properties of the complexes and not just finding complexes for which the $^3\text{MLCT}$ excited state is lower in energy than any ^3MC excited state. Though we achieved exciting results, these were far from practical applicability as they were performed at 77K. Other isomers of TQA ligand can be used for tuning the excited state properties. Metals like iridium should also be used as numerous Ir complexes have relatively longer excited-state lifetimes compared to their Ru counterparts. Also strong donating ancillary ligand groups could increase the excited state-lifetimes.

APPENDIX

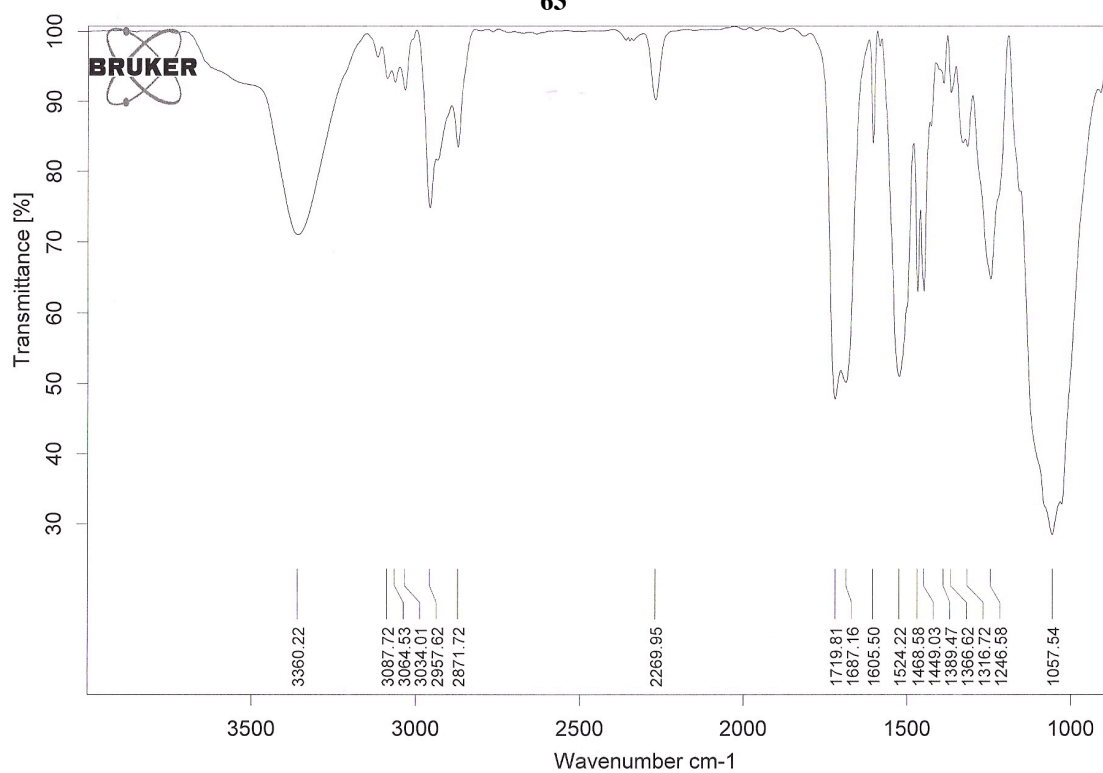


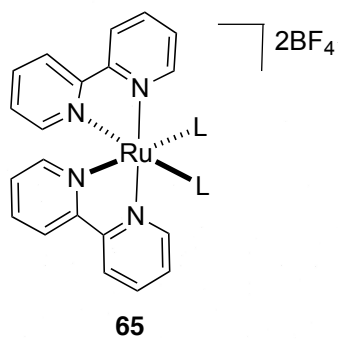
cis-[Ru(bpy)₂(**61**)₂](BF₄)₂

63

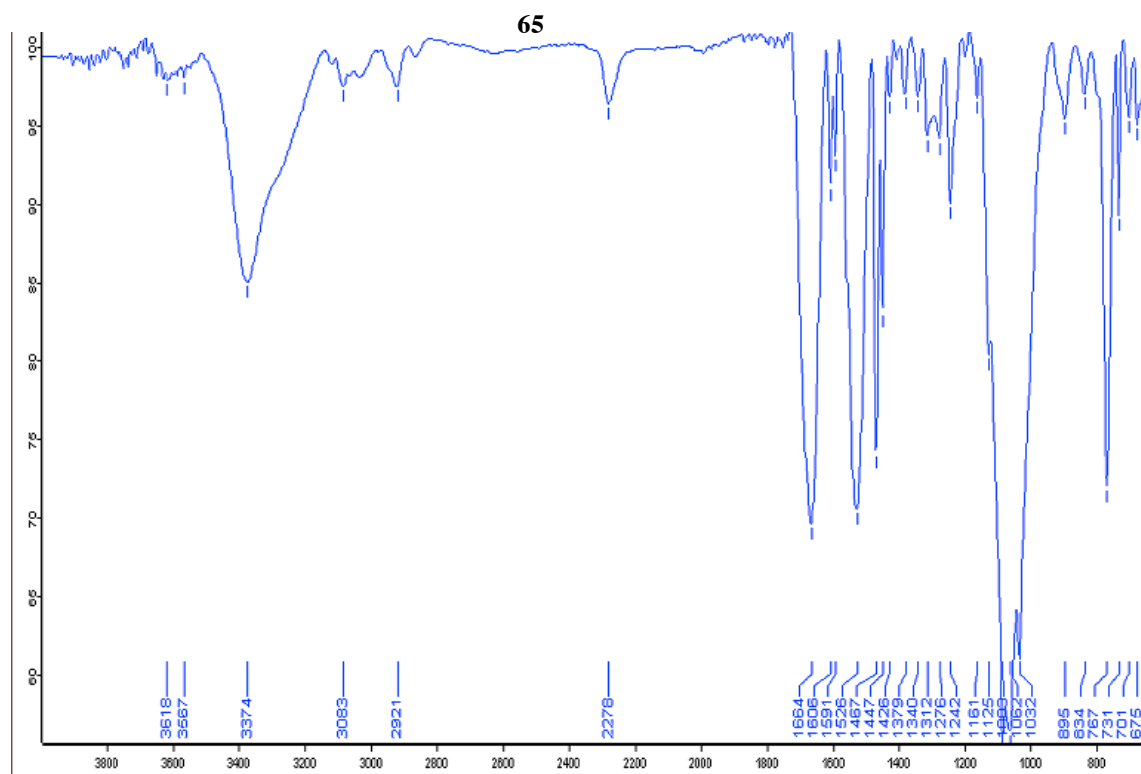
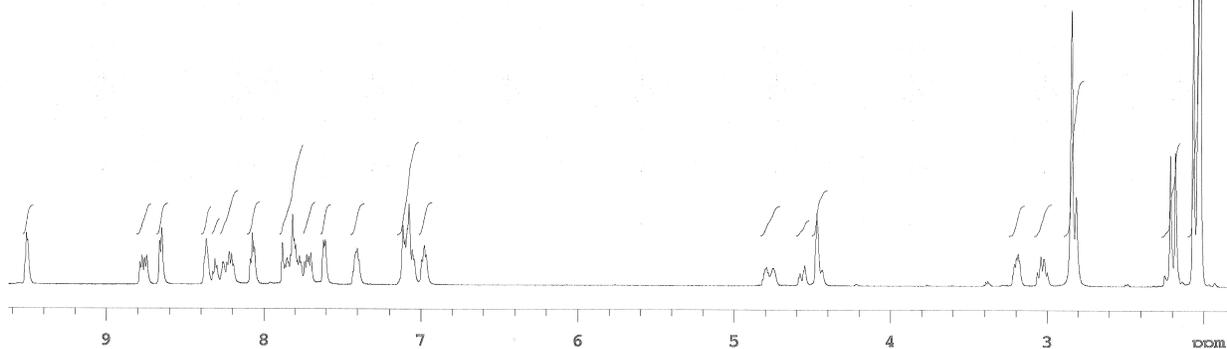
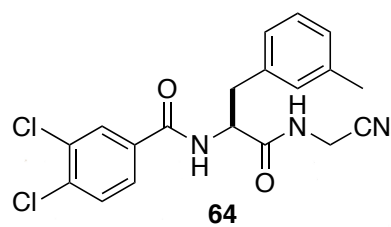


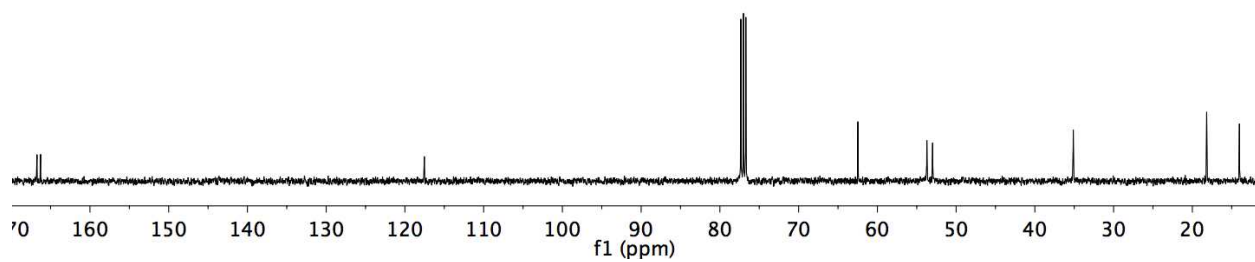
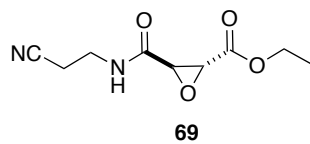
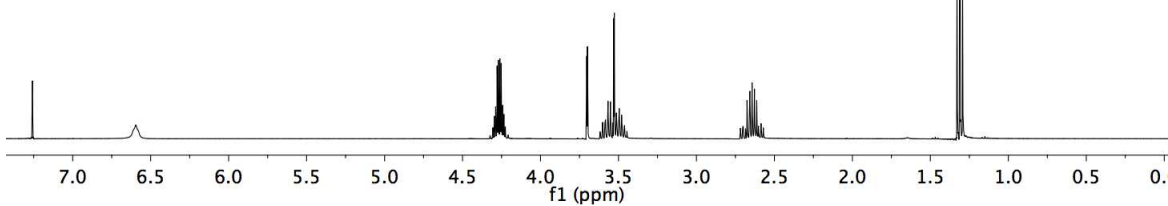
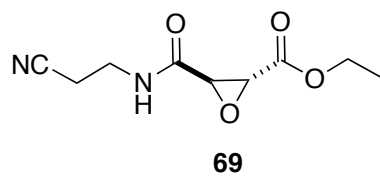
63

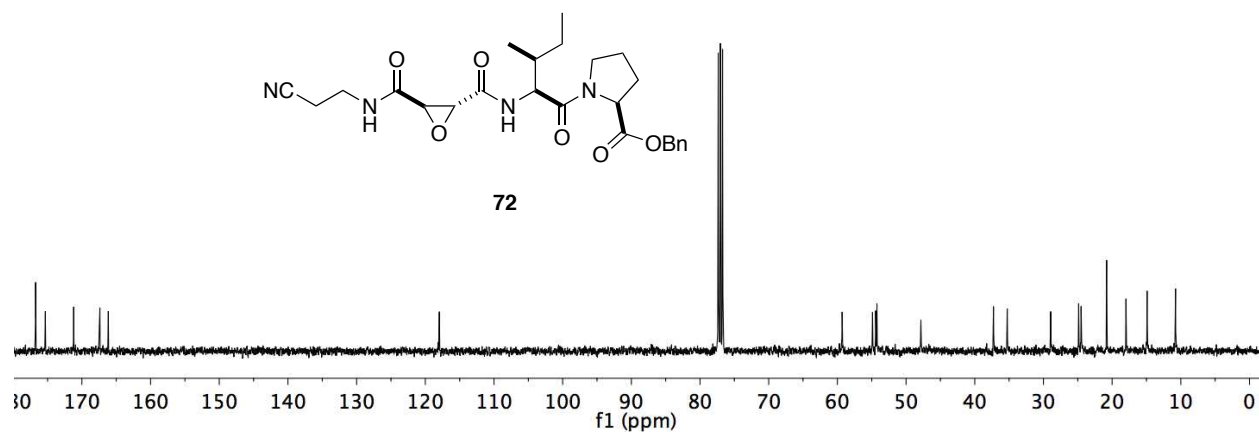
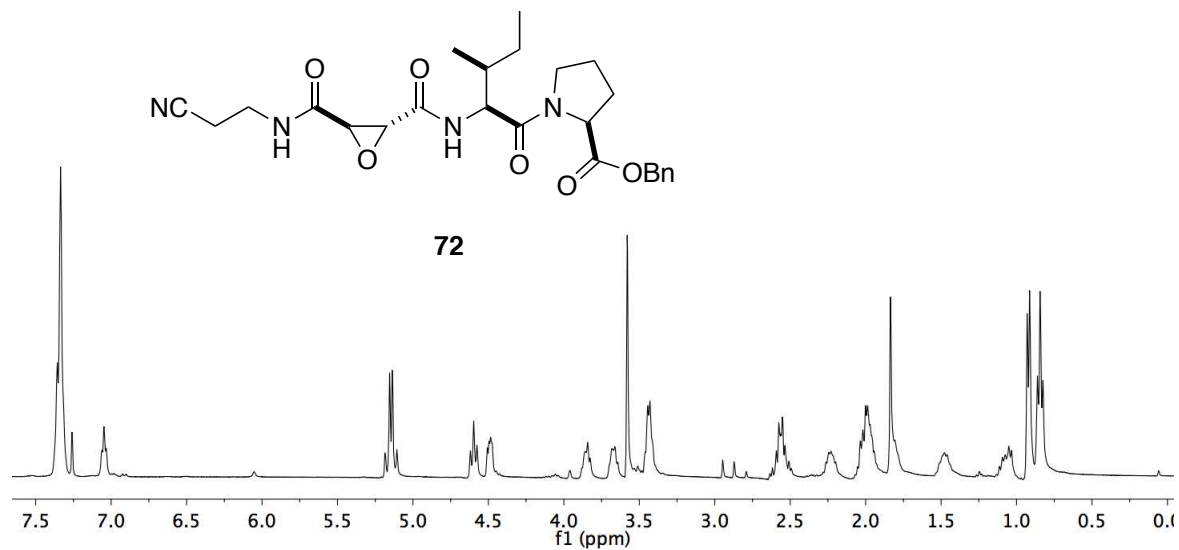


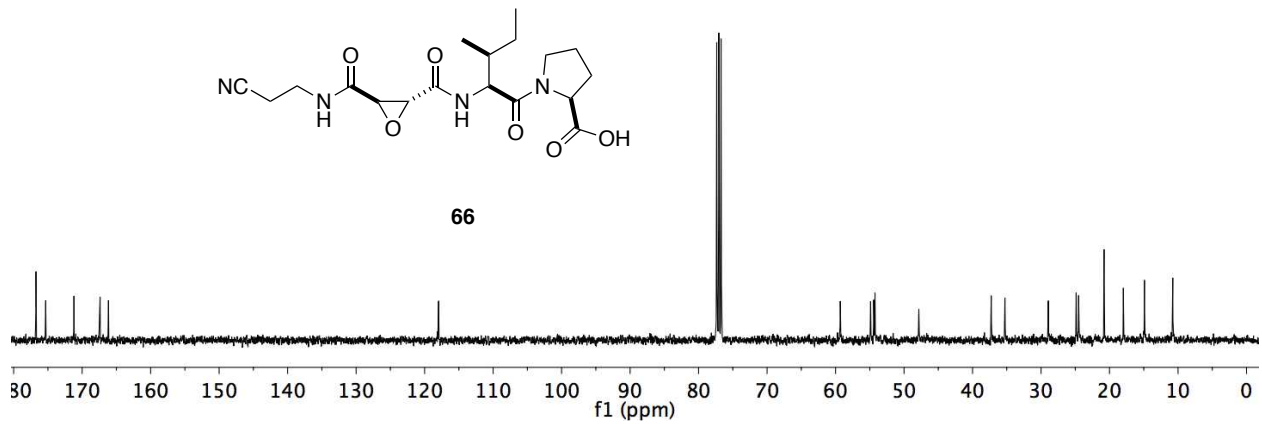
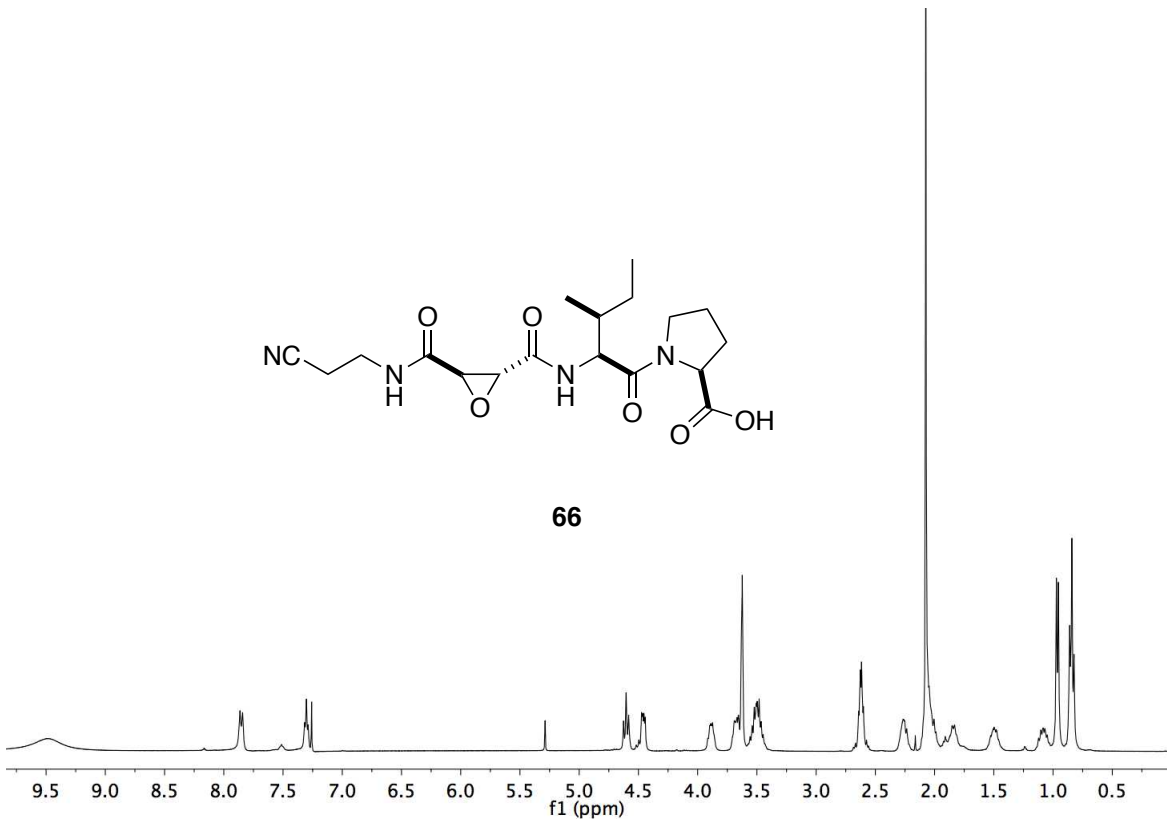


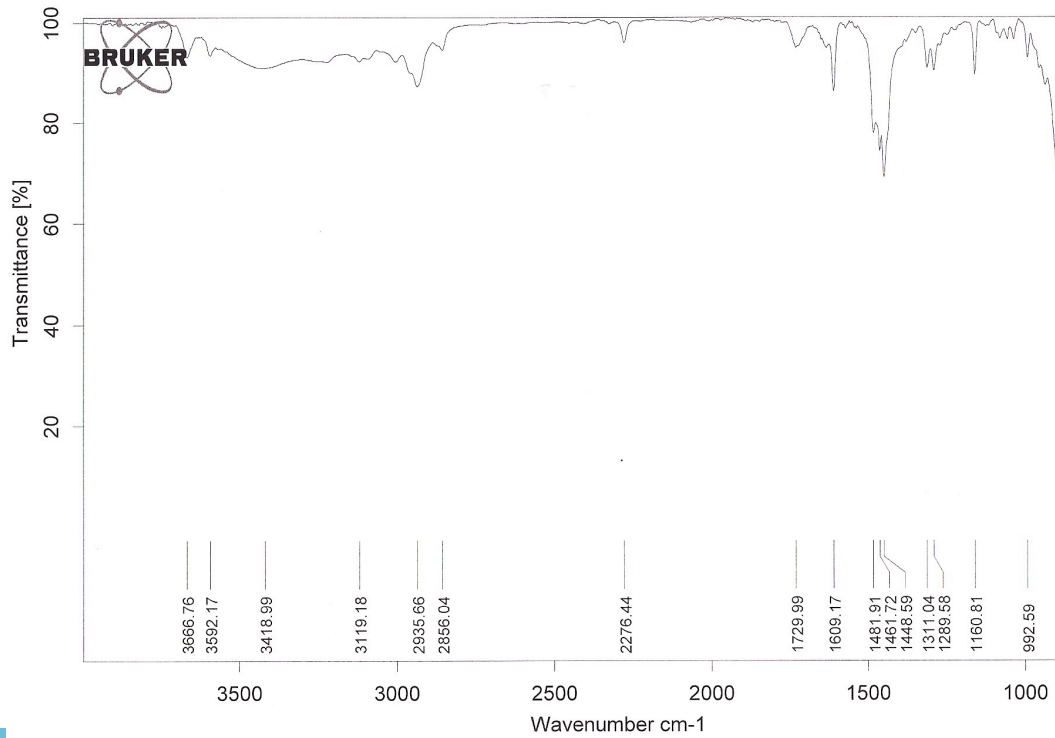
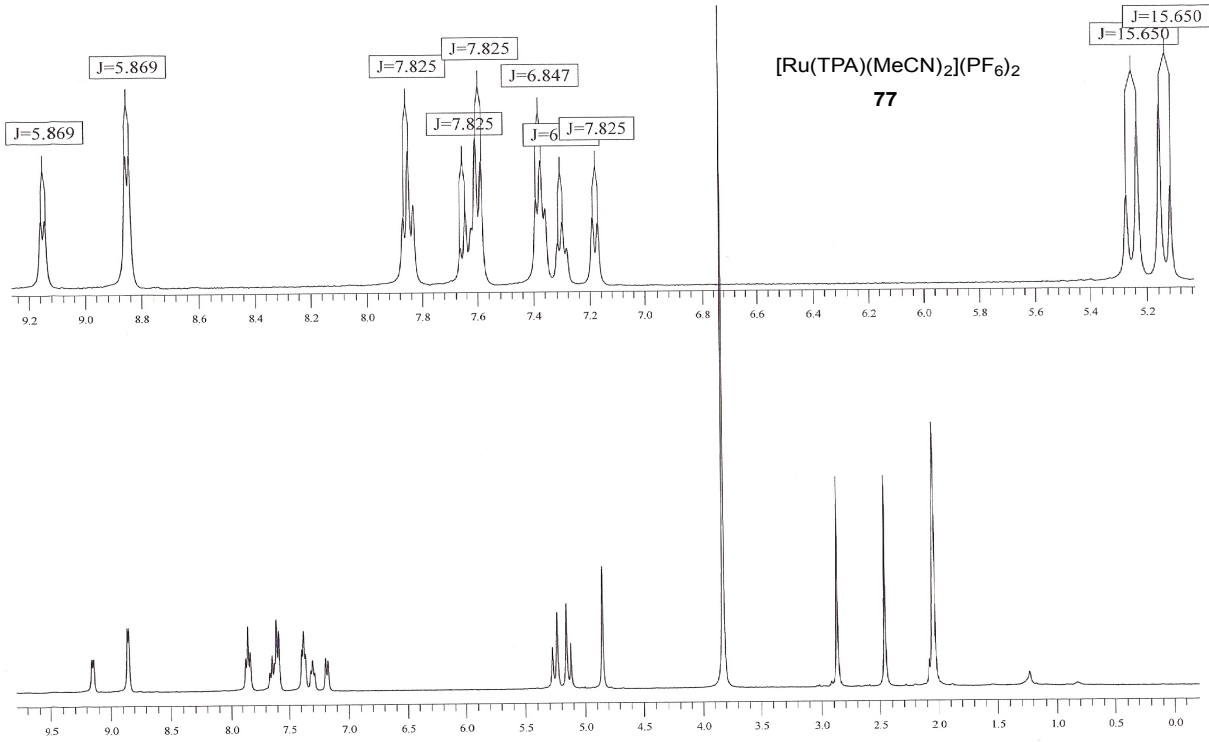
L =

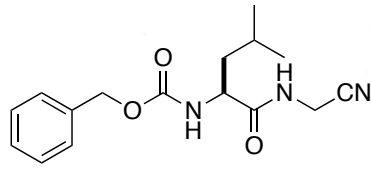
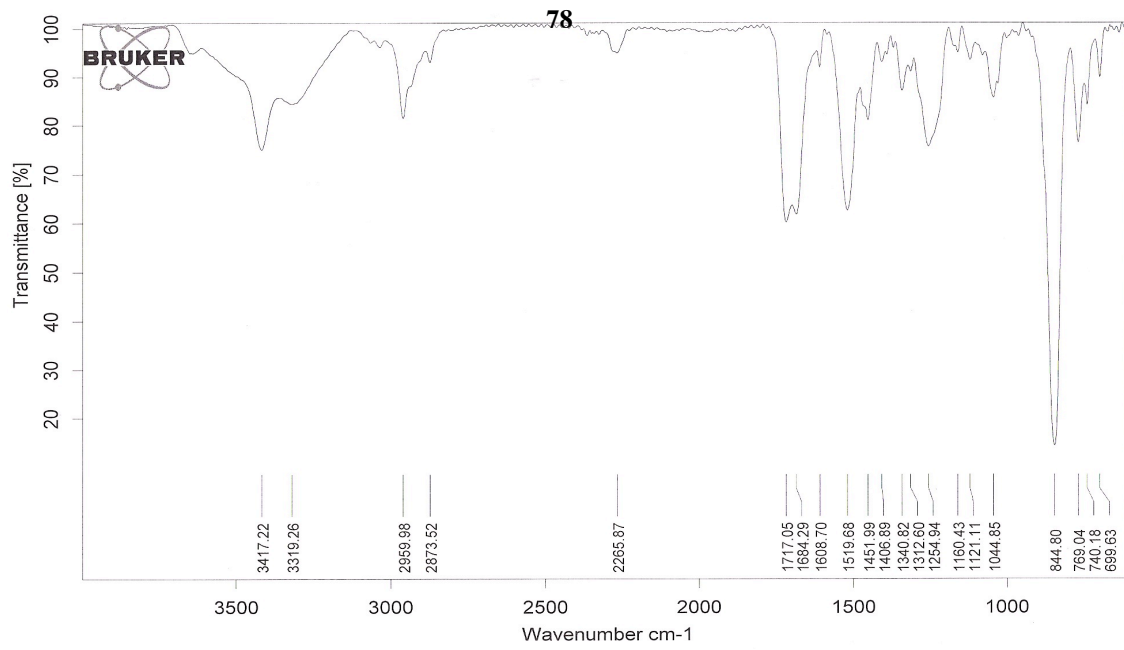
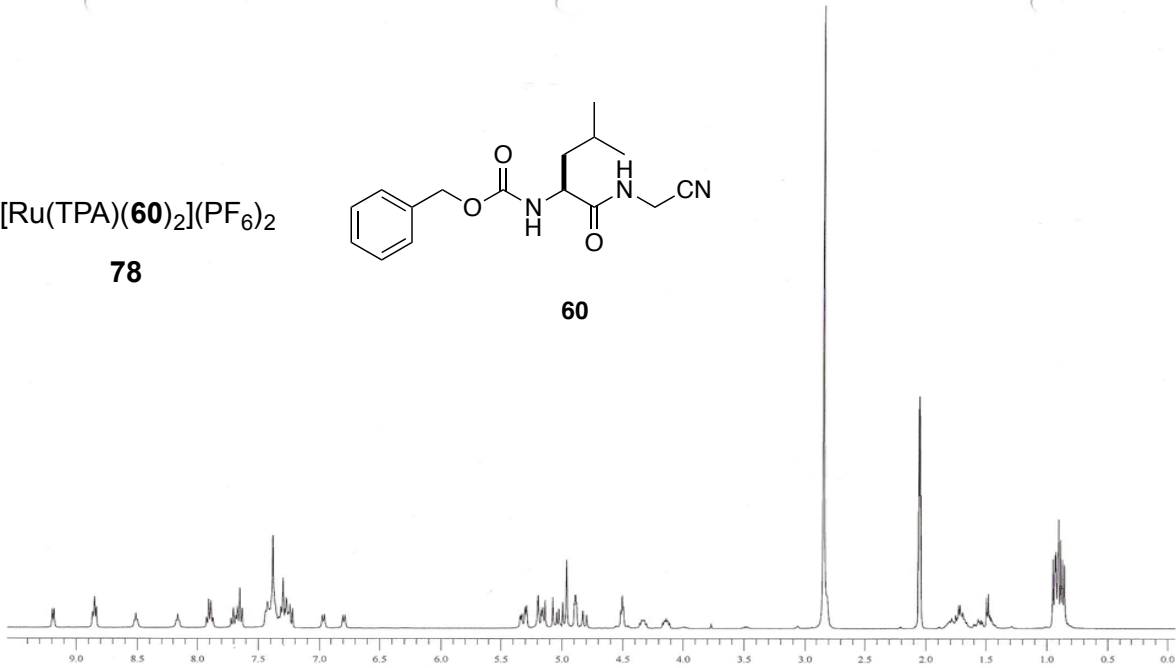


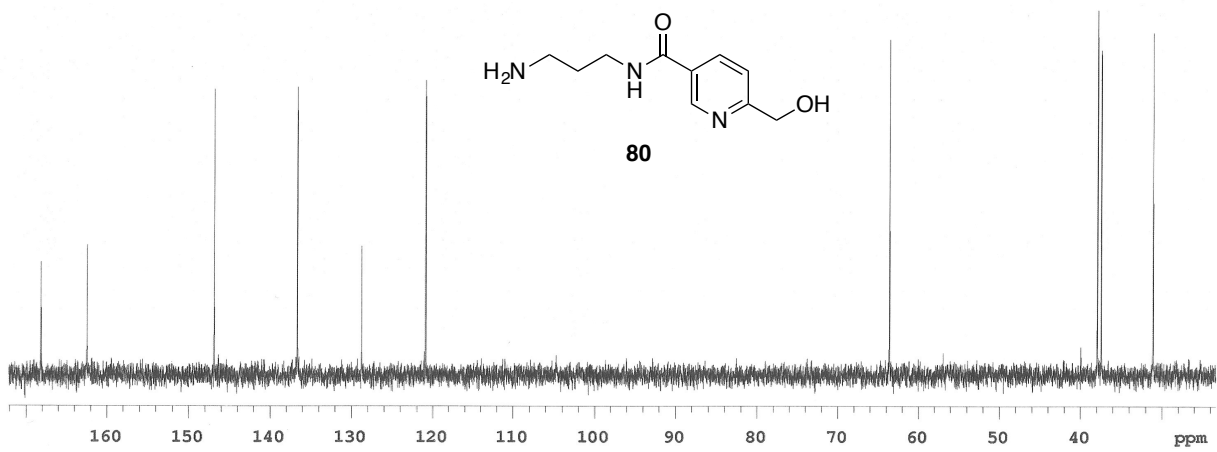
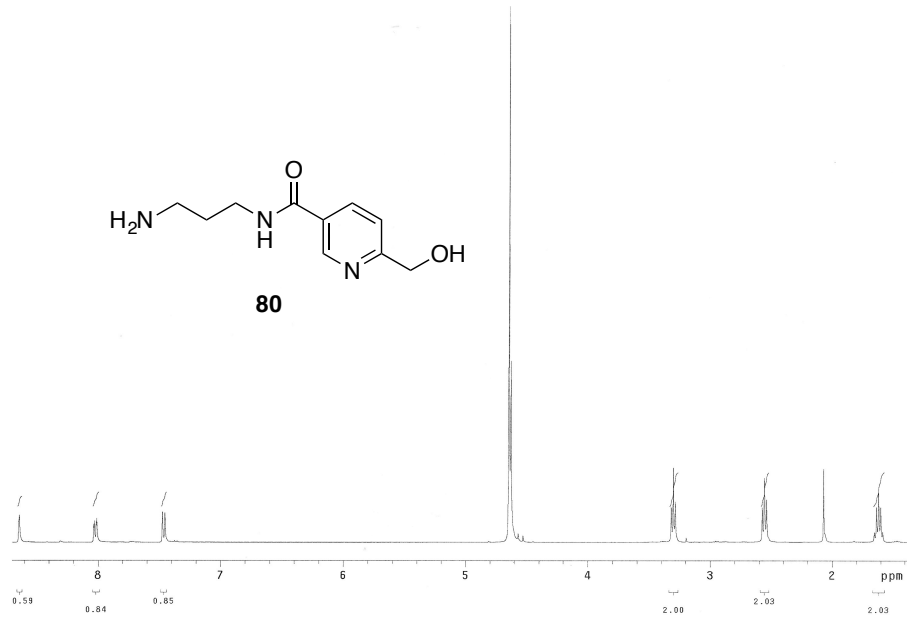


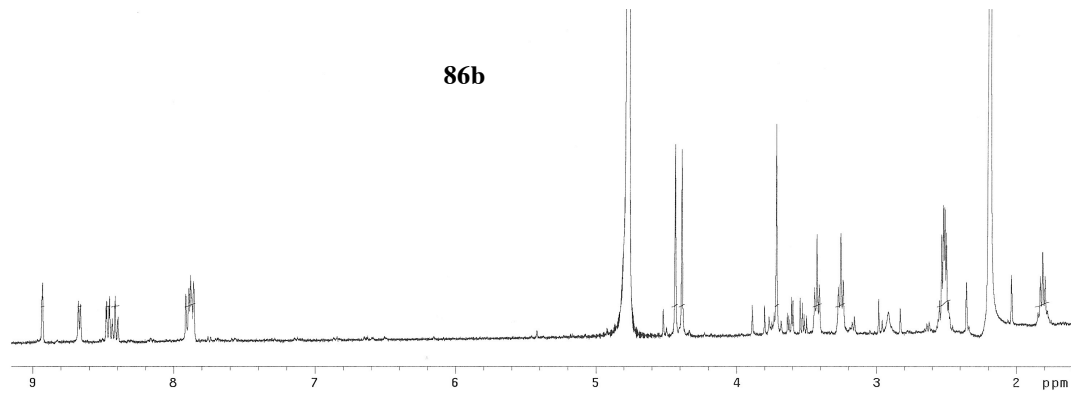
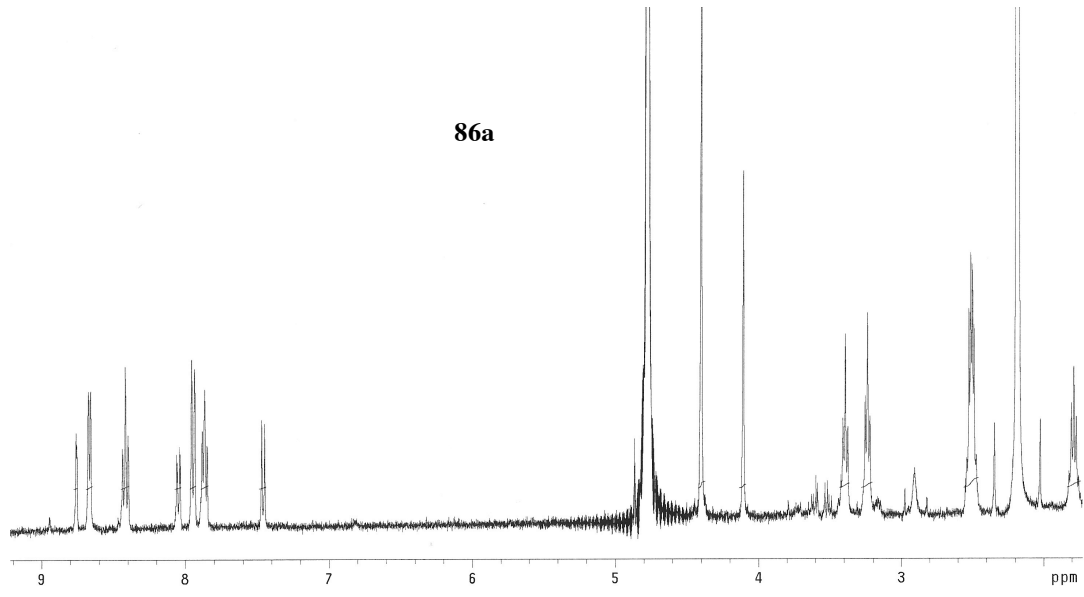


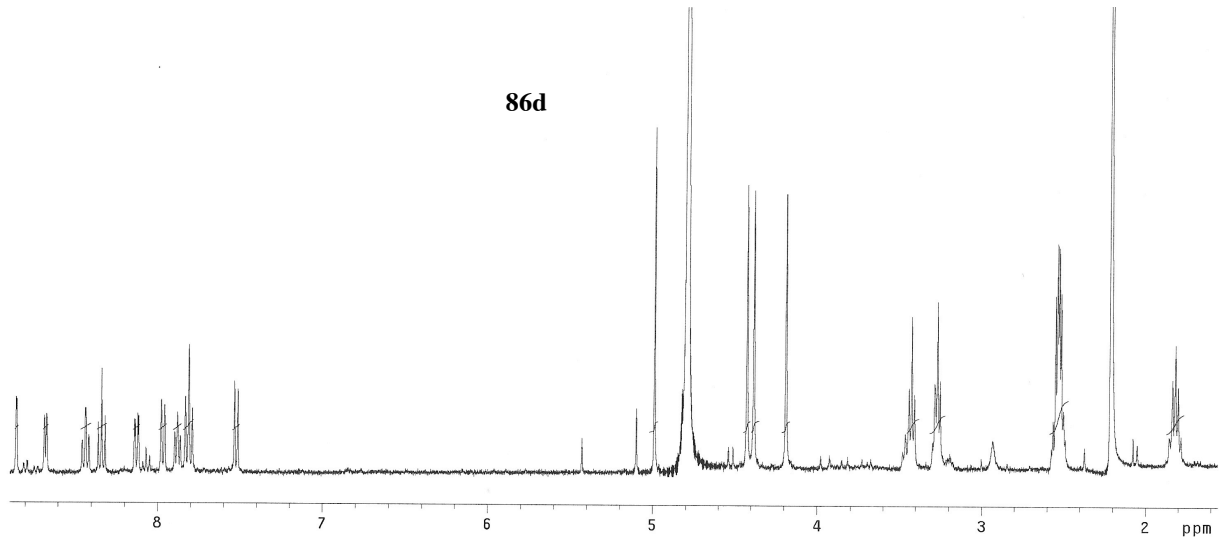
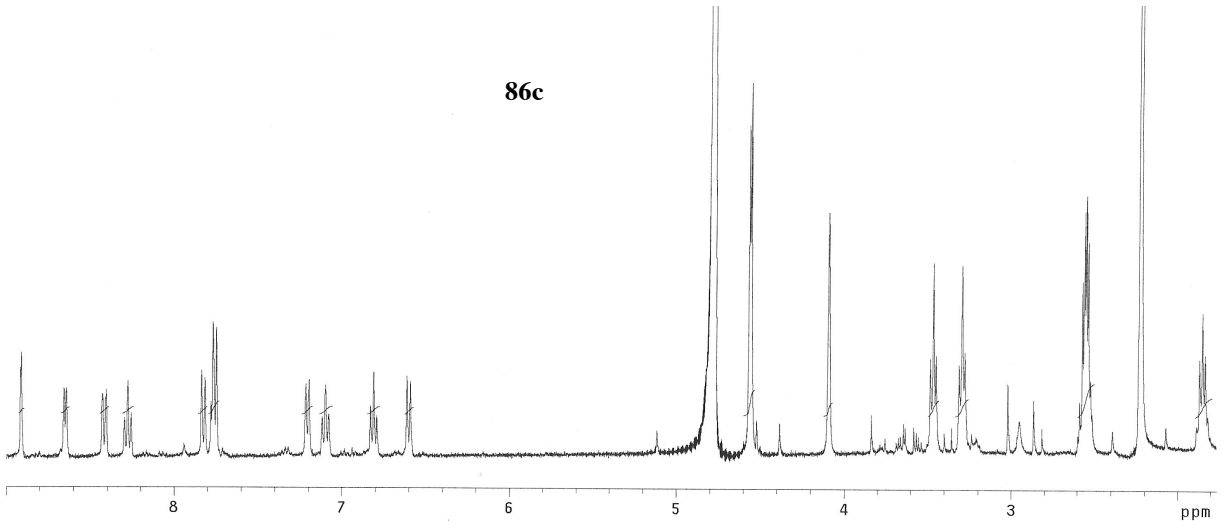


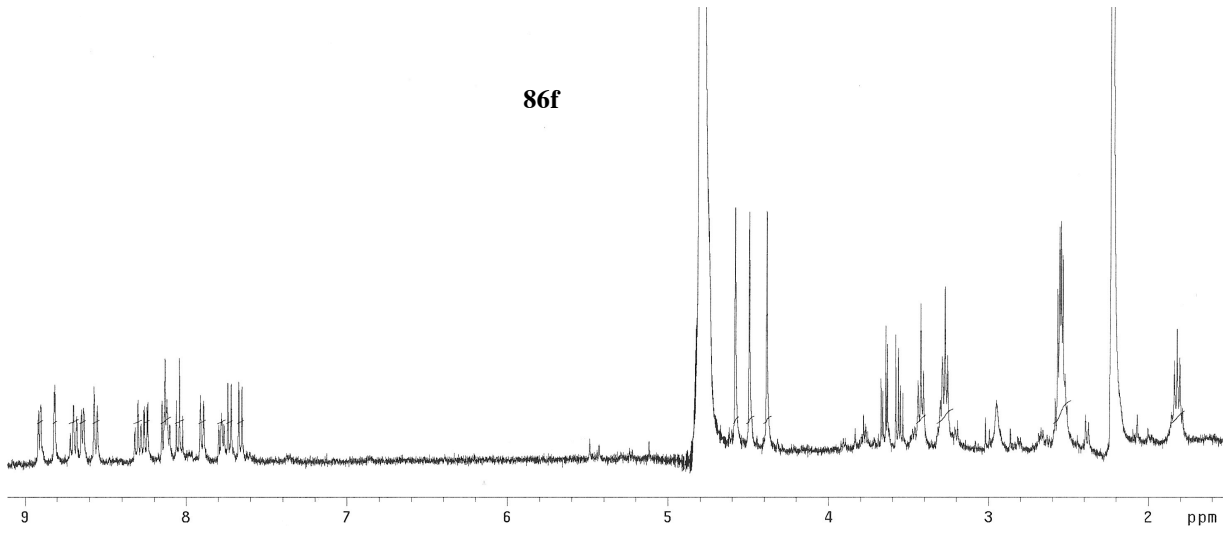
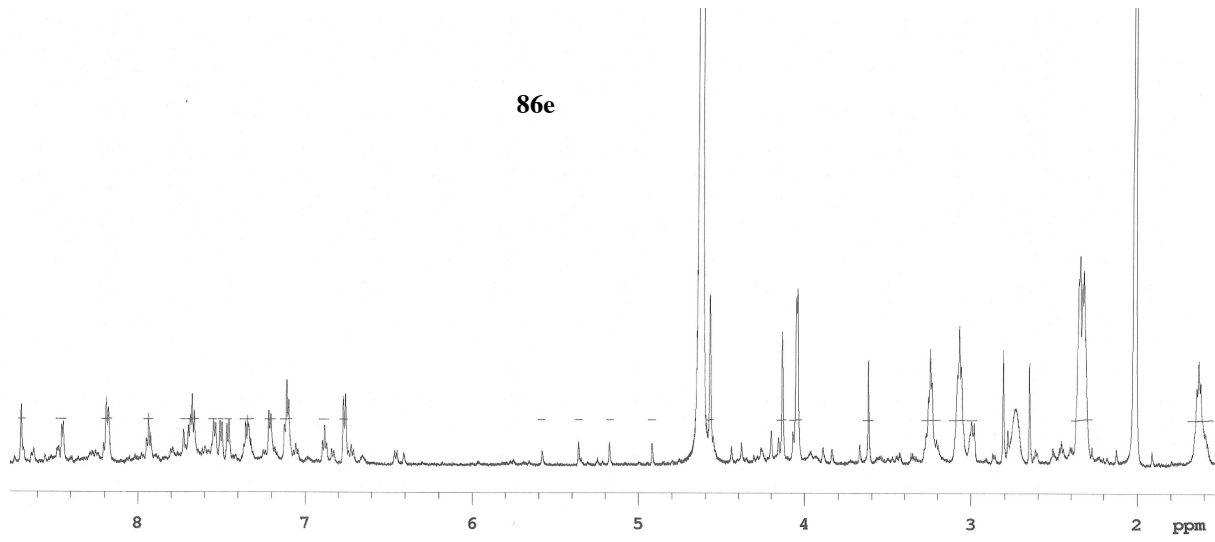


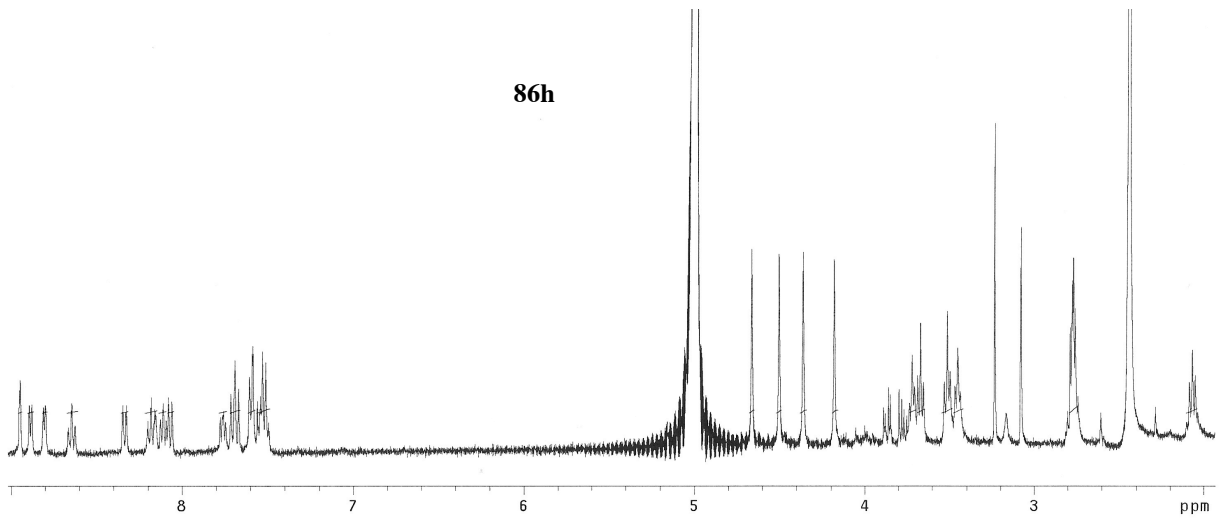
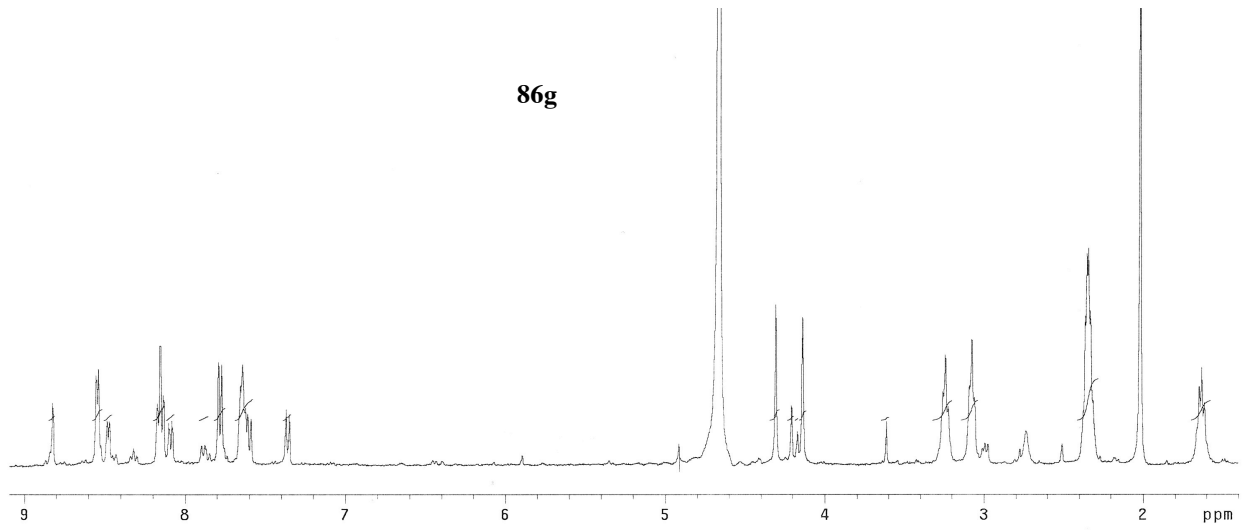
**78****60**

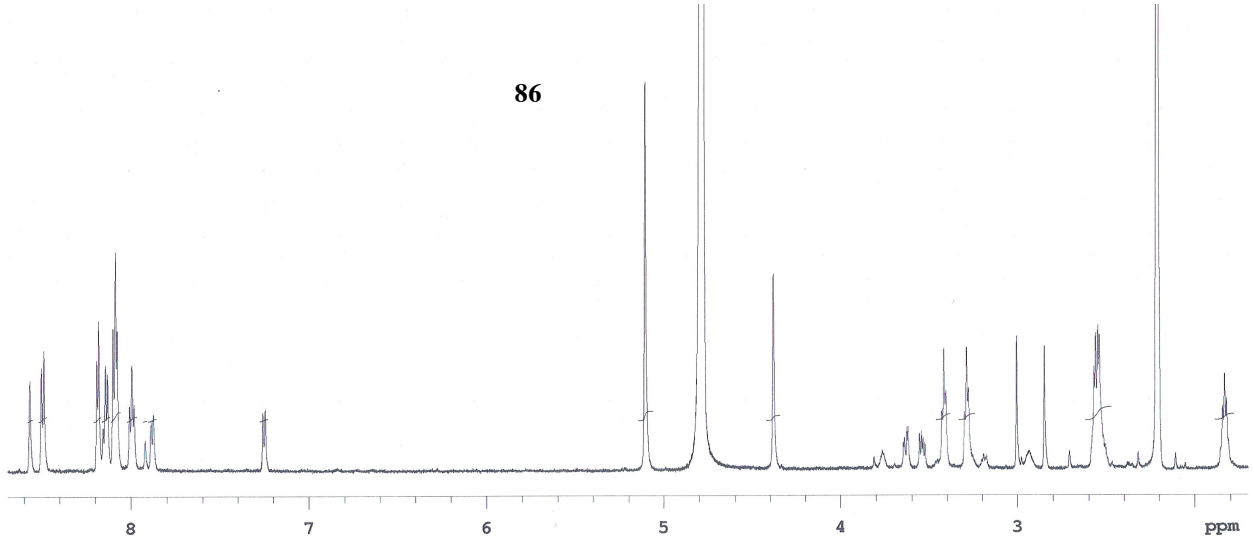
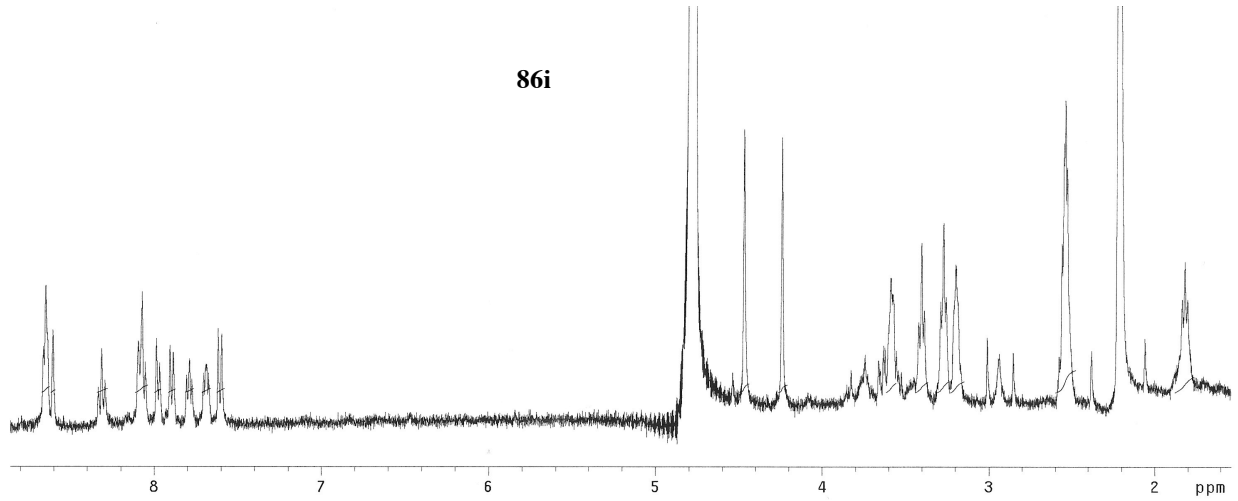


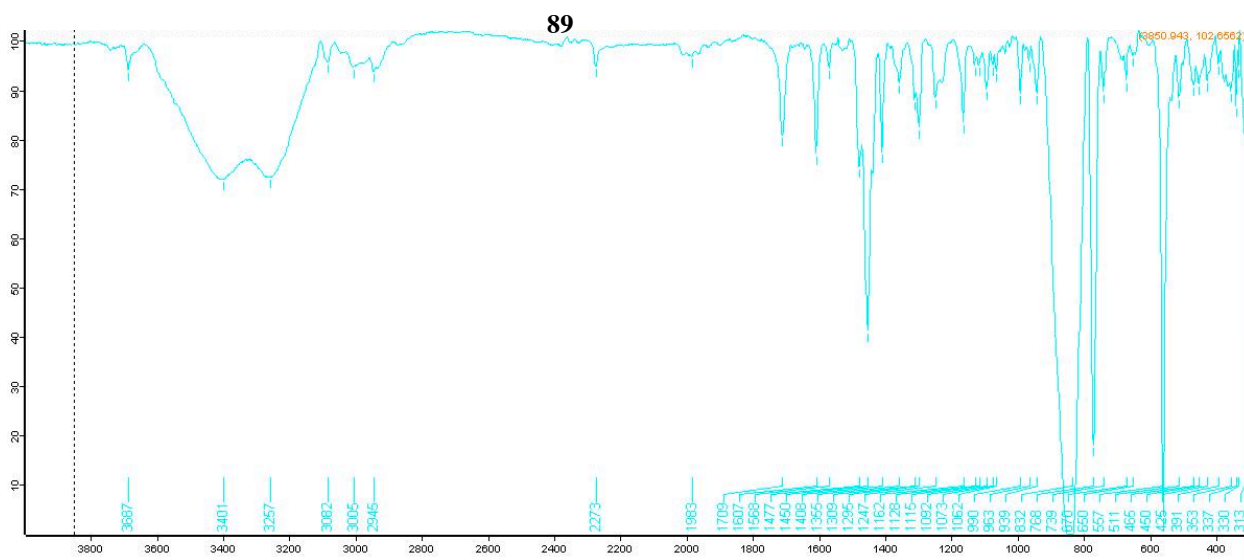
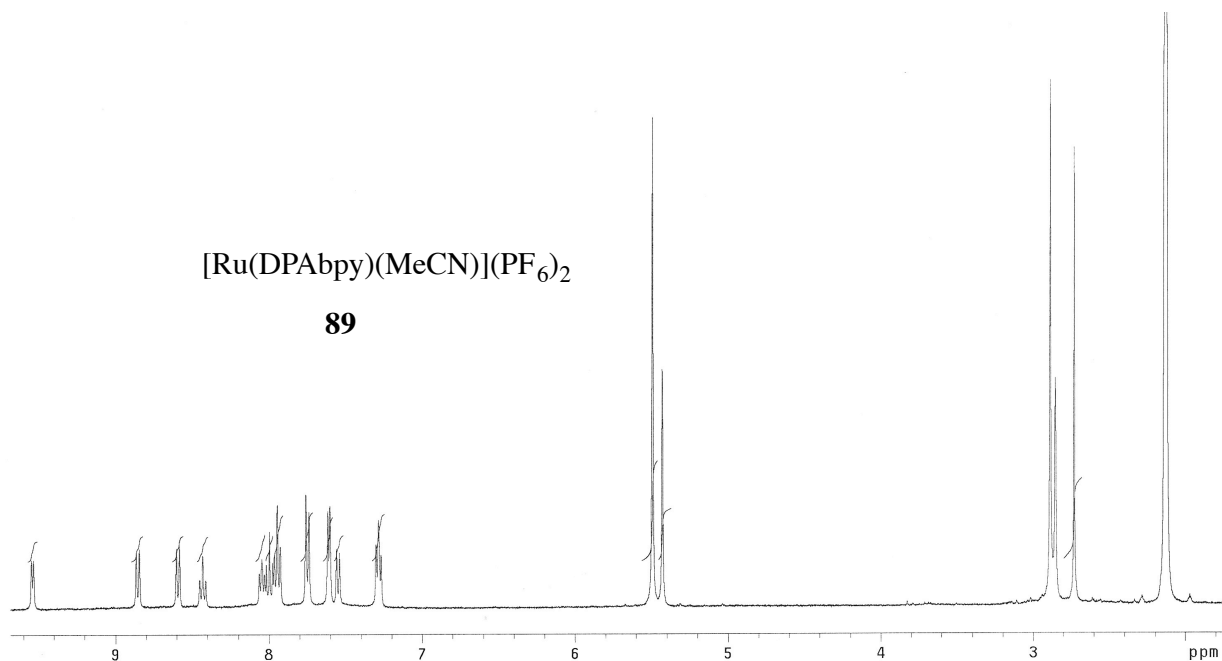


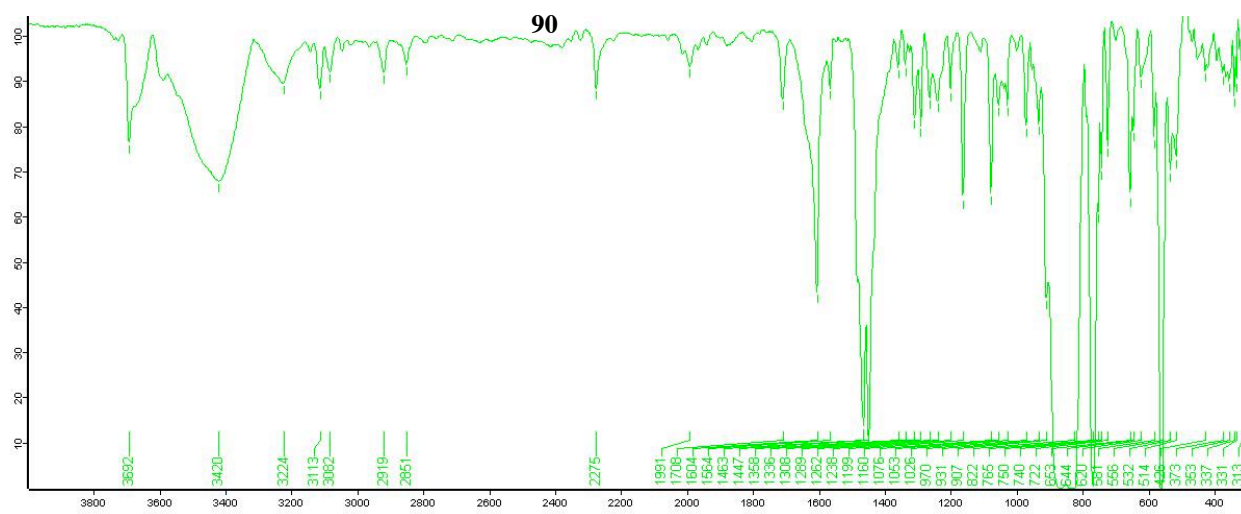
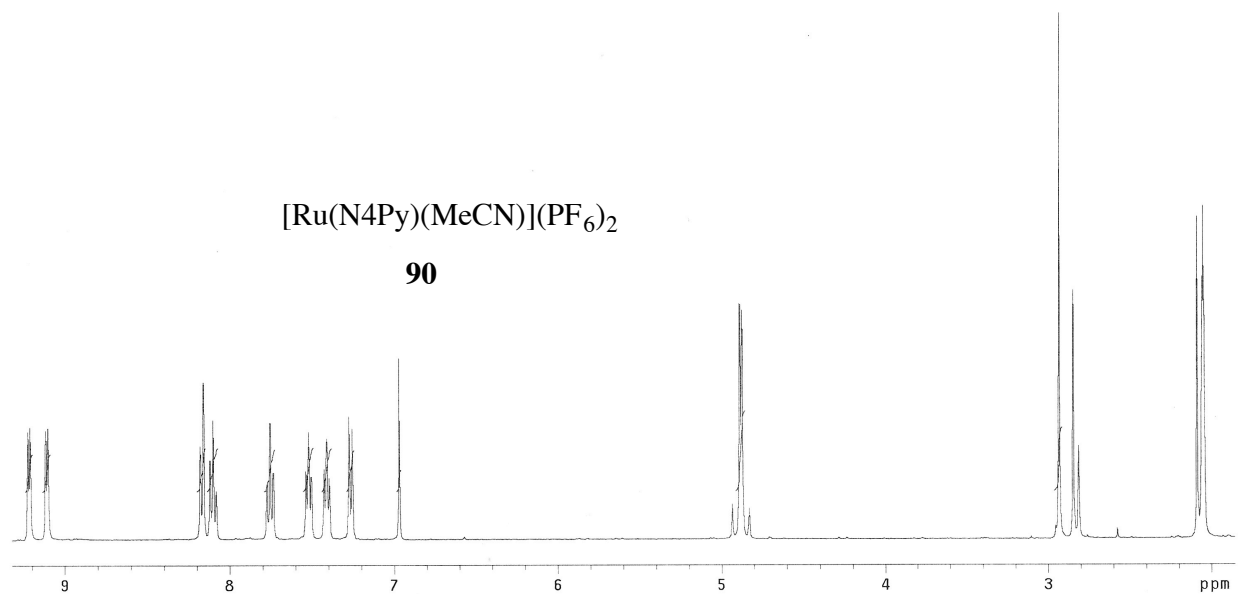


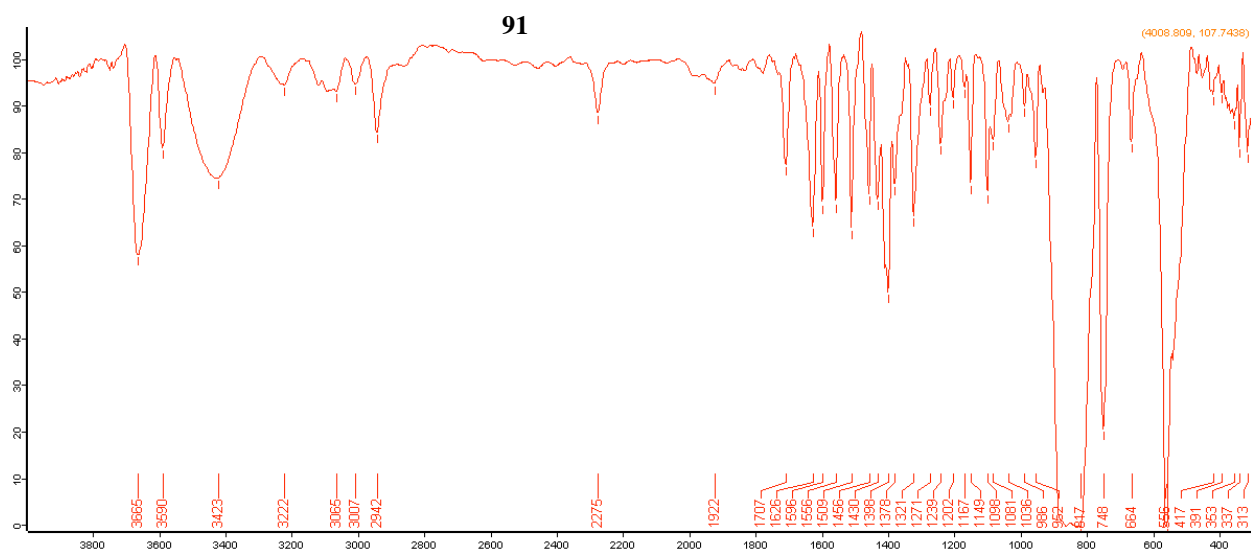
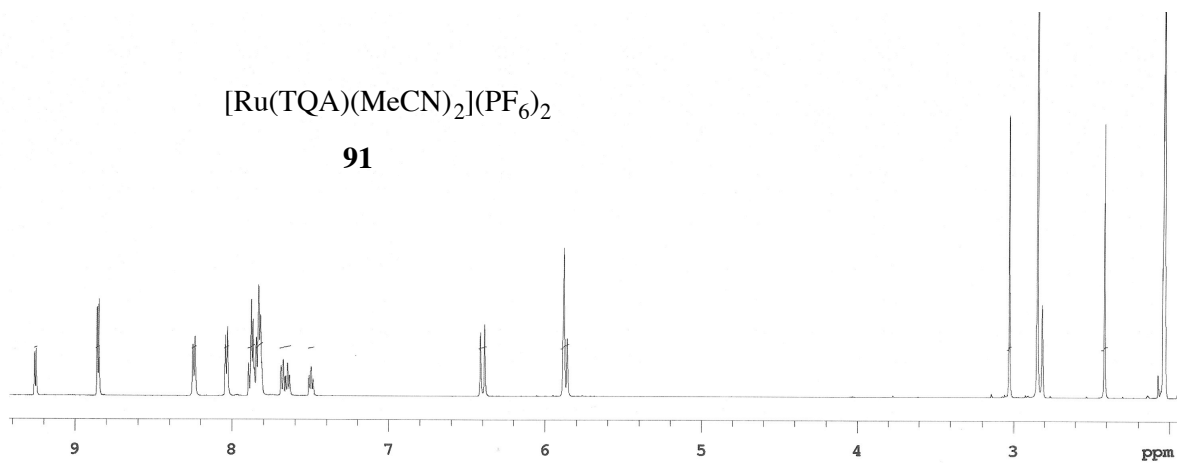


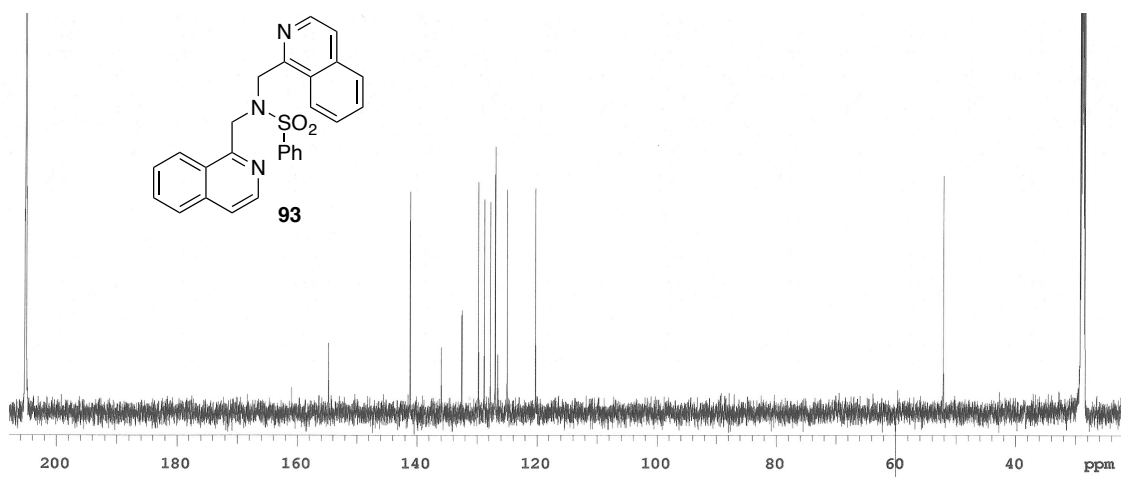
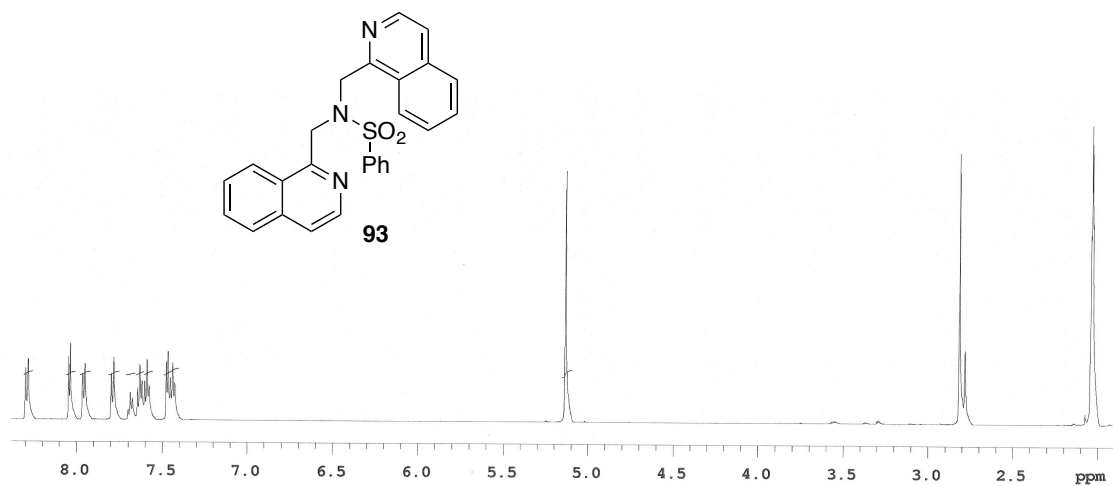




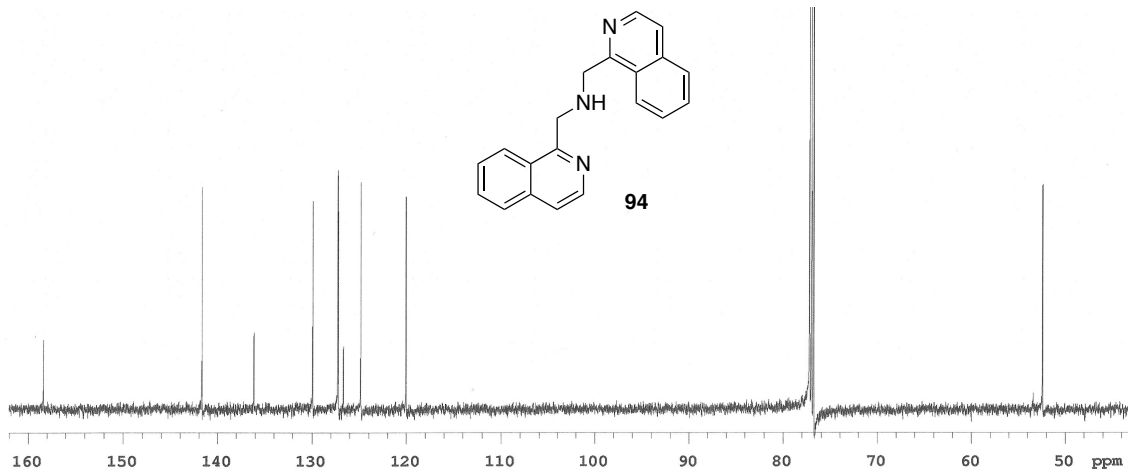
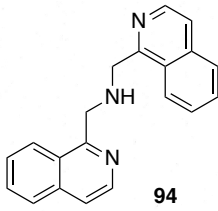
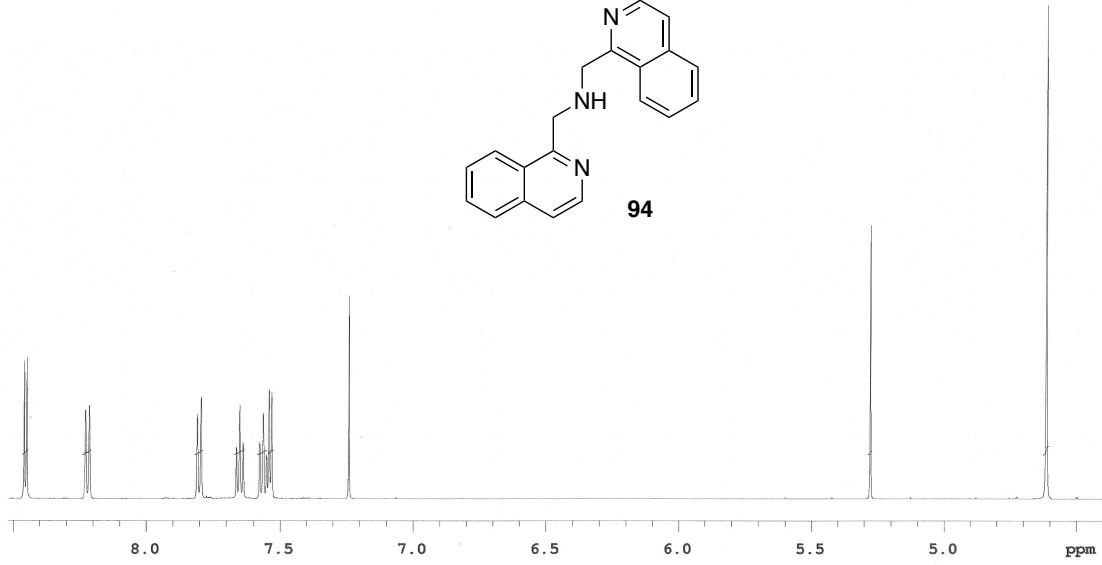
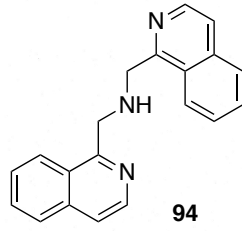


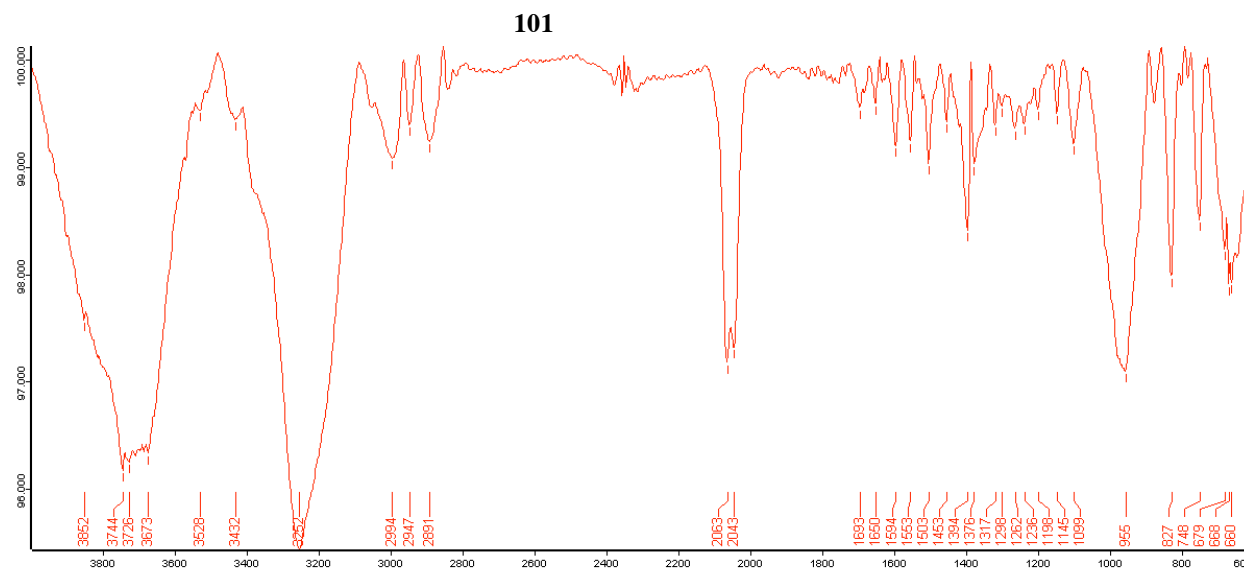
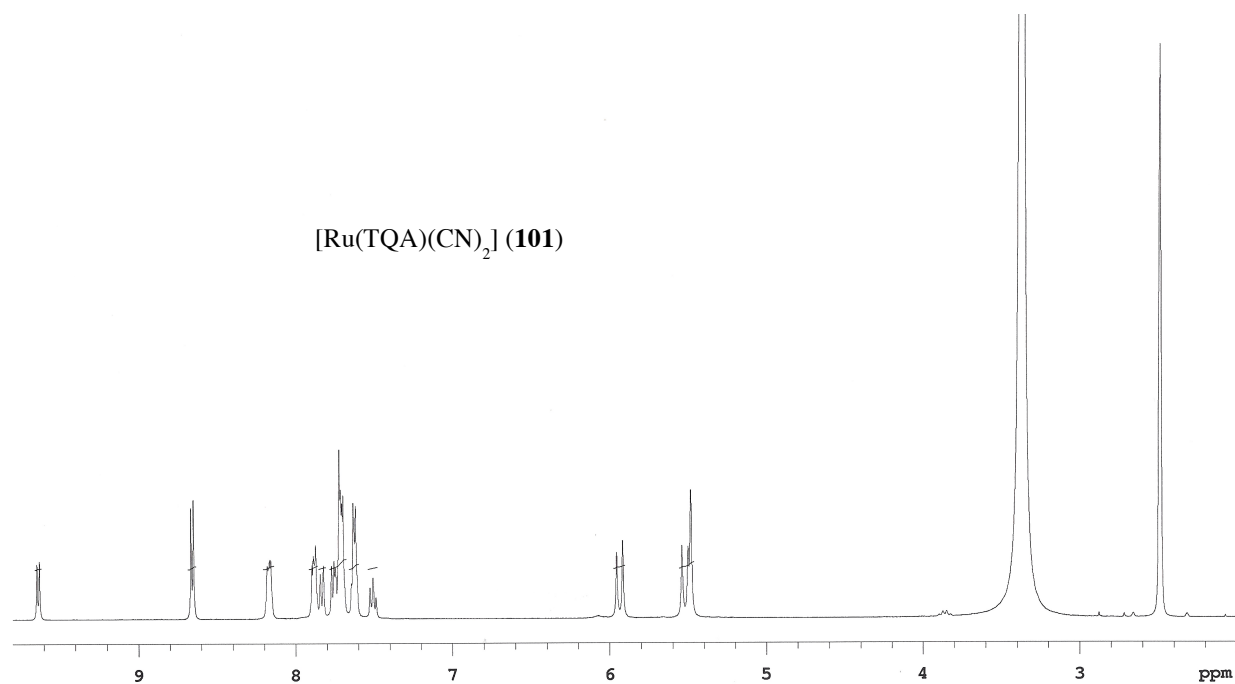


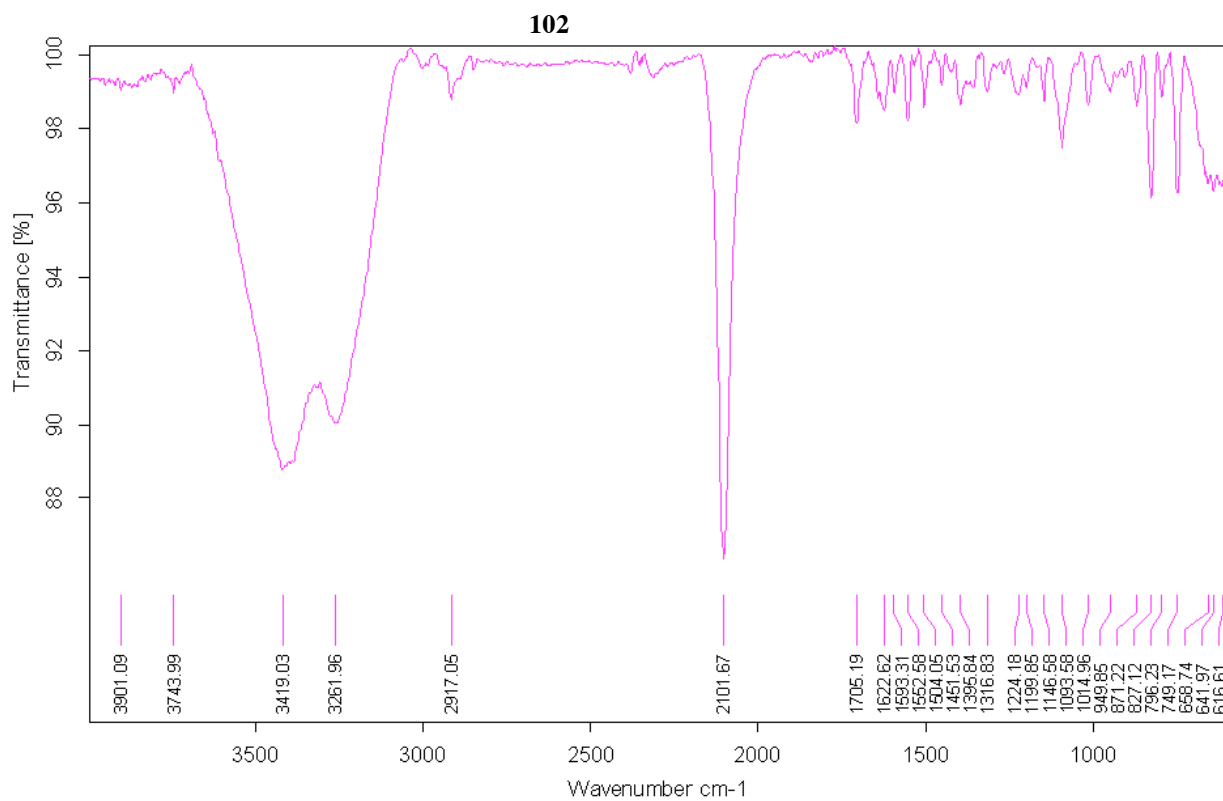
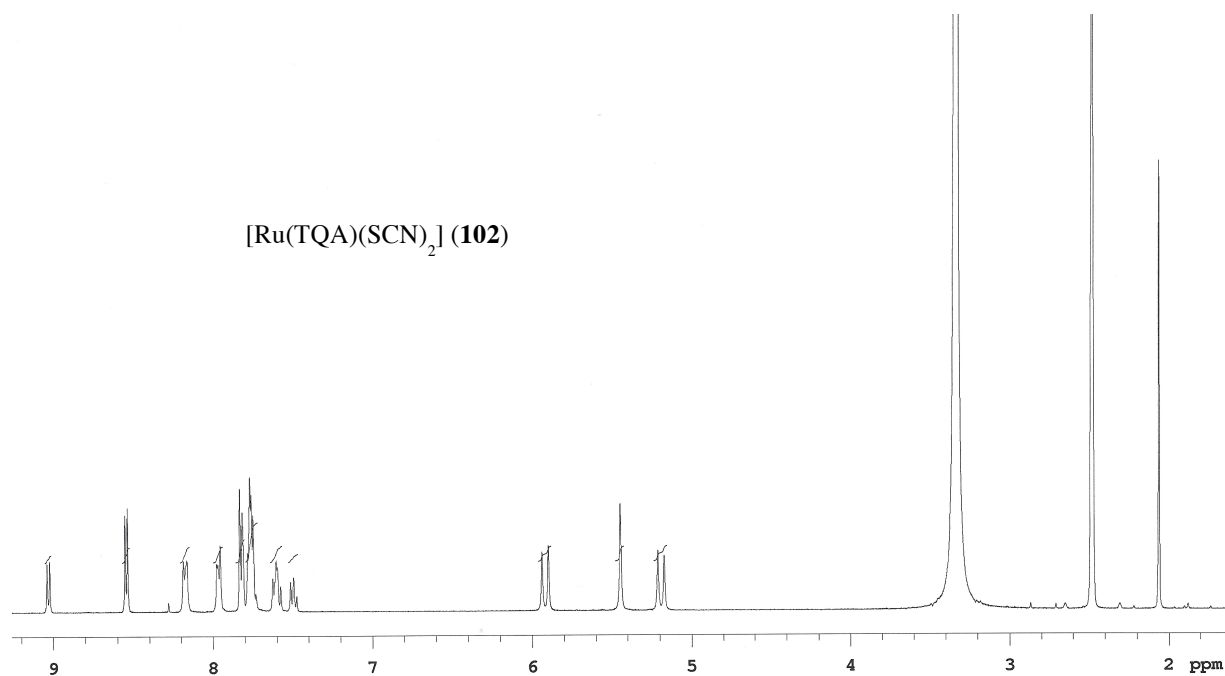
**91**



234







**JOHN WILEY AND SONS LICENSE
TERMS AND CONDITIONS**

Aug 17, 2015

This Agreement between rajgopal sharma ("You") and John Wiley and Sons ("John Wiley and Sons") consists of your license details and the terms and conditions provided by John Wiley and Sons and Copyright Clearance Center.

License Number	3691220188092
License date	Aug 17, 2015
Licensed Content Publisher	John Wiley and Sons
Licensed Content Publication	ChemMedChem
Licensed Content Title	Inhibition of Cathepsin Activity in a Cell-Based Assay by a Light-Activated Ruthenium Compound
Licensed Content Author	Tomasz Respondek,Rajgopal Sharma,Mackenzie K. Herroon,Robert N. Garner,Jessica D. Knoll,Eric Cueny,Claudia Turro,Izabela Podgorski,Jeremy J. Kodanko
Licensed Content Date	Apr 11, 2014
Pages	10
Type of use	Dissertation/Thesis
Requestor type	Author of this Wiley article
Format	Print and electronic
Portion	Full article
Will you be translating?	No
Title of your thesis / dissertation	• Synthesis and biological evaluation of nitrile-based cysteine proteases inhibitors caged with ruthenium complexes
Expected completion date	Aug 2015
Expected size (number of pages)	250
Requestor Location	rajgopal sharma 15117 e vernor highway apt 11 GROSSE POINTE, MI 48230 United States Attn: rajgopal sharma
Billing Type	Invoice
Billing Address	rajgopal sharma 15117 e vernor highway

<https://s100.copyright.com/App/PrintableLicenseFrame.jsp?publisherID...dc8aa-3ad4-468c-a4a1-bc01d68bc99c%20%20&targetPage=printablelicense>

Page 1 of 7



RightsLink®

Home

Create Account

Help



ACS Publications
Most Trusted. Most Cited. Most Read.

Title:

Solid-Phase Synthesis as a Platform for the Discovery of New Ruthenium Complexes for Efficient Release of Photocaged Ligands with Visible Light

Author:

Rajgopal Sharma, Jessica D. Knoll, Nicholas Ancona, et al

Publication: Inorganic Chemistry

Publisher: American Chemical Society

Date: Feb 1, 2015

Copyright © 2015, American Chemical Society

LOGIN

If you're a **copyright.com user**, you can login to RightsLink using your copyright.com credentials. Already a **RightsLink user** or want to [learn more?](#)

PERMISSION/LICENSE IS GRANTED FOR YOUR ORDER AT NO CHARGE

This type of permission/license, instead of the standard Terms & Conditions, is sent to you because no fee is being charged for your order. Please note the following:

- Permission is granted for your request in both print and electronic formats, and translations.
- If figures and/or tables were requested, they may be adapted or used in part.
- Please print this page for your records and send a copy of it to your publisher/graduate school.
- Appropriate credit for the requested material should be given as follows: "Reprinted (adapted) with permission from (COMPLETE REFERENCE CITATION). Copyright (YEAR) American Chemical Society." Insert appropriate information in place of the capitalized words.
- One-time permission is granted only for the use specified in your request. No additional uses are granted (such as derivative works or other editions). For any other uses, please submit a new request.

BACK

CLOSE WINDOW

Copyright © 2015 [Copyright Clearance Center, Inc.](#) All Rights Reserved. [Privacy statement](#). [Terms and Conditions](#). Comments? We would like to hear from you. E-mail us at customercare@copyright.com

REFERENCES

- (1) Davies, M. J. *Chem. Edu* **1954**, 31, 89.
- (2) Rouhi, A. M. *Chem. Eng. News Archive* **1998**, 76, 22.
- (3) Martin, B. In *Electromagnetic Fields*; ACS: 1995; Vol. 250, p 1.
- (4) Martin, B. *Electromagnetic Fields*; ACS, 1995; Vol. 250.
- (5) James, C. W.; Astumian, R. D. In *Electromagnetic Fields*; ACS: 1995; Vol. 250, p 79.
- (6) Peter, C. P. *Med. Inorg. Chem.*; ACS: 2005; Vol. 903, p 15.
- (7) Jonathan, L. S.; Susan, R. D.; Thomas, J. M.; Stephen, J. L. *Med. Inorg. Chem.*; ACS, 2005; Vol. 903.
- (8) Gibaud, S.; Jaouen, G. In *Medicinal Organometallic Chemistry*; Jaouen, G., Metzler-Nolte, N., Eds.; Springer Berlin Heidelberg: 2010; Vol. 32, p 1.
- (9) Lloyd, N. C.; Morgan, H. W.; Nicholson, B. K.; Ronimus, R. S. *Angew. Chem., Int. Ed.* **2005**, 44, 941.
- (10) Guo, Z.; Sadler, P. J. *Angew. Chem., Int. Ed.* **1999**, 38, 1512.
- (11) Dhar, S.; Kolishetti, N.; Lippard, S. J.; Farokhzad, O. C. *Proc. Natl. Acad. Sci.* **2011**, 108, 1850.
- (12) Komeda, S.; Casini, A. *Curr. Top. Med. Chem.* **2012**, 12, 219.
- (13) Wong, E.; Giandomenico, C. M. *Chem. Rev.* **1999**, 99, 2451.
- (14) Tayem, Y.; Johnson, T. R.; Mann, B. E.; Green, C. J.; Motterlini, R. *Am. J. Physiol.* **2006**, 290, F789.
- (15) Singh, T. N.; Turro, C. *Inorg. Chem.* **2004**, 43, 7260.
- (16) Loganathan, D.; Morrison, H. *Curr. Opin. Drug Discovery Dev.* **2005**, 8, 478.

- (17) Farrer, N. J.; Woods, J. A.; Munk, V. P.; Mackay, F. S.; Sadler, P. J. *Chem. Res. Toxicol.*, **23**, 413.
- (18) Cohen, S. M.; Lippard, S. J. *Prog. Nucleic Acid Res. Mol. Biol.* **2001**, *67*, 93.
- (19) Ciesinski, K. L.; Hyman, L. M.; Yang, D. T.; Haas, K. L.; Dickens, M. G.; Holbrook, R. J.; Franz, K. J. *Eur. J. Inorg. Chem.* **2010**, 2224.
- (20) Barnes, K. R.; Lippard, S. J. *Metal Ions in Biological Systems* **2004**, *42*, 143.
- (21) Cabantchik, Z. I.; Glickstein, H.; Golenser, J.; Loyevsky, M.; Tsafack, A. *Acta Haematologica* **1996**, *95*, 70.
- (22) Nobili, S.; Mini, E.; Landini, I.; Gabbiani, C.; Casini, A.; Messori, L. *Med. Res. Rev.* **2010**, *30*, 550.
- (23) Bannister, W. H. *Biochem. Educ.* **1992**, *20*, 62.
- (24) Holm, R. H.; Kennepohl, P.; Solomon, E. I. *Chem. Rev.* **1996**, *96*, 2239.
- (25) Stillman, M. *Angew. Chem. Int. Ed* **2007**, *119*, 8895.
- (26) David, S. S.; Meggers, E. *Curr. Opin. Chem. Biol.* **2008**, *12*, 194.
- (27) Cohen, S. M. *Curr. Opin. Chem. Biol.* **2007**, *11*, 115.
- (28) Haas, K. L.; Franz, K. J. *Chem. Rev.* **2009**, *109*, 4921.
- (29) Napoli, C.; Ignarro, L. J. *Annu. Rev. Pharmacool. Toxicol.* **2003**, *43*, 97.
- (30) Motterlini, R.; Clark, J. E.; Foresti, R.; Sarathchandra, P.; Mann, B. E.; Green, C. *J. Circ. Res.* **2002**, *90*, e17.
- (31) Yan, Y. K.; Melchart, M.; Habtemariam, A.; Sadler, P. J. *Chem. Commun.* **2005**, 4764.
- (32) Abrams, M. J.; Murrer, B. A. *Science* **1993**, *261*, 725.

- (33) Fricker, S. P.; Slade, E.; Powell, N. A.; Vaughan, O. J.; Henderson, G. R.; Murrer, B. A.; Megson, I. L.; Bisland, S. K.; Flitney, F. W. *Br. J. Pharmacol.* **1997**, *122*, 1441.
- (34) Suss-Fink, G. *Dalton Trans.* **2010**, *39*, 1673.
- (35) Hartinger, C. G.; Zorbas-Seifried, S.; Jakupec, M. A.; Kynast, B.; Zorbas, H.; Keppler, B. K. *J. Inorg. Biochem.* **2006**, *100*, 891.
- (36) Zayat, L.; Salierno, M.; Etchenique, R. *Inorg. Chem.* **2006**, *45*, 1728.
- (37) Zayat, L.; Noval, M. G.; Campi, J.; Calero, C. I.; Calvo, D. J.; Etchenique, R. *ChemBioChem* **2007**, *8*, 2035.
- (38) Zayat, L.; Calero, C.; Albores, P.; Baraldo, L.; Etchenique, R. *J. Am. Chem. Soc.* **2003**, *125*, 882.
- (39) Zayat, L.; Baraldo, L.; Etchenique, R. *Imaging Neurosci. Dev.* **2005**, 391.
- (40) Salierno, M.; Fameli, C.; Etchenique, R. *Eur. J. Inorg. Chem.* **2008**, 1125.
- (41) Respondek, T., *Ph.D Thesis*, **2013**.
- (42) Klan, P.; Solomek, T.; Bochet, C. G.; Blanc, A.; Givens, R.; Rubina, M.; Popik, V.; Kostikov, A.; Wirz, J. *Chem. Rev.* **2013**, *113*, 119.
- (43) Kim, M. S.; Diamond, S. L. *Bioorg. Med. Chem. Lett.* **2006**, *16*, 4007.
- (44) Adams, S. R.; Tsien, R. Y. *Annu. Rev. Physiol.* **1993**, *55*, 755.
- (45) So, P. T. C.; John Wiley & Sons Ltd.: 2007; Vol. 2, p 1201.
- (46) Gorka, A. P.; Nani, R. R.; Zhu, J.; Mackem, S.; Schnermann, M. J. *J. Am. Chem. Soc.* **2014**, *136*, 14153.
- (47) Garner, R. N.; Gallucci, J. C.; Dunbar, K. R.; Turro, C. *Inorg. Chem.* **2011**, *50*, 9213.

- (48) Sgambellone, M. A.; David, A.; Garner, R. N.; Dunbar, K. R.; Turro, C. *J. Am. Chem. Soc.* **2013**, *135*, 11274.
- (49) Goldbach, R. E.; Rodriguez-Garcia, I.; van, L. J. H.; Siegler, M. A.; Bonnet, S. *Chem. Eur. J.* **2011**, *17*, 9924.
- (50) Knoll, J. D.; Albani, B. A.; Durr, C. B.; Turro, C. *J. Phys. Chem. A* **2014**, *118*, 10603.
- (51) Mackay, F. S.; Woods, J. A.; Moseley, H.; Ferguson, J.; Dawson, A.; Parsons, S.; Sadler, P. J. *Chem. Eur. J.* **2006**, *12*, 3155.
- (52) Farrer, N. J.; Salassa, L.; Sadler, P. J. *Dalton Trans.* **2009**, 10690.
- (53) Farrer, N. J.; Sadler, P. J. *Aust. J. Chem.* **2008**, *61*, 669.
- (54) Betanzos-Lara, S.; Salassa, L.; Habtemariam, A.; Novakova, O.; Pizarro, A. M.; Clarkson, G. J.; Liskova, B.; Brabec, V.; Sadler, P. J. *Organometallics* **2012**, *31*, 3466.
- (55) Bednarski, P. J.; Mackay, F. S.; Sadler, P. J. *Anti-Cancer Agents Med. Chem.* **2007**, *7*, 75.
- (56) Salierno, M.; Marceca, E.; Peterka, D. S.; Yuste, R.; Etchenique, R. *J. Inorg. Biochem.* **2010**, *104*, 418.
- (57) Dolmans, D. E. J. G. J.; Fukumura, D.; Jain, R. K. *Nat. Rev. Cancer* **2003**, *3*, 380.
- (58) Dougherty, T. J.; Gomer, C. J.; Henderson, B. W.; Jori, G.; Kessel, D.; Korbek, M.; Moan, J.; Peng, Q. *J. Natl. Cancer Inst.* **1998**, *90*, 889.
- (59) Castano, A. P.; Mroz, P.; Hamblin, M. R. *Nat. Rev. Cancer* **2006**, *6*, 535.
- (60) Castano, A. P.; Demidova, T. N.; Hamblin, M. R. *Photodiagn. Photodyn. Ther.* **2005**, *1*, 279.

- (61) Burch, S.; London, C.; Seguin, B.; Rodriguez, C.; Wilson, B. C.; Bisland, S. K. *Clin. Orthop. Relat. Res.* **2009**, *467*, 1028.
- (62) Burch, S.; Bogaards, A.; Siewerdsen, J.; Moseley, D.; Yee, A.; Finkelstein, J.; Weersink, R.; Wilson, B. C.; Bisland, S. K. *J. Biomed. Opt.* **2005**, *10*, 034011.
- (63) Burch, S.; Bisland, S. K.; Bogaards, A.; Yee, A. J. M.; Whyne, C. M.; Finkelstein, J. A.; Wilson, B. C. *J. Orthopaed. Res.* **2005**, *23*, 995.
- (64) Bisland, S. K.; Burch, S. *Photodiagn. Photody.* **2006**, *3*, 147.
- (65) Babilas, P.; Schreml, S.; Landthaler, M.; Szeimies, R.-M. *Photodermatol. Photoimmunol. Photomed.* **2010**, *26*, 118.
- (66) Ackroyd, R.; Kelty, C.; Brown, N.; Reed, M. *Photochem. Photobiol.* **2001**, *74*, 656.
- (67) Juarranz, A.; Jaen, P.; Sanz-Rodriguez, F.; Cuevas, J.; Gonzalez, S. *Clin. Transl. Oncol.* **2008**, *10*, 148.
- (68) Ethirajan, M.; Chen, Y.; Joshi, P.; Pandey, R. K. *Chem. Soc. Rev.* **2011**, *40*, 340.
- (69) Cooke, M. S.; Evans, M. D.; Dizdaroglu, M.; Lunec, J. *FASEB J.* **2003**, *17*, 1195.
- (70) Cederbaum, A.; Lu, Y.; Wu, D. *Arch Toxicol* **2009**, *83*, 519.
- (71) Sharma, P.; Jha, A. B.; Dubey, R. S.; Pessarakli, M. *Am. J. Bot.* **2012**, *2012*, 1.
- (72) Moan, J.; Berg, K. *Photochem. Photobiol.* **1991**, *53*, 549.
- (73) Peng, Q.; Moan, J.; Nesland, J. M. *Ultrastrut. Pathol.* **1996**, *20*, 109.
- (74) Durham, B.; Caspar, J. V.; Nagle, J. K.; Meyer, T. J. *J. Am. Chem. Soc.* **1982**, *104*, 4803.
- (75) Liu, Y.; Turner, D. B.; Singh, T. N.; Angeles-Boza, A. M.; Chouai, A.; Dunbar, K. R.; Turro, C. *J. Am. Chem. Soc.* **2009**, *131*, 26.

- (76) Patra, A. K.; Mascharak, P. K. *Inorg. Chem.* **2003**, *42*, 7363.
- (77) Albani, B. A.; Peña, B.; Leed, N. A.; de Paula, N. A. B. G.; Pavani, C.; Baptista, M. S.; Dunbar, K. R.; Turro, C. *J. Am. Chem. Soc.* **2014**, *136*, 17095.
- (78) Gary, F. L.; Michael, E. H. *Enzymes in Biomass Conversion*; ACS, 1991; Vol. 460.
- (79) Fox, J. W.; Shannon, J. D.; Bjarnason, J. B. In *Enzymes in Biomass Conversion*; ACS: 1991; Vol. 460, p 62.
- (80) Hedstrom, L. *Chem. Rev.* **2002**, *102*, 4429.
- (81) Rawlings, N. D.; Barrett, A. J.; Bateman, A. *Nuc. Acids Res.* **2010**, *38*, D227.
- (82) Polgár, L. In *Handbook of Proteolytic Enzymes*; Salvesen, N. D. R., Ed.; Academic Press: 2013, p 1773.
- (83) Mohamed, M. M.; Sloane, B. F. *Nat. Rev. Cancer* **2006**, *6*, 764.
- (84) Turk, V.; Turk, B.; Turk, D. *EMBO J.* **2001**, *20*, 4629.
- (85) Turk, V.; Stoka, V.; Vasiljeva, O.; Renko, M.; Sun, T.; Turk, B.; Turk, D. *Biochim. Biophys. Acta (BBA)* **2012**, *1824*, 68.
- (86) Santamaría, I.; Velasco, G.; Cazorla, M.; Fueyo, A.; Campo, E.; López-Otín, C. *Cancer Res.* **1998**, *58*, 1624.
- (87) Saftig, P.; Hunziker, E.; Wehmeyer, O.; Jones, S.; Boyde, A.; Rommerskirch, W.; Moritz, J. D.; Schu, P.; Von Figura, K. *Proc. Natl. Acad. Sci. U.S.A* **1998**, *95*, 13453.
- (88) Reinheckel, T.; Deussing, J.; Roth, W.; Peters, C. *Biol. Chem.* 2001; Vol. 382, p 735.
- (89) Beers, C.; Burich, A.; Kleijmeer, M. J.; Griffith, J. M.; Wong, P.; Rudensky, A. *Y. J. Immunol.* **2005**, *174*, 1205.

- (90) Duncan, E. M.; Muratore-Schroeder, T. L.; Cook, R. G.; Garcia, B. A.; Shabanowitz, J.; Hunt, D. F.; Allis, C. D. *Cell*, **135**, 284.
- (91) Roth, W.; Deussing, J. A. N.; Botchkarev, V. A.; Pauly-Evers, M.; Saftig, P.; Hafner, A.; Schmidt, P.; Schmahl, W.; Scherer, J.; Anton-Lamprecht, I.; Von Figura, K.; Paus, R.; Peters, C. *FASEB J.* **2000**, *14*, 2075.
- (92) Vasiljeva, O.; Reinheckel, T.; Peters, C.; Turk, D.; Turk, V.; Turk, B. *Curr. Pharm. Des.* **2007**, *13*, 387.
- (93) Otto, H.-H.; Schirmeister, T. *Chem. Rev.* **1997**, *97*, 133.
- (94) Jedeszko, C.; Sloane, B. F. *Biol. Chem.* **2004**, *385*, 1017.
- (95) Brix, K.; Dunkhorst, A.; Mayer, K.; Jordans, S. *Biochimie* **2008**, *90*, 194.
- (96) Berdowska, I. *Clin. Chim. Acta.* **2004**, *342*, 41.
- (97) Xia, L.; Kilb, J.; Wex, H.; Li, Z.; Lipyansky, A.; Breuil, V.; Stein, L.; Palmer, J. T.; Dempster, D. W.; Bromme, D. *Biol. Chem.* **1999**, *380*, 679.
- (98) Friedrichs, B.; Tepel, C.; Reinheckel, T.; Deussing, J.; von Figura, K.; Herzog, V.; Peters, C.; Saftig, P.; Brix, K. *J. Clin. Invest.* **2003**, *111*, 1733.
- (99) Gocheva, V.; Joyce, J. A. *Cell Cycle* **2007**, *6*, 60.
- (100) Kolwijck, E.; Massuger, L. A. G.; Thomas, C. G.; Span, P.; Krasovec, M.; Kos, J.; Sweep, F. G. J. *J. Cancer Res Clin Oncol* **2010**, *136*, 771.
- (101) Jevnikar, Z.; Rojnik, M.; Jamnik, P.; Doljak, B.; Fonović, U. P.; Kos, J. *J. Biol. Chem.* **2013**, *288*, 2201.
- (102) Gabrijelcic, D.; Svetic B Fau - Spaic, D.; Spaic D Fau - Skrk, J.; Skrk J Fau - Budihna, M.; Budihna M Fau - Dolenc, I.; Dolenc I Fau - Popovic, T.; Popovic T Fau - Cotic, V.; Cotic V Fau - Turk, V.; Turk, V.

- (103) Kobayashi, H.; Moniwa, N.; Sugimura, M.; Shinohara, H.; Ohi, H.; Terao, T. *Biochim. Biophys. Acta, Molecular Cell Research* **1993**, *1178*, 55.
- (104) Szpaderska, A. M.; Silberman, S.; Ahmed, Y.; Frankfater, A. *AntiCancer Res.* **2004**, *24*, 3887.
- (105) Sinha, A. A.; Morgan, J. L.; Buus, R. J.; Ewing, S. L.; Fernandes, E. T.; Le, C.; Wilson, M. J. *AntiCancer Res.* **2007**, *27*, 3135.
- (106) Gondi, C. S.; Rao, J. S. *Expert Opin. Ther. Targets* **2013**, *17*, 281.
- (107) Yanamandra, N.; Gumidyala, K. V.; Waldron, K. G.; Gujrati, M.; Olivero, W. C.; Dinh, D. H.; Rao, J. S.; Mohanam, S. *Oncogene* **2004**, *23*, 2224.
- (108) Yan, S.; Sloane, B. F. *Biol. Chem.* **2003**, *384*, 845.
- (109) Rempel, S. A.; Rosenblum, M. L.; Mikkelsen, T.; Yan, P.-S.; Ellis, K. D.; Golembieski, W. A.; Sameni, M.; Rozhin, J.; Ziegler, G.; Sloane, B. F. *Cancer Res.* **1994**, *54*, 6027.
- (110) Murnane, M. J.; Sheahan, K.; Ozdemirli, M.; Shuja, S. *Cancer Res.* **1991**, *51*, 1137.
- (111) Sloane, B. F.; Yan, S.; Podgorski, I.; Linebaugh, B. E.; Cher, M. L.; Mai, J.; Cavallo-Medved, D.; Sameni, M.; Dosesco, J.; Moin, K. *Semi. Cancer Biol.* **2005**, *15*, 149.
- (112) Reinheckel, T.; Gocheva, V.; Peters, C.; Joyce, J. A. *Cancer Degradome*; Edwards, D., Hoyer-Hansen, G., Blasi, F., Sloane, B. F., Eds.; Springer: New York, NY, 2008, p 281.
- (113) Mai, J.; Sameni, M.; Mikkelsen, T.; Sloane, B. F. *Biol. Chem.* **2002**, *383*, 1407.

- (114) Withana, N. P.; Blum, G.; Sameni, M.; Slaney, C.; Anbalagan, A.; Olive, M. B.; Bidwell, B. N.; Edgington, L.; Wang, L.; Moin, K.; Sloane, B. F.; Anderson, R. L.; Bogyo, M. S.; Parker, B. S. *Cancer Res.* **2012**, *72*, 1199.
- (115) Vasiljeva, O.; Papazoglou, A.; Krueger, A.; Brodoefel, H.; Korovin, M.; Deussing, J.; Augustin, N.; Nielsen, B. S.; Almholt, K.; Bogyo, M.; Peters, C.; Reinheckel, T. *Cancer Res.* **2006**, *66*, 5242.
- (116) Roshy, S.; Sloane, B. F.; Moin, K. *Cancer. Metastasis Rev.* **2003**, *22*, 271.
- (117) Cavallo-Medved, D.; Sloane, B. F. *Curr. Top. Dev. Biol.* **2003**, *54*, 313.
- (118) Podgorski, I.; Linebaugh, B. E.; Koblinski, J. E.; Rudy, D. L.; Herroon, M. K.; Olive, M. B.; Sloane, B. F. *Am. J. Pathol.* **2009**, *175*, 1255.
- (119) Podgorski, I. *Future Med. Chem.* **2009**, *1*, 21.
- (120) Herroon, M. K.; Rajagurubandara, E.; Rudy, D. L.; Chalasani, A.; Hardaway, A. L.; Podgorski, I. *Oncogene* **2013**, *32*, 1580.
- (121) Bossard, M. J.; Tomaszek, T. A.; Thompson, S. K.; Amegadzie, B. Y.; Hanning, C. R.; Jones, C.; Kurdyla, J. T.; McNulty, D. E.; Drake, F. H.; Gowen, M.; Levy, M. A. *J Biol Chem* **1996**, *271*, 12517.
- (122) Garnero, P., Borel, O., Byrjalsen, I., Ferras, M., Drake, F.H., McQueney, M.S., Foged, N.T., Delmas, P.D., and Delaisse, J.M. *J. Biol. Chem.* **1998**, *273*, 32347.
- (123) Palermo, C.; Joyce, J. A. *Trends. Pharmacol. Sci.* **2008**, *29*, 22.
- (124) Leung, D.; Abbenante, G.; Fairlie, D. P. *J. Med. Chem.* **2000**, *43*, 305.
- (125) Le Gall, C.; Bellahcene, A.; Bonnelye, E.; Gasser, J. A.; Castronovo, V.; Green, J.; Zimmermann, J.; Clezardin, P. *Cancer Res.* **2007**, *67*, 9894.

(126) Kim, M. K.; Kim, H. D.; Park, J. H.; Lim, J. I.; Yang, J. S.; Kwak, W. Y.; Sung, S. Y.; Kim, H. J.; Kim, S. H.; Lee, C. H.; Shim, J. Y.; Bae, M. H.; Shin, Y. A.; Huh, Y.; Han, T. D.; Chong, W.; Choi, H.; Ahn, B. N.; Yang, S. O.; Son, M. H. *J. Pharmacol. Exp. Ther.* **2006**, *318*, 555.

(127) Altmann, E.; Aichholz, R.; Betschart, C.; Buhl, T.; Green, J.; Lattmann, R.; Missbach, M. *Bioorg. Med. Chem. Lett.* **2006**, *16*, 2549.

(128) Turk, B. *Nat. Rev. Drug Discovery* **2006**, *5*, 785.

(129) Yasuda, Y.; Kaleta, J.; Broemme, D. *Adv. Drug Delivery Rev.* **2005**, *57*, 973.

(130) Ward, Y. D.; Thomson, D. S.; Frye, L. L.; Cywin, C. L.; Morwick, T.; Emmanuel, M. J.; Zindell, R.; McNeil, D.; Bekkali, Y.; Hrapchak, M.; DeTuri, M.; Crane, K.; White, D.; Pav, S.; Wang, Y.; Hao, M.-H.; Grygon, C. A.; Labadia, M. E.; Freeman, D. M.; Davidson, W.; Hopkins, J. L.; Brown, M. L.; Spero, D. M. *J. Med. Chem.* **2002**, *45*, 5471.

(131) Greenspan, P. D.; Clark, K. L.; Tommasi, R. A.; Cowen, S. D.; McQuire, L. W.; Farley, D. L.; van Duzer, J. H.; Goldberg, R. L.; Zhou, H.; Du, Z.; Fitt, J. J.; Coppa, D. E.; Fang, Z.; Macchia, W.; Zhu, L.; Capparelli, M. P.; Goldstein, R.; Wigg, A. M.; Doughty, J. R.; Bohacek, R. S.; Knap, A. K. *J. Med. Chem.* **2001**, *44*, 4524.

(132) Bondebjerg, J.; Fuglsang, H.; Valeur, K. R.; Pedersen, J.; Nærum, L. *Bioorg. Med. Chem. Lett.* **2006**, *16*, 3614.

(133) Boxer, M. B.; Quinn, A. M.; Shen, M.; Jadhav, A.; Leister, W.; Simeonov, A.; Auld, D. S.; Thomas, C. J. *ChemMedChem* **2010**, *5*, 730.

(134) Moon, J. B.; Coleman, R. S.; Hanzlik, R. P. *J. Am. Chem. Soc.* **1986**, *108*, 1350.

(135) Frizler, M.; Stirnberg, M.; Sisay, M. T.; Guetschow, M. *Curr. Top. Med. Chem.* **2010**, *10*, 294.

- (136) Fleming, F. F.; Yao, L.; Ravikumar, P. C.; Funk, L.; Shook, B. C. *J. Med. Chem.* **2010**, *53*, 7902.
- (137) Lucas, E. C.; Williams, A. *Biochemistry* **1969**, *8*, 5125.
- (138) Oballa, R. M.; Truchon, J.-F.; Bayly, C. I.; Chauret, N.; Day, S.; Crane, S.; Berthelette, C. *Bioorg. Med. Chem. Lett.* **2007**, *17*, 998.
- (139) Loeser, R.; Schilling, K.; Dimmig, E.; Guetschow, M. *J. Med. Chem.* **2005**, *48*, 7688.
- (140) Robichaud, J.; Oballa, R.; Prasit, P.; Falguyret, J.-P.; Percival, M. D.; Wesolowski, G.; Rodan, S. B.; Kimmel, D.; Johnson, C.; Bryant, C.; Venkatraman, S.; Setti, E.; Mendonca, R.; Palmer, J. T. *J. Med. Chem.* **2003**, *46*, 3709.
- (141) Jensen, A. B.; Wynne, C.; Ramirez, G.; He, W.; Song, Y.; Berd, Y.; Wang, H.; Mehta, A.; Lombardi, A. *Clin. Breast Cancer* **2010**, *10*, 452.
- (142) Gauthier, J. Y.; Chauret, N.; Cromlish, W.; Desmarais, S.; Duong, L. T.; Falguyret, J.-P.; Kimmel, D. B.; Lamontagne, S.; Leger, S.; LeRiche, T.; Li, C. S.; Masse, F.; McKay, D. J.; Nicoll-Griffith, D. A.; Oballa, R. M.; Palmer, J. T.; Percival, M. D.; Riendeau, D.; Robichaud, J.; Rodan, G. A.; Rodan, S. B.; Seto, C.; Therien, M.; Truong, V.-L.; Venuti, M. C.; Wesolowski, G.; Young, R. N.; Zamboni, R.; Black, W. C. *Bioorg. Med. Chem. Lett.* **2008**, *18*, 923.
- (143) Peroni, A.; Zini A Fau - Braga, V.; Braga V Fau - Colato, C.; Colato C Fau - Adami, S.; Adami S Fau - Girolomoni, G.; Girolomoni, G. *Curr. Top. Med. Chem.* 2240
- (144) Kim, T. S.; Tasker, A. S. *Curr. Top. Med. Chem.* **2006**, *6*, 355.
- (145) Gondi, C. S.; Rao, J. S. *Expert. Opin. Ther. Targets.* **2013**, *17*, 281.

- (146) Respondek, T.; Garner, R. N.; Herroon, M. K.; Podgorski, I.; Turro, C.; Kodanko, J. J. *J. Am. Chem. Soc.* **2011**, *133*, 17164.
- (147) Howerton, B. S.; Heidary, D. K.; Glazer, E. C. *J. Am. Chem. Soc.* **2012**, *134*, 8324.
- (148) Brieke, C.; Rohrbach, F.; Gottschalk, A.; Mayer, G.; Heckel, A. *Angew. Chem., Int. Ed.* **2012**, *51*, 8446.
- (149) Lee, H.-M.; Larson, D. R.; Lawrence, D. S. *ACS Chem. Biol.* **2009**, *4*, 409.
- (150) Fino, E.; Araya, R.; Peterka, D. S.; Salierno, M.; Etchenique, R.; Yuste, R. *Front. Neural Circuits* **2009**, *3*, 1.
- (151) Filevich, O.; Etchenique, R. *Ruthenium Prop., Prod. Appl.* **2011**, 269.
- (152) Araya, R.; Andino-Pavlovsky, V.; Yuste, R.; Etchenique, R. *ACS Chem. Neurosci.* **2013**, *4*, 1163.
- (153) Tepel, C.; Bromme, D.; Herzog, V.; Brix, K. *J. Cell Science* **2000**, *113*, 4487.
- (154) Boonen, S.; Rosenberg E Fau - Claessens, F.; Claessens F Fau - Vanderschueren, D.; Vanderschueren D Fau - Papapoulos, S.; Papapoulos, S. *Curr. Top. Med. Chem.* 1640.
- (155) Pollard, J. W. *Nat. Rev. Cancer* **2004**, *4*, 71.
- (156) Pollard, J. W. *Nat. Rev. Immunol.* **2009**, *9*, 259.
- (157) Cruz, A. J.; Kirgan, R.; Siam, K.; Heiland, P.; Rillema, D. P. *Inorg. Chim. Acta.* **2010**, *363*, 2496.
- (158) Durham, B.; Wilson, S. R.; Hodgson, D. J.; Meyer, T. J. *J. Am. Chem. Soc.* **1980**, *102*, 600.
- (159) Kamiya, T.; Kobayashi, Y.; Kanaoka, K.; Nakashima, T.; Kato, Y.; Mizuno, A.; Sakai, H. *J. Biochem.* **1998**, *123*, 752.

- (160) Gocheva, V.; Zeng, W.; Ke, D.; Klimstra, D.; Reinheckel, T.; Peters, C.; Hanahan, D.; Joyce, J. A. *Genes. Dev.* **2006**, *20*, 543.
- (161) Salassa, L.; Ruiu, T.; Garino, C.; Pizarro, A. M.; Bardelli, F.; Gianolio, D.; Westendorf, A.; Bednarski, P. J.; Lamberti, C.; Gobetto, R.; Sadler, P. J., *Organometallics*, **2010**.
- (162) Falguyret, J.-P.; Black, W. C.; Cromlish, W.; Desmarais, S.; Lamontagne, S.; Mellon, C.; Riendeau, D.; Rodan, S.; Tawa, P.; Wesolowski, G.; Bass, K. E.; Venkatraman, S.; Percival, M. D. *Anal. Biochem.* **2004**, *335*, 218.
- (163) Ruettinger, A.; Mollenhauer, J.; Loeser, R.; Guetschow, M.; Wiederanders, B. *BioTechniques* **2006**, *41*, 469.
- (164) Desmarais, S.; Black, W. C.; Oballa, R.; Lamontagne, S.; Riendeau, D.; Tawa, P.; Duong, L. T.; Pickarski, M.; Percival, M. D. *Mol. Pharmacol.* **2008**, *73*, 147.
- (165) Rafi, S. B.; Hearn, B. R.; Vedantham, P.; Jacobson, M. P.; Renslo, A. R. *J. Med. Chem.* **2012**, *55*, 3163.
- (166) Puckett, C. A.; Ernst, R. J.; Barton, J. K. *Dalton Trans.* **2010**, *39*, 1159.
- (167) Durham, B.; Wilson, S. R.; Hodgson, D. J.; Meyer, T. J. *J. Am. Chem. Soc.* **1980**, *102*, 600.
- (168) Montalti, M.; Credi, A.; Prodi, L.; Gandolfi, M. T. *Handb. Photochem.*; 3rd ed.; CRC Press: Boca Raton, FL, 2006.
- (169) Herroon, M. K.; Rajagurubandara, E.; Rudy, D. L.; Chalasani, A.; Hardaway, A. L.; Podgorski, I. *Oncogene* **2012**, 2108.
- (170) Deiters, A. *ChemBioChem* **2010**, *11*, 47.
- (171) Respondek, T.; Sharma, R.; Herroon, M. K.; Garner, R. N.; Knoll, J. D.; Cueny, E.; Turro, C.; Podgorski, I.; Kodanko, J. J. *ChemMedChem* **2014**, *9*, 1306.

- (172) Solary, E.; Eymin, B.; Droin, N.; Haugg, M. *Cell Biol. Toxicol.* **1998**, *14*, 121.
- (173) Liang, Q.; Ouyang X Fau - Schneider, L.; Schneider L Fau - Zhang, J.; Zhang, J. *Mol. Neurodegener.*, 1750
- (174) Uchiyama, Y. *Arch. Histol. Cytol.* 9465.
- (175) Yang, C. N.; Shiao Yj Fau - Shie, F.-S.; Shie Fs Fau - Guo, B.-S.; Guo Bs Fau - Chen, P.-H.; Chen Ph Fau - Cho, C.-Y.; Cho Cy Fau - Chen, Y.-J.; Chen Yj Fau - Huang, F.-L.; Huang Fl Fau - Tsay, H.-J.; Tsay, H. J. *Neurobiol. Dis.*, 1095.
- (176) Joyce, J. A.; Pollard, J. W. *Nat Rev Cancer* **2009**, *9*, 239.
- (177) Elliott, N. T.; Yuan, F. *J. Pharm. Sci.* **2011**, *100*, 59.
- (178) Lovitt, C.; Shelper, T.; Avery, V. *J Cancer Res Clin Oncol* **2015**, *141*, 951.
- (179) Lovitt, C. J.; Shelper Tb Fau - Avery, V. M.; Avery, V. M. *Assay. Drug. Dev. Technol.*, 1557.
- (180) Sameni, M.; Cavallo-Medved, D.; Dosescu, J.; Jedeszko, C.; Moin, K.; Mullins, S. R.; Olive, M. B.; Rudy, D.; Sloane, B. F. *Clin. Exp. Metastas.* **2009**, *26*, 299.
- (181) Sameni, M.; Anbalagan, A.; Olive, M. B.; Moin, K.; Mattingly, R. R.; Sloane, B. *F. J. Vis. Exp.* **2012**, *60*, 3661.
- (182) Rothberg, J. M.; Bailey, K. M.; Wojtkowiak, J. W.; Ben-Nun, Y.; Bogyo, M.; Weber, E.; Moin, K.; Blum, G.; Mattingly, R. R.; Gillies, R. J.; Sloane, B. F. *Neoplasia* **2013**, *15*, 1125.
- (183) Jedeszko, C.; Sameni, M.; Olive, M. B.; Moin, K.; Sloane, B. F. *Curr Protoc Cell Biol* **2008**, *Chapter 4*, Unit 4.20.
- (184) Schmeichel, K. L.; Bissell, M. J. *J. Cell. Sci.* **2003**, *116*, 2377.

- (185) Linebaugh, B. E.; Sameni, M.; Day, N. A.; Sloane, B. F.; Keppler, D. *Eur. J. Biochem.* **1999**, *264*, 100.
- (186) Jedeszko, C.; Sameni, M.; Olive, M.; Moin, K.; Sloane, B. F. *Current Protocols In Cell Biology* **2008**, *39*, 4.
- (187) Montaser, M.; Lalmanach, G.; Mach, L. *Biol. Chem.* **2002**, *383*, 1305.
- (188) Lankelma, J. M.; Voorend, D. M.; Barwari, T.; Koetsveld, J.; Van der Spek, A. H.; De Porto, A. P. N. A.; Van Rooijen, G.; Van Noorden, C. J. F. *Life Sci.* **2010**, *86*, 225.
- (189) Wagenaar-Miller, R. A.; Engelholm, L. H.; Gavard, J.; Yamada, S. S.; Gutkind, J. S.; Behrendt, N.; Bugge, T. H.; Holmbeck, K. *Mol. Cell. Biol.* **2007**, *27*, 6309.
- (190) Sameni, M.; Dosescu, J.; Moin, K.; Sloane, B. F. *Mol Imaging* **2003**, *2*, 159.
- (191) Sloane, B. F.; Sameni, M.; Podgorski, I.; Cavallo-Medved, D.; Moin, K. *Annu. Rev. Pharmacool. Toxicol.* **2006**, *46*, 301.
- (192) Bogenrieder, T.; Herlyn, M. *Oncogene*, **2003**, *22*, 6524.
- (193) Mohamed, M. M.; Cavallo-Medved D Fau - Sloane, B. F.; Sloane, B. F. *Cell. Physiol. Biochem.* **2010**, *25*, 315.
- (194) Lecaille, F.; Kaleta, J.; Brömme, D. *Chem. Rev.* **2002**, *102*, 4459.
- (195) Droga-Mazovec, G.; Bojič, L.; Petelin, A.; Ivanova, S.; Romih, R.; Repnik, U.; Salvesen, G. S.; Stoka, V.; Turk, V.; Turk, B. *J. Biol. Chem.* **2008**, *283*, 19140.
- (196) Katunuma, N.; Matsunaga Y Fau - Himeno, K.; Himeno K Fau - Hayashi, Y.; Hayashi, Y. *J. Biochem.* **1980**, *88*, 1085.
- (197) Fröhlich, E. *Cell. Mol. Life Sci.* **2010**, *67*, 3947.
- (198) Berquin, I. M.; Sloane, B. F. *Adv. Exp. Med. Biol.* **1996**, *389*, 281.

- (199) Towatari, T.; Nikawa, T.; Murata, M.; Yokoo, C.; Tamai, M.; Hanada, K.; Katunuma, N. *FEBS Lett.* **1991**, *280*, 311.
- (200) Droga-Mazovec, G.; Bojič, L.; Petelin, A.; Ivanova, S.; Romih, R.; Repnik, U.; Salvesen, G. S.; Stoka, V.; Turk, V.; Turk, B. *J. Biol. Chem.* **2008**, *283*, 19140.
- (201) Hanada, K.; Tamai, M.; Yamagishi, M.; Ohmura, S.; Sawada, J.; Tanaka, I. *Agricultural. Biol. Chem.* **1978**, *42*, 523.
- (202) Hashida S Fau - Towatari, T.; Towatari T Fau - Kominami, E.; Kominami E Fau - Katunuma, N.; Katunuma, N. *J. Biochem.* **1980**, *88*, 1085
- (203) Dorman, G.; Prestwich, G. D. *Trends. Biotechnol.* **2000**, *18*, 64.
- (204) Banghart, M. R.; Sabatini, B. L. *Neuron* **2012**, *73*, 249.
- (205) Aurelio, L.; Brownlee, R. T. C.; Hughes, A. B. *Aust. J. Chem.* **2008**, *61*, 615.
- (206) Hoertz, P. G.; Staniszewski, A.; Marton, A.; Higgins, G. T.; Incarvito, C. D.; Rheingold, A. L.; Meyer, G. J. *J. Am. Chem. Soc.* **2006**, *128*, 8234.
- (207) Liu, Y.; Chouai, A.; Degtyareva, N. N.; Lutterman, D. A.; Dunbar, K. R.; Turro, C. J. *J. Am. Chem. Soc.* **2005**, *127*, 10796.
- (208) Wachter, E.; Heidary, D. K.; Howerton, B. S.; Parkin, S.; Glazer, E. C. *Chem. Commun.* **2012**, *48*, 9649.
- (209) Jabre, N. D.; Respondek, T.; Ulku, S. A.; Korostelova, N.; Kodanko, J. J. *J. Org. Chem.* **2010**, *75*, 650.
- (210) Jabre, N. D.; Korostelova, N.; Kodanko, J. J. *J. Org. Chem.* **2011**, *76*, 2273.
- (211) Whiteoak, C. J.; Nobbs, J. D.; Kiryushchenkov, E.; Pagano, S.; White, A. J. P.; Britovsek, G. J. P. *Inorg. Chem.* **2013**, *52*, 7000.

- (212) Kojima, T.; Amano, T.; Ishii, Y.; Ohba, M.; Okaue, Y.; Matsuda, Y. *Inorg. Chem.* **1998**, *37*, 4076.
- (213) Radaram, B.; Ivie, J. A.; Singh, W. M.; Grudzien, R. M.; Reibenspies, J. H.; Webster, C. E.; Zhao, X. *Inorg. Chem.* **2011**, *50*, 10564.
- (214) Weisser, F.; Hohloch, S.; Plebst, S.; Schweinfurth, D.; Sarkar, B. *Chem. Eur. J.* **2014**, *20*, 781.
- (215) Kodadek, T. *Chem. Commun.* **2011**, *47*, 9757.
- (216) Mulcahy, S. P.; Li, S.; Korn, R.; Xie, X.; Meggers, E. *Inorg. Chem.* **2008**, *47*, 5030.
- (217) Mulcahy, S. P.; Gruendler, K.; Frias, C.; Wagner, L.; Prokop, A.; Meggers, E. *Dalton Trans.* **2010**, *39*, 8177.
- (218) Sandman, K. E.; Lippard, S. J. *Cisplatin* **1999**, 523.
- (219) Chow, M. J.; Licon, C.; Wong, D. Y. Q.; Pastorin, G.; Gaiddon, C.; Ang, W. H. *J. Med. Chem.* **2014**, *57*, 6043.
- (220) Ciesienski, K. L.; Franz, K. J. *Angew. Chem. Int. Ed.* **2011**, *50*, 814.
- (221) Sharma, R.; Knoll, J. D.; Martin, P. D.; Podgorski, I.; Turro, C.; Kodanko, J. J. *Inorg. Chem.* **2014**, *53*, 3272.
- (222) Olson, J. P.; Kwon, H.-B.; Takasaki, K. T.; Chiu, C. Q.; Higley, M. J.; Sabatini, B. L.; Ellis-Davies, G. C. R. *J. Am. Chem. Soc.* **2013**, *135*, 5954.
- (223) Olson, J. P.; Banghart, M. R.; Sabatini, B. L.; Ellis-Davies, G. C. R. *J. Am. Chem. Soc.* **2013**, *135*, 15948.
- (224) Jabre, N. D.; Hryhorczuk, L.; Kodanko, J. J. *Inorg. Chem.* **2009**, *48*, 8078.

- (225) Widegren, J. A.; Weiner, H.; Miller, S. M.; Finke, R. G. *J. Organomet. Chem.* **2000**, *610*, 112.
- (226) Malik, K. Z.; Robinson, S. D.; Steed, J. W. *Polyhedron* **2000**, *19*, 1589.
- (227) Mikata, Y.; Kawata, K.; Iwatsuki, S.; Konno, H. *Inorg. Chem.* **2012**, *51*, 1859.
- (228) Roelfes, G.; Lubben, M.; W. Leppard, S.; Schudde, E. P.; Hermant, R. M.; Hage, R.; Wilkinson, E. C.; Que, L., Jr.; Feringa, B. L. *J. Mol. Cat.* **1997**, *117*, 223.
- (229) Makino, M.; Ishizuka, T.; Ohzu, S.; Hua, J.; Kotani, H.; Kojima, T. *Inorg. Chem.* **2013**, *52*, 5507.
- (230) Horton, D. A.; Bourne, G. T.; Smythe, M. L. *Chem. Rev.* **2003**, *103*, 893.
- (231) Tan, D. S. *Nat. Chem. Biol.* **2005**, *1*, 74.
- (232) Schreiber, S. L. *Science* **2000**, *287*, 1964.
- (233) Bunin, B. A.; Plunkett, M. J.; Ellman, J. A. *Proc. Natl. Acad. Sci. U. S. A.* **1994**, *91*, 4708.
- (234) Lam, K. S.; Salmon, S. E.; Hersh, E. M.; Hruby, V. J.; Kazmierski, W. M.; Knapp, R. J. *Nature* **1991**, *354*, 82.
- (235) Astle, J. M.; Simpson, L. S.; Huang, Y.; Reddy, M. M.; Wilson, R.; Connell, S.; Wilson, J.; Kodadek, T. *Chem. Biol.* **2010**, *17*, 38.
- (236) Kodadek, T. *Nat. Chem. Biol.* **2010**, *6*, 162.
- (237) Francis, M. B.; Finney, N. S.; Jacobsen, E. N. *J. Am. Chem. Soc.* **1996**, *118*, 8983.
- (238) Reetz, M. T. *Angew. Chem., Int. Ed.* **2008**, *47*, 2556.
- (239) Boussie, T. R.; Murphy, V.; Hall, K. A.; Coutard, C.; Dales, C.; Petro, M.; Carlson, E.; Turner, H. W.; Powers, T. S. *Tetrahedron* **1999**, *55*, 11699.

- (240) Knight, A. S.; Zhou, E. Y.; Pelton, J. G.; Francis, M. B. *J. Am. Chem. Soc.* **2013**, *135*, 17488.
- (241) Marshall, G. R.; Reddy, P. A.; Schall, O. F.; Naik, A.; Beusen, D. D.; Ye, Y.; Slomczynska, U. *Adv. Supramol. Chem.* **2002**, *8*, 175.
- (242) Choudhary, S.; Morrow, J. R. *Methods Mol. Biol.* **2002**, *201*, 215.
- (243) Al-Mutlaq, F.; Potvin, P. G. *J. Comb. Chem.* **2005**, *7*, 820.
- (244) Sardesai, N. Y.; Lin, S. C.; Zimmerman, K.; Barton, J. K. *Bioconjug. chem.* **1995**, *6*, 302.
- (245) Chantson, J. T.; Falzacappa, M. V. V.; Crovella, S.; Metzler-Nolte, N. *ChemMedChem* **2006**, *1*, 1268.
- (246) Kirin, S. I.; Ott, I.; Gust, R.; Mier, W.; Weyhermueller, T.; Metzler-Nolte, N. *Angew. Chem. Int. Ed.* **2008**, *47*, 955.
- (247) Noor, F.; Wuestholz, A.; Kinscherf, R.; Metzler-Nolte, N. *Angew. Chem. Int. Ed.* **2005**, *44*, 2429.
- (248) van Staveren, D. R.; Metzler-Nolte, N. *Chem. Rev.* **2004**, *104*, 5931.
- (249) Stephenson, K. A.; Banerjee, S. R.; Besanger, T.; Sogbein, O. O.; Levadala, M. K.; McFarlane, N.; Lemon, J. A.; Boreham, D. R.; Maresca, K. P.; Brennan, J. D.; Babich, J. W.; Zubieta, J.; Valliant, J. F. *J. Am. Chem. Soc.* **2004**, *126*, 8598.
- (250) Stephenson, K. A.; Zubieta, J.; Banerjee, S. R.; Levadala, M. K.; Taggart, L.; Ryan, L.; McFarlane, N.; Boreham, D. R.; Maresca, K. P.; Babich, J. W.; Valliant, J. F. *Bioconju. Chem.* **2004**, *15*, 128.

- (251) Armstrong, A. F.; Oakley, N.; Parker, S.; Causey, P. W.; Lemon, J.; Capretta, A.; Zimmerman, C.; Joyal, J.; Appoh, F.; Zubieta, J.; Babich, J. W.; Singh, G.; Valliant, J. F. *Chem. Commun.* **2008**, 5532.
- (252) Stephenson, K. A.; Reid, L. C.; Zubieta, J.; Babich, J. W.; Kung, M.-P.; Kung, H. F.; Valliant, J. F. *Bioconju. Chem.* **2008**, *19*, 1087.
- (253) Dirscherl, G.; Koenig, B. *Eur. J. Org. Chem.* **2008**, 597.
- (254) Filevich, O.; Salierno, M.; Etchenique, R. *J. Inorg. Biochem.* **2010**, *104*, 1248.
- (255) De Candia, A. G.; Marcolongo, J. P.; Etchenique, R.; Slep, L. D. *Inorg. Chem.* **2010**, *49*, 6925.
- (256) Nikolenko, V.; Yuste, R.; Zayat, L.; Baraldo, L. M.; Etchenique, R. *Chem. Commun.* **2005**, 1752.
- (257) Chakraborty, I.; Carrington, S. J.; Mascharak, P. K. *ChemMedChem* **2014**, *9*, 1266.
- (258) Halpenny, G. M.; Gandhi, K. R.; Mascharak, P. K. *ACS Med. Chem. Lett.* **2010**, *1*, 180.
- (259) Rose, M. J.; Mascharak, P. K. *Inorg. Chem.* **2009**, *48*, 6904.
- (260) Halpenny, G. M.; Mascharak, P. K. *Inorg. Chem.* **2009**, *48*, 1490.
- (261) Rose, M. J.; Mascharak, P. K. *Coord. Chem. Rev.* **2008**, *252*, 2093.
- (262) Rose, M. J.; Mascharak, P. K. *Curr. Opin. Chem. Biol.* **2008**, *12*, 238.
- (263) Eroy-Reveles, A. A.; Leung, Y.; Beavers, C. M.; Olmstead, M. M.; Mascharak, P. K. *J. Am. Chem. Soc.* **2008**, *130*, 6650.
- (264) Madhani, M.; Patra, A. K.; Miller, T. W.; Eroy-Reveles, A. A.; Hobbs, A. J.; Fukuto, J. M.; Mascharak, P. K. *J. Med. Chem.* **2006**, *49*, 7325.

- (265) Eroy-Reveles, A. A.; Leung, Y.; Mascharak, P. K. *J. Am. Chem. Soc.* **2006**, *128*, 7166.
- (266) Afshar, R. K.; Patra, A. K.; Mascharak, P. K. *J. Inorg. Biochem.* **2005**, *99*, 1458.
- (267) Halpenny, G. M.; Gandhi, K. R.; Mascharak, P. K. *ACS Med. Chem. Lett.* **2010**, *1*, 180.
- (268) Stephenson, K. A.; Reid, L. C.; Zubieta, J.; Babich, J. W.; Kung, M.-P.; Kung, H. F.; Valliant, J. F. *Bioconju. Chem.* **2008**, *19*, 1087.
- (269) Tu, Y.-J.; Mazumder, S.; Endicott, J. F.; Turro, C.; Kodanko, J. J.; Schlegel, H. B. *Inorg. Chem.* **2015**, *54*, 8003.
- (270) Jabre, N. D.; Respondek, T.; Ulku, S. A.; Korostelova, N.; Kodanko, J. J. *J. Org. Chem.* **2010**, *75*, 650.
- (271) Sankaralingam, M.; Palaniandavar, M. *Polyhedron* **2014**, *67*, 171.
- (272) Wang, X.; Vittal, J. J. *Inorg. Chem.* **2003**, *42*, 5135.
- (273) Kim, H.; Kim, K. B.; Song, E. J.; Hwang, I. H.; Noh, J. Y.; Kim, P.-G.; Jeong, K.-D.; Kim, C. *Inorg. Chem. Commun.* **2013**, *36*, 72.
- (274) Darbre, T.; Dubs, C.; Rusanov, E.; Stoeckli-Evans, H. *Eur. J. Inorg. Chem.* **2002**, 3284.
- (275) Newkome, G. R.; Puckett, W. E.; Kiefer, G. E.; Gupta, V. D.; Xia, Y.; Coreil, M.; Hackney, M. A. *J. Org. Chem.* **1982**, *47*, 4116.
- (276) Au-Yeung, H. Y.; Chan, J.; Chantarojsiri, T.; Chang, C. J. *J. Am. Chem. Soc.* **2013**, *135*, 15165.

(277) Baffert, C.; Collomb, M.-N.; Deronzier, A.; Kjaergaard-Knudsen, S.; Latour, J.-M.; Lund, K. H.; McKenzie, C. J.; Mortensen, M.; Nielsen, L. P.; Thorup, N. *Dalton Trans.* **2003**, 1765.

(278) Ife, R. J.; Catchpole, K. W.; Durant, G. J.; Ganellin, C. R.; Harvey, C. A.; Meeson, M. L.; Owen, D. A. A.; Parsons, M. E.; Slingsby, B. P.; Theobald, C. J. *Eur. J. Med. Chem.* **1989**, *24*, 249.

(279) Widegren, J. A.; Weiner, H.; Miller, S. M.; Finke, R. G. *J. Organomet. Chem.* **2000**, *610*, 112.

(280) Malik, K. Z.; Robinson, S. D.; Steed, J. W. *Polyhedron* **2000**, *19*, 1589.

(281) Young, K. J.; Takase, M. K.; Brudvig, G. W. *Inorg. Chem.* **2013**, *52*, 7615.

(282) Russell, M. G. N.; Carling, R. W.; Atack, J. R.; Bromidge, F. A.; Cook, S. M.; Hunt, P.; Isted, C.; Lucas, M.; McKernan, R. M.; Mitchinson, A.; Moore, K. W.; Narquizian, R.; Macaulay, A. J.; Thomas, D.; Thompson, S.-A.; Wafford, K. A.; Castro, J. L. *J. Med. Chem.* **2005**, *48*, 1367.

(283) Zhao, J.; Wu, W.; Sun, J.; Guo, S. *Chem. Soc. Rev.* **2013**, *42*, 5323.

(284) Polo, A. S.; Itokazu, M. K.; Murakami Iha, N. Y. *Coord. Chem. Rev.* **2004**, *248*, 1343.

(285) Svanberg, K.; Bendsoe, N.; Axelsson, J.; Andersson-Engels, S.; Svanberg, S. J. *Biomed. Opt.* **2010**, *15*, 041502.

(286) Gorman, A.; Killoran, J.; O'Shea, C.; Kenna, T.; Gallagher, W. M.; O'Shea, D. F. *J. Am. Chem. Soc.* **2004**, *126*, 10619.

(287) McDonnell, S. O.; Hall, M. J.; Allen, L. T.; Byrne, A.; Gallagher, W. M.; O'Shea, D. F. *J. Am. Chem. Soc.* **2005**, *127*, 16360.

- (288) Kamkaew, A.; Lim, S. H.; Lee, H. B.; Kiew, L. V.; Chung, L. Y.; Burgess, K. *Chem. Soc. Rev.* **2013**, *42*, 77.
- (289) O'Connor, A. E.; Gallagher, W. M.; Byrne, A. T. *Photochem. Photobiol.* **2009**, *85*, 1053.
- (290) Zhao, Q.; Li, F.; Huang, C. *Chem. Soc. Rev.* **2010**, *39*, 3007.
- (291) Sun, Y.; Wang, S. *Inorg. Chem.* **2009**, *48*, 3755.
- (292) Sun, Y.; Hudson, Z. M.; Rao, Y.; Wang, S. *Inorg. Chem.* **2011**, *50*, 3373.
- (293) Williams, J. A. G. *Top. Curr. Chem.* **2007**, *281*, 205.
- (294) Vezzu, D. A. K.; Ravindranathan, D.; Garner, A. W.; Bartolotti, L.; Smith, M. E.; Boyle, P. D.; Huo, S.-Q. *Inorg. Chem.* **2011**, *50*, 8261.
- (295) Zeitler, K. *Angew. Chem., Int. Ed.* **2009**, *48*, 9785.
- (296) Narayanam, J. M. R.; Stephenson, C. R. J. *Chem. Soc. Rev.* **2011**, *40*, 102.
- (297) Tucker, J. W.; Stephenson, C. R. J. *J. Org. Chem.* **2012**, *77*, 1617.
- (298) Zhao, J.; Ji, S.; Wu, W.; Wu, W.; Guo, H.; Sun, J.; Sun, H.; Liu, Y.; Li, Q.; Huang, L. *RSC Adv.* **2012**, *2*, 1712.
- (299) You, Y.; Nam, W. *Chem. Soc. Rev.* **2012**, *41*, 7061.
- (300) Sauvage, J. P.; Collin, J. P.; Chambron, J. C.; Guillerez, S.; Coudret, C.; Balzani, V.; Barigelletti, F.; De Cola, L.; Flamigni, L. *Chem. Rev.* **1994**, *94*, 993.
- (301) Sun, L.; Hammarstrom, L.; Akermark, B.; Styring, S. *Chem. Soc. Rev.* **2001**, *30*, 36.
- (302) Islam, A.; Sugihara, H.; Arakawa, H. *J. Photochem. Photobiol., A* **2003**, *158*, 131.
- (303) Lomoth, R.; Magnuson, A.; Sjoedin, M.; Huang, P.; Styring, S.; Hammarstroem, L. *Photosynth. Res.* **2006**, *87*, 25.

- (304) Esswein, A. J.; Nocera, D. G. *Chem. Rev.* **2007**, *107*, 4022.
- (305) O'Regan, B.; Graetzel, M. *Nature* **1991**, *353*, 737.
- (306) Schramm, F.; Meded, V.; Fliegl, H.; Fink, K.; Fuhr, O.; Qu, Z.; Klopper, W.; Finn, S.; Keyes, T. E.; Ruben, M. *Inorg. Chem.* **2009**, *48*, 5677.
- (307) Brown, D. G.; Sanguantrakun, N.; Schulze, B.; Schubert, U. S.; Berlinguette, C. *P. J. Am. Chem. Soc.* **2012**, *134*, 12354.
- (308) Ragazzon, G.; Verwilt, P.; Denisov, S. A.; Credi, A.; Jonusauskas, G.; McClenaghan, N. D. *Chem. Commun.* **2013**, *49*, 9110.
- (309) Sharma, R.; Knoll, J. D.; Ancona, N.; Martin, P. D.; Turro, C.; Kodanko, J. J. *Inorg. Chem.* **2015**, *54*, 1901.
- (310) Nakamoto, K. *Infrared and Raman Spectra of Inorganic and Coordination Compounds. Part B*; Wiley: New York, 1997.
- (311) Kohle, O.; Ruile, S.; Gratzel, M. *Inorg. Chem.* **1996**, *35*, 4779.
- (312) Kasha, M. *Discuss. Faraday Soc.* **1950**, *9*, 14.
- (313) Mazumder, S.; Thomas, R. A.; Lord, R. L.; Schlegel, H. B.; Endicott, J. F. *Can. J. Chem.* **2014**, *92*, 996.
- (314) Odongo, O. S.; Heeg, M. J.; Chen, Y.-J.; Xie, P.; Endicott, J. F. *Inorg. Chem.* **2008**, *47*, 7493.
- (315) Xie, P.; Chen, Y.-J.; Uddin, M. J.; Endicott, J. F. *J. Phys. Chem. A* **2005**, *109*, 4671.
- (316) Lord, R. L.; Allard, M. M.; Thomas, R., A.; Odongo, O. S.; Schlegel, H. B.; Chen, Y.-J.; Endicott, J. F. *Inorg. Chem.* **2013**, *52*, 1185.
- (317) Tyson, D. S.; Bialecki, J.; Castellano, F. N. *Chem. Commun.* **2000**, 2355.

- (318) Kos, J.; Werle, B.; Lah, T.; Brunner, N. *Int. J. Biol. Markers*, **2000**, *15*, 84.
- (319) Abrahamson, M.; Alvarez-Fernandez, M.; Nathanson, C.-M. *Biochem. Soc. Symp.* **2003**, *70*, 179.
- (320) Watson, C. J.; Kreuzaler, P. A. *J Mammary Gland Biol Neoplasia* **2009**, *14*, 171.
- (321) Joyce, J. A.; Hanahan, D. *Cell Cycle* **2004**, *3*, 1516.
- (322) Wiczerzak, E.; Drabik, P.; Lankiewicz, L.; Oldziej, S.; Grzonka, Z.; Abrahamson, M.; Grubb, A.; Broemme, D. *J. Med. Chem.* **2002**, *45*, 4202.
- (323) Sadaghiani, A. M.; Verhelst, S. H. L.; Gocheva, V.; Hill, K.; Majerova, E.; Stinson, S.; Joyce, J. A.; Bogoy, M. *Chem. Biol.* **2007**, *14*, 499.
- (324) Powers, J. C.; Asgian, J. L.; Ekici, O. D.; James, K. E. *Chem. Rev.* **2002**, *102*, 4639.
- (325) Murata, M.; Miyashita, S.; Yokoo, C.; Tamai, M.; Hanada, K.; Hatayama, K.; Towatari, T.; Nikawa, T.; Katunuma, N. *FEBS Lett.* **1991**, *280*, 307.
- (326) Huang, L.; Lee, A.; Ellman, J. A. *J. Med. Chem.* **2002**, *45*, 676.

ABSTRACT**SYNTHESIS AND BIOLOGICAL EVALUATION OF NITRILE-BASED INHIBITORS OF CYSTEINE PROTEASES CAGED WITH RUTHENIUM COMPLEXES**

by

RAJGOPAL SHARMA**December 2015****Advisor:** Jeremy J. Kodanko, Ph.D.**Major:** Chemistry (Organic)**Degree:** Doctor of Philosophy

Light activated compounds can be used as tools for understanding and solving numerous biological problems. This dissertation focuses on developing ruthenium-based photocages for caging nitrile-based cysteine protease inhibitors. Four research areas pertaining to this dissertation, i) metals in medicine, ii) photocages in biological applications, iii) photodynamic therapy and iv) cysteine cathepsin proteases were briefly surveyed in the introductory chapter. Next, Ru(bpy)₂ group was utilized for synthesizing nitrile-based caged CTSK and CTSB inhibitors. Light activated release of inhibitors, followed by toxicity and stability data were studied. Cathepsin enzyme activity inhibition in 2D and 3D assays were established. This work showcased the applicability of ruthenium complexes in photocaging cathepsin inhibitors for gaining spatiotemporal control over enzyme inhibition. Later we reported that ruthenium (II) tri(2-pyridylmethyl)amine, a polypyridyl ligand distinct from the established Ru(bpy)₂ class, is an effective caging group for nitriles that provides high levels of control over cathepsin activity with light. Also a library approach was developed by solid phase that provides rapid access to new complexes for screening photochemical behavior. Ligands designed to tune spectral properties of the ruthenium-based photocaging group were synthesized in parallel fashion on

resin. The library was processed to form caged ruthenium complexes bound to resin, then subsequently cleaved and analyzed for photochemical reactivity. Three compounds identified from this screen were synthesized by solution phase and characterized spectroscopically and photochemically. Data were in good agreement with compounds from solid phase, thus validating the predictive power of our library approach. Finally new ruthenium complexes based on TQA ligand were developed and studied for excited state lifetimes.

AUTOBIOGRAPHICAL STATEMENT

RAJGOPAL SHARMA

EDUCATION

2011 – 2015	Ph.D in Organic Chemistry Wayne State University, Detroit, MI, USA
2007 – 2009	M.Sc in Organic Chemistry Osmania University, Hyderabad, India
2004 – 2007	B.Sc in B.Z.C (Botany, Zoology and Chemistry) Osmania University, Hyderabad, India

AWARDS AND HONORS

- Dr. Cal Stevens Memorial Scholarship, Wayne State University – 2015
- Summer Dissertation Fellowship, Wayne State University – Summer 2015
- James C. French Graduate Award, Wayne State University – Awarded for most outstanding fourth year organic graduate student – 2014
- Rumble Graduate Fellowship, Wayne State University – 2014 - 2015
- Graduate Teaching Award, Wayne State University – 2011 and 2012
- KYD certification (Know Your Development) – Dr. Reddy's Laboratories, India – 2011
- Excellence in Innovation – Dr. Reddy's Laboratories, India – 2010
- Best value creation through functional excellence – API R&D – Dr. Reddy's Laboratories, India – 2010
- Complex product development – Dr. Reddy's Laboratories, India – 2009

PUBLICATIONS AND PRESENTATIONS

- “Ruthenium Tris(2-pyridylmethyl)amine as an Effective Photocaging Group for Nitriles” **Sharma, R.;** Knoll, J. D.; Martin, P. D.; Podgorski, I.; Turro, C.; Kodanko, J. J. *Inorg. Chem.* **2014**, 53, 3273.
- “Inhibition of Cathepsin Activity in a Cell – Based Assay by Light Activated Ruthenium Compounds” Respondek, T.; **Sharma, R.;** Herroon, M. K.; Graner, R. N.; Knoll, J. D.; Cueny, E.; Turro, C.; Podgorski, I.; Kodanko, J. J. *Chem. Med. Chem.* **2014**, 9, 1306.
- “Solid Phase Synthesis as a Platform for Discovery of Light - Activated Metal complexes” **Sharma, R.;** Ancona, N.; Kodanko, J. J. *Inorg. Chem.* **2015**, 54, 1901.
- “Tuning Polypyridyl based Ruthenium Complexes for Effective Light Harvesting by Prolonged Excited State Lifetimes” - **Sharma, R.;** Thomas, R.; Endicott, J. F.; Kodanko, J. J. *manuscript under revision*.
- “Visualizing Inhibition of Proteolysis by a Light-Activated Ruthenium Compound in Live Breast Cancer Cells” – Ramalho, D. S.; **Sharma, R.;** Aggarwal, N.; Chalasani, A.; Sameni, M.; Vieira, P. C.; Knoll, J.; Turro, C.; Kodanko, J. J.; Sloane, B. F. *manuscript under revision*.
- “Light Mediated Directed Release of Cysteine (Cathepsin and Caspase) Protease Inhibitors” poster presentation given at 14th Graduate Chemistry Symposium, Wayne State University, Detroit, MI, October **2012**.
- “Development of Ruthenium Complexes as Photocaging Groups” oral presentation at 16th Graduate Chemistry Symposium, Wayne State University, Detroit, MI, October **2014**.
- “Development of Ruthenium Complexes as Photocaging Groups” poster presentation at 24th Inter-American Photochemical Society (I-APS) meeting – Sarasota, Florida, January **2015**.